SOLAR RADIATION RELATED CLIMATE CHANGE PROJECTIONS FOR THE UK

YIENG WEI THAM

BEng (Hons) Mechanical Engineering

MSc. Energy and Environment

A thesis submitted in partial fulfilment of the requirements of Edinburgh Napier University, for the award of Doctor of Philosophy

June 2011

ABSTRACT

This research is mainly focussed on solar radiation in the UK. It can be divided into four main areas; evaluation of models, analysis of the relations between temperature and solar radiation, critical analysis of the projected future data for the UK and the improvement to the UKCP09 Weather Generator (WG).

From the evaluations of models carried out, the Liu-Jordan model performs well for estimating the average hourly global and diffuse radiation. At the individual hourly level however, a number of problems were observed. Regarding clear-sky radiation models, for semi-arid climatic conditions Page model was found to be suitable and for humid climates Yang model is recommended. As for all-sky radiation models, the MRM and Yang model were selected. For the UK, the MRM was found to perform better than the Yang model.

Furthermore, a study was carried out to analyse the relationship between temperature and solar radiation. The development of temperature-based mathematical models to obtain mean-daily irradiation was established. A procedure to decompose daily to hourly temperatures was evaluated with respect to world-wide locations and its performance found to be satisfactory.

As part of the UKCP09/COPSE project, detailed analysis on the future projected data was carried out to critically evaluate sol-air temperature and the likely change that may occur in the key climatic variables, i.e. temperature, sunshine duration and solar irradiation. Drastic increase of sol-air temperatures and shifting trend of daylight illuminance were found. Furthermore, a sensitivity test was also carried out to analyse the effects of each input variables on sol-air temperature.

As a result of the present investigations and communications with the UKCP personnel a new version of WG was released with appropriate modifications. A comparison of the now old- and new WG data sets has been made. Improvements in ratio of diffuse to global radiation and sunshine datasets were found.

ACKNOWLEDGEMENTS

I would like to thank my Director of Studies, Professor Tariq Muneer for giving me this great opportunity to study for my PhD. Furthermore, thank you for your constant support, guidance, motivation, and giving me the undivided attention throughout the course of my research. In addition I would like to thank my supervisor, Mr Brian Davison for the support and advice that you have given me. I would also like to thank the technician Mr Bill Campbell and administrative staff at the Faculty and the School of Engineering and Built Environment who were always so helpful and supportive.

I am grateful to the Engineering and Physical Sciences Research Council (EPSRC) which provided the research funding.

Last but not least, I would like to express my heartfelt thanks to my family members and friends. Without their continuous support and endless love, completion of this thesis would not have been possible.

DECLARATION

I hereby declare that the work presented in this thesis was solely carried out by myself at Edinburgh Napier University, Edinburgh, except where due acknowledgement is made, and that is has not been submitted for any other degree.

……

Yieng Wei Tham (CANDIDATE)

……..

Date:

Table of Contents

List of Figures

List of Tables

Nomenclature

a, b = site-specific coefficients

CO_2 = carbon dioxide

c', c_0, c_{01}, c_{02}, c_1, c_{11}, c_{12} = equation coefficients

cc = cloud cover

COPSE = COincident Probabilistic climate change weather data for a Sustainable built Environment

D = earth-sun distance, m

DBR = Ratio of diffuse- to beam irradiance on horizontal surface

DEC = solar declination, degree

DRG = diffuse to global solar radiation ratio

DSWF = Downward Short-Wave Flux

DSY = Design Summer Years

$\overline{D}$ = monthly-averaged daily diffuse irradiation, kWh/m^2

$\overline{d}$ = monthly-averaged hourly diffuse irradiation, Wh/m^2

d', d_0, d_{01}, d_{02}, d_1, d_{11}, d_{12} = equation coefficients

dbt = dry bulb temperature, °C

$\overline{E}$ = monthly-averaged extraterrestrial radiation, kWh/m^2

G = global solar irradiance, W/m^2

GHGs = green house gases

$\overline{G}$ = monthly-averaged daily global irradiation, kWh/m^2

$\bar{g}$ = monthly-averaged hourly global irradiation, Wh/m^2

$\bar{G}_{clear}$ = average clear-day global irradiation, kWh/m^2

gsr = hourly global solar radiation, Wh/m^2

H = maximum possible sunshine duration

h = actual sunshine duration

I_B = beam irradiance on horizontal surface, W/m^2

I_{Bc} = beam irradiance on horizontal surface under a clear sky, W/m^2

I_D = diffuse irradiance on horizontal surface, W/m^2

I_{Dc} = diffuse irradiance on horizontal surface under a clear sky, W/m^2

I_{Do} = diffuse irradiance under over cast sky horizontal surface, W/m^2

I_E = extraterrestrial irradiance on horizontal surface, W/m^2

I_G = global irradiance, W/m^2

I_{Gc} = global irradiance under a clear sky on horizontal surface, W/m^2

I_{SC} = solar constant, W/m^2

IPCC = Intergovernmental Panel on Climate Change

$J^{'}$ = the day angle

k = hourly diffuse ratio

$\bar{k}$ = weighted mean of hourly diffuse ratio

K_B = Ratio of beam to extraterrestrial irradiance on horizontal surface

K_d = solar distance,

K_D = Ratio of diffuse to extraterrestrial irradiance on horizontal surface

K_N = Ratio of normal to extraterrestrial irradiance on horizontal surface

K_r = empirical coefficient, dimensionless

$\overline{K}_T$ = monthly averaged clearness index

LAT = latitude, degree

MBE = Mean Bias Error

ME = Model Efficiency

MetD = Meteorological office datasets

m = optical air mass

m' = pressure corrected optical air mass

N = astronomical day length, hour

n = average daily hours of bright sunshine, hour

r_D = ratio of hourly to daily diffuse radiation.

r_{DC} = ratio of computed hourly to daily diffuse radiation.

r_{D_LJ} = r_D predicted by Liu and Jordan's regression model

r_{Dn} = r_D predicted by proposed new model

$r_{Dc,am}$ = ratio of computed hourly to daily global radiation before noon.

$r_{Dc,ave}$ = average ratio of computed hourly to daily global radiation.

$r_{Dc,pm}$ = ratio of computed hourly to daily global radiation after noon.

$r_{Dm,am}$ = ratio of measured hourly to daily diffuse radiation before noon.

$r_{Dm,ave}$ = average ratio of measured hourly to daily diffuse radiation.

$r_{Dm,pm}$ = ratio of measured hourly to daily diffuse radiation after noon.

r_G = ratio of hourly to daily global radiation.

r_{GC} = ratio of computed hourly to daily global radiation.

$r_{Gc,am}$ = ratio of computed hourly to daily global radiation before noon.

$r_{Gc,ave}$ = average ratio of computed hourly to daily global radiation.

$r_{Gc,pm}$ = ratio of computed hourly to daily global radiation after noon.

$r_{Gm,am}$ = ratio of measured hourly to daily global radiation before noon.

$r_{Gm,ave}$ = average ratio of measured hourly to daily global radiation.

$r_{Gm,pm}$ = ratio of measured hourly to daily global radiation after noon.

r_s = ground albedo.

$r_\alpha^{'}$ = albedo of cloudless sky.

r^2 = coefficient of determination

RMSE= Root Mean Square Error

R_o = mean solar radius, m

SF = sunshine fraction

SOLALT = solar altitude, °

T = temperature, °K

T_{LK} = Linke turbidity factor

$Trd(n)$ = diffuse transmittance for any given day

UKCP = United Kingdom Climate Projections

UKCIP = United Kingdom Climate Impacts Programme

UN = United Nation

WAZ = orientation of surface, degree

WAZS = orientation of surface due to south, degree

$x_{o,i}$ = measured variable

$x_{p,i}$ = computed variable

$\overline{x_o}$ = average of the measured variable

Y = measured value

Yc = computed value

Ym = mean measured value

Z = Ratio of hourly temperature elevation to daily range {= $\frac{T_h - T_{\min}}{T_{\max} - T_{\min}}$}, dimensionless

z = station height, m

Greek

$\beta =$ Ångström turbidity coefficient

ε = percentage error, %

μ_o = thickness of the ozone layer, cm

$\rho =$ atmospheric pressure, mbar

ρ_o = standard atmospheric pressure, mbar

ω = hour angle, degree

ω_s = Sunset hour angle, degree

σ = Stefan Boltzmann constant, W/m^2K^4

σ_k = standard deviation of hourly diffuse ratio

τ_B = beam transmittance

τ_D = diffuse transmittance

τ_α = Mie scattering transmittance

τ_c = cloud extinction transmittance

τ_a = aerosol transmittance

τ_g = gas transmittance

τ_o = ozone transmittance

τ_r = Rayleigh transmittance

τ_w = water-vapour transmittance

1.0 Introduction

In this chapter, an introductory discussion about climate change and green house gases (GHGs) emissions was conducted. Later in this chapter, discussion of how this research is aimed to fill the gap in current research will also be presented.

1.1 Climate change

According to the United Nation (UN) (UNFCCC 1994) climate change is a change in climate that is attributed either directly or indirectly to human activity that alters the composition of the global atmosphere and which is in addition to natural climate variability observed over comparable time periods.

Energy from the sun is absorbed by oceans, land and air and the rest is reflected back to the space. The energy absorbed by the land and oceans are released to the atmosphere as heat. This heat is then absorbed by GHGs and later re-emits it back to the earth surface. This heat will keep the earth comfortably warm but the increased GHGs concentrations intensify this effect and increase the temperature. In-depth discussion of energy flow will be carried out in Chapter 2. Figure 1.1.1 shows the overview of the solar energy absorptions and reflections.

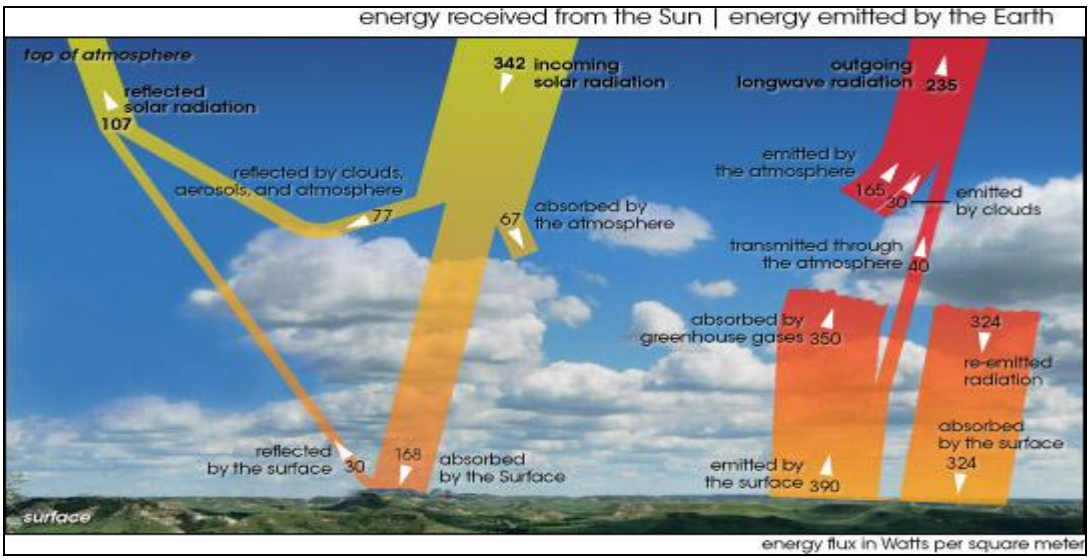

Figure 1.1.1 Energy cycle from the sun (Kiehl and E.Trenberth 1997)

From the process mentioned above, assessment from the Intergovernmental Panel on Climate Change (IPCC) reported measurements recording an increase of 0.74 ± 0.18°C in mean global surface temperature from 1906 to 2005 against a baseline of 14°C from Sims (Sims 2004) and predicted a rise by 1.4 to 5.8°C during the remainder of the 21st century (IPCC 2007). This estimate was produced by running different global climate models at different emission scenarios. Different emission scenarios give a range of temperature predictions. If humans limit GHGs emissions (low growth), then the temperature change over the next century will be smaller than that predicted if humans do not limit emissions (high growth). Prediction from the IPCC model shows that warming will be greatest in the Arctic and over land.

A similar rising trend in temperature was also reported by the UK Meteorological Office, a possible rise of future temperature of 4°C by 2070 due to high levels of carbon dioxide (CO_2) emissions but in the plausible worst case scenario, this rise would occur by 2060 (Betts, Sanderson, Hemming et al. 2009). Furthermore, Hansen et. al., reported that the global mean temperature anomaly, 0.57°C (about 1°F) warmer than the 1951-1980 mean, continues the strong warming trend of the past thirty years that has been confidently attributed to the effect of increasing human-made GHGs (Hansen, Sato, Ruedy et al. 2007). This may cause warmer summers than the 2003 heat wave which was considered the hottest summer since 1500 (Black, Blackburn and Harrison 2004; Lutherbacher, Dietrich, Xoplanki et al. 2004; Schar, Vidale, Luthi et al. 2004). Furthermore, a 2003-type summer is predicted to be about average by the 2040s (Scott, Stone and Allen 2004).

The Climatic Research Unit and the UK Meteorological Office Hadley Centre jointly compiled the global temperature record time from 1850 till 2010 to show the increased trend in global temperature. Figure 1.1.2 shows this global temperature record.

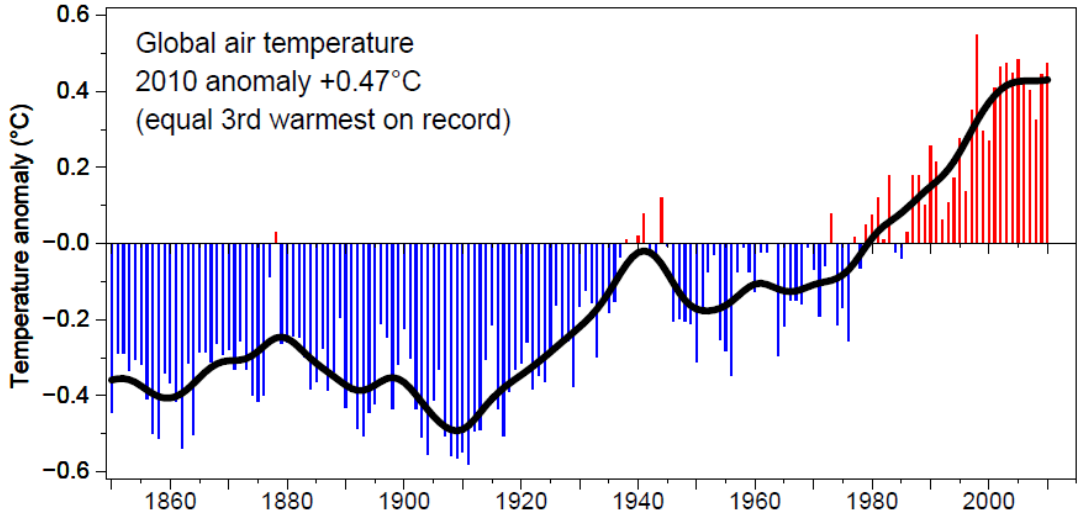

Figure 1.1.2 The combined global land and marine surface temperature record from 1850 to 2010 (Jones 2011)

The earth's surface is warm because there is a natural blanket to trap the long wave radiation emitted from its surface. This natural blanket is called the greenhouse effect from the GHGs. GHGs consist of water vapour, CO_2, methane, ozone, oxygen etc and clouds. Of all these GHGs, water vapour and CO_2 have the greatest effect in absorbing and emitting the heat from both the sun and earth. The higher concentration of CO_2 traps more heat or radiation emitted from the earth's surface hence increased the earth temperature. On the other hand, clouds do have the same effects of blanketing as the GHGs but its reflectivity offsets the effect.

One of the main GHG contributors is the burning of fossil fuels. The use of fossil fuels which release a large amount of CO_2 to the atmosphere contributes to the effect of global warming. Figure 1.1.3 shows the concentration of CO_2 in the atmosphere at Mauna Loa in Hawaii from 1959 to 2008.

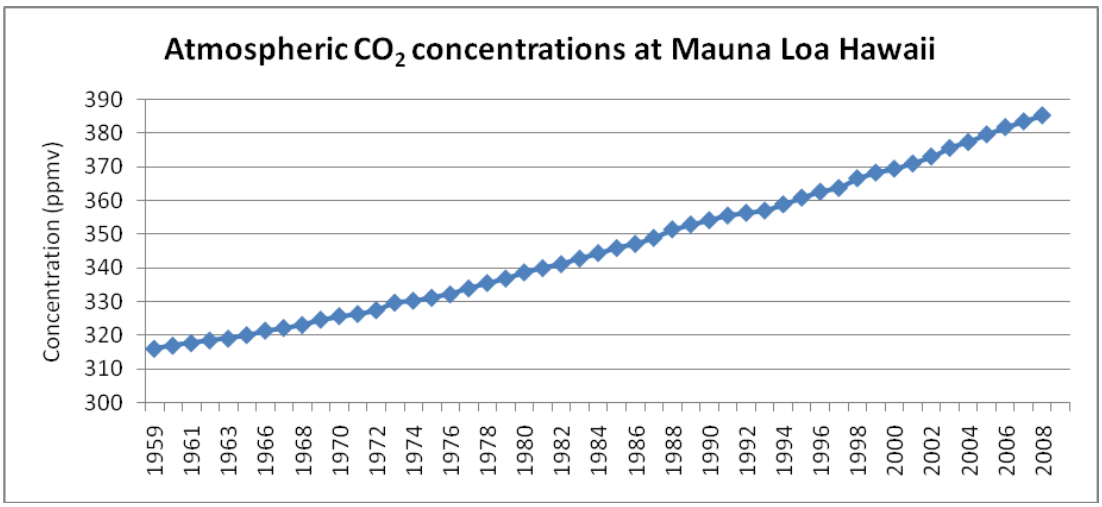

Figure 1.1.3 Concentration of CO_2 in the atmosphere at Mauna Loa in Hawaii (Keeling, Piper, Bollenbacher et al. 2009)

The annual average concentrations of CO_2 rose from 316 parts per million by volume (ppmv) in 1959 to 385 ppmv in 2008. This represents an average annual growth rate of 1.4 ppmv per year in the in situ values at Mauna Loa (Keeling, Piper, Bollenbacher et al. 2009). The current CO_2 concentration amounts to about 390 ppmv (Latif 2010). A drop in the ocean storage of carbon from 48% to 41% was observed caused mainly from fossil fuel emissions since the pre-industrial era. This shows that the ocean uptake does not seems to keeping with pace with the increase of CO_2 emission (Sabine CL 2010). The increased trend of CO_2 concentration is in line with the increased trend of temperature as shown above in Figures 1.1.2 and 1.1.3.

The result of increased global temperature, IPCC (IPCC 2007) - since 1993 melting glaciers and ice caps contributed about 28% of the sea level rise whilst thermal expansion of the oceans has contributed to 57% and polar ice sheets contributed the remaining 15%. Hence this resulted in the mean sea level rising by 10 to 20cm with an average rate increase of about 3.1 ± 0.7mm per year from 1993 to 2003.

As a result from the aforementioned changes in CO_2 and temperature, the frequency and intensity of extreme weather events have changed in the past 50 years making climate change one of the main global challenges today.

1.2 Impacts of climate change

Climate change affects every aspect of human life. Economic losses are unavoidable due to climate change impacts such as extreme weather, including floods, droughts and storms. According to the Stern Review (2006) if action is not taken to curb carbon emissions, climate change could cost between 5 and 20 percent of the annual global gross domestic product. This poses an increased threat to poorer nations where extra monetary funds are needed to address climate change impacts. Examples of extreme events in 2010 such as the monsoon-related floods in Pakistan, the summer heat wave in Russian and drought in the Amazon have affected millions of people and huge amounts of money are needed for redevelopment of the affected areas.

Besides that, climate change directly impacts health. The World Health Organisation (WHO 2009) stated that people die every year from the side-effects of global warming with increased deaths in heat waves, and in natural disasters such as floods, as well as changing patterns of life-threatening vector-borne diseases such as malaria and other existing and emerging infectious diseases. According to the IPCC (IPCC 2007) those people living in poverty would be worst affected by the effects of climate change.

Furthermore, the Organisation for Economic Co-operation and Development (OECD 2008) has shown potential water related tensions between nations that share common freshwater reserves - where 47% of the world's population will live in areas of high water stress in 2030. On top of that, to meet increasing demands for food and bio-fuels, world agricultural land use will need to expand by an estimated 10% by 2030. Hence this poses an increased pressure on agriculture and biodiversity development. "A statistical analysis of the historical temperature-yield relationship indicates that at the global scale, warming from 1981-2002 very like offset some of the yield gains (for maize, wheat and barley) from technological advances, rising CO_2 and other non-climatic factors". Yield for rice, soy and sorghum were less affected (Lobell and Field 2007).

Global warming is predicted to increase generally with latitude. A study suggested that warming in the tropics even with relatively small magnitude is

likely to have deleterious consequences on the local ecosystem. This is because tropical species are currently living very close to their optimal temperature and are as a result sensitive to temperature change (Calosi, Bilton and Spicer 2008; Deutsch, Tewksbury, Huey et al. 2008). Consequently, the greatest extinction risks from global warming may be in the tropics where there is greatest biological diversity. (Williams, Jackson and Kutzbach 2007)

Scientists around the world are working around the clock to better understand the Earth's climate systems; as a result, climate projection tools have been developed to provide a better understanding of future climate so that adaptations and mitigations measures can be taken.

1.3 Project overview

Refer to the previously mentioned consequences of climate change; reduction of GHGs is an essential step to reduce the trapped sun's energy or solar irradiation. The UK Climate Impacts Programme (UKCIP) has produced projections of future climate for the UK to provide the UK with a platform to understand climate change. This research is part of the Coincident Probabilistic climate change weather data for a Sustainable built Environment (COPSE) project. The main study of this research work is to study and analyse in detail projections of future solar irradiation in the UK. Validations of solar radiation models for the UK were carried out to determine the best model to predict solar irradiation.

1.4 Objectives and aims

The aims of this research are to study and analyse in detail the future projections of solar profile in the UK and hence determine the best model to predict solar radiation. The objectives are:

- To examine in detail solar radiation data from the UKCIP projections for consistencies.
- To critically analyse the likely changes that may occur in the key climate variables, i.e. temperature, sunshine duration and solar irradiation.

- To critically analyse sol-air temperature for different orientations and different type of surface i.e. dark- and light coloured surface.
- To analyse the trend of daylight illuminance through the frequencies of occurrence of illuminance.
- To evaluate solar radiation models for UK climate conditions using statistical evaluation techniques.
- To study the relationship between solar radiation and temperature.

1.5 Thesis outline

Chapter 1 gives the introduction to the thesis, which broadly covers an overview of climate change. The chapter begins with an overview of the basic concept of how the earth is warmed by the sun, the change in global temperature, the global GHGs scenario and also the causes and effects of climate change. Later in this chapter also outlines the background, aims and objectives and key areas which this thesis will investigate further.

Chapter 2, deals with literature review which will cover in detail the effects of solar radiation on earth climate system, the need of solar radiation measurement, the type of solar measurements equipment and their uncertainties and errors, quality control procedures, statistical evaluation techniques, photovoltaic development and the UK Feed-in tariffs (FITs). The development of UKCIP starting from its history up to the present and discussion on the development of weather generator (WG) will be presented.

Chapter 3 covers validation of solar radiation models. This chapter will start with a brief review of the solar radiation models that will be evaluated i.e. Page radiation model, Yang model and Meteorological Radiation Model. Measured data from around the world and the whole UK were used in these validations. Furthermore, detail method to decompose average-daily to average-hourly solar radiation will also be validated. Attempt to further improvement to the model will also be discussed in detail.

Chapter 4 presents a study on the relation between solar radiation and temperature. Data from around the world mainly for the northern hemisphere were used in this study. Statistical evaluation techniques were used to study the correlation between solar radiation and temperature.

Chapter 5 will discuss in detail the analysis of sol-air temperature and day light illuminance. Data sets from the UKCP09 were used in this study along with the historical measured data for three locations i.e. Bracknell (London), Manchester and Edinburgh to critically analyse the likely change in sol-air temperature and daylight illuminance. Extreme clear day and long sunshine duration was found and reported to the UKCP.

Chapter 6 will present all communications with the UKCP modellers. All emails of communications are attached as Appendix B. Communications regarding proposed steps to check the sunshine data are also presented later in this chapter. Analyses of the new WG data sets were carried out and compared with the now old version WG data sets.

Chapter 7 draws important conclusions from each aspect of the presented work. The potential for future work is also discussed.

1.6 Concluding remarks

This chapter provides an introduction to climate change and the effects of solar radiation to the earth climate system. Detail temperature change and increased of GHGs concentrations were discussed. Furthermore, effects of climate change from the economic, health, biodiversity and political aspects were also presented. Later, the research objectives and aims and the outline of the thesis were stated.

2.0 Literature review

This chapter comprises a core aspect of the research work. Firstly, it presents the fundamental concepts in relation to solar radiation and earth climate and the equations that are needed to obtain the basic functions of solar radiation models. Then, it discusses solar radiation measurements and its developments. Furthermore, it discusses the methods of quality control procedures of solar data and statistical evaluation techniques. Development of photovoltaic and the UK feed-in tariffs will also be discussed.

2.1 Earth climate system

The earth climate system basically depends on the energy emitted from the Sun i.e. the climate system is powered by solar radiation. The upwards and downwards flows of energy which circulate vertically are the main factor for climate study. Its presence at the earth's surface is necessary for the provision of food for mankind. Thus it is important to be able to understand the physics of solar radiation and in particular to determine the amount of energy intercepted by the earth's surface. There are three fundamental ways to change the radiation balance of the Earth (IPCC 2007):

1) Changing the incoming solar radiation (e.g., by changes in Earth's orbit or in the Sun itself)

2) Changing the fraction of solar radiation that is reflected (called 'albedo'; e.g., by changes in cloud cover, atmospheric particles or vegetation)

3) Altering the long-wave radiation from Earth back towards space (e.g., by changing greenhouse gas concentrations).

Figure 2.1.1 shows the mean energy flow from the sun to the surface of the earth.

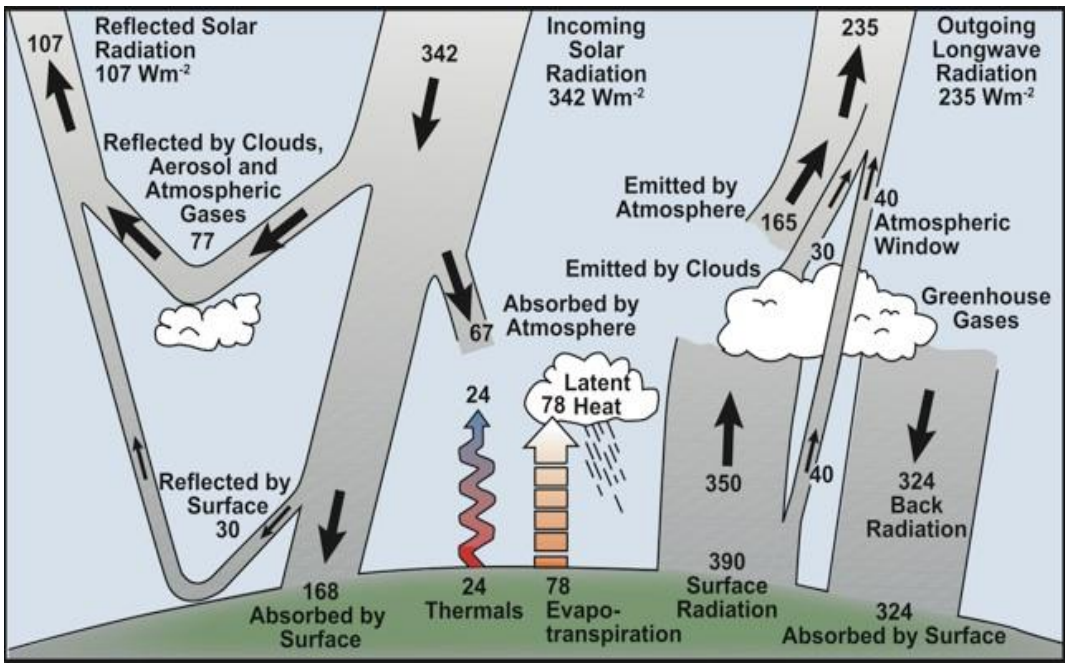

Figure 2.1.1 Mean vertical energy flows from the sun (atmosphere and surface), in Watts per square metre. (IPCC 2007)

The two most important flows of solar energy are the 342 W/m^2 which enters the troposphere and the 390 W/m^2 emanated from the earth surface in the form of infrared waves. The balance between the incoming and outgoing energy is 0 on both the planet's surface and the tropopause.

Approximately 240 W/m^2 of mean energy flow from the sun is absorbed by the earth of which 70 W/m^2 are absorbed directly by the gases and clouds in the atmosphere. The planet's surface absorbs the remaining 170 W/m^2 which pass through the air.

The total radiation reaching the earth's surfaces consists of direct or beam and diffuse radiation. Direct or beam radiation is the radiation directly from the sun to the earth surface without any kind of reflection. The diffuse radiation is the sun's radiation which reaches the earth's surface from any direction which has been diverted several times through the atmosphere. In clear or sunny days, direct or beam radiation is higher than the diffuse radiation, whilst on the contrary, during cloudy days, diffuse radiation exceeds the direct radiation.

The mean energy flow of 240 W/m^2 was calculated based on the flow of solar radiation which reaches the surface of the atmosphere on a plane perpendicular to the sun's rays. The electromagnetic spectrum of the sun is close to the black body radiation. Stefan Boltzmann described black body radiation with the equation:

$$B = \sigma T^4 \tag{2.1.1}$$

Where B is the radian flux density emitted from a black body of temperature T and σ is the Stefan-Boltzmann constant 5.67x10^{-8} W/m^{2}K^4.

To obtain the solar constant (I_{SC}) the following equation may be used:

$$I_{SC} = \sigma T^4 \left(\frac{R_o}{D} \right)^2 \tag{2.1.2}$$

Where the sun surface temperature T =5770K, the mean solar radius (R_o) =6.96x10^{8}m and the earth-sun distance (D) = 1.496x10^{11}m or 1 astronomical unit. Hence the solar constant obtained is equal to 1360 W/m^2. The mean value of solar constant given by composites of measurements is near 1365.5 W/m^2 (Fröhlich 2006). However, measurement from the total irradiance monitor on the SORCE satellite launce in 2003 yield similar variation with the values persistently lower at 1361 W/m^2(Kopp, Lawrence and Rottman 2005). The latest Earth-observing satellite developed by NASA, called Glory, will be launched on February 2011. Glory will improve the understanding of aerosol contributions to global climate change and help maintain a record of total solar irradiance (NASA 2011). This may help to resolve the discrepancy in the solar constant value.

The Earth's global albedo best estimate is very close to 0.3 (Loeb, Wielicki, Doelling et al. 2009). There is no scientific theory to indicate that the albedo has been and remained constant, and a change of 1% in its value can have a large impact on the earth's climate system (Raval and Ramanathan 1989). Taking the current earth albedo, the mean energy absorbed by the Earth is therefore 240 W/m2 ((1 -0.3) x 342 = 240 W/m^2). The higher the albedo the more light or

radiation is reflected from the surface. For example, the albedo of deserts is higher than for forests or jungles and the albedo of snow-covered tundra landscape is higher than that of a snow-covered landscape covered by boreal forests.

Hence from discussions above, any changes in solar irradiation and earth surface landscape will effect greatly on its climate system. Understanding of the course of future solar irradiation is essential.

2.2 UK greenhouse gases

To help reduce the effect of climate change, the UK is working hard toward reducing its GHG emissions. According to the Climate Change Act 2008 (DEFRA 2008), the UK target to reduce its GHG emissions by at least 80% by 2050 relative to 1990 emission. Figure 2.2.1 shows GHG emissions from 1990 to 2009. From 1990, the UK emission of GHGs have decreased a total of about 28% from 781.6 million tonnes of CO_2 equivalent ($MtCO_2e$) to 563.6 $MtCO_2e$. The largest contribution of GHGs came from the energy supply sector with 35 percent, followed by transport sector (22 percent), business (15 percent), residential (14 percent), agriculture (9 percent) and others accounted for the remaining 5 percent were waste management, public and land industrial process. There was a decrease of about 0.7 percent in the Land Use, Land Use Change and deforestation and forest management (LULUCF) sector.

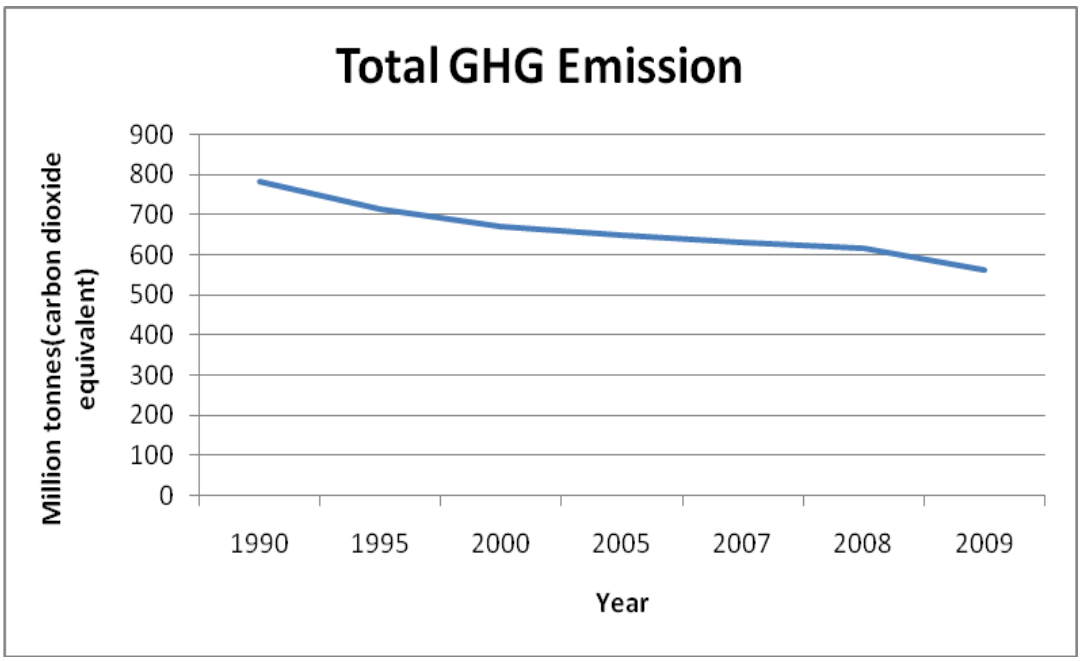

Figure 2.2.1 Total green house gases (GHGs) emission for the UK from 1990 to 2009 (DECC 2011)

When compared with the base level at year 1990, the energy supply sector has reduced emissions by 28 percent, the business sector by 24 percent, the agriculture sector by 21 percent, the waste management sector by 68 percent, industrial process sector by 81 percent and public sector by 41 percent. There was a slight increase in the transport sector with 0.1 percent. Table 2.2.1 shows the GHGs emission by each sector.

From the reduction trend, it seems that the UK government is working hard to achieve its target to reduce GHG emissions by 80 percent by year 2050.

Table 2.2.1 GHGs emission according to sector; million tonnes of CO_2 equivalent ($MtCO_2e$) (DECC 2011).

Year	1990	1995	2000	2005	2007	2008	2009
Energy Supply	272.1	233.9	218.6	227.9	226.1	219.2	195
Transport	122.1	122.6	127.3	131.1	132.4	127.6	122.2
Business	112.4	107.6	110.5	103.1	99.1	97.4	85.9
Residential	80.8	82.3	90.1	87.8	81.5	83.4	78.6
Agriculture	63	60.8	57.3	53.4	50.5	50	49.5
Waste Management	59	46.1	31.5	20	19.1	18.5	17.9
Industrial Process	54.3	44.8	24.4	18	17.9	16.4	10.4
Public	14.1	13.7	11.7	11	9.3	9.3	8.2
LULUCF	3.9	2.4	0.4	-3	-3.6	-4	-4.1
Total	**781.6**	**714.3**	**672**	**649.4**	**632.2**	**617.7**	**563.6**

2.2.1 UK CO_2 emission

Of all the man made GHGs, carbon dioxide (CO_2) accounted for 86 percent of the total emissions (DECC 2011). A total of 474 million tonnes (Mt) of CO_2 were emitted in the year of 2009. Figure 2.2.2 shows the CO_2 emission for the UK. A sharp decrease was observed when comparing year 2009 to 2008. This may be due to the fall in energy demand which was cause by the effects of the economic crisis in 2008-2009.

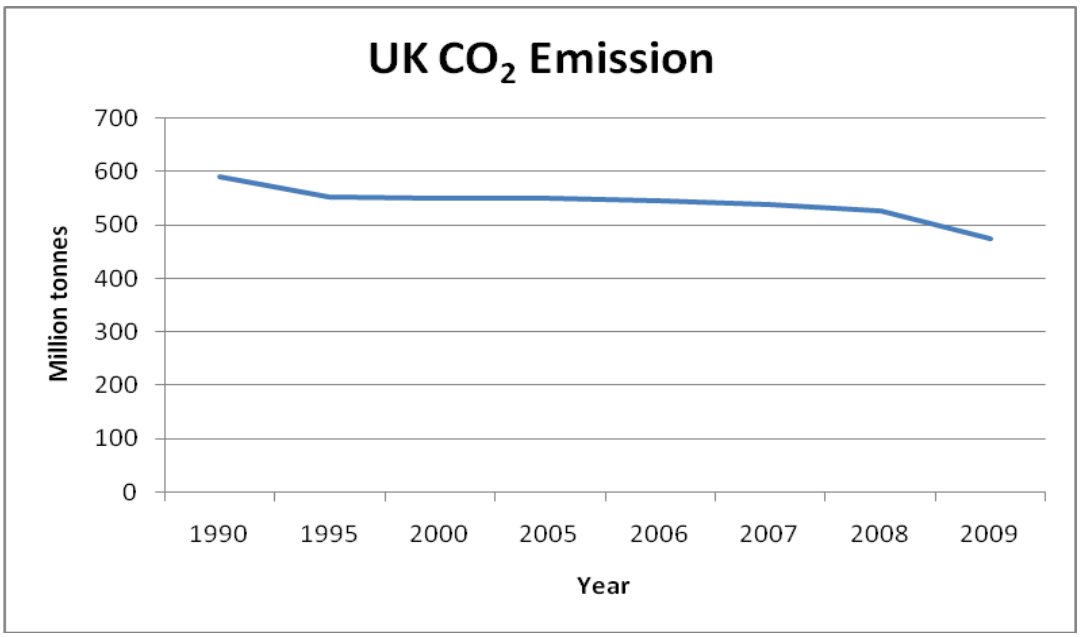

Figure 2.2.2 UK CO_2 emission from 1990 to 2009 (DECC 2011).

A detail breakdown of CO_2 for each main sector is shown in Table 2.2.2. The energy supply sector accounted for the highest amount of CO_2 emission which was 185 Mt or 39 percent, follow by road transport sector 113 Mt (24 percent), business sector 76 Mt (16 percent), residential sector 75 Mt (16 percent) and other sectors 25 Mt (5 percent). A comparison was carried out to compare the 1990 base level with the 2009 emission. A total of 116 Mt of CO_2 was reduced. Energy supply sector CO_2 emission decreased by 56 Mt, business sector by 34 Mt, residential sector by 4 Mt and other sectors by 25 Mt. Contrarily, the road transport sector saw an increase of almost 4 Mt of emission.

The aforementioned global economic crisis seems to have had a big impact on the UK where reduction of CO_2 emission is evident across all sectors since 2008. The drastic fall in energy supply may be due to the decrease in energy demand which cause the reduction of emission from power stations. Furthermore, it may be due to the increase used of nuclear power than coal and natural gas.

Table 2.2.2 CO_2 emission according to sector; million tonnes (Mt) (DECC 2011)

Year	1990	1995	2000	2005	2006	2007	2008	2009
Energy Supply	241	210	202	216	220	216	209	185
Road Transport	109	111	116	120	120	121	117	113
Business	110	104	104	94	91	89	87	76
Residential	79	81	87	84	82	78	80	75
Other	50	46	40	36	33	33	31	25
Total	**590**	**551**	**549**	**550**	**546**	**538**	**525**	**474**

2.2.2 UK Methane emission

Methane is the second largest GHG of UK emissions for the year 2009 which is about 8 percent. The main contributors to methane emission were the agriculture sector which accounted for 41 percent and landfill sites which accounted for 37 percent. Figure 2.2.3 shows UK methane emissions.

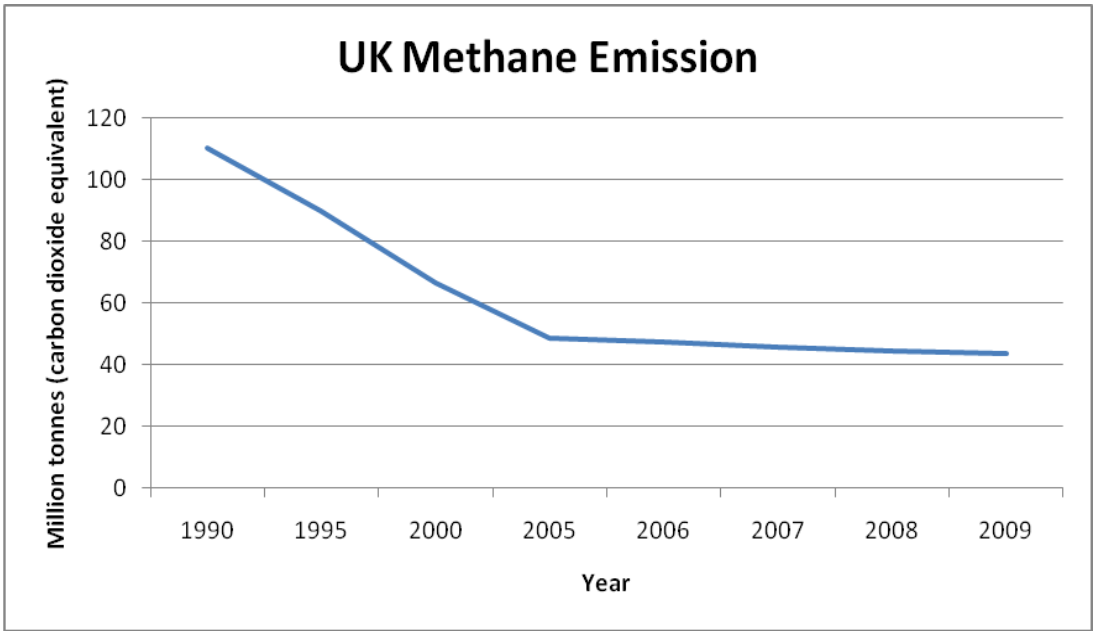

Figure 2.2.3 UK methane emission from 1990 to 2009 (DECC 2011)

When comparing methane emission between the base level of 1990 and 2009, a total reduction of 67 $MtCO_2e$ was achieved. A drastic reduction was found in landfill sector which was 72 percent and in the agriculture sector reduced by 19 percent. A drastic reduction was found from 1995 till 2005 this may be due to the implementation of the European Union (EU) Landfill Directive (DEFRA 2009). This directive changed the way waste was disposed of and helped to drive waste up the hierarchy through waste minimisation and increased levels of re-use, recycling and energy recovery. Table 2.2.3 shows the breakdown of methane emission by each sector.

Table 2.2.3 Methane emission according to sector; million tonnes of CO_2 equivalent ($MtCO_2e$) (DECC 2011)

Year	**1990**	**1995**	**2000**	**2005**	**2006**	**2007**	**2008**	**2009**
Agriculture	22.3	21.7	20.3	19.2	18.9	18.8	18.3	18
Landfill	56.1	43.6	29.3	17.8	17.4	16.9	16.4	15.9
Gas leakage	8.5	8.1	6.7	4.9	4.6	4.7	4.4	4.3
Coal mines	18.3	12.6	7	4.1	3.8	2.6	2.8	2.9
Other	5.2	4.2	3.3	2.6	2.5	2.7	2.6	2.5
Total	**110.4**	**90.1**	**66.7**	**48.6**	**47.2**	**45.7**	**44.5**	**43.6**

2.2.3 UK Nitrous oxide emission

Nitrous oxide is the third potential global warming GHG where it accounted for 6 percent of total of the UK GHGs emissions in 2009. A total of 33 $MtCO_2e$ reduction of nitrous oxide were found when comparing the 2009 emission with the 1990 base level. Figure 2.2.4 shows the emission of nitrous oxide in the UK from 1990 to 2009.

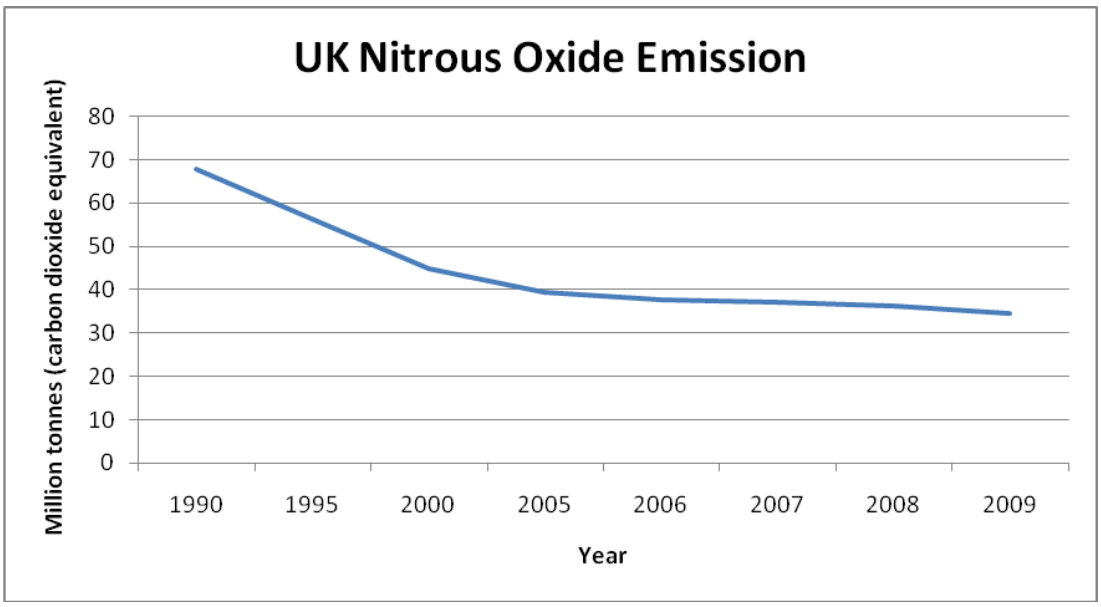

Figure 2.2.4 UK nitrous oxide emission from 1990 to 2009 (DECC 2011)

The main contributor of nitrous oxide was the agriculture sector which accounted for 79 percent of total emission in 2009. A drastic decrease was found in industrial processes between 1995 and 2000. This was due to the reduction in acid production with a total reduction of 9 $MtCO_2e$ of nitrous oxide. Table 2.2.4 shows the emission of nitrous oxide for each sector.

Table 2.2.4 Nitrous oxide emission according to sector; million tonnes of CO_2 equivalent ($MtCO_2e$) (DECC 2011).

Year	**1990**	**1995**	**2000**	**2005**	**2006**	**2007**	**2008**	**2009**
Agriculture	35.5	33.8	32.2	29.6	28.3	27.6	27.6	27.4
Industrial process	24.7	14.9	5.6	3	2.4	2.8	2.5	1.2
Road transport	1.2	1.7	1.6	1.3	1.3	1.2	1.1	1
Other	6.4	5.8	5.6	5.6	5.6	5.5	5.3	5
Total	**67.7**	**56.3**	**44.9**	**39.5**	**37.7**	**37.2**	**36.4**	**34.6**

2.3 Solar data collection

An accurate estimation of the amount of solar radiation reaching the surface of the earth is needed to study the effects of climate change as mentioned in the previous section. Measurements of diffuse and global solar radiation on horizontal surface are normally carried out by the national agency i.e. the national Meteorological Office. This section will discuss measurement instruments, instruments error and operational errors.

2.3.1 Measurement equipment

According to the European Solar Radiation Atlas (ESRA), solar radiation measurements can be broadly classified as ground-based measurements derived from geostationary satellites which measures the energy reflected by the system (earth/atmosphere) in different wavelength bands (ESRA 2000). Types of measuring equipment are as follows:

Pyranometer

This instrument measures global solar radiation. Figure 2.3.1 shows the structure of the CM11 Kipp and Zonen pyranometer. The pyranometer has a spectral response of between 335 and 2200 nm. A thermal detector in the sensing element responds to the total power absorbed from the solar radiation at any spectral distribution. The absorption of radiation on the black disk generates heat and the heat energy flows to the heat sink through a thermal resistance. The temperature difference across the thermal resistance of the disk is converted into a small voltage which can be detected by the logging system or computer. To avoid temperature fluctuation and reduce thermal radiation losses to the atmosphere, the pyranometer is built with a double glass envelope and silica gel crystal is used to prevent moisture within the pyranometer. Periodic cleaning of the glass dome is recommended as debris may be collected over time. The working principle of the pyranometer given here is as discussed by Muneer (Muneer 2004).

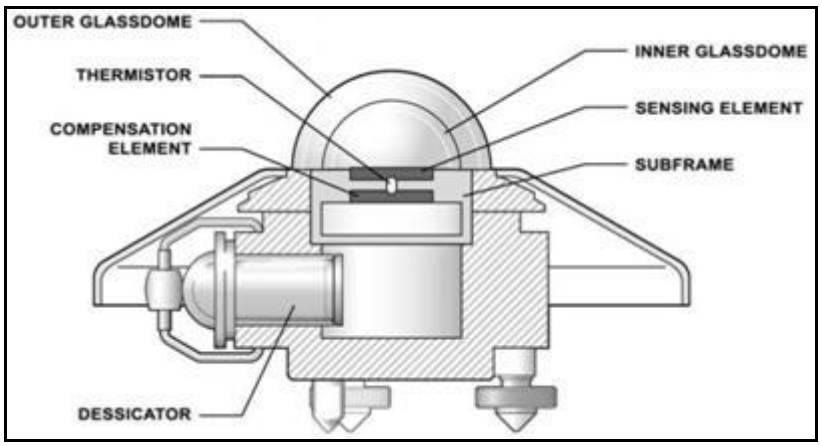

Figure 2.3.1 Kipp & Zonen CM11 pyranometer (Anon).

Pyranometer with shading device

This type of pyranometer measures the diffuse solar radiation. The shadow ring or disk shades the sun's direct beam from the pyranometer. Figure 2.3.2 shows a Kipp & Zonen CM11 pyranometer with shadow ring. The shadow ring needs to be adjusted according to the sun's declination angle. A more expensive approach has been designed to track the sun's declination, where the disk will move accordingly or synchronous with the sun's movement; hence it produces a more accurate estimation of diffuse radiation. Figure 2.3.3 shows the shade ring correction factors for the measurement of diffuse sky radiation.

Figure 2.3.2 Kipp & Zonen CM11 Pyranometer with shading device (Clima).

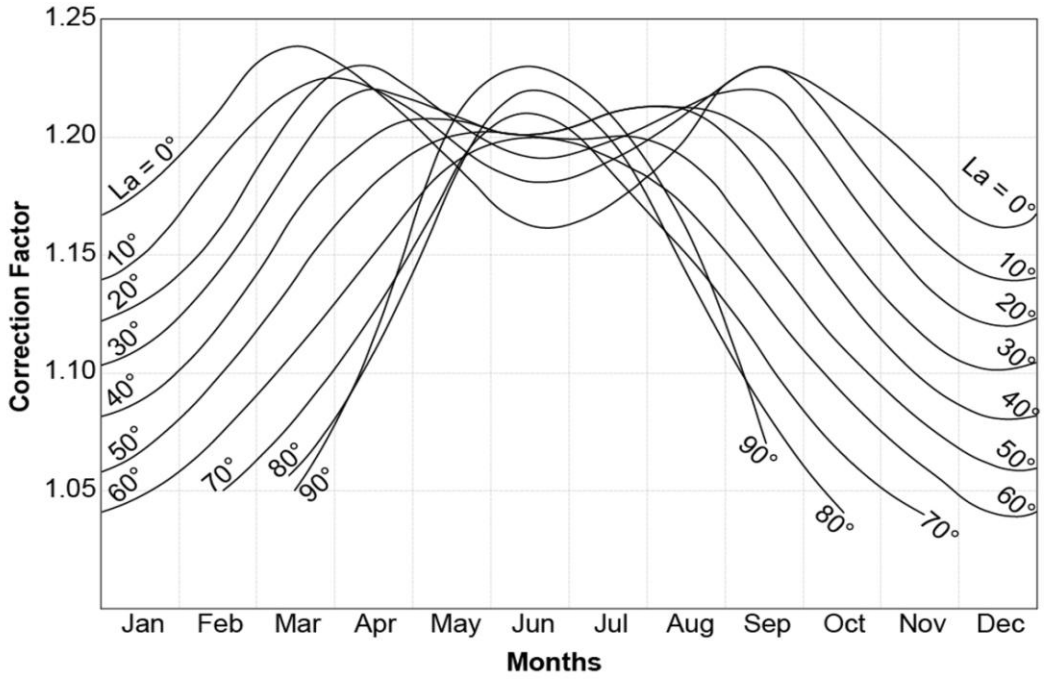

Figure 2.3.3 Shade ring correction factors for measured sky diffuse radiation. (Coulson 1975)

The World Meteorological Organization (WMO) classified pyranometer according to features such as stability, sensitivity etc. Classifications of pyranometer are divided into three classes, i.e. first-, second- and third class. The same features of classification apply to pyrheliometer where they are only divided into two classes, first- and second class as mentioned before. The WMO characteristics of operational pyranometers are shown in Table 2.3.1.

Table 2.3.1 WMO Characteristic of operational pyranometer. (WMO 2006)

Characteristic	**High quality[1]**	**Good quality[2]**	**Moderate quality[3]**
Response time (95 per cent response)	< 15s	< 30s	< 60s
Zero offset:			
(a) Response to 200 W/m^2 net thermal radiation (ventilated)	7 W/m^2	15 W/m^2	30 W/m^2
(b) Response to 5 K/h change in ambient temperature	2 W/m^2	4 W/m^2	8 W/m^2
Resolution (smallest detectable change)	1 W/m^2	5 W/m^2	10 W/m^2
Stability (change per year, percentage of full scale)	0.8	1.5	3
Directional response for beam radiation (the range of errors caused by assuming that the normal incidence responsivity is valid for all directions when measuring, from any direction, a beam radiation whose normal incidence irradiance is 1 000 W/m^2)	10 W/m^2	20 W/m^2	30 W/m^2
Temperature response (percentage maximum error due to any change of ambient temperature within an interval of 50K)	2	4	8
Non-linearity (percentage deviation from the responsivity at 500 W/m^2 due to any change of irradiance within the range 100 to 1 000 W/m^2)	0.5	1	3
Spectral sensitivity (percentage deviation of the product of spectral absorptance and spectral transmittance from the corresponding mean within the range 0.3 to 3 µm)	2	5	10
Tilt response (percentage deviation from the responsivity at 0° tilt (horizontal) due to change in tilt from 0° to 90° at 1 000 W/m^2 irradiance)	0.5	2	5
Achievable uncertainty, 95 per cent confidence level:			
Hourly totals	3%	8%	20%
Daily totals	2%	5%	10%

Note:

(1) Near state-of-the-art, suitable for use as a working standard; maintainable only at stations with special facilities and staff.

(2) Acceptable for network operations.

(3) Suitable for low-cost networks where moderate to low performance is acceptable.

Pyrheliometer

A pyrheliometer is used to measure beam (direct) radiation at normal incidence. Figure 2.3.4 shows a DN5 pyrheliometer used in an active tracking system. The long barrel of the pyrheliometer may be seen below the glass dome of the pyranometer in this picture. This equipment is equipped with a sun tracking system to enable it to measure direct radiation as the sun moves. Inside the pyrheliometer there is a collimator with an optimum aperture of 6° which can

completely include the sun's disc. A multi junction thermopile which converts the heat from the sun's radiation to an electrical signal is used so that the data can be read and recorded by data logger. To obtain the equivalent radiant energy flux (W/m^2) a calibration factor is applied. Other types of pyrheliometer are shown in Figure 2.3.5 and 2.3.6. Table 2.3.2 shows the characteristics of operational pyrheliometers.

Figure 2.3.4 Middleton Solar-DN5 pyrheliometer (in active solar tracking system) (Anon)

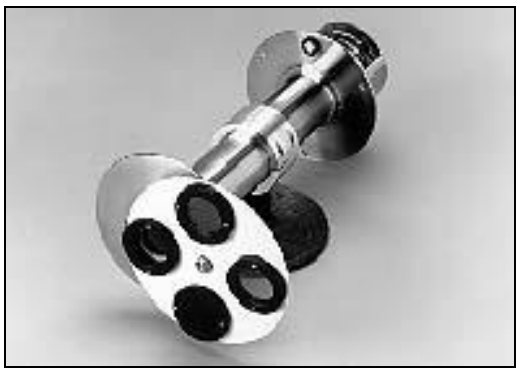

Figure 2.3.5 Eppley Normal Incidence Pyrheliometer (EPLAP).

Figure 2.3.6 The EKO-Instrument's Sky scanner MS-321LR (Instruments 2004)

The direct equipment cost of a pyrheliometer is approximately six times that a shaded pryranometer (Muneer 2004). Since the measurement cost of direct normal radiation is high, a simple relationship relating horizontal of global (I_G), diffuse (I_D) and beam (I_B) radiation may be used to estimate the latter component. That equation is:

$$I_G = I_D + I_B \sin SOLALT \tag{2.3.1}$$

where *SOLALT* is the solar altitude.

According to Perez et. al. (Perez, Ineichen and Seals 1990) and Gueymard (Gueymard 2003a), the present state of solar radiation and daylight model is such that they are approaching the accuracy limits set out by the measuring equipment. Hence, modelling procedures are now used to cross-check measurement data.

Table 2.3.2 WMO characteristic of operational pyrheliometers (WMO 2006).

Characteristic	High quality[1]	Good quality[2]
Response time (95 per cent response)	<15s	<30s
Zero offset (response to 5 K/h change in ambient temperature)	2 W/m^2	4 W/m^2
Resolution (smallest detectable change in W/m^2)	0.5	1
Stability (percentage of full scale, change/year)	1	0.5
Temperature response (percentage maximum error due to change of ambient temperature within an interval of 50 K)	1	2
Non -linearity (percentage deviation from the responsivity at 500 W/m^2 due to the change of irradiance within 100 W/m^2 to 1 100 W/m^2)	0.2	0.5
Spectral sensitivity (percentage deviation of the product of spectral absorptance and spectral transmittance from the mean within the range 0.3 to 3 µm)corresponding	0.5	1
Tilt response (percentage deviation from the responsivity at 0° tilt (horizontal) due to change in tilt from 0° to 90° at 1 000 W/m^2 irradiance)	0.2	0.5
Achievable uncertainty, 95 per cent confidence level (see above)		
1 minute totals,		
per cent	0.9	1.8
kJ/m^2	0.56	1
1 hour totals,		
per cent	0.7	1.5
kJ/m^2	21	54
daily totals,		
per cent	0.5	1
kJ/m^2	200	400

Notes:

(1) Near state-of-the-art, suitable for use as a working standard; maintainable only at stations with special facilities and staff.

(2) Acceptable for network operations

Pyrgeometer

A Pyrgeometer is used to measure long wave radiation which falls within the infrared radiation spectrum (4.5µm to 100µm). It consists of a thermopile with a 200nm to 100µm radiation band sensitivity, a dome mirror with solar blind filter coating which eliminates shortwave radiation, a temperature sensor which measures the body temperature of the instrument and a sun shield to reduce heat from radiation. Figure 2.3.7 shows an EKO MS-202 pyrgeometer.

Figure 2.3.7 EKO M-S202 pyrgeometer (Instruments 2005)

Albedometer

The term ‘ground albedo’ or simply ‘albedo’ is often used interchangeably with ‘ground reflectance’. On the other hand, as Monteith (Monteith 1959) has pointed out, the term ‘albedo’ or ‘whiteness’ refers to the reflection coefficient in the visible range of the spectrum, whereas ‘reflectance’ denotes the reflected fraction of short-wave energy. The importance of knowing the albedo for the determination of radiation balance of macro- and microclimates is well known. A good estimate of albedo of the surrounding terrain is a prerequisite for representative calculations related to the energy balance of vegetation, amount of potential transpiration, energy interception of walls, windows, roofs and solar energy collectors. Therefore the small- and large-scale variation of albedo is of interest. The variation in albedo is spatial and temporal owing to the changing landscapes of the earth and due to the seasonal presence of snow and to some extent moisture deposition.

As the name of the instrument suggests, it measures the reflected radiation as well as the global radiation. Figure 2.3.8 shows an albedometer. Generally albedometer is constructed with two pyranometers. One is facing upwards to measure incident global radiation and the other facing downward to measure the ground-reflected radiation. Both pyranometers provide output individually. Albedo can be calculated from the output data of the two pyranometers. To obtain the albedo value, the equation below may be used:

$$Albedo = \frac{reflected \quad radiation}{global \quad radiation} \tag{2.3.2}$$

Figure 2.3.8 Kipp & Zonen CMA 6 Albedometer (Envco 2009)

Sunshine Recorder

According to the WMO definition of sunshine duration is,

'*sunshine duration during a given period is defined as the sum of that sub-period for which the direct solar irradiance exceeds 120 W/m^2*.' (WMO 2003)

In many countries, diurnal duration of bright sunshine is measured at a wide number of places. For over a century these data have been measured using the well-known Campbell-Stokes sunshine recorder as shown in Figure 2.3.9, which uses a solid glass spherical lens to burn a trace of the sun on a treated paper, the trace being produced whenever the beam irradiation is supposedly above the above-mentioned critical level. Although the critical threshold varies loosely with the prevailing ambient conditions, the sunshine recorder is an economic and robust device and hence used widely.

The limitations of the Campbell–Stokes sunshine recorder are well known and have been discussed in *Observers' Handbook* (1969), Painter (Painter 1981) and Rawlins (Rawlins 1984). Some of the associated limitations with this device are that the recorder does not register a burn on the card below a certain level of incident radiation (about 150–300 W/m^2). On a clear day with a cloudless sky the burn does not start until 15–30 minutes after sunrise and usually ceases about the same period before sunset. This period varies with the season. On the other hand under periods of intermittent bright sunshine the burn spreads. The diameter of the sun's image formed by the spherical lens is only about 0.7 mm, however, a few seconds' exposure to bright sunshine may produce a burnt width of about 2 mm. As such, intermittent sunshine may be indistinguishable from a longer period of continuous sunshine. In the past a more sophisticated photoelectric sunshine recorder called the Foster sunshine switch (N.B. Foster 1953) has been used by the US Weather Service. This device incorporates two photovoltaic cells, one shaded and the other exposed to solar beam. Incident beam irradiation above a given threshold produces a differential output from the above two cells, the diurnal duration of which determines the hours of bright sunshine.

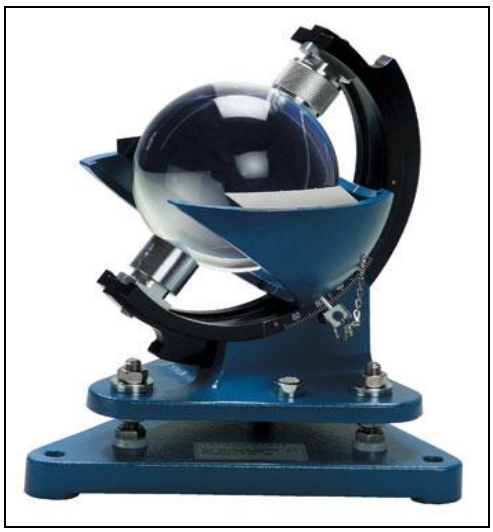

Figure 2.3.9 240-1070-L Campbell-Stokes Pattern Sunshine Recorder (NovaLynx 2011).

2.3.2 Uncertainties and errors

2.3.2.1 Instrument error and uncertainties

Errors are unavoidable in measurement e.g. random and equipment error. Angus (Angus 1995) has provided an account for the measurement errors associated with solar radiation and illuminance measurement. Furthermore, some common errors do occur such as lack of maintenance either of instruments or data recording equipment calibration error and sometime unsuitable equipment (ESRA 2000). The most general type of error associated with the sensors and equipments are as follow:

1. Cosine response
2. Azimuth response
3. Temperature response
4. Spectral selectivity
5. Non-linearity
6. Thermal instability
7. Stability
8. Zero offset due to nocturnal radiative cooling

Of all the errors, the cosine error is the most apparent and widely recognised. This error occurs when the sensor responds to the angle at which the radiation strikes the sensing area. The error becomes greater when the angle of the sun becomes more acute i.e. at sunrise and sunset (at latitude angle of the sun below 6°). To avoid this error, recorded data at sunrise and sunset have to be excluded.

The imperfection of the glass dome causes the azimuth error. This is an inherent manufacturing error which yields a similar percentage error as the cosine effect as mentioned above. As for the azimuth error, the temperature response is an individual fault for each cell. The percentage errors due to fluctuations in the sensor's temperature are reduced because the photometers are thermostatically controlled. However, some pyranometers have a less elaborate temperature control system like the CM11 pyranometer. This

pyranometer relies on the two glass dome to prevent large temperature swing. To avoid this, ventilation of the instruments is recommended.

Spectral absorbance of the black paint and the spectral transmission of the glass is the spectral selectivity dependant of a pyranometer. Only small percentage errors of measurements are contributed to by this effect. Each sensor processes a high level of stability with the deterioration of the cell resulting in approximately ±1% change in the full scale measurement per year. A Pyranometer with all black receivers is barely in thermal equilibrium outdoors, hence, thermal energy exchange between the absorbing sensor, dome and sky, results in a net thermal offset in the thermopile voltage signal where this offset is site dependent (Myers 2005).

2.3.2.2 Measurement uncertainties

An accuracy of 2-3% for daily summation were estimated by Drummond (Drummond 1956) with a first class pyranometer. But for hourly summation, it is in excess of 5% even with carefully calibrated equipment (Muneer and Fairooz 2002). Halthore (Halthore 1999) reported that the uncertainties in measurement of diffuse irradiance is ±5 W/m^2 at a 75% confidence limit and ±8 W/m^2 at 95% confidence limit. Furthermore, Myers reported that possible range of measurement errors of uncertainties for pyranometer is between +25 to -100 W/m^2 and ±25 W/m^2 for pyrheliometer measurement under clear sky condition.

2.3.2.3 Operational Errors

Operational errors are self-explanatory as listed below:

i. Complete or partial shade-ring misalignment.
ii. Dust, snow, dew, water droplets, birds dropping, etc.
iii. Shading caused by building structures
iv. Station shut down
v. Incorrect sensor levelling
vi. Electric fields in the vicinity of cables
vii. Improper application of diffuse shade ring correction
viii. Inaccurate programming of calibration constant

ix. Mechanical loading on cables

x. Orientation and/or improper screening of the vertical sensors from ground-reflected radiation.

To avoid the above noted operational errors, operators have to take extra care to ensure that all instruments are in good condition with periodic preventive maintenance scheduled.

2.4 Quality control procedures of solar data

Data quality assessment is a process or procedure to avoid spurious data to be included in the data set. Gueymard and Kembezidis pointed out that even though a data set has passed the quality assessment process or procedure, the data must be examined for its uncertainty that has been transferred from a measuring sensor to the actual measurement (Geuymard and Kambezidis 2004). In this section, a summary of a few assessment methods which have been published in journals and trusted website will be discussed.

United State National Renewable Energy Laboratory (NREL)-1993(NREL 1993)

The US NREL developed a quality assessment procedure which was named SERI QC. This procedure will assess the three radiation data elements namely global horizontal, diffuse horizontal and direct normal. A summary of the key features are discussed as follow:

- At the beginning, SERI QC will perform one element test by defining a range of acceptable values of K_t,K_d or K_n between minimum and maximum depending on the element that is being tested based on air mass regimes and month of the year. Where:

K_t = Clearness index or global horizontal transmittance

= Global horizontal radiation / extraterrestrial horizontal radiation

K_d = Diffuse horizontal transmittance

= Diffuse horizontal radiation / extraterrestrial horizontal radiation

K_n = Direct normal transmittance

= Direct normal radiation / extraterrestrial direct normal radiation.

- If the zenith angle is less than or equal to 80° and with all three elements present then SERI QC will perform a three-element test. A range of acceptable values will be define so that the equation $K_t = K_d + K_n$ is satisfied within the arbitrary error limit of ± 0.03 which accounts for the measurement uncertainties.
- If the data pass the three element test or two elements pass the one element test, SERI QC will perform a two element test by defining a range of acceptable values within the boundaries empirically to determine three different air mass regimes for each month using collected data from the site.
- Flags are assigned to the data after the test. The flagging system of SERI QC permits the assignment of uncertainties which depend on the nature of the test performed (one, two or three elements) and the distance by which the data point exceed the expected limit.

For up to date information regarding about the procedure, please referred to the following website: http://rredc.nrel.gov/solar/pubs/seri_qc/

Commision Internationale de l'éclairage (CIE) automatic quality control (Kendrick 1994)

A brief summary of the five tests in CIE quality control for radiation and illuminance is presented here.

1. A rough boundary limit for global and diffuse irradiance and direct irradiance is set to be less than the extraterrestrial irradiance.
2. To ensure consistency, it utilises the redundancy between three solar radiation components or the diffuse component such as to be less than

the global component plus a 10% allowance for shade ring correction where the beam component is not measured.

3. Each aspect of the global irradiance and illuminance is tested i.e. north, east, south and west.
4. Inter-comparisons tests between irradiance and illuminance.
5. Tests to compare the zenith luminance with either diffuse irradiance or illuminance.

Note that CIE noted that automatic testing should not be performed when global irradiance is below 20 W/m^2 and solar elevation is less than 4°.

Page model

The Page model is based on the work undertaken for the production of the European Solar Radiation Atlas (ESRA) and the Charted Institution of Building Services Engineers (CIBSE) Guide on weather and solar data (Page 1997; ESRA 2000). Page sets out the following steps to control all daily totals of solar radiation data:

- Values for global solar radiation have to be less than the extraterrestrial radiation and sunshine values have to be less than or equal to corresponding astronomical values.
- Solar radiation values have to be lie within the range of the expected clear-sky extreme values by considering the influence of the atmospheric layer.
- Basic relationship between different radiation components should be fulfilled.
- Values of solar radiation parameters have to be in a specific range compared to nearby station's values with allowance for spatial variability.
- The variation of relative terms of the Ångstrőm regression should lie within a definite range.

Muneer and Fairooz quality control procedure(Muneer and Fairooz 2002)

This quality control procedure consists of four levels of tests which emphasize on the global and diffuse radiation. The procedure was developed based on CIE recommendation for first level test and the Page irradiance model for fourth level test. Those levels of tests are summarised as follow:

1. Adopted from CIE quality control;
   $0<G<1.2\ E_n$
   $0<D<0.8\ E_n$
   E_n is the normal incidence extraterrestrial irradiance, G is the global irradiance and D is the diffuse irradiance
2. Consistency test between diffuse and global irradiation and between global and horizontal extraterrestrial irradiation.
3. Test based on an expected diffuse ratio-clearness index envelop. This check is to make sure that the diffuse irradiation data conforms to the limit set out by the envelope of acceptance.
4. Check on the quality of diffuse irradiance is performed by comparing its value with the diffuse irradiance under two extreme conditions as defined by Page.

A further test is carried out on the diffuse and global irradiance by investigating the Linke turbidity values e.g. when the Linke turbidity value is less than 2.5 or greater than 12, a close inspection of the corresponding data is required.

Refering to the graphical procedure as mentioned in test level three above, Younes et. al.(Younes, Claywell and Muneer 2005) proposed a new standard deviation procedure to produce an envelope of acceptance. This procedure basically categorises diffuse ratio-clearness index in band of k_t. For any given band of k_t, outliers are identified as data points lying outside the envelope which is defined by $\bar{k} \pm 2\sigma_k$ boundaries.

2.5 Statistical evaluation techniques

Slope of the best-fit line, s

The slope of the best-fit line, given by Eq. (2.5.1), between the computed and measured variable is desired to be as close as possible to unity. Slope values exceeding one indicate overestimation, while slope values under one indicate underestimation of the computed variable,

$$s = \frac{\sum \left(Y_m - \bar{Y}_m\right)\left(Y_c - \bar{Y}_c\right)}{\sum \left(Y_m - \bar{Y}_m\right)^2} \tag{2.5.1}$$

Note that Y_c is the calculated value of the dependent variable and Y_m is the measured or observed value, and $\bar{Y}_m$ is the mean value of the measured variable.

Coefficient of determination, r^2

The coefficient of determination (r^2) is the ratio of explained variation to the total variation. r^2 lies between zero and one.

$$r^2 = \left[\frac{\sum \left(Y_m - \bar{Y}_m\right)\left(Y_c - \bar{Y}_c\right)}{\sqrt{\sum \left(Y_m - \bar{Y}_m\right)^2 \sum \left(Y_c - \bar{Y}_c\right)^2}} \right]^2 \tag{2.5.2}$$

A high value of r^2, indicating a lower unexplained variation, is desirable. r^2 is often used to judge the adequacy of a regression model, but it should not be the sole criterion for choosing a particular model. In the present context r^2 provides an indication of the order of scatter between Y_c and Y_m. Further information may be obtained in Montgomery and Peck (Montgomery and Peck 1992) and Draper and Smith (Draper and Smith 1998).

Root mean squared error, RMSE

The root mean squared error (RMSE) gives a value of the level of scatter that the model produces. This is an important statistical test as it highlights the readability and repeatability of the model. It provides a term-by-term comparison

of the actual deviation between the predicted and the measured values. Since it is a measure of the absolute deviation, RMSE is always positive. A lower absolute value of RMSE indicates a better model. Mathematically, it is given by the following equation:

$$RMSE = \sqrt{\sum\left[\frac{(Y_c - Y_m)^2}{n}\right]} \tag{2.5.3}$$

Mean bias error, MBE

The mean bias error (MBE) provides an indication of the trend of the model, whether it has a tendency to under-predict or over-predict the modelled values. MBE can be expressed either as a percentage or as an absolute value. Nevertheless, within a data set an overestimation of one observation can cancel an underestimation of another. A MBE nearest to zero is desired. It is given by the following equation:

$$MBE = \frac{\sum(Y_c - Y_m)}{n} \tag{2.5.4}$$

Mean of absolute deviations, MAD

Another metric that is often employed in such analysis is the mean of absolute deviations, MAD and is given by,

$$MAD = \frac{\sum|Y_c - Y_m|}{n} \tag{2.5.5}$$

Unlike MBE, the MAD metric provides an insight into the scatter between Y_c and Y_m. Note that the MAD is similar to RMSE and provides a measure of absolute deviations.

Non-dimensional MBE, MAD and RMSE

The above formulae provide MBE, MAD and RMSE, which have the same physical units as the dependent variable, Y. In some instances non-dimensional MBE (NDMBE), MAD (NDMAD) and RMSE (NDRMSE) are required. These are obtained as follows,

$$NDMBE = \frac{\sum\left[\frac{(Y_c - Y_m)}{Y_m}\right]}{n} \tag{2.5.6}$$

$$NDMAD = \frac{\sum\left|\left[\frac{(Y_c - Y_m)}{Y_m}\right]\right|}{n} \tag{2.5.7}$$

$$NDRMSE = \sqrt{\frac{\sum\left[\frac{(Y_c - Y_m)}{Y_m}\right]^2}{n}} \tag{2.5.8}$$

2.6 The need for computer-generated solar radiation data

Measuring and recording solar irradiation are an expensive affair. Due to the high cost including of well trained personnel, there are not many stations that measure solar irradiation. Horizontal hourly and sub-hourly diffuse and beam irradiance are required by engineers for the estimation of global irradiance. For stations which do not record all these parameters, or for sites which simply do not record any solar irradiation information, a simple but reasonably accurate method is required to estimate solar irradiance. This will help designers and engineers to design buildings and energy applications.

2.7 Review of solar radiation models

In this section, solar radiation models that were widely used and tested in the UK will be discussed. These models are Page Radiation Model, Yang Model and Meteorological Radiation Model.

2.7.1 Page Radiation Model (PRM)

The Page Radiation Model (PRM) evolved from the development of the European Solar Radiation Atlas (ESRA) (ESRA 2000).

Clear-sky radiation model

This cloudless sky model predicts the irradiation on horizontal surfaces as a function of solar altitude and air mass 2 Linke turbidity factors, after incorporating the standard corrections to mean solar distance. The cloudless sky, direct-beam and diffuse irradiance on the horizontal surface are separately estimated and global irradiance is obtained by summing up the aforementioned components. This model was originally developed by Page and Lebens (Page and Lubens 1986).

Estimation of direct-beam irradiation

As above, the solar beam normal depends on solar altitude and the Linke turbidity factor. The sun-earth distance varies slightly around the year due to the orbit of the sun which is slightly eccentric. Hence this influences the extraterrestrial irradiation. The correction factor use within ESRA to allow varying of solar distance K_d is expressed as follow:

$$K_d = 1.0 + 0.03344\cos(J' - 280) \quad (2.7.1.1)$$

where J' is the day angle, which is the day number divided by 365.25.

The beam irradiation to normal surface is calculated as follow:

$$I_{Bn} = I_E K_d \exp[-m \times 0.8662 T_{LK} \delta_r(m)] \quad (2.7.1.2)$$

Where *m* is the optical air mass corrected for station pressure, T_{LK} is the air mass Linke turbidity factor and δ_r is the Rayleigh optical depth at air mass *m*. Equation to calculate beam irradiation on horizontal surface is as followed:

$$I_{Bc} = I_{Bn} \sin SOLALT \quad (2.7.1.3)$$

where *SOLALT* is solar altitude and I_{Bn} is the normal beam irradiation. Besides air mass 2 Linke turbidity factor the model uses some other inputs which are vapour pressure, atmospheric pressure and present weather code.

Estimation of clear-sky diffuse irradiation

The diffuse irradiation increases as the sky become more turbid and the beam irradiation decreases. This model depends on two factors which are solar altitude and air mass 2 Linke turbidity factor. There are two stages in this model. First, the diffuse transmittance $Trd(n)$ value for day *n* is established which is the theoretical diffuse irradiation on horizontal surface where the sun is vertically overhead for the selected air mass 2 Linke turbidity factor. The second order polynomial expression is used:

$$Trd(n) = -21.657 + 41.752T_{LK} + 0.51905(T_{LK})^2 \quad (2.7.1.4)$$

Later, the evaluation of solar elevation function, *F(SOLALT)* by using the following equation:

$$F(SOLALT) = C(0) + C(1)\sin SOLALT + C(2)\sin^2 SOLALT \quad (2.7.1.5)$$

The following expressions are used to find *C(0), C(1)* and *C(2)* which are only dependant on air mass 2 Linke turbidity factor:

$$C(0) = 0.26463 - 0.061581T_{LK} + 0.0031408(T_{LK})^2 \quad (2.7.1.6a)$$

If $Trd(n) \times C(0) < 3W/m^2$ then $C(0) = 3/Trd(n)$ (2.7.1.6b)

$$C(1) = 2.0402 + 0.018945T_{LK} - 0.011161(T_{LK})^2 \quad (2.7.1.6c)$$

$$C(2) = -1.3025 + 0.039231T_{LK} + 0.0085079(T_{LK})^2 \quad (2.7.1.6d)$$

The cloudless sky diffuse irradiation is as follow:

$$I_{Dc} = K_d \times Trd(n) \times F(SOLALT) \quad (2.7.1.7)$$

Hence the global irradiation under clear-sky conditions is obtained as follow:

$$I_{Gc} = I_{Dc} + I_{Bc} \tag{2.7.1.8}$$

2.7.2 Yang model

Yang clear-sky model

Yang *et. al.* (Yang, Huang and Tamai 2001; Yang, Koike and Ye 2006) developed a broadband radiative transfer model by simplifying Leckner's spectral model (Leckner 1978). The radiative transmittances which are taken into account in this model are Rayleigh scattering (τ_r), ozone absorption (τ_o), gas absorption (τ_g), water vapour absorption (τ_w), and aerosol extinction (τ_a). Formulae for these quantities rely on values for the Ångström turbidity coefficient (β), precipitable water vapour (ω) and thickness of the ozone layer (u_o). Total beam and diffuse transmittances (τ_B and τ_D respectively) are calculated as shown in Eqs. 2.7.2.1 and 2.7.2.2.

$$\tau_B = \tau_r * \tau_o * \tau_g * \tau_w * \tau_a - 0.013 \tag{2.7.2.1}$$

$$\tau_D = \tau_o * \tau_g * \tau_w (1 - \tau_r * \tau_a) + 0.013 \tag{2.7.2.2}$$

where:

$$\tau_r = \exp\left[-0.008735m'(0.5475 + 0.0142m' - 0.0003834m'^2 + 0.00000459m'^3)^{-4.08}\right]$$

$$\tau_o = \exp\left[-0.0365(m\mu_o)^{0.7136}\right]$$

$$\tau_o = \exp\left[-0.0117m'^{0.3139}\right]$$

$$\tau_w = \min\left[1.0,\ \ 0.909 - 0.036\ln(mw)\right]$$

$$\tau_a = \exp\left\{-m\beta\left[0.6777 + 0.1464m\beta - 0.00626(m\beta)^2\right]^{-1.3}\right\}$$

The formulation to obtain β and μ_o as reported by Yang et. al. (Yang, Huang and Tamai 2001)

$$\beta = \overline{\beta} + \Delta\beta$$

$$\overline{\beta} = (0.025 + 0.1\cos LAT)\exp(-0.7z/1000) \text{ and } \Delta\beta = \pm(0.02 \sim 0.06)$$

z is the station height in meter above sea level.

$$\mu_o = 0.44 - 0.16\left\{\left[(LAT - 80)/60\right]^2 + \left[(d - 120)/(263 - LAT)\right]^2\right\}^{0.5}$$

$$d = DN \text{ for } DN < 300$$

else: $d = DN - 366$

The horizontal beam and diffuse irradiance are then obtained by multiplication of their respective transmittances with instantaneous extraterrestrial irradiance, I_E.

$$I_{Dc} = I_E \times \tau_D \quad (2.7.2.3)$$

$$I_{Bc} = I_E \times \tau_B \quad (2.7.2.4)$$

Total global irradiance under clear sky conditions is then calculated as:

$$I_{Gc} = I_{Dc} + I_{Bc} \quad (2.7.2.5)$$

Yang all-sky model

Yang *et al* (Yang 2006) further developed the model for all sky conditions and tested it against global data sets. The cloud extinction transmittance is the ratio of surface- to clear-sky radiation as shown below;

$$\tau_C = I_G / I_{Gc} \quad (2.7.2.6)$$

All other radiative transmittances have been included in Eqs. (2.7.2.1) and (2.7.2.2); hence it is assumed that the radiation extinction in cloud layer is a function of sunshine duration (Ångström 1924). The estimation of the cloud transmittance for hourly, daily and monthly mean daily radiation may be obtained from the following equations respectively.

For hourly radiation,

$$\tau_C = 0.4435 + 0.3976\frac{h}{H} + 0.1589\left[\frac{h}{H}\right]^2, \text{ if } h>0 \qquad (2.7.2.7a)$$

τ_c = 0.2560 if h=0

For daily radiation,

$$\tau_C = 0.2505 + 1.1468\frac{h}{H} - 0.3974\left[\frac{h}{H}\right]^2 \qquad (2.7.2.7b)$$

For monthly mean daily radiation,

$$\tau_C = 0.2777 + 0.8636\frac{h}{H} - 0.1413\left[\frac{h}{H}\right]^2 \qquad (2.7.2.7c)$$

where h is the actual sunshine duration and H the maximum possible sunshine duration. Eqs (2.7.2.7a) to (2.7.2.7c) are constrained by the condition that τ_c = 1 if $\frac{h}{H}$=1. Once τ_c is obtained, I_G is then calculated via Eq (2.7.2.6). Note that the quantity $\frac{h}{H}$ in Eqs (2.7.2.7a) to (2.7.2.7c) is the sunshine fraction (SF) for a certain time period i.e. hourly, daily or monthly.

2.7.3 Meteorological radiation model

Generally the Meteorological radiation model (MRM) theories may be traced back to the work of Chandrasekhar and Elbert (Chandrasekhar and Elbert 1954), Sakera (Sakera 1956), Coulson (Coulson 1959), Dave (Dave 1964) and Kambezidis et. al. (Kambezidis, Psiloglou and Synodinou 1997). Kambezidis and Papanikolaou (Kambezidis and Papanikolaou 1989), presented the complete set of sub-models and an improved version was then presented by Muneer and Gul (Muneer and Gul 1998).

The MRM only used ground-based meteorological data which can be easily available from local meteorological station or offices and on websites. Those data are atmospheric pressure, relative humidity or wet bulb temperature, sunshine duration and air temperature or dry bulb temperature. From these data, MRM estimates horizontal global, beam and diffuse irradiance.

The MRM can provide high accuracy during clear-sky condition but worst during overcast condition. At low solar altitude, the model provides an unreasonably high value. Note that, readers could avoid this by incorporating in the model an exclusion of the estimation of solar irradiance at solar altitude of less than 7°. This method was found to be effective in dealing with broadband and spectral irradiance estimation.

MRM for clear-sky

MRM clear-sky diffuse model was based on the work of Dave (Dave 1979), Bird and Hulstrom (Bird and Hulstrom 1979) and Pisimanis et. al. (Pisimanis, Notaridou and Lalas 1987). The equations for the model are as follow:

$$I_D = I_E \tau_{\alpha\alpha} \tau_g \tau_o \tau_w \left[\frac{0.5(1-\tau_r)}{1-m+m^{1.02}} + \frac{0.84(1-\tau_{\alpha s})}{1-m+m^{1.02}} \right] \quad (2.7.3.1)$$

$$\tau_{\alpha\alpha} = 1 - 0.1(1-\tau_\alpha)(1-m+m^{1.06}) \quad (2.7.3.2)$$

$$\tau_{\alpha s} = 10^{-0.045^{m'0.7}} \quad (2.7.3.3)$$

Global horizontal irradiance I_G is given as:

$$I_G = (I_B + I_D)\left[\frac{1}{1 - r_s r_\alpha^{'}}\right] \quad (2.7.3.4)$$

Where r_s is the ground albedo (0.2 is always used) and $r_\alpha^{'}$ = 0.0685+0.17(1- r_α) is the albedo of cloudless sky. τ_α is the Rayleigh scattering transmittance computed at *m*=1.66.

MRM for overcast sky

For overcast sky, MRM estimates the global irradiation, I_G same as diffuse irradiation, I_D hence, Eq. (2.7.3.1) may be used. Overcast sky is the most difficult to model due to the sky condition because it is difficult to differentiate between dense and dark cloud with thin cloud. These two types of clouds registered no sunshine duration. Further, irradiation may be widely different.

MRM for non-overcast sky

The MRM is based on regressions between the ratio of hourly diffuse horizontal irradiation (I_D) to beam horizontal irradiation (I_B) and beam clearness index. Note that the above two quantities are herein referred as DBR = I_D / I_B and $K_B = I_B / I_E$. Muneer et. al. (Muneer, Gul, Kambezedis et al. 1996; Muneer, Gul and Kambezedis 1998; Muneer and Gul 2000) have expressed the relationship between the above two dimensionless variables in the form of a power function;

$$\text{DBR} = a(K_B)^b \quad (2.7.3.5)$$

They validated the MRM using data from the UK and Japan; the coefficients to be used in Eq. (2.7.3.5) for the UK are *a*= 0.285 and *b*= -1.00648.

The calculated beam horizontal-irradiation (I_B) is a function of the extraterrestrial horizontal-irradiation attenuated by the SF and atmospheric transmittances, thus

$$I_B = I_E * SF * \tau_r \tau_o \tau_g \tau_w \tau_\alpha \quad (2.7.3.6)$$

Once I_B is calculated, I_D is then calculated via Eq (2.7.3.5). The calculated beam and diffuse horizontal-irradiation is then summed to obtain the calculated global horizontal irradiation (I_G).

For more in-depth discussion reference is made to Muneer book section 3.3.4 (Muneer 2004)

2.8 Photovoltaic (PV)

The name photovoltaic (PV) comes from the process of converting light (photons) to electricity (voltage). This process is known as the PV effect. Generally there are three generations of PV cells.

First generation is the traditional solar cells made from silicon. There are two types of solar cells in this generation namely mono-crystalline and poly-crystalline. The main difference between these two types of cells is its manufacturing process. Mono-crystalline cells are cut from a single crystal of silicon which makes them very smooth in texture and the thickness of the slice can be seen. Mono-crystalline cells are the most expensive to produce but they are the most efficient. Due to their rigidness, they must be mounted in a rigid frame for protection.

Polycrystalline (or Multi-crystalline) cells are made from a slice cut from a block of silicon where these cells consist of a large number of crystals. This gives them a dotted reflective appearance and the thickness of the slice is visible. These types of cell are slightly less efficient but also slightly cheaper than mono-crystalline cells. They also need to be mounted in a rigid frame.

The second generation is the amorphous cells which are manufactured by placing a thin film of amorphous (non crystalline) silicon onto a wide range of surfaces. This type of cells is the least efficient but also the cheapest. Due to the amorphous flexible nature of the thin layer and it can be manufactured on a flexible surface where the whole photovoltaic solar panel will be flexible. There

is one downside of these cells is that their power output reduces over time especially during the first few months then they are basically stable. The quoted output could be achieved after this period.

The third generation made from different types new materials besides silicon, of which are solar inks using conventional printing press technologies, solar dyes, and conductive plastics (NREL 2009).

2.8.1 UK feed-in tariffs for PV

Feed-in tariffs (FITs) are not a new concept and have been successfully used in Germany since 1991. They have since been taken up by other countries such as Denmark, Spain and France. The feed-in tariff varies in Europe is between 40 to 50 eurocents, being adjusted depending on the size and location of the system. Increased rates are paid for islands (Celik, Muneer and Clarke 2009).

In the UK the proposal aims to help install generating capacity that will meet 2% of the UK's electricity consumption by 2020, which translates to approximately eight Terra Watt hour (Gipe 2009). The UK (FITs) was available on 1st April 2010 but it is not available in Northern Ireland - although this is under review (EST-UK 2011). This scheme covers the following technologies for electricity generation up to the installation size of 5 Mega Watts (MW):

- Solar electricity (PV) (roof mounted or stand alone)
- Wind turbine (building mounted or free standing)
- Hydroelectricity
- Anaerobic digestion
- Micro combined heat and power (micro CHP) (limited to a pilot at this stage)

Qualified participants of the FITs are benefited in the following 3 ways:

1. Generation tariff – the energy supplier will pay a set rate for each unit (or kWh) of electricity generated by the participant. This rate will change each year for new entrants to the scheme (except for

the first 2 years), but once you join you will continue on the same for 25 years for PV. The FITs rates are shown in Table 2.8.1.1.

2. Export tariff - a further 3p/kWh are paid to participant from the energy supplier for each unit of electricity that is export back to the electricity grid, when it is not used on site.
3. Energy bill savings –savings on electricity bills, because electricity generated from PV to power all electrical appliances, the participant reduce the amount of electricity buy from the electricity supplier. The amount may vary depend on how much of the electricity is generated and used on site.

Table 2.8.1.1 Generation tariffs for PV till 2020 (DECC 2010).

Technology	Scheme Year	Tariff level for new installations in period (p/kWh) [NB tariffs will be inflated annually]											**Tariff lifetime (years)**
		Year 1: 1/4/10 – 31/03/11	Year 2: 1/4/11 – 31/3/12	Year 3: 1/4/12 – 31/3/13	Year 4: 1/4/13 – 31/03/14	Year 5: 1/4/14 – 31/03/15	Year 6: 1/4/15 – 31/03/16	Year 7: 1/4/16 – 31/03/17	Year 8: 1/4/17 – 31/03/18	Year 9: 1/4/18 – 31/03/19	Year 10: 1/4/19 – 31/03/20	Year 11 : 1/4/20 – 31/03/21	
PV	≤4 kW (new build**)	36.1	36.1	33	30.2	27.6	25.1	22.9	20.8	19	17.2	15.7	25
PV	≤4 kW (retrofit**)	41.3	41.3	37.8	34.6	31.6	28.8	26.2	23.8	21.7	19.7	18	25
PV	>4-10 kW	36.1	36.1	33	30.2	27.6	25.1	22.9	20.8	19	17.2	15.7	25
PV	>10-100 kW	31.4	31.4	28.7	26.3	24	21.9	19.9	18.1	16.5	15	13.6	25
PV	>100kW-5MW	29.3	29.3	26.8	24.5	22.4	20.4	18.6	16.9	15.4	14	12.7	25

2.8.2 Current PV in the UK

The PV installation in the UK saw a gradual increase from 10.9 Mega Watt electricity (MWe) to 265 MWe for the period from 2005 to 2009. An average increase of 4 MWe per year was observed. The total energy generated from PV increased from 8 Giga Watt hour (GWh) in 2005 to 20 GWh in 2009. Throughout this period of time, several incentives were implemented i.e. Major Potovoltaic Demostration Programme between 2002 and 2006, and the Low Carbon Building Programme between April 2006 to May 2010. Recently the UK government introduced the FITs in April 2010 as discussed above. This may be the main reason for the steady increase of PV use in the UK. Table 2.8.2.1 and Figure 2.8.2.1 show the PV generation and installation capacity in the UK.

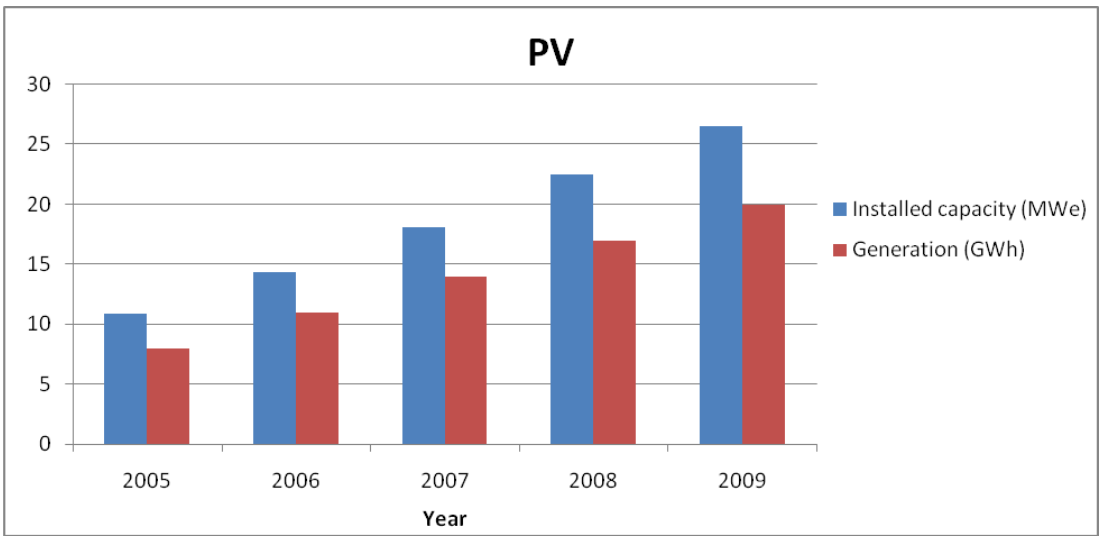

Figure 2.8.2.1 PV installation and generation in the UK (MacLeay, Harris and Annut 2010)

2.9 UKCP09

To make the UK well prepared for climate change, the UK government established The UK Climate Impacts Programme (UKCIP) in 1997 to help co-ordinate scientific research into the impacts of climate change, and to help organisations adapt to those unavoidable impacts. The majority of UKCIP's funding is from the Department for Environment, Food and Rural Affairs (Defra) (UKCIP 2010).

UKCP09 is the most comprehensive package produced to date and is the fifth generation of UK climate projection. Probabilistic projections of climate change are provided based on quantification of the known sources of uncertainty. A User Interface (UI) is provided to facilitate access to the projections and a User Guidance is available to support decisions using UKCP09. An analytical tool which is the Weather Generator (WG) together with the Threshold Detector is offered to support users in exploring potential impacts, vulnerabilities and adaptation options.

Three types of climate information available from the UKCP09 are:

- Probabilistic projections
- Marine and coastal projections
- Observed climate and climate trends

The projections are provided from 2010 to the end of this century at seven 30-year time periods and at a 25 km spatial resolution.

UKCP09 provides vast amount of information to users. To avoid users getting flooded with too much information, and facilitate its use, UKCP organised the information into three categories i.e. key findings, published material and customised output.

A peer review panel was set up to check and verify the methodology and outputs throughout their development, examine the methodologies used to produce the climate projections and the marine and coastal projections, as well as the WG (Jones, Kilsby, Harpham et al. 2009).

The UKCP09 will evolve with time based on experience gained; therefore new functions are being added and existing ones modified. Besides that the User Guidance and science reports will also evolve with periodic updates reflecting such evolution and the addition of the extras. Hence it is recommended that users should ensure that most up-to-date versions of the User Guidance and science reports are used. For further information on updates the following link is provided: http://ukclimateprojections.defra.gov.uk/content/view/932/9/

The following section will discuss only the WG tool which is used in this study. In-depth details and information about UKCP09 can be accessed through its website at: http://ukclimateprojections.defra.gov.uk/

2.10 UKCP09 Weather Generator

To generate future data, there are several methods i.e. extrapolating statistical method (degree-day method), imposed offset method, stochastic weather model and global climate models (Guan 2009).

The UKCP09 Weather Generator (WG) uses stochastic weather model. It is a downscaling tool that is used to generate statistically plausible daily and hourly time series that comprise of a set of climate variables at a 5 km resolution. These series of variables are consistent with the underlying 25 km resolution climate projections. The method used is the Neyman-Scott Rectangular Processes (NSRP) model (Jones, Kilsby, Harpham et al. 2009) which is similar to the one used by Burton et al (Burton, Fowler, Blenkinsop et al. 2010), Kilsby et al (Kilsby, Jones, Burton et al. 2007) and Cowpertwait et al (Cowpertwait, Kilsby and O'Connell 2002).

It can produce a minimum of 100 daily (and hourly) time series from 30 to 1000 years in length. The user specifies the number of years where options are available for daily and hourly outputs. There are no graphical products available through the UKCP09 UI based on the WG outputs. Figure 2.10.1 shows procedures that are used to generate climate variables from the WG output. These procedures were extracted from the WG report (Jones, Kilsby, Harpham et al. 2009).

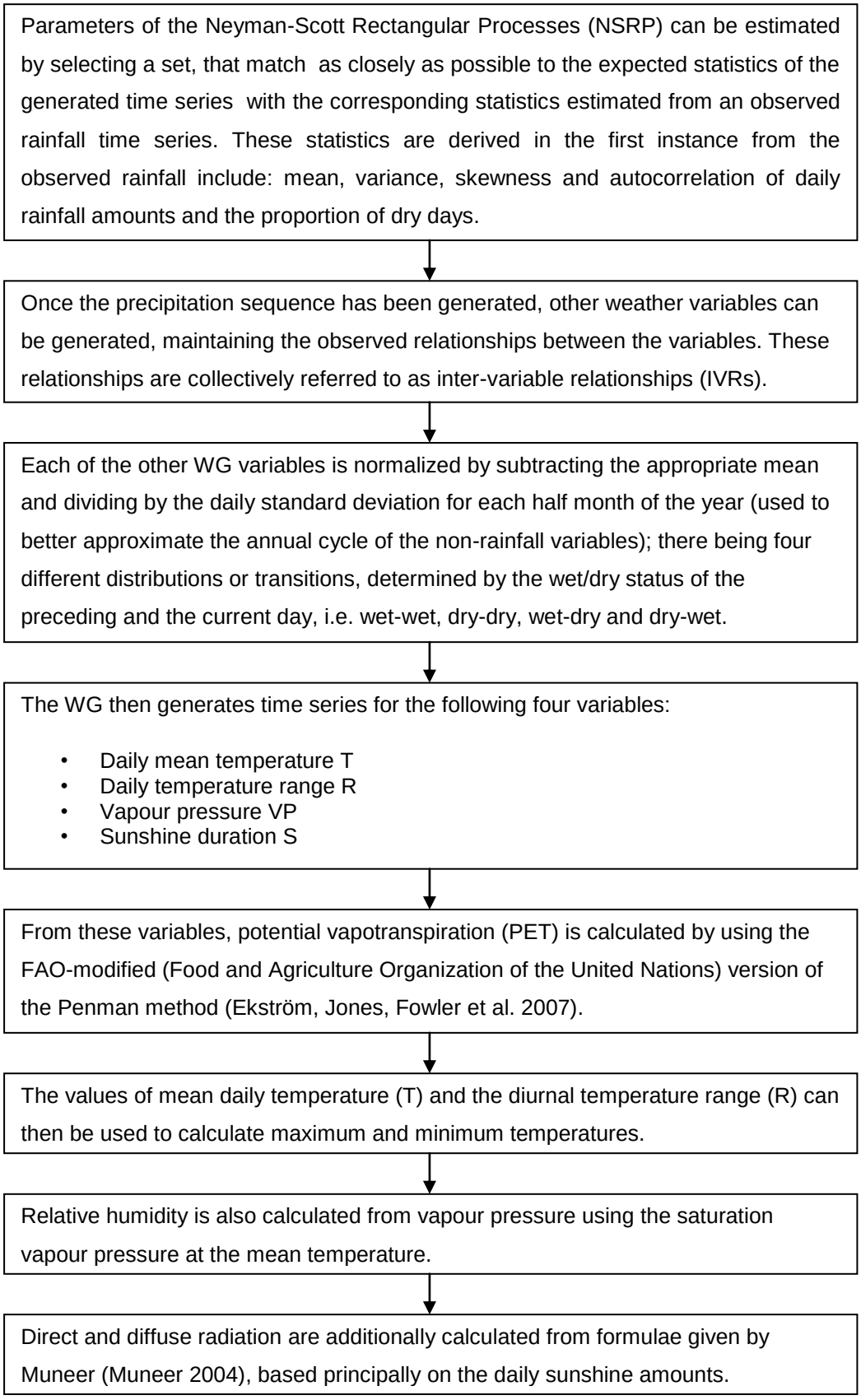

Figure 2.10.1 Procedures used to produce the WG output variables (Jones, Kilsby, Harpham et al. 2009).

The WG output consists of a set of files as follows:

1. Control run – 100 time series of 30 years for the baseline period.

2. Future climate runs – minimum of 100 time series of user-defined runs perturbed using a given future climate. The number and length of the time series can be set within specified limits by the user when configuring the WG request within the UKCP09 UI (the default is 30 years and 100 time series).

3. WG driving statistics file – presenting the absolute values of variable statistics used to drive the WG. This is similar to the change factor file, but provides absolute values rather than transformations of climate change values.

4. Metadata – includes information on the request parameters selected, internal WG settings, seed values and model variant IDs used.

The output variables of the WG are default outputs and the user cannot reduce the amount of output variables. The output variables for each run either daily or hourly time series are as below:

Daily time series variables:

- Year, month, day, day count within year, transition, mean total daily precipitation rate (mm/day), minimum daily temperature (ºC), maximum daily temperature (ºC), vapour pressure (hPA), relative humidity (%), sunshine hours (hours), downward diffuse radiation (Wh/m^2), direct radiation (Wh/m^2), and potential evapotranspiration (mm/day)

Hourly time series variables:

- Year, month, day, hour, total hourly precipitation (mm), mean hourly temperature (ºC), vapour pressure (hPA), relative humidity (%), sunshine (fraction of an hour), downward diffuse radiation (Wh/m^2), and direct radiation (Wh/m^2).

The output file from the WG comprises of two types of formats i.e. comma-separated (*.csv) and the CF-NetCDF (portable binary data) formats. For this study, hourly time series in the ‘csv’ file format was selected.

2.11 Conclusions

In this chapter, discussion of how solar irradiation affects the earth climate system, the UK current GHG emissions, measurement equipment and their errors and uncertainties, quality control of data, statistical evaluation techniques and a review of solar radiation models were covered. Furthermore, discussion on the UKCIP is also presented.

To conclude, a clear understanding of the amount of solar radiation received by the earth’s surface is very important. Furthermore, the understanding of how users use energy in the UK needs to be explored in depth (Janda 2011). From the current GHG emissions trend and the FITs that were introduced, the UK government is working forward to achieve its target to combat climate change.

3.0 Evaluation of models

Measured solar radiation data is scarce due to the high cost of measurement equipment and the need for well trained personnel as discussed in Chapter 2. Hence, computational models are needed to fill this gap. This chapter will discuss in detail the types of models and evaluations that have been carried out.

3.1 Evaluation of hourly averaged solar irradiation models

Concerns about energy efficiency in building design and the sustainable generation of electricity from solar energy have led to the need for accurate estimates of solar irradiation. Meteorological measurements available from locations around the world can be used as the basis for such estimates, but are severely limited in the detail they can provide. The majority of stations, for example, do not collect solar data and those that do usually only provide daily measurements, whereas many current applications require estimates by hour or even by minute. Climate simulation systems, for example, such as the weather generator described by Kilsby *et al.*(Kilsby, Jones, Burton et al. 2007) require at least hourly data to validate their output. Liu and Jordan's model fills gaps in the sparse data available by enabling the estimation of both beam and diffuse hourly irradiation from its daily counterpart.

This evaluation work reports on a comparison of measured hourly data from 16 UK locations with values calculated using Liu and Jordan's model. Various researchers have carried out similar evaluations as described in the next section, and certain weaknesses have already been identified. However, a rigorous evaluation has not previously been performed using data from the UK. The present aims are therefore:

a) to identify discrepancies between measured and calculated values for the UK dataset, and therefore to suggest possible approaches to improvement if at all possible.

b) to evaluate the applicability of the Liu-Jordan model to a northern European location in comparison to similar studies carried out at lower latitudes.

3.1.1 Review of models and previous work

Solar radiation incident on any given surface can be decomposed into two components, the direct or beam component emanating from the sun, and a diffuse component which results from multiple reflections and scattering due to particles in the atmosphere. The diffuse component may also include reflections from the ground and local surroundings where the surface in question is sloped rather than horizontal. Differentiating between the two components is vital for accurate calculations in most solar energy applications; however, a number of steps may be required to arrive at realistic estimates at an appropriate level of detail for a given location depending on the basic data available. Where no actual measurements of solar irradiation are available, for example, the calculation scheme would involve the steps shown in Figure 3.1.1. As stated above for the sake of generality Figure 3.1.1 shows the computational flow for any general surface, i.e. one which may have a given orientation and slope. With each successive step errors would be conflated, and the accuracy of each individual stage is therefore crucial.

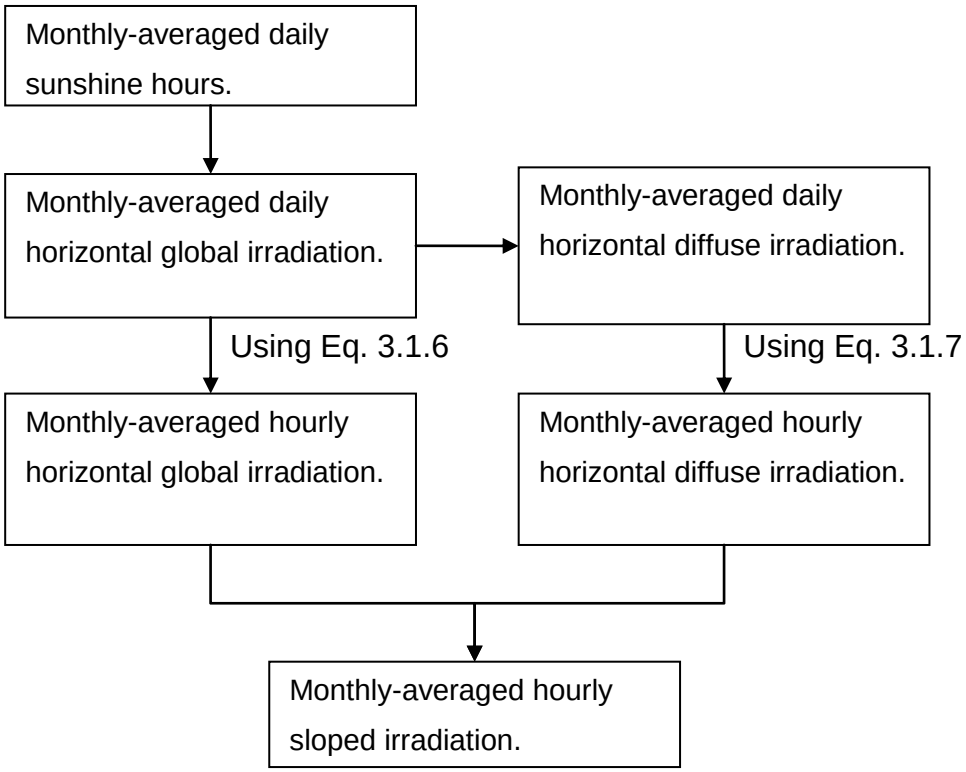

Figure 3.1.1 Calculation scheme for monthly-averaged hourly sloped irradiation.

Very many locations around the world record sunshine duration and this parameter may reliably be used to obtain monthly-averaged daily irradiation. The second step would then incorporate the Liu and Jordan model presently under discussion to obtain hourly irradiation as indicated in Figure 3.1.1. Original work by Ångström (Ångström 1924) on the estimation of daily global irradiation was based on a comparison of monthly-averaged daily values with a clear-sky figure. This method was refined by several other researchers (Page 1961; Lof 1966; Schulze 1976; Hawas and Muneer 1983; Nagrial and Muneer 1984; Grag and Grag 1985; Turton 1987; Jain and Jain 1988) all of whom developed models of the form shown in Eq. 3.1.1

$$\overline{G} = \overline{E}\left[a + b(n/N)\right] \qquad (3.1.1)$$

where $\overline{G}$ = monthly-averaged daily global irradiation

$\overline{E}$ = monthly-averaged extraterrestrial radiation

a, b = site-specific constant coefficients

n = average daily hours of bright sunshine

N = day length

n/N = fractional possible sunshine

N in the above formula is derived from the sunset hour angle using the following equations:

$$\omega_s = \cos^{-1}(\tan Lat \tan DEC) \tag{3.1.2}$$

$$N = (2\omega_s / 15) \tag{3.1.3}$$

where ω_s = sunset hour angle

LAT = latitude

DEC = declination (angular position of the sun with respect to the equatorial plane at solar noon)

The sunset hour angle, given in degrees, is a measure of the rotation of the Earth between solar noon and sunset. $2\omega_s$ therefore precisely describe the length of a given astronomical day. Some simple mathematics shows that a rotation of 15^o of arc corresponds to one hour.

The success of models of the form of Eq. 3.1.1 relies on the compilation of appropriate coefficients for different locations; however, Suehrcke (Suehrcke 2000) has proposed an alterative relationship which eliminates this additional overhead. Using the notion of a clearness index $\overline{K}_T=(\overline{G}/\overline{E})$ and a

corresponding reference value for clear-sky conditions ($\overline{G}_{clear}/\overline{E}$), Suehrcke's formulation is as shown in Eq. 3.1.4.

$$\overline{G}/\overline{E} = (n/N)(\overline{G}_{clear}/\overline{E}) \tag{3.1.4}$$

Arguing that since $\overline{G}_{clear}/\overline{E}$ varies only within the very limited range of 0.65 to 0.75, Suehrcke proposed using a single constant value of 0.7 making Eq. 3.1.4 applicable in any location given the single local value of n, the average daily hours of bright sunshine. Work by Driesse and Thevenard (Driesse and Thevenard 2002) has demonstrated the validity of this approach using 70000 data points from 700 worldwide sites. The latter authors demonstrated a root mean square variation of 12% around the relationship predicted by Suehrcke. The 'universal' model can therefore provide acceptable estimates of monthly-averaged daily global irradiation in the absence of site-specific coefficients.

Addressing the problem of decomposing global irradiation into its components, Liu and Jordan (Liu and Jordan 1960) developed a model similar to that shown in Eq.3.1.5 in which the ratio of monthly-averaged daily diffuse irradiation ($\overline{D}$) to monthly-averaged daily global irradiation ($\overline{G}$) is expressed as a function of $\overline{K}_{\mathrm{T.}}$ Two sets of coefficients for Eq. 3.1.5 are available, one by Page (Page 1977) for use in temperate climates, and one for desert and tropical locations by Hawas and Muneer (Hawas and Muneer 1984).

$$\overline{D}/\overline{G} = 1.00 - 1.13\overline{K}_T \tag{3.1.5}$$

$a = 1.00, b = 1.13$: Page (Page 1977)

$a = 1.35, b = 1.61$: Hawas and Muneer (Hawas and Muneer 1984)

Using Eqs. 3.1.1-3.1.5 it is thus possible to obtain $\overline{G}$ and then $\overline{D}$ from monthly-averaged sunshine data. In the remainder of this evaluation the subject of discussion shall be the progression of hourly, horizontal irradiation estimation.

To provide a model to decompose averaged-daily to averaged-hourly values, Liu and Jordan (Liu and Jordan 1960) built on earlier work by Whillier (Whillier

1956) to develop a set of regression curves which represent the ratio of hourly to daily global solar irradiation at a series of time intervals from solar noon. This approach was validated by Collares-Pereira and Rabl (Collares-Pereira and Rabl 1979) who obtained Eq. 3.1.6 using a least-squares fit.

$$r_G = \frac{\pi}{24}\left(a' + b'\cos\omega\right)\frac{\cos\omega - \cos\omega_s}{\sin\omega_s - \omega_s\cos\omega_s} \tag{3.1.6}$$

where a' = $0.409 + 0.5016\sin(\omega_s - 1.047)$

b' = $0.6609 - 0.4767\sin(\omega_s - 1.047)$

r_G = ratio of hourly to daily global irradiation, $\overline{g}/\overline{G}$

Liu and Jordan's theoretical model for the ratio of hourly to daily diffuse irradiation is given in Eq. 3.1.7.

$$r_D = \frac{\pi}{24}\frac{\cos\omega - \cos\omega_s}{\sin\omega_s - \omega_s\cos\omega_s} \tag{3.1.7}$$

where r_D = ratio of hourly to daily diffuse irradiation, $\overline{d}/\overline{D}$

The above Lui and Jordan model was found to be one of the best model by Koussa et al (Koussa, Malek and Haddadi 2009). Other methods for obtaining hourly irradiation figures, such as the 'daily integration model' described by Gueymard (Geuymard 2000) have been proposed. However, Gueymard's model has been shown to produce very similar results to the Liu-Jordan model, at least in the case of Hawas and Muneer's Indian data. Weather generators such as the one described by Kilsby *et al.* (Kilsby, Jones, Burton et al. 2007) also use linear regression to derive values for a range of meteorological variables including sunshine duration. They do not, however, attempt to model global and diffuse irradiation directly. The Liu-Jordan model therefore remains the object of evaluation here.

Hawas and Muneer (Hawas and Muneer 1984) compared measurements from 13 locations in India taken between 1957 and 1975 to the values predicted by the model and found a general agreement for the r_G model. Average values for r_G and r_D are shown in Figure 3.1.2 as points while the solid lines indicate the values predicted by Eqs.3.1.6 and 3.1.7 for 0.5, 1.5, 2.5, 3.5, 4.5 and 5.5 hours from solar noon.

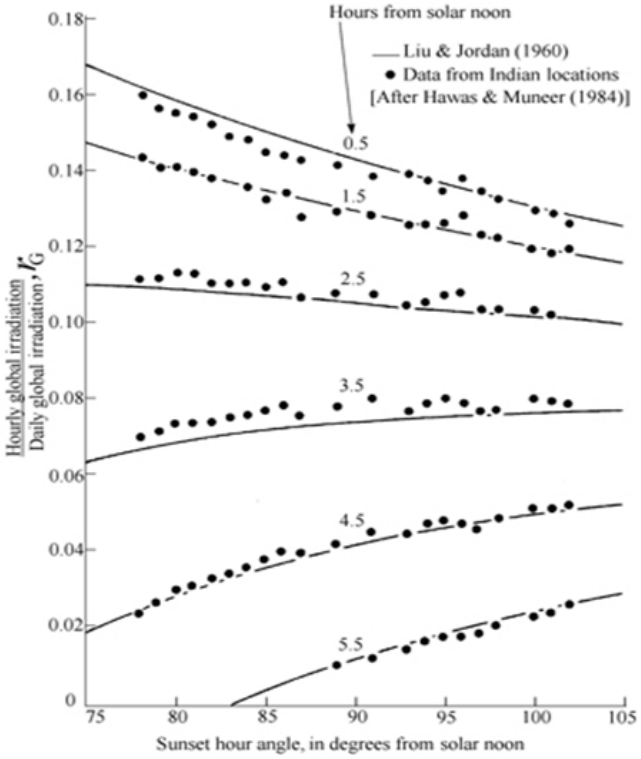

Figure 3.1.2 Ratio of hourly to daily global irradiation (Muneer 2004).

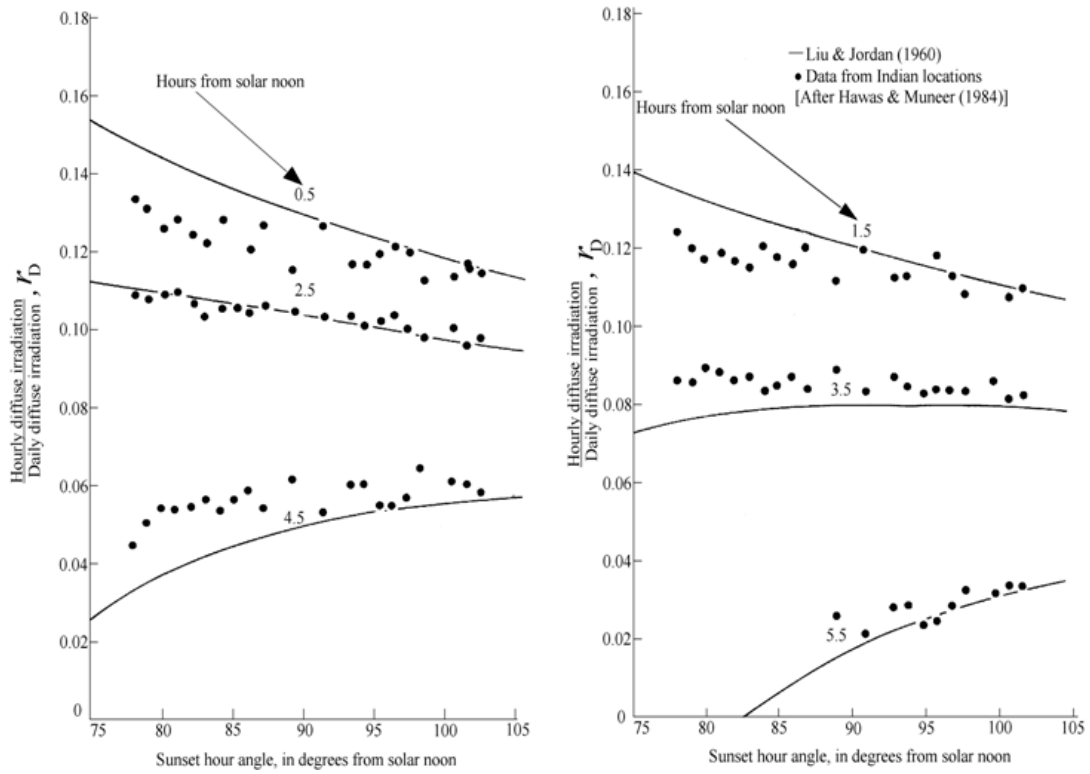

Figure 3.1.3 Ratio of hourly to daily diffuse irradiation (Muneer 2004).

Notwithstanding the agreement with Liu and Jordan's model for global irradiation, Hawas and Muneer (Hawas and Muneer 1984) found that the Indian data differed markedly from the values predicted by Eq. 3.1.7 for diffuse irradiation. A compressed range of r_D is evident in Figure 3.1.3 where the average data points from the Indian recording stations are superimposed on Liu and Jordan's regression curves for the same time values as in Figure 3.1.2. Plotting individual values of r_D rather than average values as a function of sunset hour angle for a particular displacement from solar noon (Figure 3.1.4) reveals how great the scatter is, and demonstrates that the Liu-Jordan diffuse model is not suitable for estimating individual, hour by hour diffuse irradiation. Hawas and Muneer attribute the discrepancy to local conditions, and the extent to which the Liu-Jordan model is applicable elsewhere is still an appropriate subject of investigation. This is underlined by Iqbal's (Iqbal 1979) results which show good agreement with the Liu-Jordan model for three Canadian locations. To summarise, therefore, it has been shown by previous researchers that the decomposition of daily to hourly global irradiation can be performed with a fairly

high level of accuracy for long-term averaged data but not when hour-by-hour estimates are required.

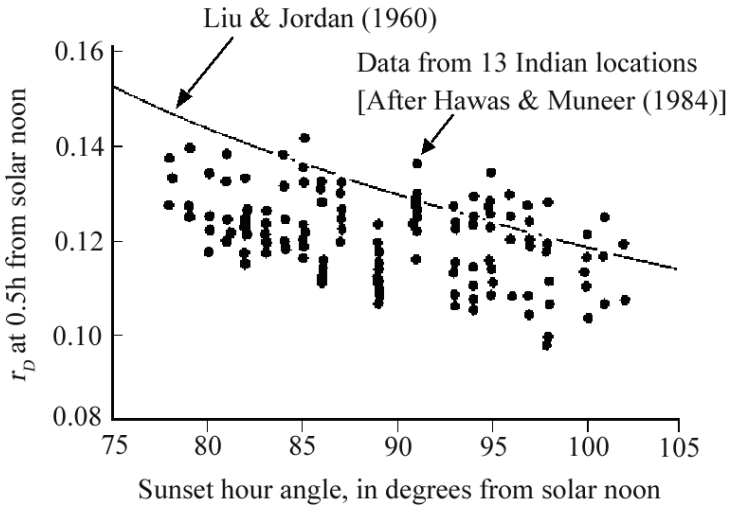

Figure 3.1.4 Individual values of r_D at 0.5h from solar noon (Muneer 2004).

Iqbal raised a further question in relation to Liu and Jordan's models for global and diffuse irradiation concerning the asymmetrical distribution of irradiation on either side of solar noon. At one of the Canadian sites in particular, a consistently lower level of global irradiation was observed in the morning compared to the afternoon. Similarly, Saluja and Robertson (Saluja and Robertson 1983) reported differences in computed values of yearly averages of irradiation on east and west facing surfaces for Aberdeen, Easthampstead and Kew compared to other UK locations. Like the variations observed by Hawas and Muneer (Hawas and Muneer 1984), these observations suggest that local factors need to be taken into account when estimating hourly irradiation.

A further feature of Hawas and Muneer's (Hawas and Muneer 1984) analysis of the Indian data was to investigate potential relationships between r_D and $\overline{K}_T$. Where the Liu-Jordan model predicts a constant value for r_D at a given displacement from solar noon, Hawas and Muneer found a clear tendency for r_D to decrease with $\overline{K}_T$ as shown in Figure 3.1.5. This work will evaluate the Liu and Jordan's regression curves for the UK taking into account the discrepancies discussed above.

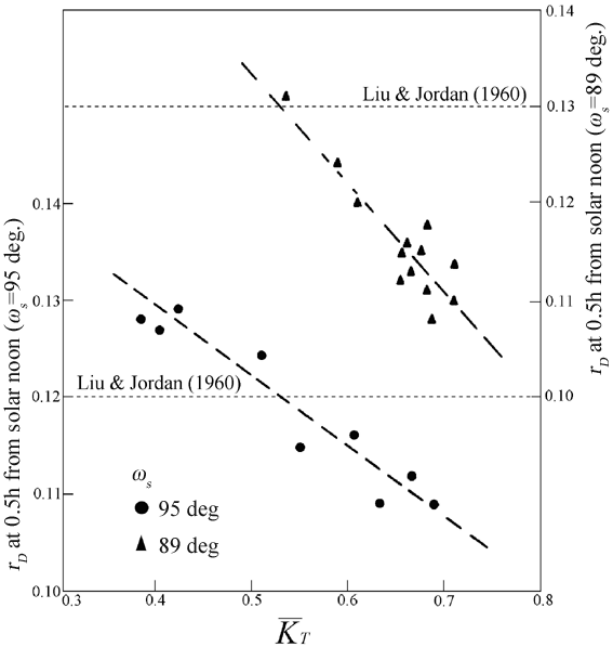

Figure 3.1.5 r_D at 0.5h from solar noon for two fixed values of ω_S (Muneer 2004).

3.1.2 Methodology

Computed values of r_D and r_G derived using Liu and Jordan's models are compared against measured data from 16 UK recording stations. Percentage error, calculated by Eq.3.1.8, is used to show the divergence of the Liu and Jordan model from the measured values.

$$\varepsilon = 100\frac{(c-m)}{m} \tag{3.1.8}$$

where ε = percentage error

c = calculated value after Liu and Jordan

m = measured value

This work is based on the measured UK data set that was provided by the UK Meteorological Office to the CIBSE Guide J (CIBSE 2002) panel members. T

Muneer led the work of solar radiation group under the overall coordination of G Levermore. Note that the above data set contained measured hourly radiation and other climatic parameters for a total of 20 stations, of which only three (Bracknell, Manchester and Edinburgh) were selected for inclusion in CIBSE Guide J. T Muneer was also responsible for undertaking the quality control for the solar radiation data as discussed in Chapter 2 which was the Muneer and Fairooz method (Muneer and Fairooz 2002). The time periods covered by the station subsets range from 12 to 26 years. Table 3.1.1 shows the list of the data that have presently been used.

Table 3.1.1 Details of the data used in the present evaluation and their sources.

Station	No. Years data	Latitude	Missing/ Erroneous Hours	Total hours	% Missing Hours
Camborne	13(1982-1994)	50.37	444	62842	0.71
Crawley	13(1980-1992)	51.08	334	62808	0.53
Bracknell	20(1975-1994)	51.38	223	100307	0.22
London	20(1976-1995)	51.52	*	93830	0
London (wcb)	20(1975-1994)	51.52	1455	89774	1.62
Aberporth	20(1975-1994)	52.13	650	92298	0.70
Hemsby	15(1981-1995)	52.25	613	61153	1.00
Manchester	13(1982-1994)	53.47	*	61424	0
Finningley	12(1983-1994)	53.48	107	56724	0.19
Aughton	13(1982-1994)	53.55	548	61326	0.89
Aldergrove	26(1968-1994)	54.65	3984	112634	3.54
Edinburgh	17(1976-1992)	55.85	*	79591	0
Mylnefield	19(1975-1993)	56.45	186	87485	0.21
Dunstaffnage	20(1975-1994)	56.47	102	91945	0.11
Aberdeen	20(1975-1994)	57.17	12	97191	0.01
Stornoway	13(1982-1994)	58.22	769	54304	1.42

* Completed data for these locations were produced by the CIBSE Solar Data Task Group.

Percentages of missing or erroneous hours were calculated for the stations in Table 3.1.1 by dividing the total missing hours by the total recorded hours with global and diffuse values at the location. The station with the highest number of missing hours was Aldergrove with 3.54% and the lowest was Aberdeen with just 0.01%. Only three out of 16 stations were missing more than 1% of data.

Prior to the present analysis, the raw data files were pre-processed using a series of computer programmes written in Visual Basic for Applications (VBA) which also made use of the processing features of Microsoft Excel. On completion of a stage of pre-processing, results were saved in a new file to minimise file size and to prevent accidental data loss. The pre-processing consisted of the steps shown in Figure 3.1.6.

The first filtering stage simply removed unwanted meteorological data from the files. The second stage identified and removed erroneous secondary values for global or diffuse radiation. Several criteria were used in this step including:

- the value for diffuse radiation greater than that for global radiation
- missing radiation data.
- negative or zero radiation values.

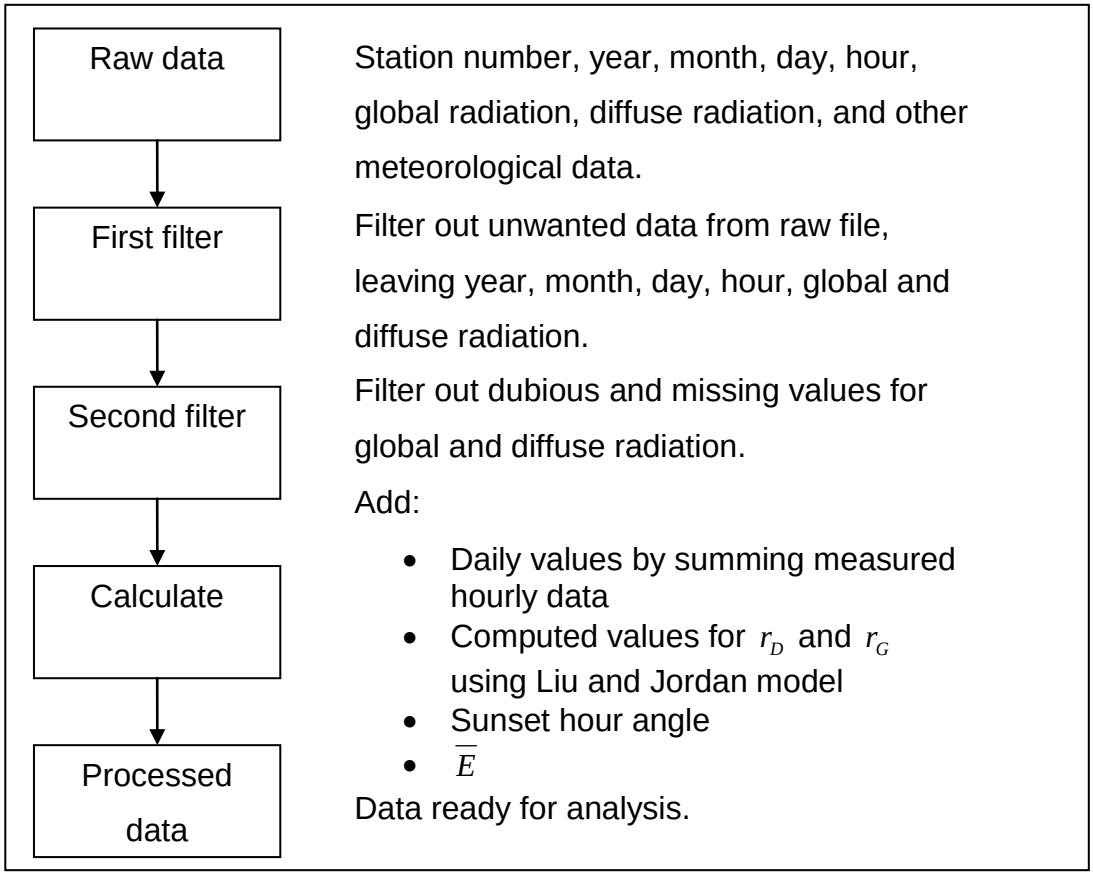

Figure 3.1.6 Flow chart for the pre-processing of raw solar radiation data

After the second filter, calculated values were added to the data which was then stored in an Excel file for later analysis. Eqs 3.1.6 and 3.1.7 were used to calculate monthly averaged hourly global and diffuse irradiation.

The operation of the VBA programmes was cross validated using another statistical software package (SPSS version 14).

3.1.3 Results and discussion

Having calculated the appropriate figures for monthly-averaged global and diffuse radiation, percentage error was used to show the deviation of the measured values from those predicted by the Liu and Jordan model. Better agreement was found for global radiation than for diffuse radiation for all 16 locations. Since a similar trend was observed in all 16 cases, two stations

Bracknell and Stornoway were selected to illustrate the differences. Bracknell used to be the UK Meteorological Office Headquarters, with higher quality data recorded than elsewhere and is also in close proximity to London. Stornoway is one of the most northerly of the UK stations.

An examination of the percentage error at Bracknell shows a reasonably good fit between the measured data and the Liu-Jordan model for global radiation. At Bracknell the error is normally distributed around zero, with 38.7% points lying in the ±10 percentage range, and 66.9% of the data in the ± 20 percentage range.

At Stornoway, 80% of the percentage data lies in the range of -10 to -30 percent showing that the Liu-Jordan model consistently underestimates global radiation for this location

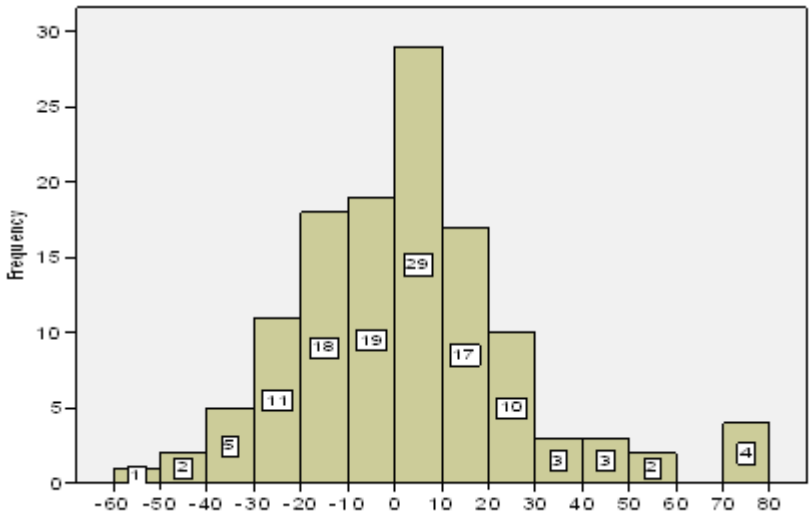

Figure 3.1.7 Histogram of percentage error of global radiation for Bracknell.

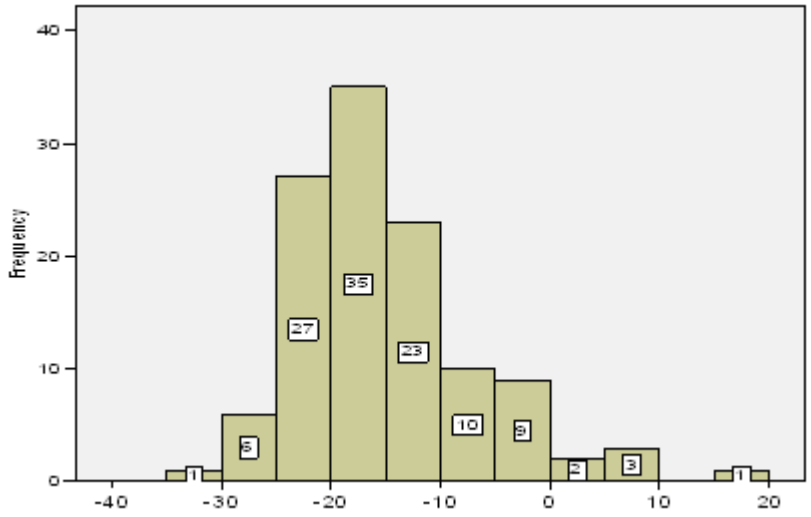

Figure 3.1.8 Histogram of percentage error of global radiation for Stornoway.

In the case of diffuse radiation, Figure 3.1.9 shows that 77.2% of the data population for Bracknell lies in the ±20 percentage error range. A negative shift in comparison with the plot for global radiation (Figure 3.1.7). The error for Stornoway shown in Figure 3.1.10 exhibits the same trend as the global radiation data where the data population is once again skewed towards negative errors. Around 94 percent of the error lies in the error range of -30 to 0 percent.

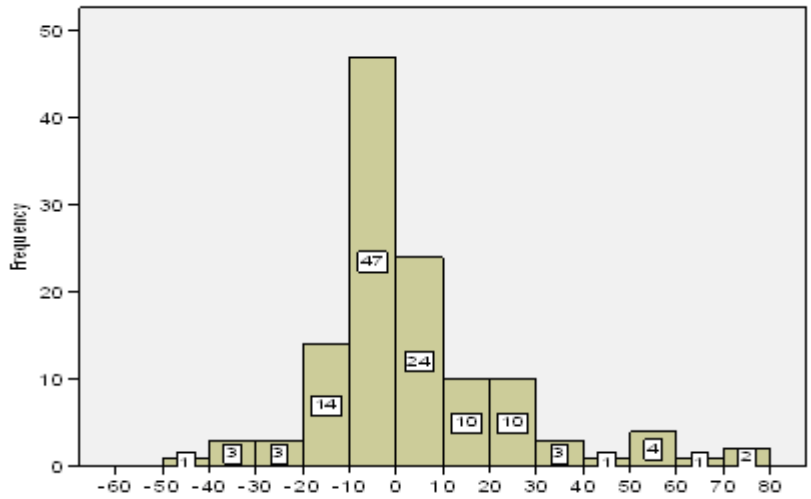

Figure 3.1.9 Histogram of percentage error of diffuse radiation for Bracknell.

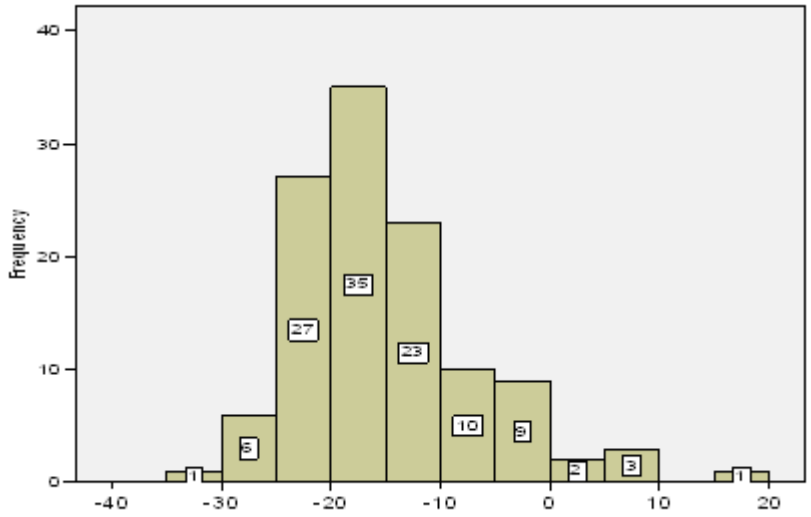

Figure 3.1.10 Histogram of percentage error of diffuse radiation for Stornoway.

In summary, weaknesses in the Liu-Jordan model are obvious for higher latitudes. Table 3.1.2 summarises the distribution of error in the total dataset.

Table 3.1.2 Summary of percentage error in the total dataset.

Error band, W/m^2	% of total data population, global radiation	% of total data population, diffuse radiation
±10	22.5	54.9
±20	50.7	95.8
±30	64.8	100

Further analysis was done to evaluate the expression of r_G and r_D derived by Liu and Jordan. Measured values for r_G and r_D before and after solar noon were plotted against sunset hour angle. Values of r_G from Eq. 3.1.6 and r_D from Eq. 3.1.7 for 0.5, 2.5 and 4.5 hours from solar noon were superimposed on the same graphs for comparison. Figures 3.1.11-3.1.16 therefore contain three sets of points for each time value. Note that in Figures 3.1.11-3.1.16, r_{GC} is the ratio of computed hourly to daily global radiation and r_{DC} is the ratio of computed hourly to daily diffuse radiation. Furthermore, in Figures 3.1.11, 3.1.12, 3.1.14

and 3.1.15 the variation of measured forenoon and afternoon values is compared against the computed ratios.

Figure 3.1.11 shows that for Bracknell the expression for r_{GC} underestimates the global radiation before noon and overestimates after noon for displacements of 2.5 and 4.5 hours. At 0.5 hours from solar noon, the expression of r_{GC} agrees well with the measured values with slightly less accurate estimates at low sunset angles.

For Stornoway in contrast, the expression for r_{GC} gives a good estimate of global radiation for all three displacements from solar noon as shown in Figure 3.1.12. The problem of over- and underestimating global radiation still occurs at low sunset angle as in Figure 3.1.11 for Bracknell.

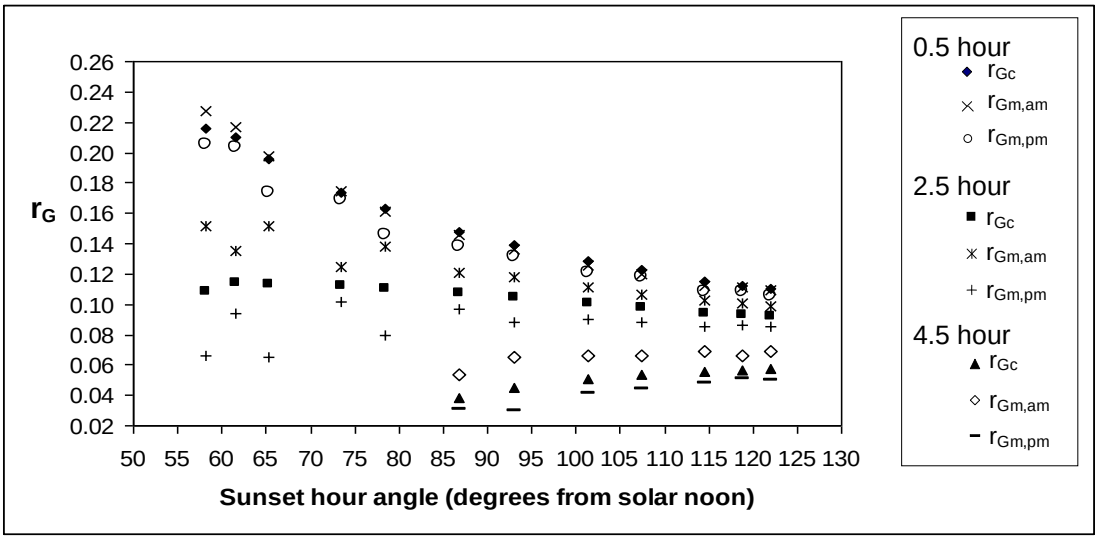

Figure 3.1.11 Ratio of measured hourly to daily total global radiation for different hours of the day vs sunset hour angle for Bracknell station.

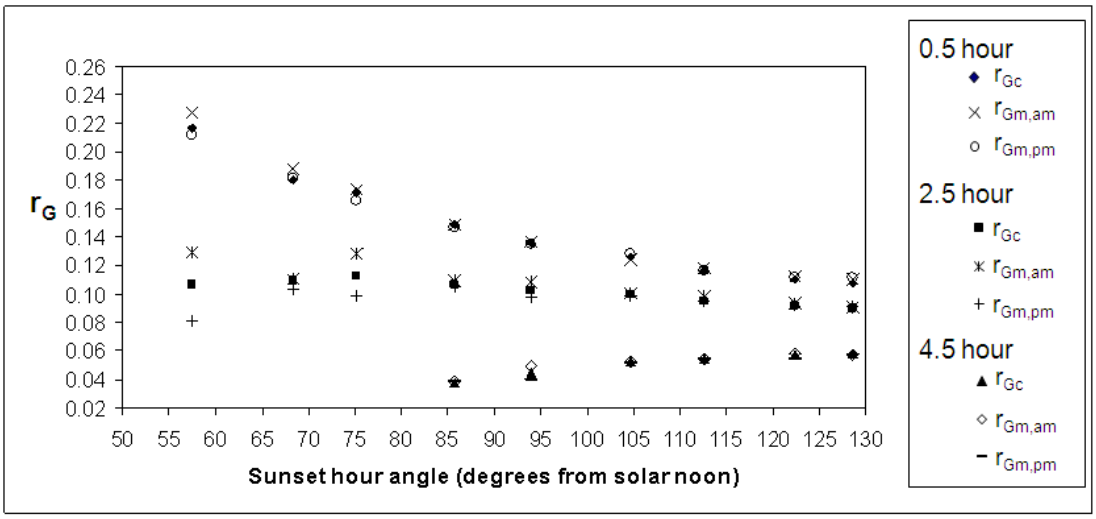

Figure 3.1.12 Ratio of measured hourly to daily total global radiation for different hours of the day vs. sunset hour angle for Stornoway station

The over- and underestimation of global and diffuse radiation which is evident in Figure 3.1.11 and 3.1.12 disappears when pre- and post-noon values are aggregated as shown in Figure 3.1.13. The errors cancel each other out, and the impression is one of a good fit. However, since this study interested in accurate values for any given hour, this is misleading.

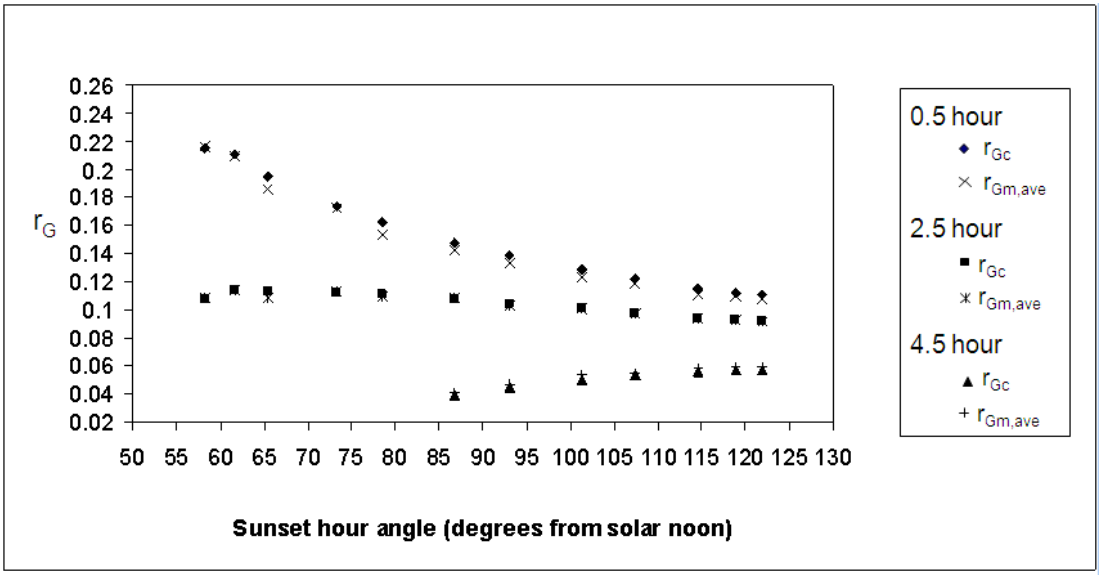

Figure 3.1.13 Average ratio of measured hourly to daily total global radiation for different hours of the day vs. sunset hour angle for Bracknell station.

The corresponding plot of the hourly ratio of diffuse radiation for Bracknell in Figure 3.1.14 follows a similar pattern to that for r_G in Figure 3.1.11. The expression of r_{DC} for 0.5 hours from solar noon correlates well with the measured values except for a small over- and underestimate at low sunset hour angle, while at 2.5 and 4.5 hours from solar noon, the expression for r_{DC} underestimates before noon and overestimates after noon.

For Stornoway, the expression for r_{DC} provides good estimation for all the hours as shown in Figure 3.1.15.

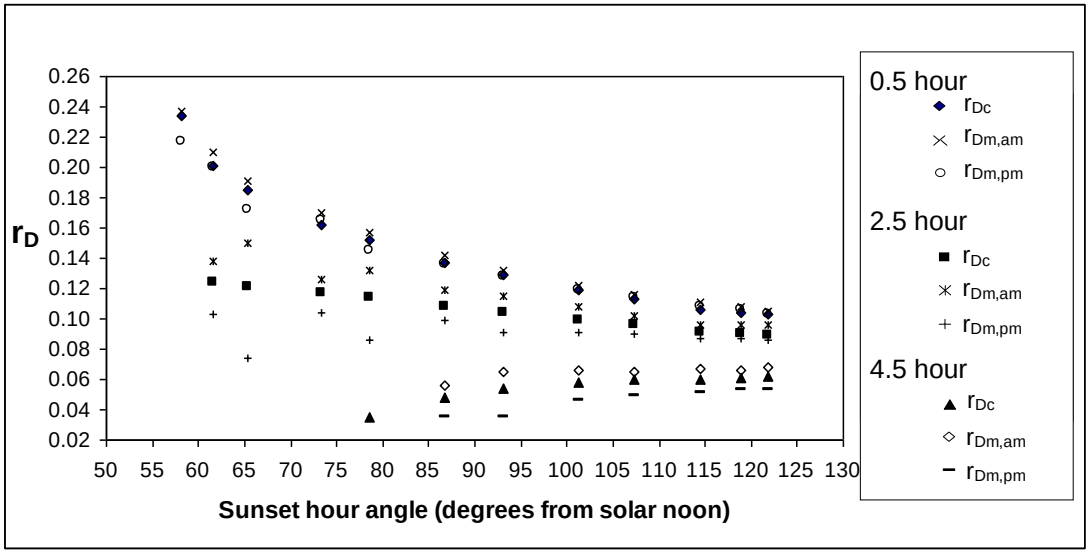

Figure 3.1.14 Ratio of measured hourly to daily diffuse radiation for hours of the day vs. sunset hour angle for Bracknell station.

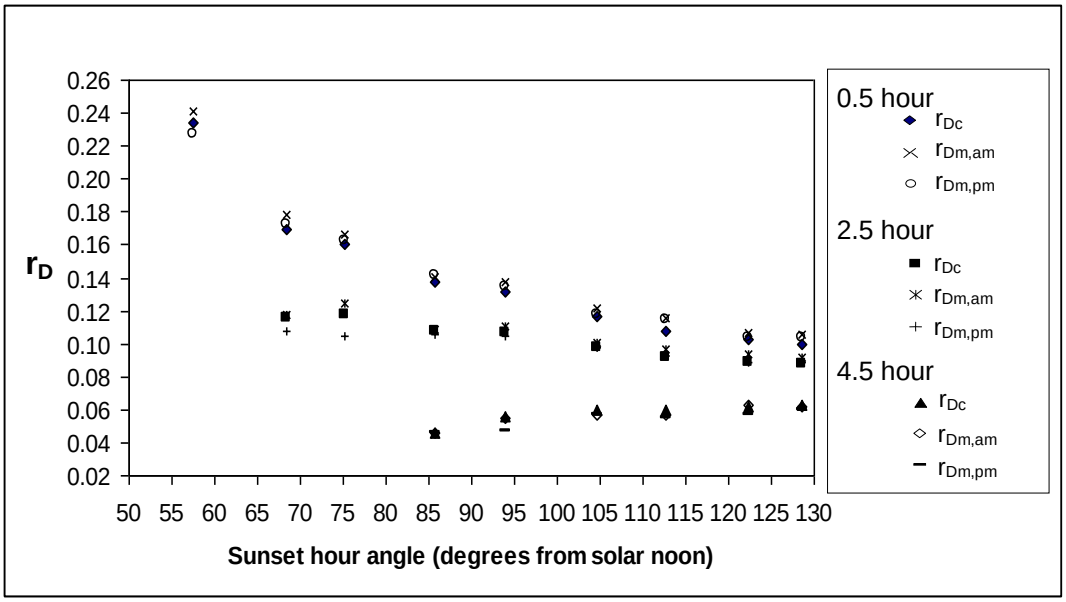

Figure 3.1.15 Ratio of measured hourly to daily diffuse radiation for different hours of the day vs. sunset hour angle for Stornoway station.

The effect of plotting the average of the measured values for r_D against sunset hour angle conceals the differences before and after solar noon as for r_G and gives the impression of a good fit with the calculated values as exemplified in Figure 3.1.16 for the Bracknell station. This suggests that the Liu-Jordan model needs to be refined to take account of this asymmetry.

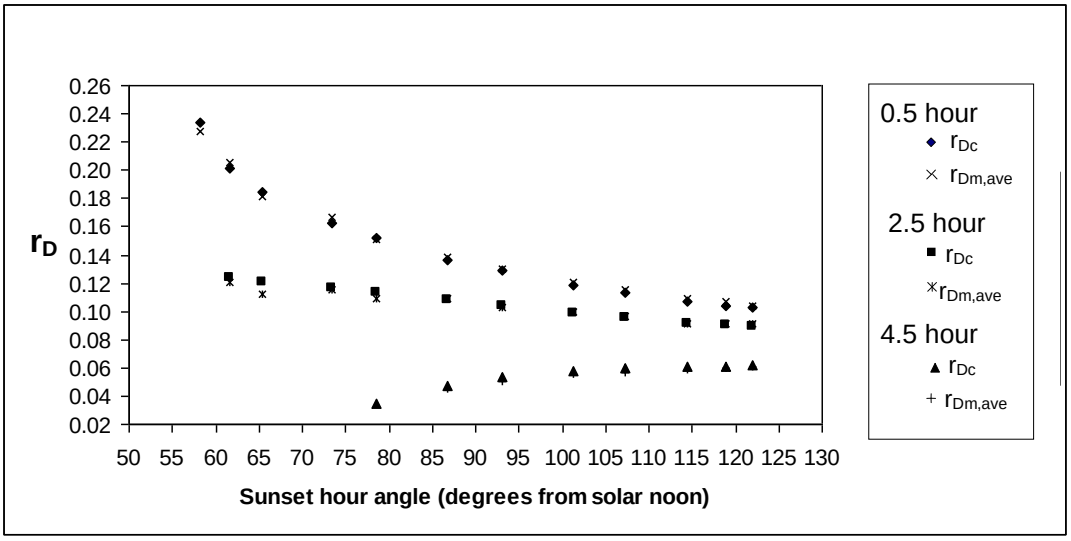

Figure 3.1.16 Average ratio of measured hourly to daily diffuse radiation for different hours of the day vs. sunset hour angle for Bracknell station

Location-specific effects are evident in the charts above, with a more marked spread of measured values for r_D at Bracknell, for example, than for Stornoway, and the extent of the local effect can be illustrated using a similar approach to Hawas and Muneer (Hawas and Muneer 1984). Plotting individual values of r_D at Bracknell rather than averages against sunset hour angle for a particular displacement from solar noon clearly shows an unacceptable degree of scatter in Figure 3.1.17.

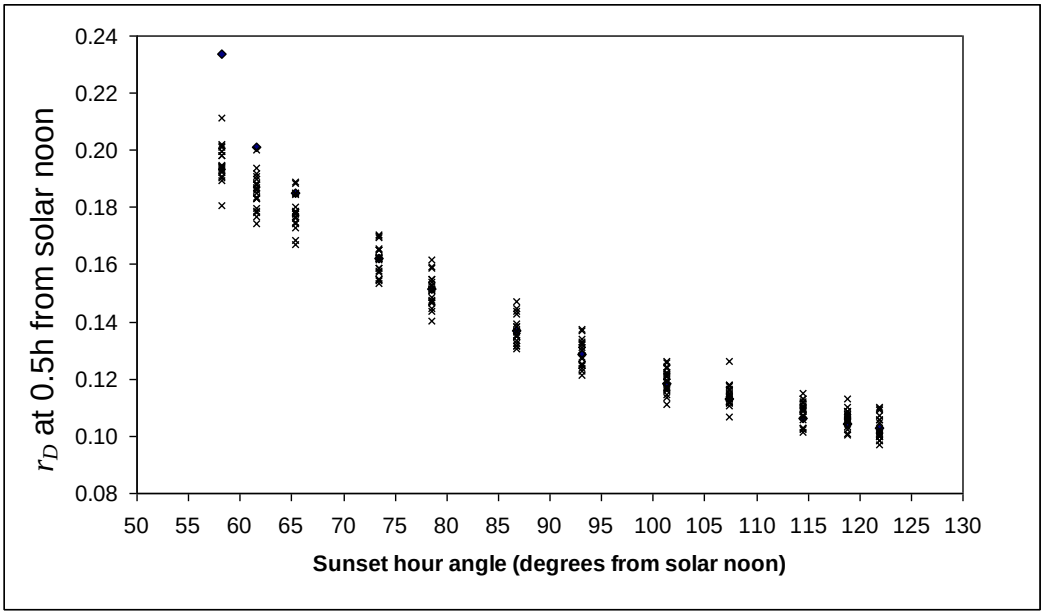

Figure 3.1.17 Individual (not averaged) values of r_D at Bracknell station before noon at 0.5h from solar noon.

3.1.4 Possible improvement

Given the observation by Hawas and Muneer (Hawas and Muneer 1984) that r_D tended to decrease as a function of $\overline{K}_T$ for the Indian locations studied, the author suggested that a systematic relationship between r_D and $\overline{K}_T$ might exist. An attempt was carried out to improve the Liu and Jordan's r_D regression model by taking into consideration the effect of $\overline{K}_T$.

Starting from the standard form of Liu and Jordan's model for r_D as shown in Eq. 3.1.7, a further term was introduced as in the Liu and Jordan model for global radiation shown in Eq. 3.1.6. The proposed model is shown in Eq. 3.1.9.

$$r_D = \frac{\pi}{24}\left(c' + d'\cos\omega\right)\frac{\cos\omega - \cos\omega_s}{\sin\omega_s - \omega_s\cos\omega_s} \tag{3.1.9}$$

Where;

$$c' = c_0 + c_1\sin(\omega_s - 1.047) \tag{3.1.10}$$

$$d' = d_0 - d_1\sin(\omega_s - 1.047) \tag{3.1.11}$$

Crucially, the coefficients c' and d' are not constants, but are themselves functions of $\overline{K}_T$ derived by linear regression as shown in Eqs. 3.1.12-3.1.15.

$$c_0 = c_{01} + c_{02}\overline{K}_T \tag{3.1.12}$$

$$c_1 = c_{11} + c_{12}\overline{K}_T \tag{3.1.13}$$

$$d_0 = d_{01} + d_{02}\overline{K}_T \tag{3.1.14}$$

$$d_1 = d_{11} + d_{12}\overline{K}_T \tag{3.1.15}$$

Using SPSS 14, the values of the further coefficients were derived, and the values are shown in Table 3.1.3.

Table 3.1.3 Coefficient values for new r_D regression model.

Coefficient	Value
c_{01}	-51.780
c_{02}	914.039
c_{11}	-0.072
c_{12}	0.078
d_{01}	6.972
d_{02}	-119.682
d_{11}	0.029
d_{12}	0.076

The derived coefficient values were then substituted to the Eqs. 3.1.10 and 3.1.11 to get the value of c' and d'. The performance of the proposed refinement (r_{Dn}) compared to Liu and Jordan's original model (r_{D_LJ}) was carried out by plotting the calculated values from both models against measured values of r_D.

The r^2 value of the r_{D_LJ} plot as calculated by SPSS 14 is 0.976, and for the r_{Dn} plot r^2 is 0.979 as shown in Figures 3.18 and 3.19 respectively.

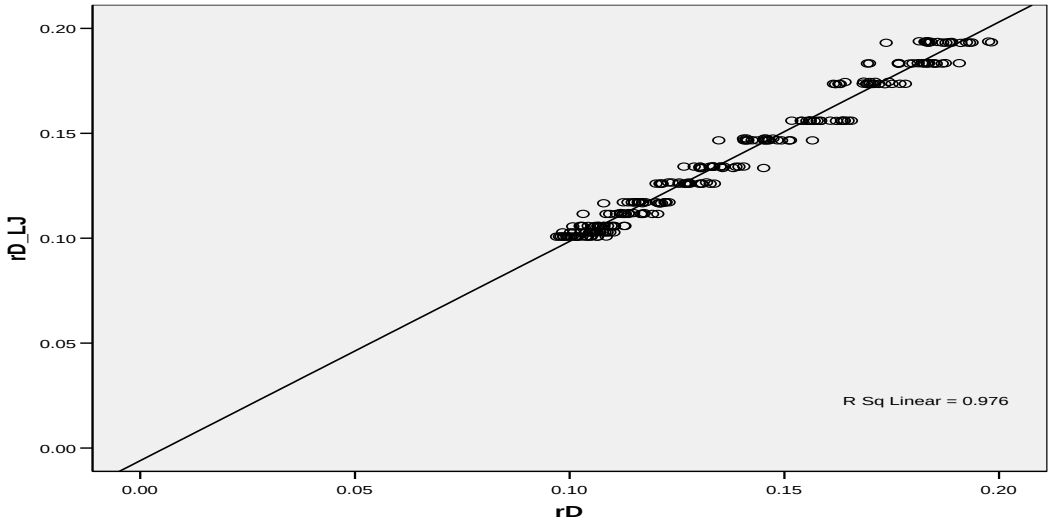

Figure 3.1.18 Liu and Jordan r_{D_LJ} regression model against measured r_D value.

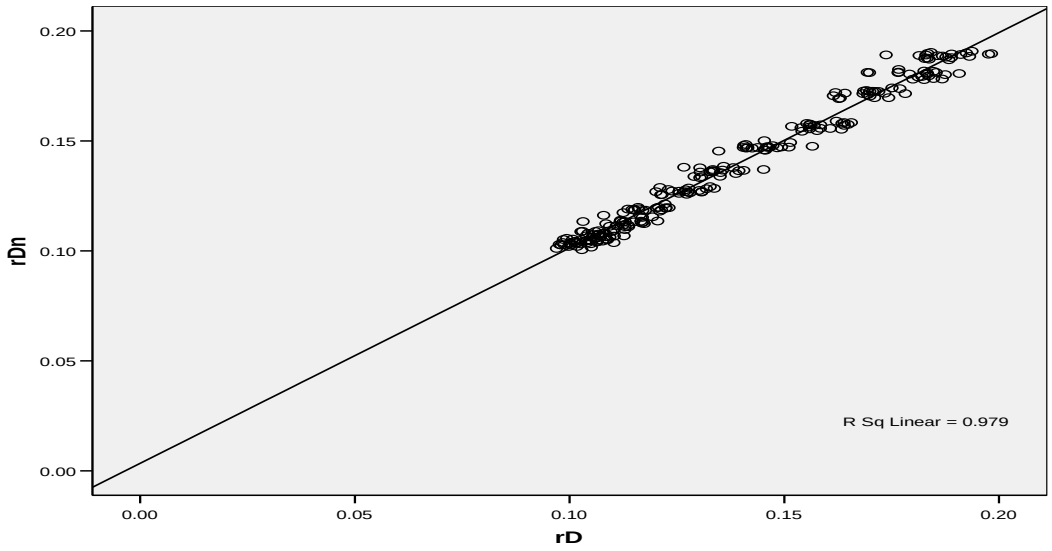

Figure 3.1.19 New proposed regression model r_{Dn} against measured r_D value.

The difference between the two models is negligible, and the proposed inclusion of $\overline{K}_T$ cannot therefore be said to bring any additional precision to the estimates produced. This was further checked by performing a similar comparison to that done by Hawas and Muneer (Hawas and Muneer 1984) for the Indian data. Measured values of r_D were plotted against $\overline{K}_T$ for two fixed values of ω_s. The results are shown in Figure 3.1.20.

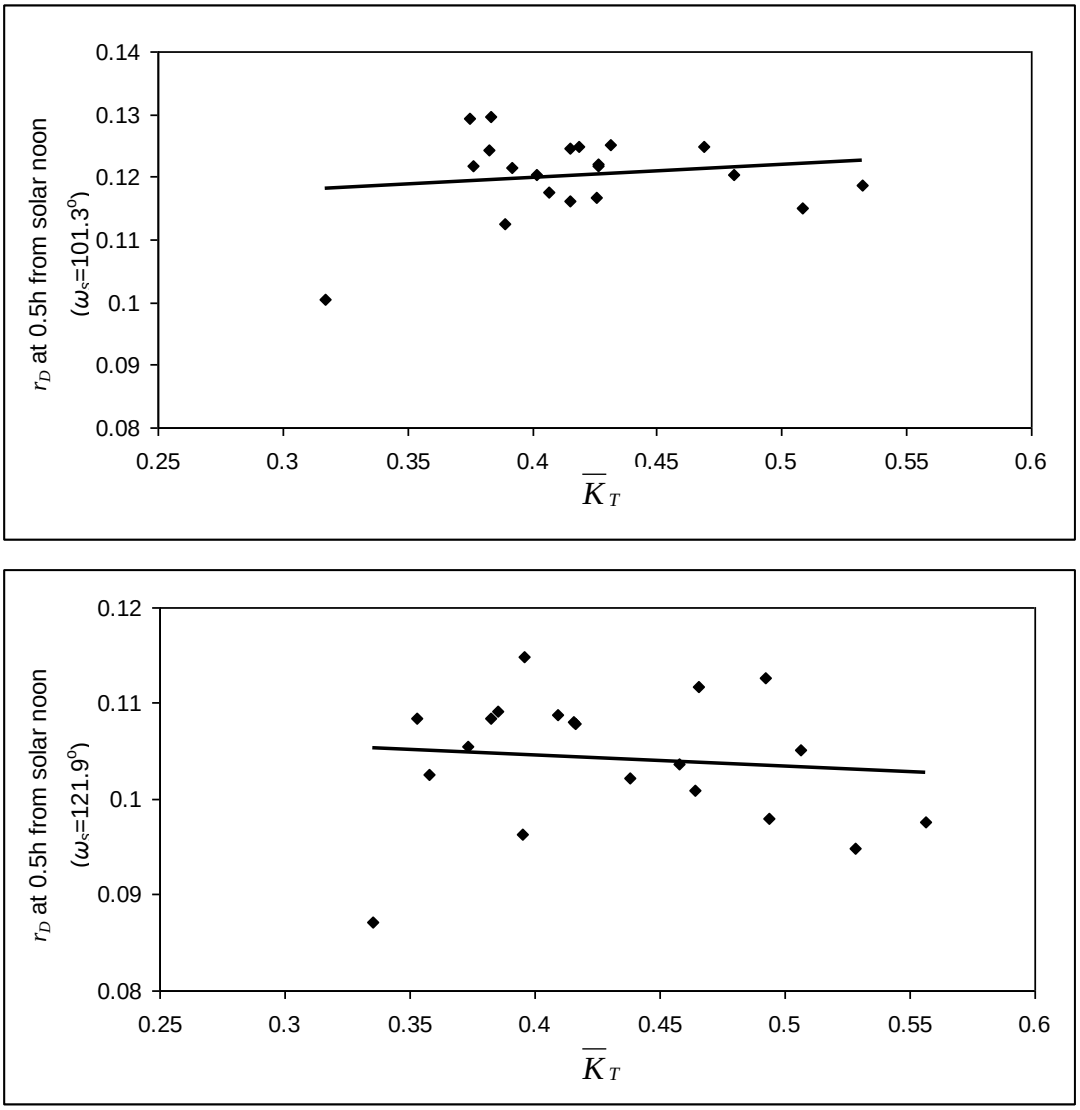

Figure 3.1.20 r_D at 0.5h from solar noon for two fixed values of ω_s for the Bracknell station.

In contrast to the Indian data shown in Figure 3.1.5, the plots for Bracknell do not show a consistent decreasing trend for r_D as a function of $\overline{K}_T$. Both are much flatter, and in the case of a sunset hour angle of 101.3°, r_D actually increases with $\overline{K}_T$. The strong correlation seen by Hawas and Muneer could be explained by the consistency of the solar climate in India compared to the much more unpredictable distribution of clear weather in the UK. These climatic differences are illustrated in Figures 3.1.21 and 3.1.22 by plotting frequencies of K_T for India and the UK.

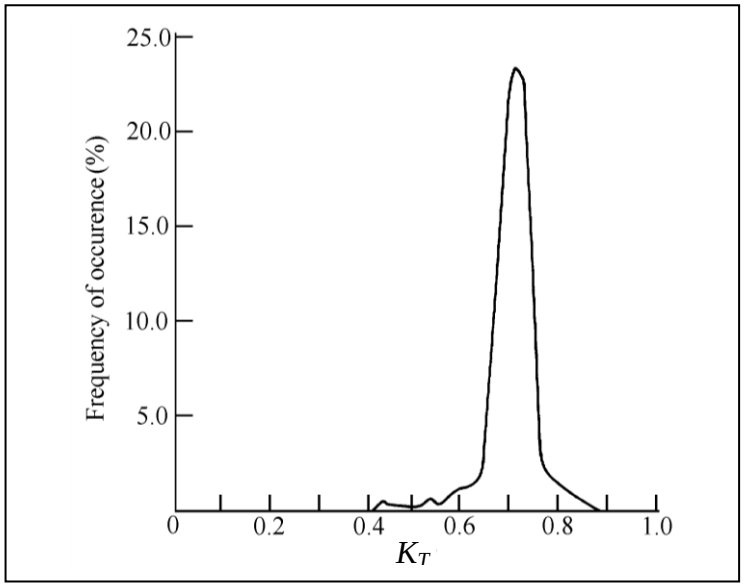

Figure 3.1.21 Frequency of occurrence of K_T for an Indian location.

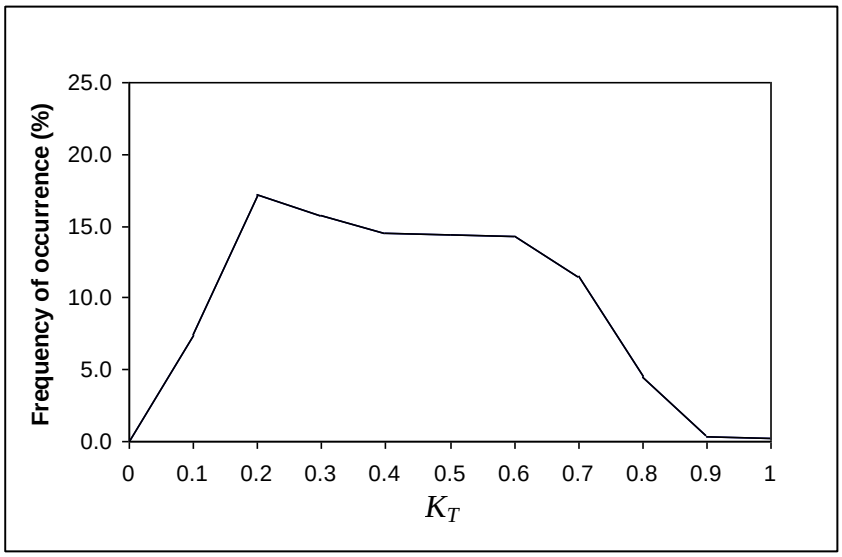

Figure 3.1.22 Frequency of occurrence of K_T for a UK location (Bracknell).

3.2 Evaluation of clear sky radiation model

Often clear sky solar radiation data are needed, such as in air-conditioning applications. In the present study, two clear sky solar radiation models were evaluated. The two chosen models were developed by Page (ESRA 2000) and Yang et. al. (Yang, Huang and Tamai 2001). These models were evaluated for four different locations namely, Aswan in Egypt, Bahrain, Gerona in Spain and Jodphur in India.

Evaluations of these models were carried out by comparing the computed values generated by the models with the site measured data. Statistical indicators were used to determine the performance of these models. Those statistical indicators are:

- the slope of the best fit regression line between computed and measured values
- the coefficient of determination value (R^2)
- the mean bias error (MBE)
- the root mean square error (RMSE).

Please refer to Chapter 2 for the detail explanation of the above mentioned statistical indicators. The main purpose of this evaluation is to provide the user with simple procedures to estimate solar radiation under a clear-sky condition. The above mentioned tests were incorporated to evaluate the accuracy of these models operating under different climatic conditions. Previous evaluations of these models by other researches such as Gueymard (Gueymard 2003a; Gueymard 2003b), Madkour *et al* (Madkour, El-Metwally and Hamed 2006), Salazar (Salazar 2011) and Tang et al (Tang, Yang, He et al. 2010) for Yang model and Ineichen (Ineichen 2006) for Page model showed that these two models were amongst the best to estimate radiation under clear-sky conditions. Reviews of these models were discussed in Chapter 2.

Note that the current evaluation offers the following additional merits:

a) Data from world-wide locations, covering a range of climates i.e. from near-arid to temperate conditions have been used.
b) A complete algorithmic approach, including the software that was expressly developed is being provided.
c) A rigorous set of statistical procedures were used to get a better understanding of the models under validations.

3.2.1 Data

Two types of data were used for this evaluation. These are measured clear-sky solar radiation data and data obtained from reputable Internet sources comprising maximum, minimum and mean daily temperature, daily relative humidity, Linke turbidity factor and daily atmospheric pressure at sea level. Detailed information about all of these data will be discussed in the following sub-sections.

3.2.1.1 Measured data

A total of four locations were selected for this evaluation study. Table 3.2.1 shows the geographical details for these locations and data period. Measured data sets for the locations were obtained by the following methods:

Table 3.2.1 Details of data used in the present evaluation.

Location	Latitude(N)	Longitude(E)	Data Period
Aswan	23.58º	32.47º	Jan.1992-Dec.1995
Bahrain	26.22º	50.65º	Mar. 2000-Jan. 2002
Jodphur	26.30º	73.01º	Jan. - Dec. 1971
Gerona	41.98º	2.81º	Jan.-Dec 1995

3.2.1.1a Jodphur, India.

The Indian Meteorological Department has published measured data of solar radiation from different locations in India (Meteorological Office 1980). Jodhpur has a predominant clear-sky climate. One year's data were extracted from the

above publication. This data set consists of daily bright sunshine duration and hourly horizontal global and diffuse solar radiation.

To select clear sky data set, daily fractional sunshine was obtained by dividing the measured sunshine duration with the astronomical day-length. A value of 0.8 for the above parameter was used as the criterion for the determination of a clear day. This value was chosen according to the WMO standard as discussed in Chapter 2. During the early and late hours of the day, the direct normal irradiance (DNI) does not exceed the above threshold criteria set by WMO. Thus by close observation of the early/late hours' irradiance it was found appropriate to set the above critical limit to a value of 0.8.

3.2.1.1b Aswan, Egypt.

The Aswan data set was provided by Dr. El-Metwally from the Physics Department of Suez Canal University in Egypt. The four-year data set (1992-1995) comprised hourly direct normal irradiance (DNI) at selected hours of 0900, 1100, 1300 and 1600 measured at local time. These data were measured by using a Link-Feussner pyrheliometer which was mounted at Aswan (Madkour, El-Metwally and Hamed 2006).

The hourly normal-incidence pyrheliometric data were converted to horizontal values using the procedure given in Chapter 2. To filter out cloudy days and part-cloudy data the beam to extraterrestrial irradiance ratio was used as the determination parameter. It will be shown in Section 3.2.1.1c that a clearness index that exceeds a value of 0.75 assures clear-sky conditions. Note that the clearness index is defined as the ratio of horizontal global- to extraterrestrial irradiance. By using regression analysis and the above discussion on clearness index it may be shown that the global- to extraterrestrial irradiance ratio of 0.8 is equivalent to the beam- to extraterrestrial irradiance ratio of 0.5. All hourly ratios of less than 0.5 were filtered out.

3.2.1.1c Bahrain

This data set was collected at the international airport at Muharaq with clear unobstructed views. The data covers a period of 22 months from March 2000 to

January 2002. The data were recorded as a joint collaboration between Edinburgh Napier University and Bahrain Meteorological Office. The dataset consists of 5-minute averaged records for four vertical surfaces with aspects of north, east, south and west and horizontal global and diffuse irradiance. Hourly-integrated data were then produced. These data were once again found to be of high quality as reported in an earlier publication by Muneer and Fairooz (Muneer and Fairooz 2002).

Clear-sky data for this location was also filtered using clearness index (ratio of horizontal global to extraterrestrial irradiance) as the determination parameter. A clearness index in excess of 0.75 was used to select clear-sky data as shown by Muneer (Muneer 2004) in the regression curves for worldwide locations.

3.2.1.1d Gerona, Spain

This data set recorded over one year (1995), was provided by the University of Gerona, Spain. The data were recorded at every eight minutes interval. Once again hourly-integrated data were created at first, and then passed through the clear-sky filter detailed above.

3.2.1.2 Data from the Internet

The different input parameters needed for incorporation within the Page and Yang models can be obtained by accessing the Internet. For the Page model, the values of Linke turbidity and atmospheric pressure are required and Figure 3.2.1 shows the flow chart for obtaining this basic data. The referred websites provide daily meteorological data. The atmospheric pressure correction used within the Page model does not make any significant difference to the final output, i.e. the estimated values were found to change by less than 0.01 percent. Hence, it is recommended that the above corrective step is ignored.

For the Yang model, parameters such as mean, maximum and minimum temperature, relative humidity and atmospheric pressure are needed to obtain Ångström turbidity coefficient, precipitable water and ozone layer (cm). The procedure to obtain all of the above input parameters is shown in Figure 3.2.2.

All files discussed in Figures 3.2.1 and 3.2.2 can be downloaded from the Education and Training on Renewable Energy Systems for Housing (ETRESH) website that is hosted by the author (http://www.etresh.eu/downloads.htm).

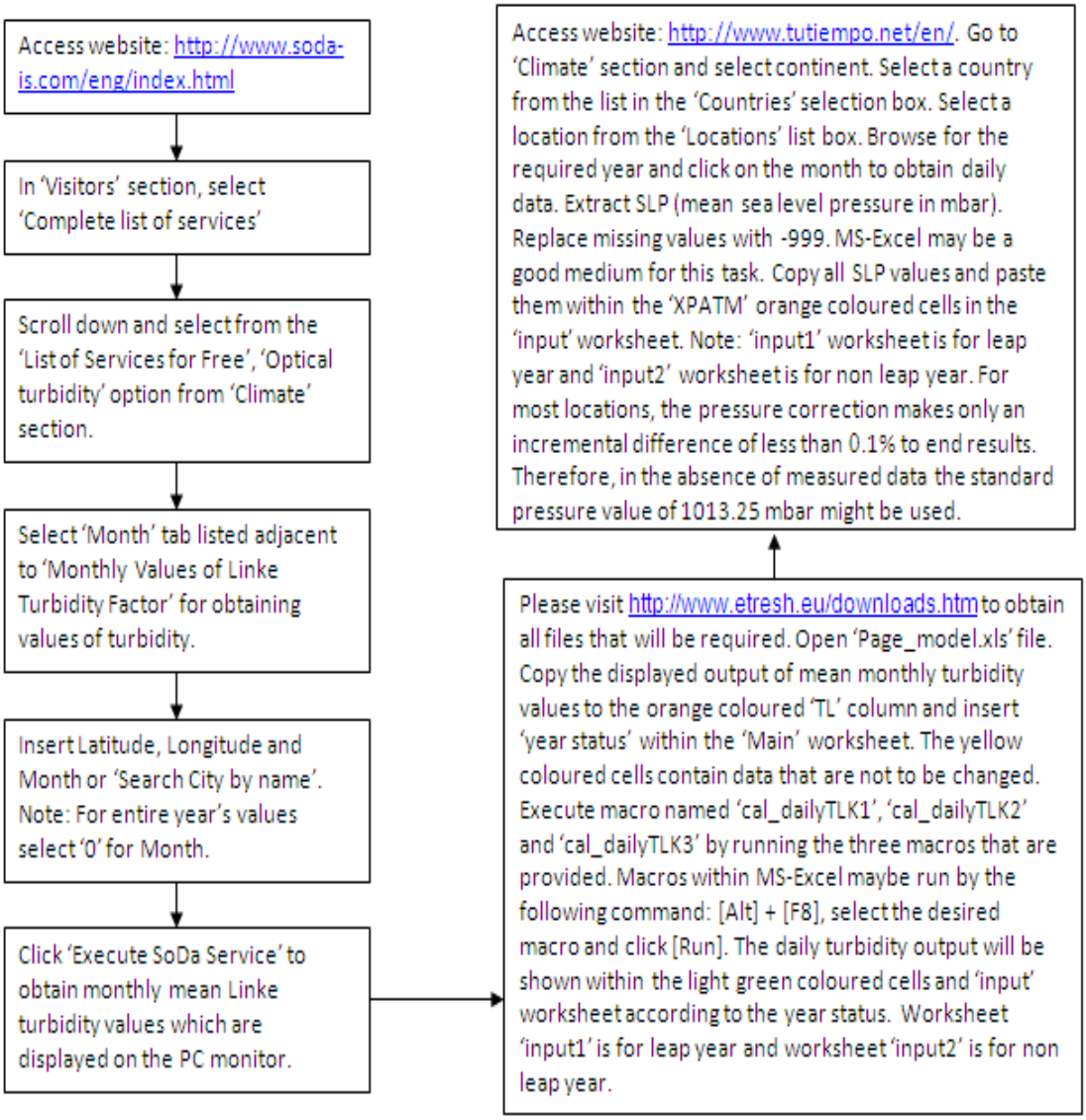

Figure 3.2.1 Flow diagram for Page clear-sky model.

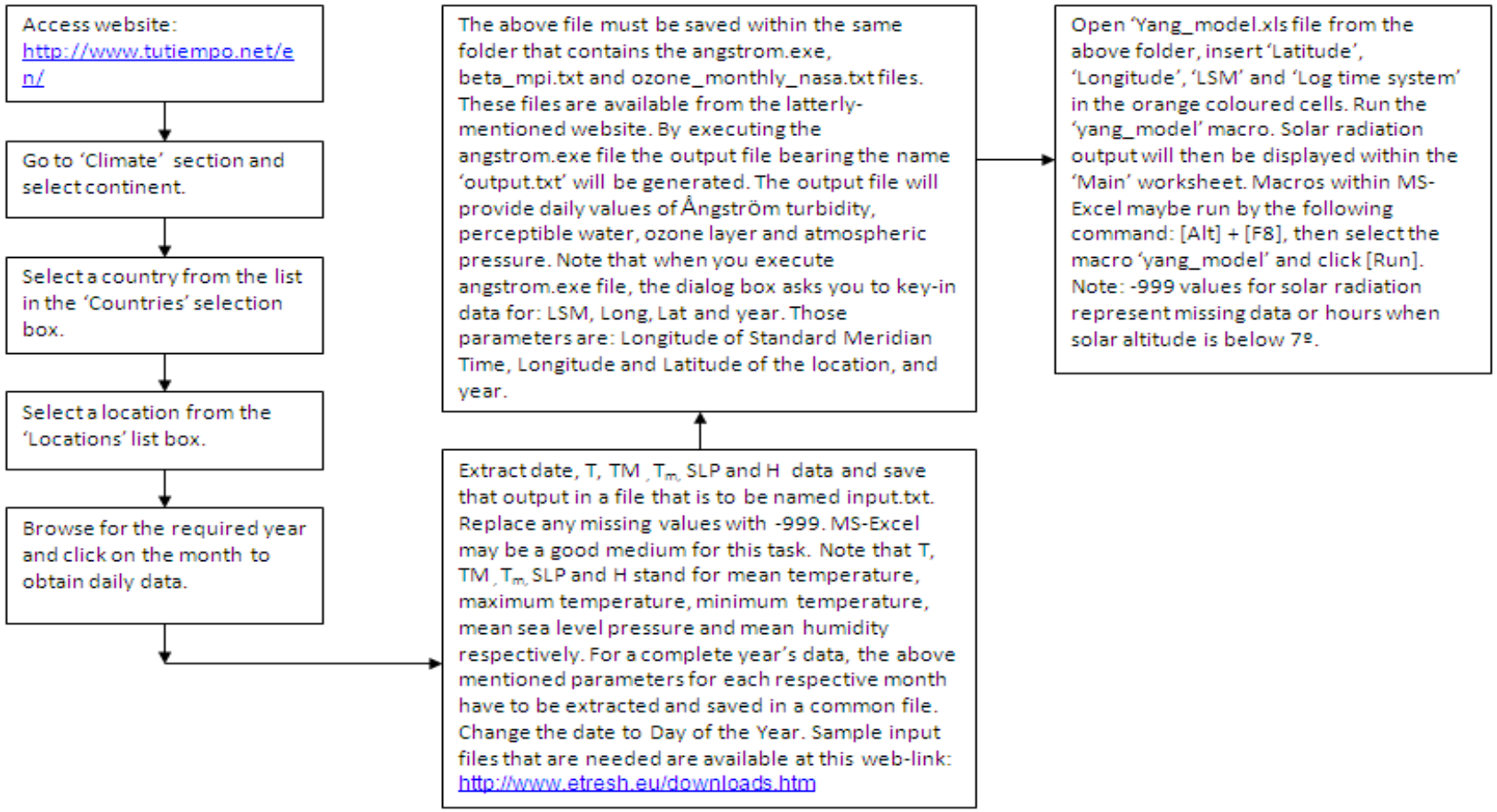

Figure 3.2.2 Flow diagram for Yang clear-sky model.

3.2.2 Results and discussions

The results of all the statistical indicators that were used to evaluate the two models are shown in Table 3.2.2. The r^2 values from the table show that the Yang model performed better than the Page model at Bahrain where the Yang model's r^2 value is 0.05 higher than that of the Page model. For Aswan and Jodphur, the Yang model's r^2 is just 0.01 higher than the Page model whereas for Gerona, the Yang model's r^2 value is 0.03 higher than the Page model. Hence, for the three latter locations both models perform with almost equal accuracy.

The averaged slope value for Aswan shows that the Page model performs better than the Yang model even though both models show slight under-estimation of computed solar radiation. Figures 3.2.3 and 3.2.4 show the scatter plots of the two models for Aswan for the year 1992. For Bahrain, the Yang model out-performs the Page model by a significant margin. Figures 3.2.5 and 3.2.6 show a sample scatter plot for Bahrain for the year 2001. The slope of the best fit-line shows that for Jodphur location, the Yang model over-estimates solar radiation by a considerable margin. However, for this location, the Page model performs very well. The corresponding scatter plots are shown in Figures 3.2.7 and 3.2.8. Lastly, for Gerona the slope values show that Page model performs better as compared to Yang model. The scatter plots are shown in Figures 3.2.9 and 3.2.10.

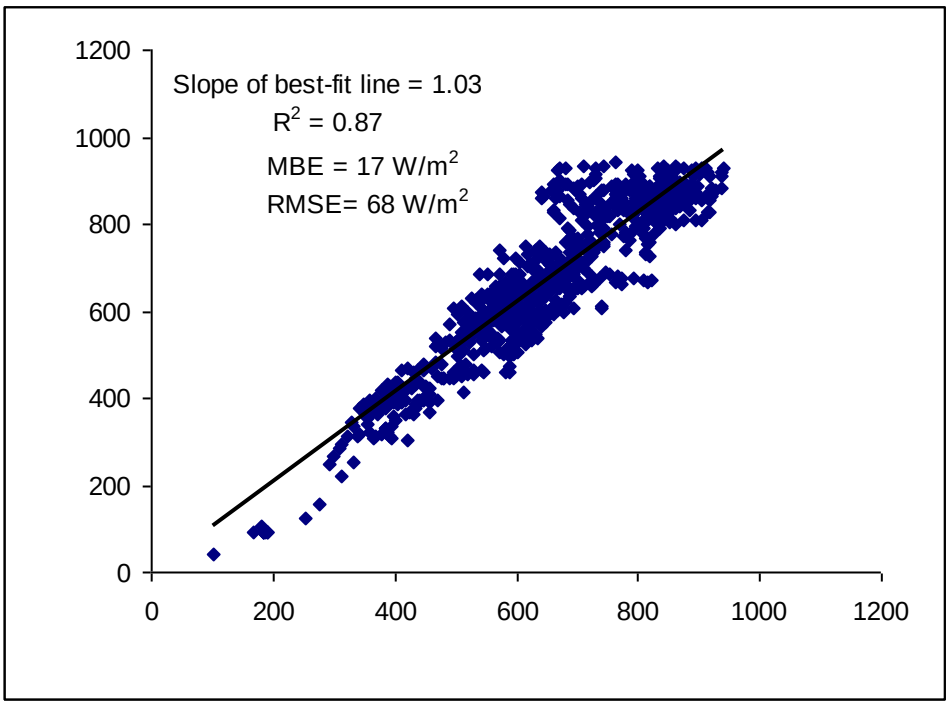

Figure 3.2.3 Page model's performance for Aswan 1992 (x-axis: measured- and Y-axis: computed irradiation, W/m^2)

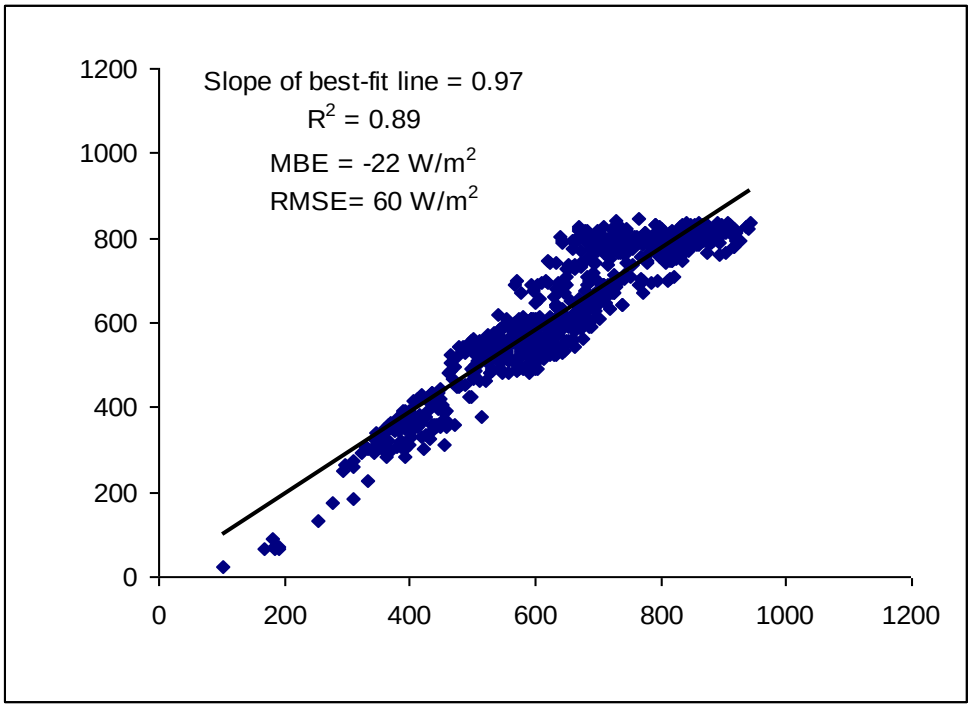

Figure 3.2.4 Yang model's performance for Aswan 1992 (x-axis: measured- and Y-axis: computed irradiation, W/m^2)

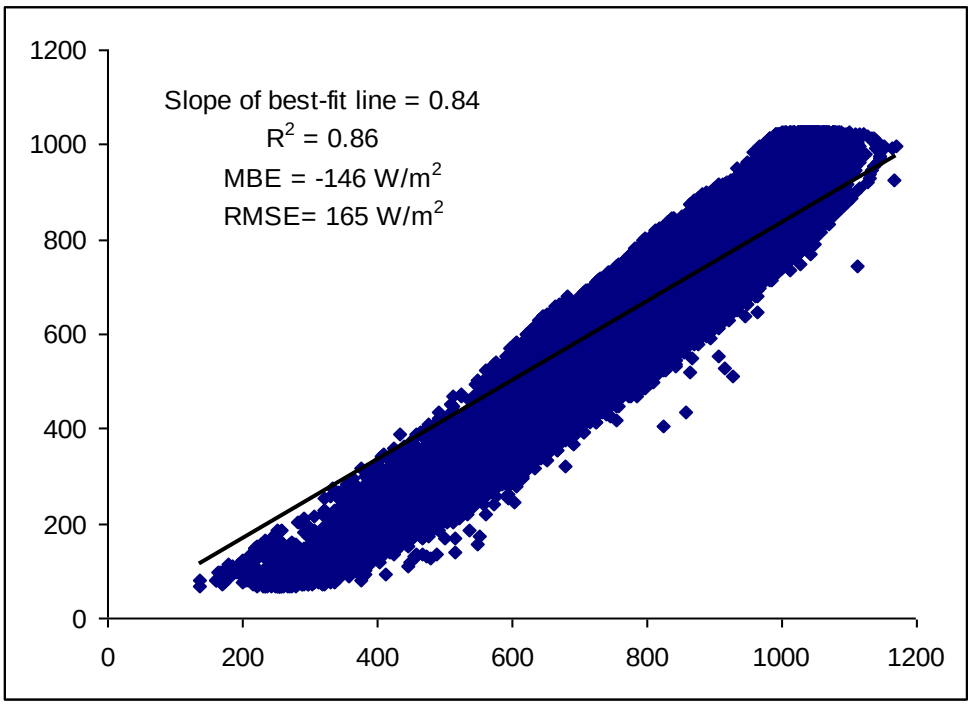

Figure 3.2.5 Page model's performance for Bahrain 2001(x-axis: measured- and Y-axis: computed irradiation, W/m^2)

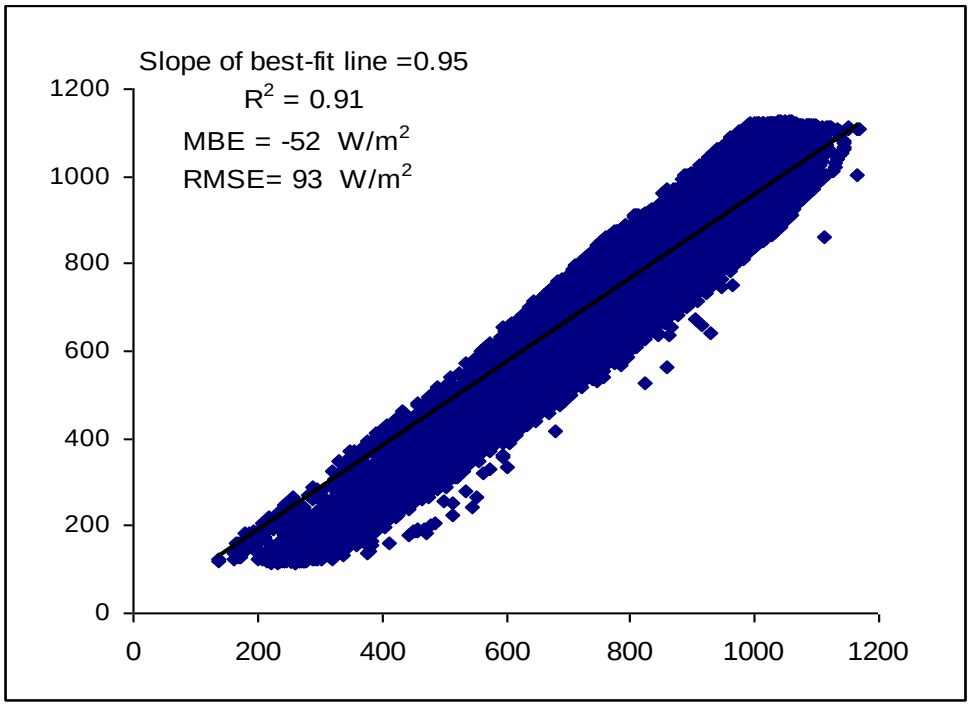

Figure 3.2.6 Yang model's performance for Bahrain 2001(x-axis: measured- and Y-axis: computed irradiation, W/m^2)

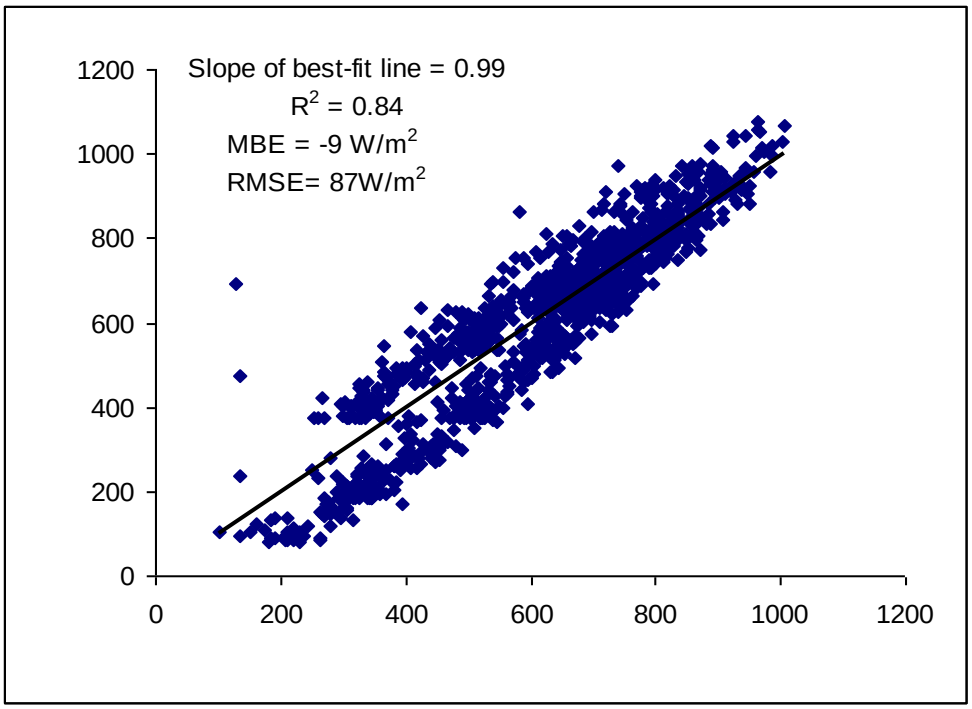

Figure 3.2.7 Page model's performance for Jodphur 1971(x-axis: measured- and Y-axis: computed irradiation, W/m^2)

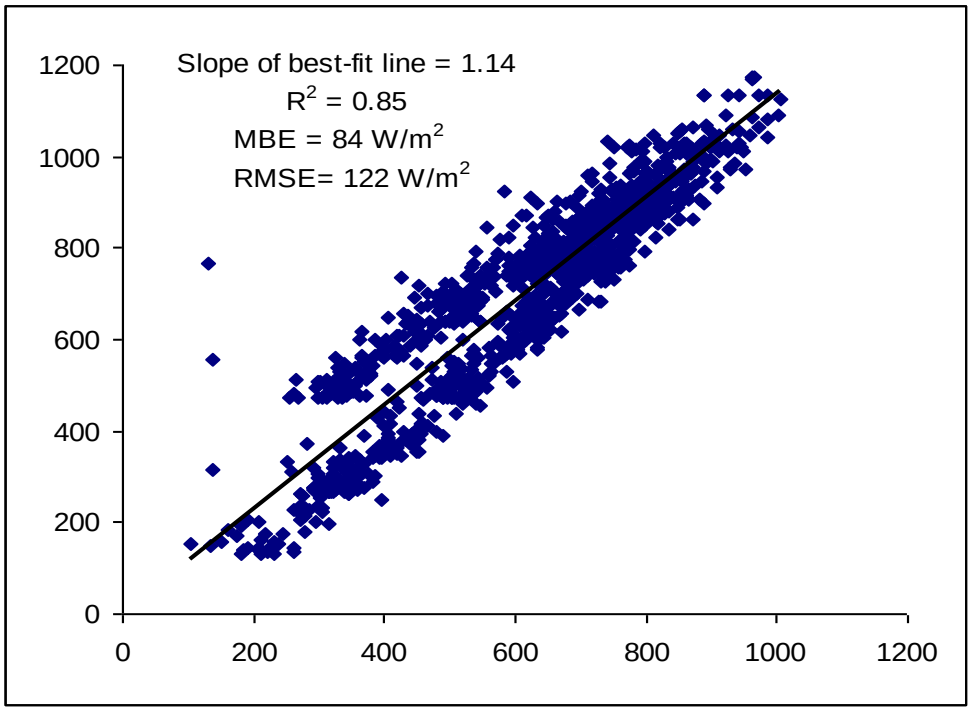

Figure 3.2.8 Yang model's performance for Jodphur 1971(x-axis: measured- and Y-axis: computed irradiation, W/m^2)

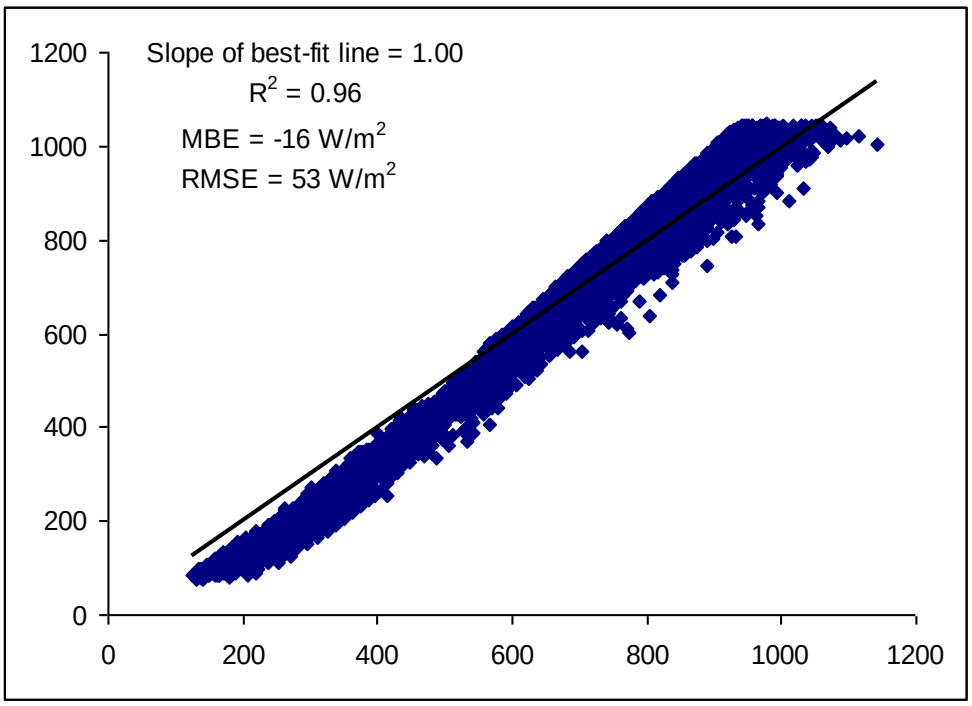

Figure 3.2.9 Page model's performance for Gerona (x-axis: measured- and Y-axis: computed irradiation, W/m^2)

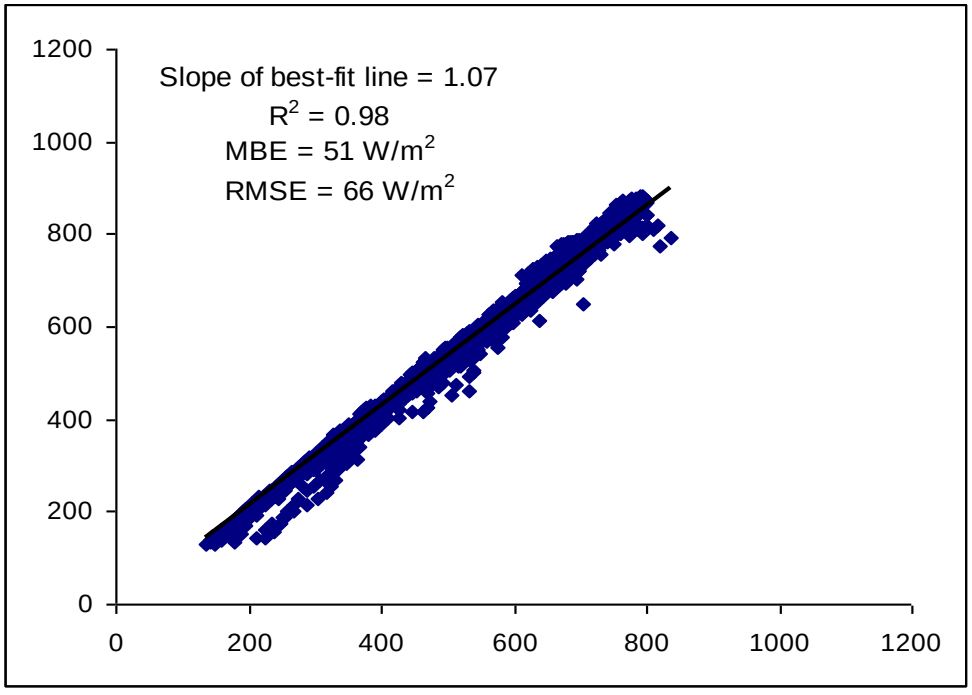

Figure 3.2.10 Yang model's performance for Gerona (x-axis: measured- and Y-axis: computed irradiation, W/m^2)

The MBE results show this parameter is in good agreement with the slope results. The Page model shows that it under-estimates solar radiation for all four locations whereas the Yang model under-estimates for Bahrain and Aswan, but over-estimates for Jodphur and Gerona. For Aswan, Jodphur and Gerona locations, the Page model performs better than the Yang model. However for Bahrain the result is the other way round and the Yang model performs better.

In Table 3.2.2, the RMSE values show that for Aswan and Jodphur locations, the Page model performs better than the Yang model. As for Bahrain and Gerona, the contrary is true.

By way of exploring the daily time series, a more detailed evaluation is shown for one location, Gerona. Three individual days were chosen from the data set where the highest daily radiation, lowest daily radiation and average daily radiation were recorded. As shown in Figure 3.2.11, it is evident that both models show good performance for days with high to mean daily radiation, although the Page model has the upper hand. As for lower daily radiation, Yang model performs better than Page model. The above findings are reinforced via data shown in Table 3.2.3.

Results from the statistical analysis, indicate that Page model performs better than the Yang model at two locations - Jodphur and Aswan. These may be explained by the fact that for these dry, semi-arid locations Linke turbidity factor plays an important role. As for Bahrain, the Yang model out-performs the Page model due to this location's proximity to sea with a more humid climate. The Yang model takes into consideration an account of precipitable water vapour as one of its main input parameters. Hence for humid climatic conditions, the Yang model is recommended. The result for Gerona shows that both models perform at the same level of accuracy. This may be due to the climate in Gerona being in between semi arid and humid.

Table 3.2.2 Results of statistical analysis.

		Page model				Yang model				
Location	**Year**	**R^2**	**Slope**	**MBE(W/m^2)**	**RMSE(W/m^2)**	**R^2**	**Slope**	**MBE(W/m^2)**	**RMSE(W/m^2)**	**No Points**
Aswan	1992	0.87	1.03	17	68	0.89	0.97	-22	60	815
	1993	0.87	0.95	-34	78	0.89	0.90	-70	94	761
	1994	0.92	0.90	-64	80	0.93	0.85	-99	109	319
	1995	0.88	0.95	-38	81	0.90	0.89	-73	96	525
	Averages	**0.89**	**0.96**	**-30**	**77**	**0.90**	**0.90**	**-66**	**90**	**2420**
Bahrain	2000	0.87	0.84	-139	158	0.92	0.96	-47	88	13696
	2001	0.86	0.84	-146	165	0.91	0.95	-52	93	20615
	2002	0.82	0.80	-123	137	0.87	0.97	-29	75	505
	Averages	**0.85**	**0.83**	**-136**	**153**	**0.90**	**0.96**	**-43**	**85**	**34816**
Jodphur	1971	**0.84**	**0.99**	**-9**	**87**	**0.85**	**1.14**	**84**	**122**	**1127**
Gerona	1995	**0.96**	**1.00**	**-16**	**53**	**0.98**	**1.07**	**51**	**66**	**6695**

Table 3.2.3 Comparison of three selected daily values.

	Page model		Yang model		Daily total (kWh/m^2)
	MBE(W/m^2)	**RMSE(W/m^2)**	**MBE(W/m^2)**	**RMSE(W/m^2)**	
Highest daily value	8	39	71	80	12.75
Mean daily value	-12	23	73	75	8.07
Lowest daily value	-59	59	20	27	2.47

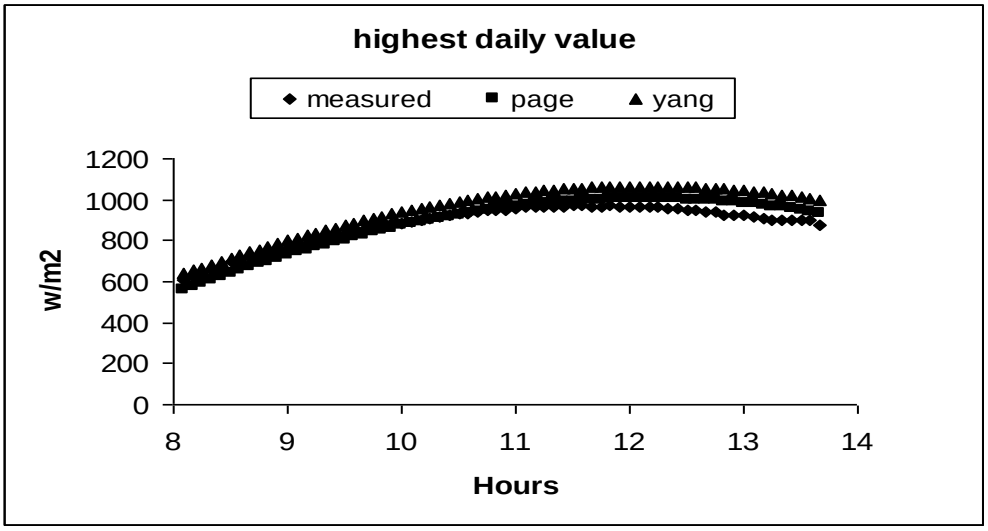

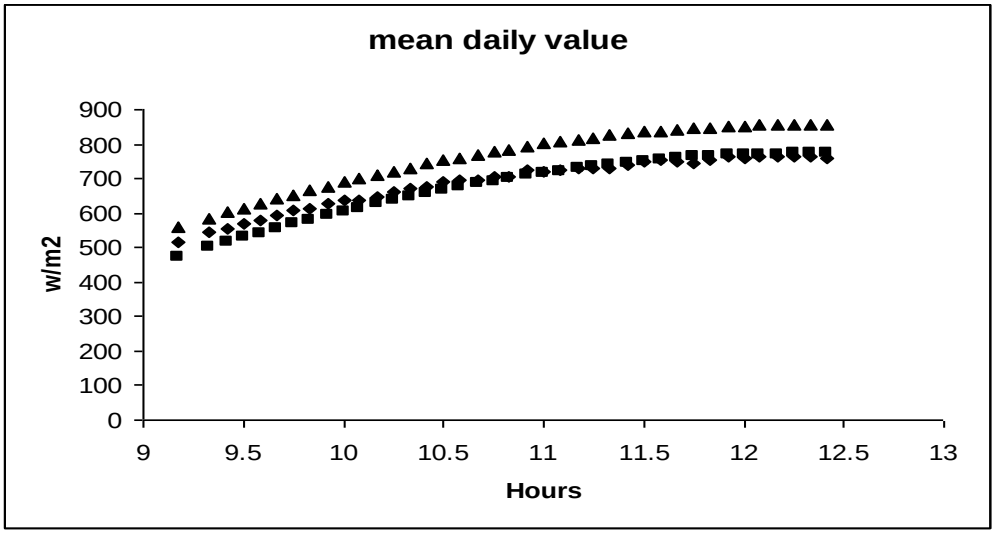

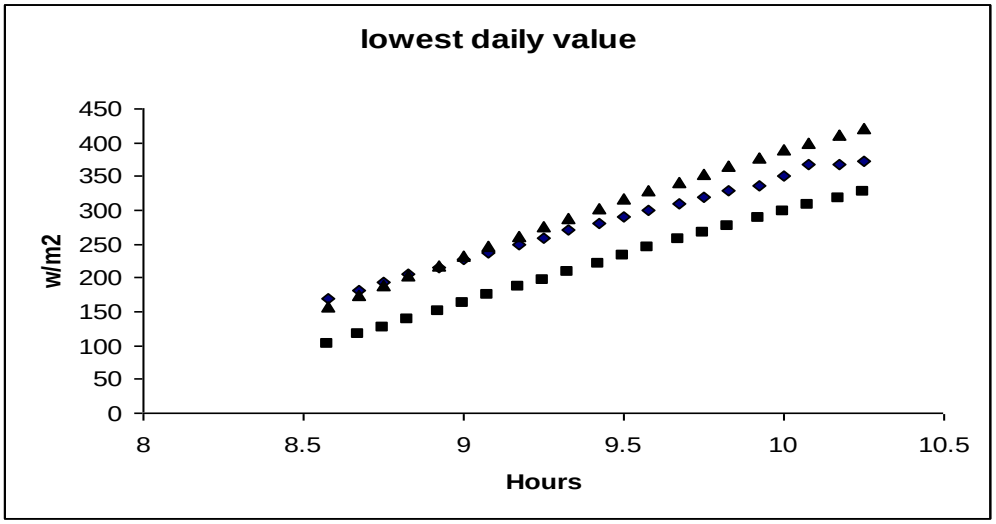

Figure 3.2.11 Daily values time series plots.

It is evident that both models did not perform well in estimating solar irradiation below 400 W/m^2 as shown in Figures 3.2.3 to 3.2.10. This may be due to seasonal effects such as low solar elevation during winter and hence higher air mass with consequential larger attenuation of beam irradiance. This is further illustrated in Figure 3.2.11 where the lowest daily values for a winter day and the highest values observed for a summer day.

Future research may be undertaken using a combination of the Linke turbidity, precipitable water vapour and ozone layer data so that a truly universal clear-sky radiation model could be developed. Furthermore, seasonal effects may be taken into consideration as well.

3.3 Evaluation of simple all-sky model to estimate solar radiation for United Kingdom

In this section, the all-sky model developed by Yang *et al* (Yang 2001) which uses widely available input parameters such as temperature and precipitation was chosen. A comparison was also carried out at the end of this evaluation with the Meteorological Radiation Model (MRM) developed and rigorously tested by Muneer *et al* (Muneer, Gul, Kambezedis et al. 1996; Muneer, Gul and Kambezedis 1998; Muneer and Gul 2000)

Evaluations of this model were carried out by comparing the computed values generated by the model with the site measured data, as reported by the UK Meteorological Office. Statistical indicators were used to determine the performance of this model. Those statistical indicators are:

- the slope of the best fit regression line between computed and measured values
- coefficient of determination value (r^2) for the above best fit line
- mean bias error (MBE)
- root mean square error (RMSE).

The above mentioned tests were incorporated to evaluate the accuracy of the above mentioned models operating under different sky conditions. Previous

evaluations of this model by other researches such as Gueymard (Gueymard 2003a; Gueymard 2003b) and Madkour *et al* (Madkour 2006) showed that the Yang model was amongst the best to estimate radiation.

3.3.1 Data

Two types of data were used for this evaluation study. These are measured solar radiation data and data obtained from reputable Internet sources comprising maximum, minimum and mean daily temperature, daily relative humidity and daily atmospheric pressure at sea level. Detailed information about all of these data will be presented in the following sections. Note that review of these two models were discussed in Chapter 2.

3.3.1.1 Measured data

The present dataset for UK is the one used by the UK Chartered Institution of Buildings Services Engineers (CIBSE) for the production of its Guides A & J. Long term hourly data from across the UK from three locations spanning a wide range of latitude from the lowest at 50º37'N to the highest at 58 º22'N was used for the above purpose. T Muneer coordinated the work of CIBSE's solar data task group and in that capacity he was responsible for undertaking the data quality control. The reader is referred to Muneer and Fairooz (Muneer and Fairooz 2002) for further details. The time periods covered by the station subsets range from 1991 to 1994. Table 3.3.1 shows the list of the data that have presently been used. Note that sunshine data for Camborne was extracted from a nearby station, i.e. Plymouth.

Table 3.3.1 Details of data used in the present study.

Location	**Latitude**	**Longitude**	**Data Period**
Camborne	50.37º(N)	5.53º(W)	1991-1994
London	51.51º(N)	0.12º(W)	1991-1994
Stornoway	58.22º(N)	6.23º(W)	1991-1994

3.3.1.2 Data from the Internet

For the Yang model, parameters such as mean, maximum and minimum temperature, relative humidity and atmospheric pressure are needed to obtain Ångström turbidity coefficient, precipitable water and ozone layer thickness (cm). These parameters were extracted from the http://www.tutiempo.net/en/ website.

3.3.2 Results and discussions

Results of statistical evaluations of the Yang model for UK locations are shown in Table 3.3.2. The slope of the best fit line for all locations show that the model over-estimates solar radiation. London shows the highest over-estimation and Stornoway the lowest. The r^2 value for Camborne shows that the model does not perform well. This is attributed to the distance of the location where sunshine duration input parameter was extracted, i.e. Plymouth. For the remaining two locations, the r^2 values show that the model performs satisfactorily with the average values of 0.91 for London and 0.80 for Stornoway.

Table 3.3.2 Statistical performance for hourly radiation estimation for UK locations - Yang model

Location	Year	Slope	r^2	MBE(W/m^2)	RMSE(W/m^2)
Camborne	1991	1.15	0.67	63	160
	1992	1.11	0.71	49	150
	1993	1.11	0.68	52	152
	1994	1.14	0.70	58	155
	Average	**1.13**	**0.69**	**56**	**154**
London	1991	1.24	0.91	65	108
	1992	1.23	0.92	61	104
	1993	1.20	0.91	56	100
	1994	1.20	0.91	58	103
	Average	**1.22**	**0.91**	**60**	**104**
Stornoway	1991	1.12	0.80	36	105
	1992	1.11	0.81	33	103
	1993	1.10	0.79	30	102
	1994	1.12	0.81	40	106
	Average	**1.11**	**0.80**	**35**	**104**

The MBE values show good agreement with the slope value where Stornoway has the lowest average value of over-estimation which is 35 W/m^2, follow by Camborne with the average value of 56 W/m^2 and lastly London with the highest average value of 60 W/m^2. As for the RMSE values, Camborne has the highest average value of 154 W/m^2 which is caused by data related problems mentioned before. The remaining two stations have the same average value which is 104 W/m^2. This shows that the RMSE values are in good agreement with the r^2 values. Figures 3.3.1 to 3.3.3 show one year performance plot for all locations under discussion.

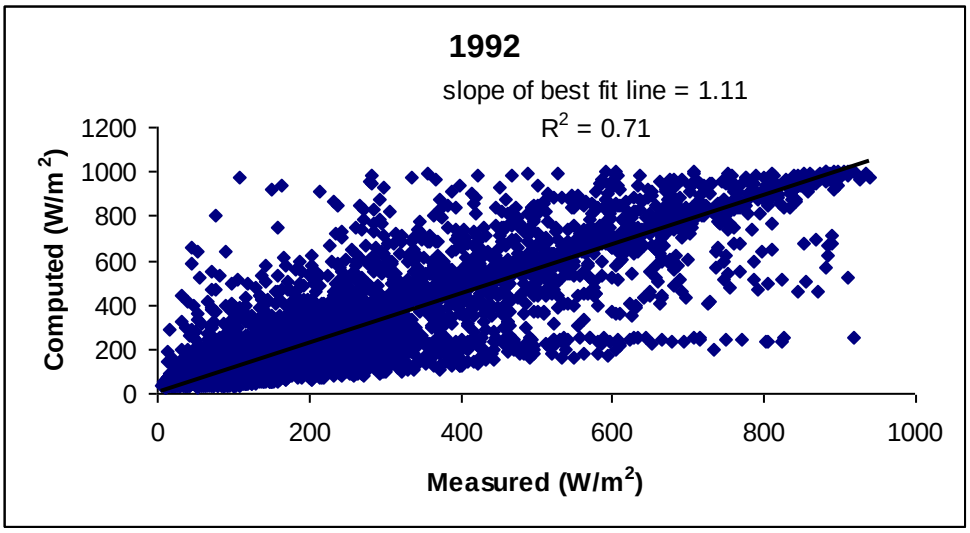

Figure 3.3.1 Yang model's performance for Camborne.

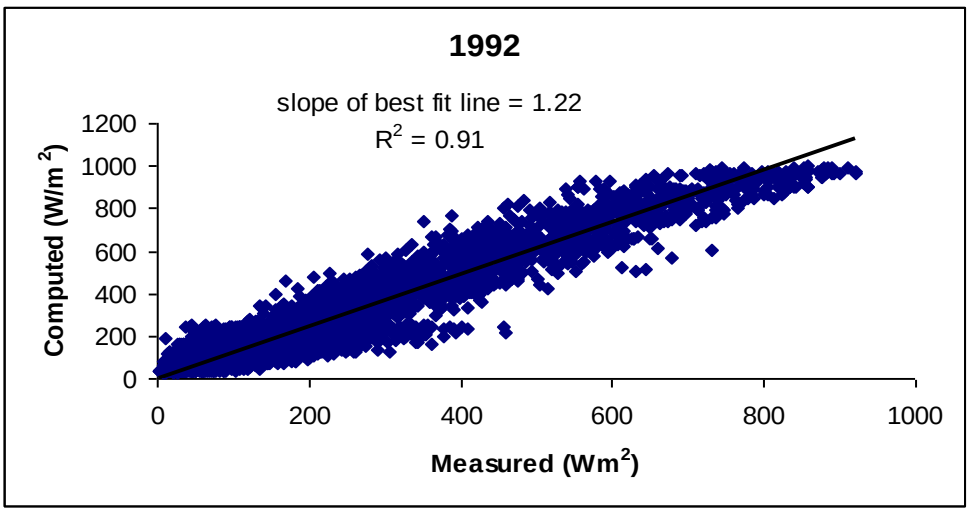

Figure 3.3.2 Yang model's performance for London.

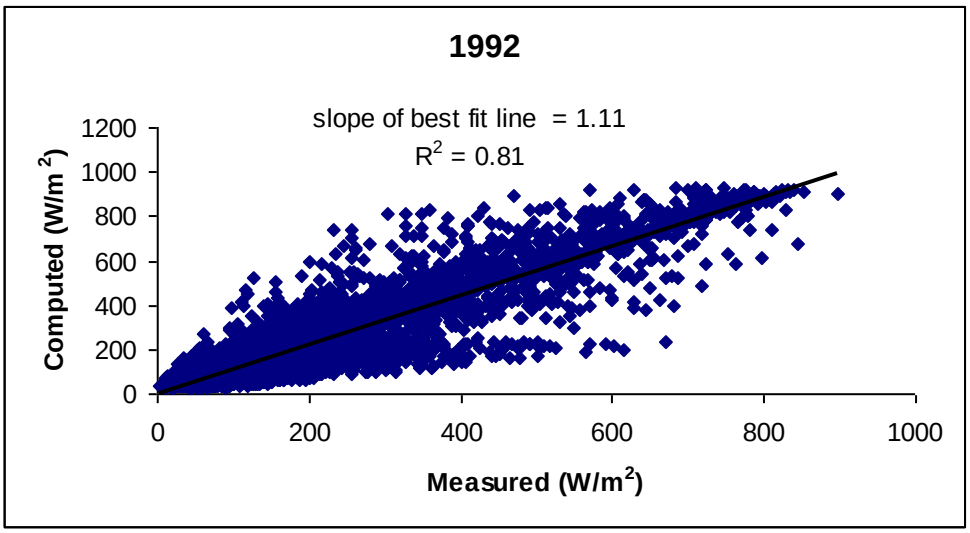

Figure 3.3.3 Yang model's performance for Stornoway.

An in-depth comparison of the Yang model and the MRM was carried out for all stations. Table 3.3.3 to 3.3.7 show side by side comparison of the models. The comparisons were carried out by dividing radiation data into five bands which were 0 to 200 W/m^2, 200 to 400 W/m^2, 400 to 600 W/m^2, 600 to 800 W/m^2 and 800 to 1000 W/m^2. Note that the MBE and RMSE were expressed in percent in Table 3.3.3 to 3.3.7.

Table 3.3.3 Models comparison at 0 to 200 W/m^2 radiation range.

		MBE(%)		**RMSE(%)**	
Location	**Year**	Yang	MRM	Yang	MRM
Camborne	1991-92	47	31	108	63
	1993-94	50	41	108	79
London	1991-92	32	33	61	50
	1993-94	32	36	61	58
Stornoway	1991-92	28	11	68	39
	1993-94	31	15	53	44

Table 3.3.4 Models comparison at 200 to 400 W/m^2 radiation range.

		MBE(%)		RMSE(%)	
Location	**Year**	Yang	MRM	Yang	MRM
Camborne	1991-92	26	8	67	32
	1993-94	24	9	65	35
London	1991-92	23	13	41	23
	1993-94	18	13	39	29
Stornoway	1991-92	12	4	47	18
	1993-94	13	9	46	20

Table 3.3.5 Models comparison at 400 to 600 W/m^2 radiation range.

		MBE(%)		RMSE(%)	
Location	**Year**	Yang	MRM	Yang	MRM
Camborne	1991-92	14	-0.4	41	26
	1993-94	14	5	42	28
London	1991-92	28	10	35	17
	1993-94	25	7	33	15
Stornoway	1991-92	11	-4	34	12
	1993-94	10	-4	33	11

Table 3.3.6 Models comparison at 600 to 800 W/m^2 radiation range.

		MBE(%)		RMSE(%)	
Location	**Year**	Yang	MRM	Yang	MRM
Camborne	1991-92	8	-4	26	10
	1993-94	5	-4	26	12
London	1991-92	21	7	24	7
	1993-94	19	7	22	5
Stornoway	1991-92	11	-2	20	5
	1993-94	8	-4	20	5

Table 3.3.7 Models comparison at 800 to 1000 W/m^2 radiation range.

		MBE(%)		RMSE(%)	
Location	**Year**	Yang	MRM	Yang	MRM
Camborne	1991-92	-0.3	-8	23	16
	1993-94	4	-8	16	19
London	1991-92	12	2	13	16
	1993-94	12	4	13	7
Stornoway	1991-92	7	-5	11	10
	1993-94	7	-4	8	10

For the 0 to 200 W/m^2 radiation range, both models show poorer performance with high MBE and RMSE values. The Yang model has the highest values of 50 and 108 percent respectively. On the other hand, the MRM has the corresponding values of 41 and 79 percent respectively. The 0-200 W/m^2 radiation band includes data under overcast sky. Note that nearly all radiation predictive models tend to collapse under overcast conditions due to their inability to differentiate between thin and heavy overcast. Either of the two weather parameters, i.e. sunshine (= 0 hours) and cloud-cover (8 oktas) would suggest overcast condition without providing any further information on their type, colour or amount of layers. Both models show improvement in their performance as the radiation range increases.

In the 400-600 W/m^2 range, an improved performance from both models was observed. Specifically, the MBE of the MRM was 10 percent in this range compared to 41 percent in the 0-200 W/m^2 range, and the RMSE measure was also improved at 28 percent compared to 79 percent in the lower energy band. A similar improvement is observed in the case of the Yang model. However, an increasing tendency for the MRM to under-estimate the solar irradiation at higher radiation levels was observed. This is evident from Tables 3.3.3-3.3.7 in which the value of MBE for the MRM drops further below zero in each successively higher radiation range. In contrast, the statistics for the Yang model both tend towards zero, indicating a gradual improvement in performance as the absolute radiation level increases.

Despite the contrasting behaviour of the models with increasing absolute radiation, the RMSE figures indicate that the MRM still outperforms the Yang model in all of the selected radiation ranges. Because the RMSE represents an absolute deviation from the expected behaviour, the consistently lower RMSE values for the MRM indicate better performance regardless of whether the error is positive (over-estimation) or negative (under-estimation).

The poorer performance of the Yang model is attributed to the UK sky conditions. Since it is derived from its clear-sky model, the Yang model would not be expected to perform well where the clearness index (K_T) is less than 0.75, the benchmark set by Muneer (Muneer 2004) using regression curves for

worldwide locations. Figures 3.3.4-3.3.6 show that the clearness index in all of the UK locations used here rarely exceeds this threshold.

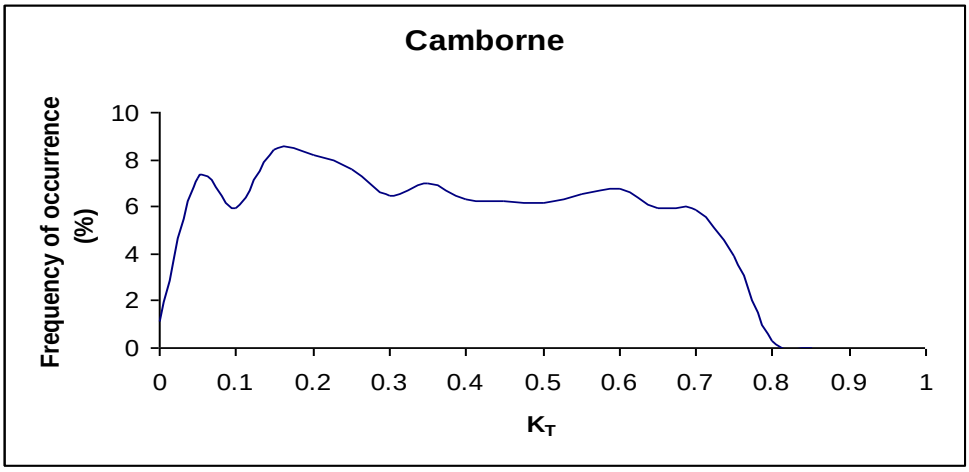

Figure 3.3.4 Clearness index for Camborne.

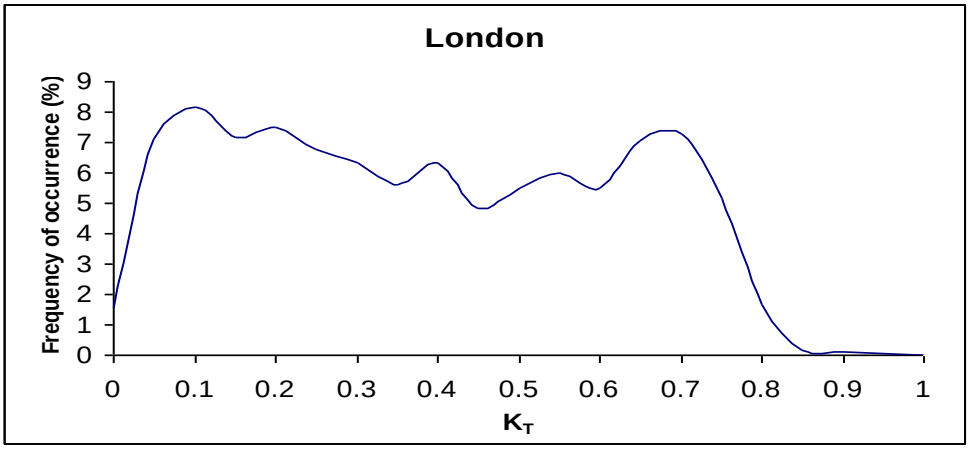

Figure 3.3.5 Clearness index for London.

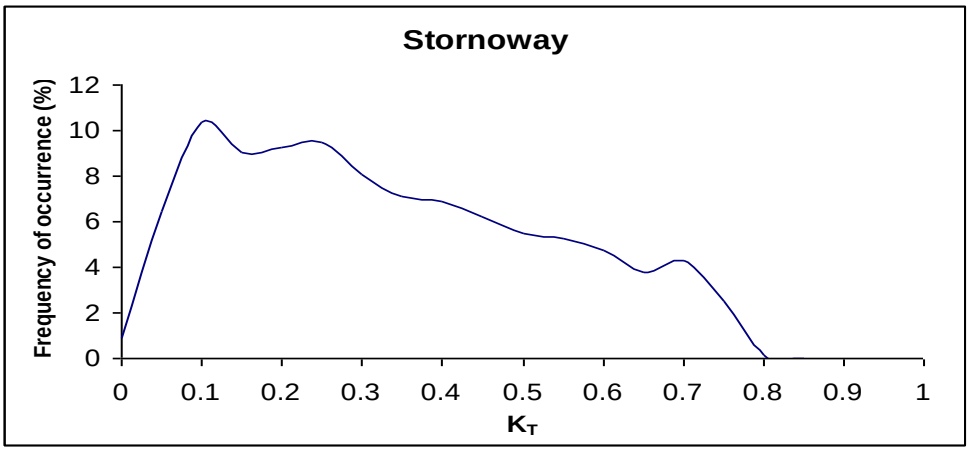

Figure 3.3.6 Clearness index for Stornoway.

As discussed earlier, accurate estimation of solar irradiation at lower radiation levels is a challenge for any model. Figures 3.3.7-3.3.9 show the distribution of measured solar radiation at all three locations during the period one year, an average of 3723 distinct values. Above 400 W/m^2, both the MRM and the Yang model perform well, but would therefore only provide reasonably reliable estimates for the UK in fewer than 50 percent of cases given the available energy. In the 200-400 W/m^2 range, however, the MRM shows a distinctly better performance than the Yang model, and this is an advantage in the UK where an average of 25.6 percent of radiation falls into that range.

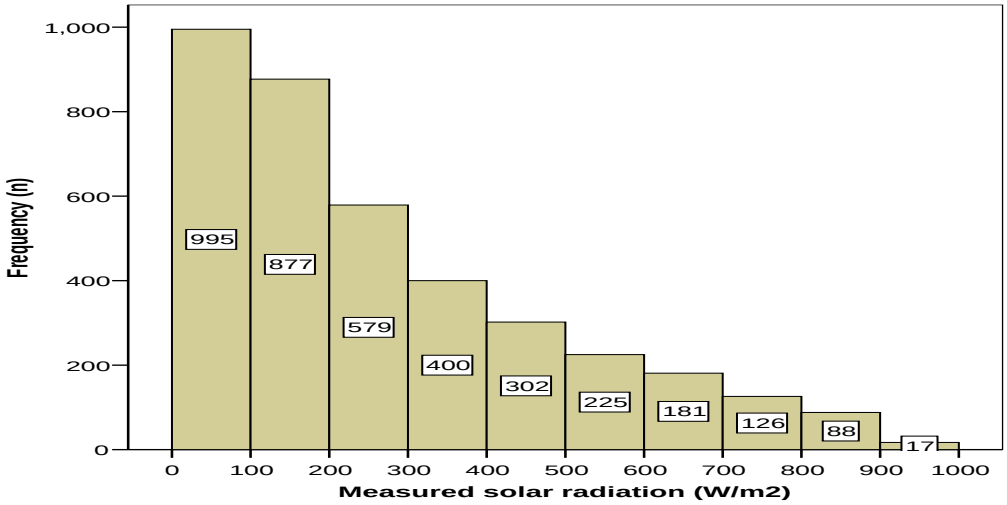

Figure 3.3.7 Measured radiation distribution for Camborne.

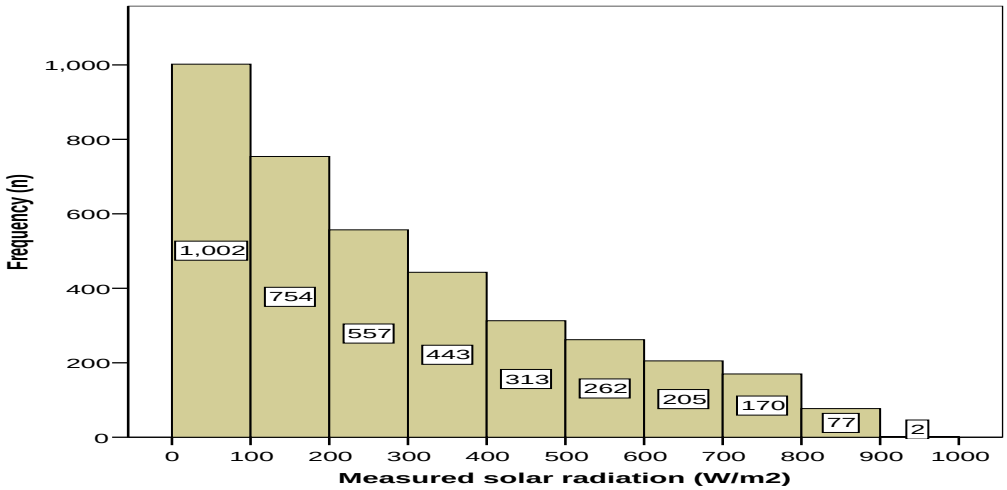

Figure 3.3.8 Measured radiation distribution for London.

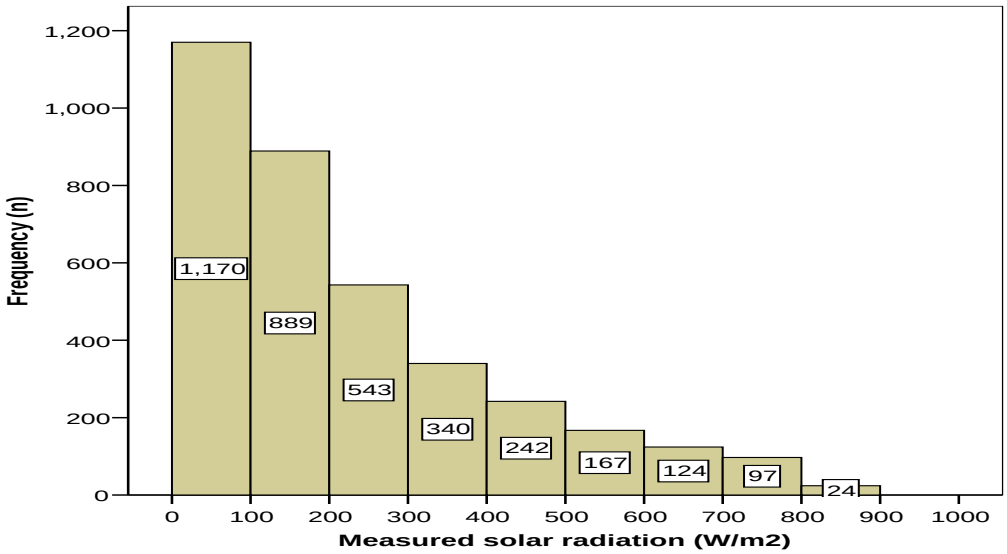

Figure 3.3.9 Measured radiation distribution Stornoway.

All the programmes used in this chapter have been uploaded to the Education and Training on Renewable Energy Systems for Housing (ETRESH) website: http://www.etresh.eu/downloads.htm. This website is free and everyone is welcome to use all the programmes listed on the website's [Download] section.

3.4 Conclusions

From the evaluation works above, the following conclusions were drawn:

1. The Liu-Jordan model performs well for estimating the average hourly global and diffuse radiation. At the individual hourly level however, a number of problems were observed. At low sunset angles, the values predicted by the model were less reliable. Given the low absolute solar energy available at such angles though, this was not seen as a major defect.

Local .meteorological conditions appear to have an effect as demonstrated by the investigation of the effect of $\overline{K}_T$ on the calculated values. A consistent effect of $\overline{K}_T$ was not evident from the UK data in contrast to earlier findings from other locations.

A general weakness, however, was the model's inability to take account of the asymmetric distribution of radiation across solar noon. Because of this it

underestimates global and diffuse radiation before noon and overestimates after noon for most of the UK locations. These observations are in agreement with Hawas and Muneer (Hawas and Muneer 1984) who were using data from recording stations in India. This particular weakness of the Liu-Jordan model cannot therefore be assumed to be location-specific, since it is evident in data from such widely different climates.

2. For clear-sky models, the Page model performs better than the Yang model in semi-arid interior climatic locations as shown in the Aswan and Jodphur results. As for the Yang model, it performs better than Page model in high humidity locations such as Bahrain. For mild climatic locations like Gerona, both models show good results. Hence, this can be concluded that for semi-arid interior climatic conditions Page model is suitable to be used and for humid climates Yang model is recommended. It has also been proposed that there is room for further improvement of the two models under discussion.

3. From the comparison of two all-sky solar radiation models, a consistently better overall performance was observed for the MRM than for the Yang model. In the 200-400 W/m^2 range, the higher accuracy of the MRM was particularly evident, which makes it the more suitable for use in the UK where conditions are frequently overcast and radiation levels typically fall below 400 W/m^2. Hence this evaluation once again supports that the MRM is the most suitable model for estimating solar radiation for UK.

Table 3.3.8 below shows the summary of the applicability of each model which has been evaluated in this chapter.

Table 3.3.8 Summary of model's applicability.

Model	**Application**
Liu and Jordan	Decomposes average daily to average hourly data for all climatic conditions.
Page clear sky	Semi-arid interior climatic condition.
Yang clear sky	Humid climate condition.
MRM	For the UK.

4.0 Temperature and solar radiation relation

Note that the work in this section has been carried out in collaboration with Eulalia Jadraque Gago from University of Granada, Spain.

Solar radiation affects the earth's weather processes which determine the natural environment as previously discussed in Chapter 2. Thus it is important to be able to understand the physics of solar radiation and in particular to determine the amount of energy intercepted by the earth's surface. The initial research related to solar radiation carried out by Ångström (Angstrom 1924) and others was concerned with the relationship between irradiation and the sunshine duration. Since then research in this field has come a long way. Today, a considerable amount of information is available on mathematical models that relate solar radiation to other meteorological parameters such as temperature, cloud-cover, rain amount, humidity and even visibility. However, the parameter that has the largest measurement network is the ambient temperature. The aim of this work is to investigate the inter-relationship between:

- Mean-daily solar radiation and mean, maximum and minimum temperature,
- Daily mean, maximum and minimum temperature, and
- Hourly temperature and the corresponding mean-daily maximum and minimum temperature.

4.1 Introduction

The understanding of the climatological study of radiation is however comparatively new. Until 2010 there were only three stations in northwest Europe with irradiation records exceeding an 85-year period. In the UK it was only in the 1950s that the Meteorological Office installed Kipp solarimeters. By contrast, however, temperature has been recorded the world over at very many locations and for a much longer period, e.g. the oldest records for temperature for Central England have existed since 1659! In India, to give another example, the number of sites with temperature records is 161, but only 18 stations

measure irradiation. Likewise, respectively, in Malaysia and Spain there exist 41- and 113 stations that measure temperature, but only 9- and 33 stations record irradiation. Table 4.1.1 provides information on the start dates for temperature records for England.

Table 4.1.1 Start dates for temperature measurement for Central England.

Year	Parameter recorded
1659	Monthly-mean temperature
1772	Daily-mean temperature
1878	Daily- and monthly-mean, maximum and minimum temperature

It has also been pointed out by Thorton and Running (Thornton and Running 1999) and Rivington et al (Rivington M., Matthews K.B. and K. 2002) that even in the most developed countries such as the US and Britain the landmass area covered by solar radiation network is less than 1%. Globally this figure is much less.

Solar irradiation availability of arbitrary surfaces is a prerequisite in many sciences. For example, agricultural meteorology, photobiology, animal husbandry, daylighting, comfort air-conditioning, building sciences and solar energy utilisation, all require this information. For most of the above applications monthly-averaged or daily solar radiation data is adequate.

The worldwide use of energy is rising by 2.5% a year, most of which is attributable to the accelerated consumption in the developed and now developing countries. It has been estimated that, from a sustainability viewpoint the developed countries will have to cut their use of energy by a factor of 10 within a generation. Proponents of solar energy have gone to the extent that they are calling for a complete substitution of conventional sources of energy with renewables. Their thesis is that the use of fossil fuels for energy production, even in minor quantities would merely postpone the collapse of the global environment.

The past three decades have seen a boom in the construction of energy efficient buildings which use solar architectural features to maximise the exploitation of daylight, solar heat, solar-driven ventilation and solar PV electricity. These applications require hourly solar radiation and temperature data.

In most areas of the world, especially in the developing countries, solar radiation measurements are not easily available due to the excessive cost and effort that is involved. Air temperatures, on the contrary, are routinely measured at most meteorological stations. As will be shown in the subsequent section, NASA provides a useful resource in terms of satellite observed data for monthly irradiation and temperature. There is, however, a need to break down the daily data into the respective hourly components, as there is a significant swing of hourly temperature within any given day.

4.2 Presently available information

There are two, reliable sources that provide information on the two of the most basic meteorological parameters: monthly-mean temperature and solar radiation. These sources are the NASA website http://eosweb.larc.nasa.gov/cgi-bin/sse/retscreen.cgi?email=rets@nrcan.gc.ca and TUTIEMPO that is maintained by http://www.tutiempo.net/en/. NASA has produced a grid map of the world with information available for any given latitude and longitude. The solar radiation data is an estimate that has been produced from satellite-based scans of terrestrial cloud-cover. Typical tabulated information that may be downloaded from this source is shown in Table 4.2.1. Note that NASA does not provide the mean-daily maximum and minimum temperature. TUTIEMPO on the other hand provides daily mean, maximum and minimum temperature data for any given location. The data is based on measurements carried out by a wide network of meteorological stations and hence these latter data are more reliable. One of the sub-tasks of this work is also to check the reliability of the NASA temperature records by comparing them against the TUTIEMPO set. Table 4.2.2 presents a sample of the TUTIEMPO data set. Note that the NASA data is available on a mean-monthly basis whereas the latter data is

downloadable on a day-by-day basis. Thus by extension of the present work one may obtain irradiation estimates for daily irradiation using the TUTIEMPO data. The present study deals with mean-monthly estimates.

Table 4.2.1 Monthly-mean solar radiation and temperature for Madrid (40.38 N, 3.78 W) Source: http://eosweb.larc.nasa.gov/cgi-bin/sse/retscreen.cgi?email=rets@nrcan.gc.ca

Month	Air temperature (°C)	Daily solar radiation - horizontal (kW·h/m^2/d)
January	2.4	2.03
February	4.0	2.96
March	7.9	4.29
April	10.7	5.11
May	15.8	5.95
June	21.6	7.09
July	24.8	7.20
August	24.0	6.34
September	19.3	4.87
October	13.3	3.13
November	7.1	2.13
December	3.6	1.70

Table 4.2.2 Sample of the TUTIEMPO data set for M.adrid (40.38 N, 3.78 W) for May 2010. Source: www.TuTiempo.net

Day	Tmean	Tmax	Tmin
1	17.8	23.2	12.0
2	17.5	23.3	10.0
3	11.1	15.7	8.0
4	9.1	13.5	3.0
5	10.8	17.4	1.0
6	12.5	18.3	2.0
7	12.6	19.3	7.0
8	11.9	17.0	7.0
9	13.4	17.0	10.0
10	12.9	17.0	9.0
11	12.7	17.4	6.4
12	11.7	16.6	9.0
13	9.3	14.4	6.0
14	9.9	14.0	4.5
15	11.4	16.8	5.6
16	14.7	21.3	5.8
17	18.0	25.2	6.8
18	20.7	27.5	10.5
19	22.0	28.2	11.6
20	20.0	26.4	12.0
21	22.4	28.6	13.0
22	23.4	29.7	14.5
23	23.1	29.7	15.0
24	22.1	28.6	15.0
25	19.3	24.4	14.6
26	19.6	24.3	13.0
27	19.8	24.0	13.5
28	18.1	23.0	12.4
29	21.3	27.3	11.0
30	25.0	30.5	14.0
31	26.5	34.0	16.0

This section is concluded by pointing out two things that qualify this study, i.e. (i) NASA data is based on satellite observations that represent inferred values of irradiation. In contrast, TuTiempo provides ground-*measured* data for temperature. Hence, if reliable regressions are available between irradiation and mean temperature then the latter data may be used to obtain more realistic estimates of irradiation. (ii) TuTiempo provides mean-minimum and maximum temperatures. Those can be used to decompose daily- to hourly temperatures.

4.3. Previous work

As mentioned above solar radiation can be estimated by means of empirical relations using other available meteorological observations such as (a) mean-daily sunshine duration, (b) cloud-cover, (c) ambient temperature along with precipitation and/or humidity, or (d) ambient temperature as the sole regressor. An exhaustive review of the above methods is available in standard references (Muneer and Saluja 1985; Colliver 1991; Muneer 2004). In this study effort has been concentrated on models that exclusively deal with ambient temperature as the sole predictor or regressor and as such models dealing with other meteorological parameters are not dealt here. The theme of the present work stems from the logic that temperature records have existed for a very long time and also the measurement network is indeed very wide. Hence an irradiation model of the type that is presently proposed would be of benefit, particularly for those in the developing countries where there is a dearth of measured irradiation data. Even for the sparse irradiation network there is the challenge of careful maintenance of solarimeters that is required on a day-to-day basis, particularly the due care that is associated with diffuse radiation measurement. In this respect a discussion on the lack of care of shade-ring adjustment and the corresponding errors has been enumerated by Muneer (Muneer 2004).

As pointed out above solar radiation affects the earth's weather processes. After cooling of the land mass during the night sensible heating resulting from irradiation absorption effects is responsible for ambient temperature variations, so it is possible to obtain a relationship between temperature and solar radiation. The landmark work in this respect was carried out by Campbell

(Campbell 1977). Using this argument, Bristow and Campbell (Bristow and Campbell 1984), suggested a relationship for global solar radiation, as a function of irradiation and the difference between maximum and minimum temperature.

Hargreaves and Samani (Hargreaves and Samani 1982) suggested that solar radiation can be estimated from the above-mentioned difference between maximum and minimum air temperatures, and introduced an empirical coefficient K_r. Hargreaves (Hargreaves 1994) recommended the value of K_r to be 0.16 for interior regions and 0.19 for coastal regions. Annandale et al (Annandale, Jovanovic, Benadé et al. 2002) introduced a correction factor for the empirical coefficient to account for effects of reduced atmospheric thickness on solar radiation. Allen (Allen 1995) obtained K_r as a function of the location altitude to take account of the volumetric heat capacity of the atmosphere (see Eq. 4.3.1).

Allen (Allen 1997) suggested the use of a self-calibrating model to estimate mean monthly global solar radiation following the work of Hargreaves (Hargreaves and Samani 1982). Samani (Samani 2000) developed an empirical relationship between K_r and the difference between air temperature extremes. Meza and Varas (Meza and Varas 2000) evaluated the behaviour of models of Allen (Allen 1997) and Bristow and Campbell (Bristow and Campbell 1984) and inter-compared their results.

Using data from 40 stations covering contrasting climates, Thornton and Running (Thornton and Running 1999) present a reformulation of the Bristow and Campbell model for daily solar radiation, based on daily observations of temperature, humidity and precipitation.

Liu and Scott (Liu and Scott 2001), evaluated the accuracy and applicability of several models for estimating daily value of solar radiation across Australia for different situations, i.e. using the work of McCaskill (McCaskill 1990a; McCaskill 1990b) when only rainfall data was available, the work of Bristow and Campbell (Bristow and Campbell 1984), Richardson (Richardson 1985) and Hargreaves

and Riley (Hargreaves, Hargreaves and Riley 1985) when only temperature data were available, and the work of De Jong and Stewart (De Jong and Stewart 1993) and Hunt et al (Hunt, Kuchar and Swanton 1998) when data for rainfall and temperature were available.

Zhou et al (Zhou, Wu and Yan 2005) validated and compared the above models to predict monthly average daily global radiation on a horizontal surface based on data from 69 meteorological stations in China. Their work was then extended to select the model with the highest accuracy that was then deployed to obtain a geographical distribution of solar radiation across China.

In their landmark work Bandyopadhyay et al (Bandyopadhyay, Bhadra, Raghuwanshi et al. 2008) estimated solar radiation by using nearly all of the above models that deal with temperature as the sole predictor and reported on the relative accuracy of those models. The work of Bandyopadhyay et al (Bandyopadhyay, Bhadra, Raghuwanshi et al. 2008) was based on data from 29 stations that were distributed throughout India. The methods compared were Hargreaves (Hargreaves 1994), Annandale (Annandale, Jovanovic, Benadé et al. 2002), Allen (Allen 1995; Allen 1997), Samani (Samani 2000), and Bristow and Campbell (Bristow and Campbell 1984). The estimated solar radiation values were then compared to measured solar radiation (or solar radiation estimated from measured sunshine hours with locally calibrated Angstrom coefficients), to check the suitability of these methods under Indian conditions. The conclusion drawn by Bandyopadhyay et al (Bandyopadhyay, Bhadra, Raghuwanshi et al. 2008) was that the original Hargreaves (Hargreaves 1994) method performed overall best for Indian locations. The methods due to Allen (Allen 1995), Samani (Samani 2000) and Bristow and Campbell (Bristow and Campbell 1984) were found to be inferior with the latter being the poorest of the lot. The Hargreaves (Hargreaves 1994) method may be summarised thus,

$$\overline{G} = K_r (T_{max} - T_{min})^{0.5} \overline{E} \qquad (4.3.1)$$

4.4 Presently proposed models

The present work is developed around the philosophy that for a great many locations around the world the only parameter that may be available is the mean ambient temperature. Furthermore, the model is simple in its constitution. It has been constructed with the ease of use in mind. Presently, three types of models are proposed that respectively deal with (i) mean-daily irradiation, (ii) mean-hourly irradiation, and (iii) hourly temperature. These are presented in the subsequent sections. Figure 4.4.1 shows the information-flow diagram for the present computational scheme.

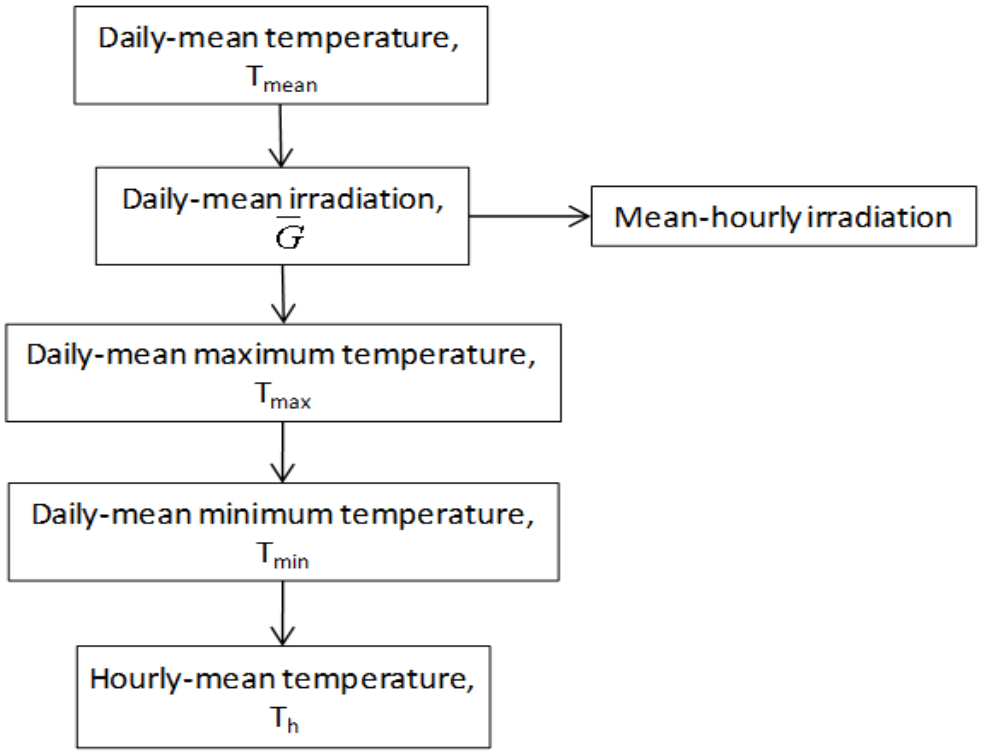

Figure 4.4.1 Flow diagram for obtaining hourly solar irradiation and temperature from mean-daily temperature.

4.4.1 Models for mean-daily irradiation

Table 4.4.1 presents a list of all locations that have been selected for the present monthly-mean database. Note that 20 locations have been selected for the 40-60 degree north. The temporal split was created in two broad categories, i.e. the heating period represented by the January-June months and the cooling

by the July-December period. For the southern hemisphere the split would obviously be reversed. The present study, being the first of its kind, is being restricted to the northern hemisphere and an extension may easily be undertaken for the southern part of the globe as pointed out above.

Table 4.4.1 Locations selected for the present monthly-mean database

Location	Latitude	Longitude	Altitude
Barcelona	41.28	2.06	4
Rome	41.95	12.50	18
Sofia	42.65	23.38	586
Sapporo	43.06	141.33	26
Varna	43.20	27.91	41
San Sebastian	43.35	-1.80	5
Cannes	43.53	6.95	3
Toulouse	43.63	1.36	152
Florence	43.80	11.20	40
Bologna	44.53	11.30	36
Milan	45.43	9.28	107
Timisoara	45.76	21.25	86
Odessa	46.43	30.76	42
Quebec	46.80	-71.38	70
Graz	47.00	15.43	340
Budapest	47.43	19.26	151
London	51.51	-0.11	5
Moscow	55.75	37.63	156
Edinburgh	55.95	-3.35	41
St. Petersburg	59.96	30.30	4

Data was extracted from two sources, i.e. the NASA- and the TuTiempo websites. The former website provides information on $\overline{G}$ and T_{mean}. However, to obtain hourly temperatures one needs mean-daily T_{min} and T_{max}. Hence the

latter data were obtained from the TuTiempo website. The next step was to obtain regressions between $\overline{G}$ and T_{mean}, the logic being that T_{mean} is available much more widely in terms of spatial and temporal coverage as pointed out in Section 4.1.

Figure 4.4.2 shows an example of regressions between $\overline{G}$ and T_{mean} for one the location. Two points are worth mentioning. Firstly, there is a strong correlation between the two parameters under discussion and, secondly, the higher values of r^2.

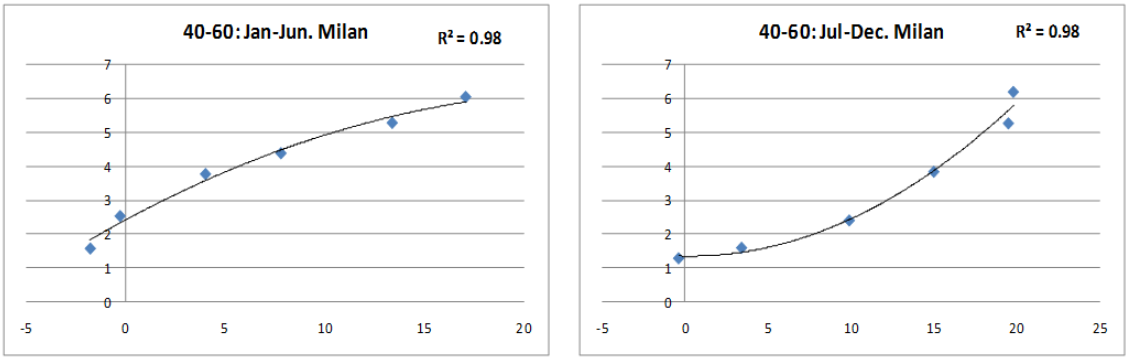

Figure 4.4.2 Regression between mean-daily irradiation ($\overline{G}$) and temperature (T_{mean}) for one location at latitude 40-60º. x-axis: T_{mean}, y-axis: $\overline{G}$.

Tables 4.4.2-4.4.4 provide the r^2 values for the regressions under discussion, for all locations. The above discussion is thus further reinforced. It is therefore recommended that the presently proposed relationships be used, with confidence, for locations 40-60 degree north latitude.

Table 4.4.2 Regression between mean-daily irradiation ($\overline{G}$) and temperature (T_{mean}): all locations.

Location	Latitude	$\overline{G}$ - T_{mean}	
		January-June	July-December
		r^2	r^2
Barcelona	41.28	0.96	0.96
Rome	41.95	0.97	0.97
Sofia	42.65	0.96	0.99
Sapporo	43.06	0.97	0.97
Varna	43.20	0.99	0.99
San Sebastian	43.35	0.99	0.98
Cannes	43.53	0.98	0.97
Toulouse	43.63	0.99	0.99
Florence	43.80	0.99	0.98
Bologna	44.53	0.99	0.98
Milan	45.43	0.98	0.98
Timisoara	45.76	0.99	0.99
Odessa	46.43	0.99	0.99
Quebec	46.80	0.98	1.00
Graz	47.00	0.99	0.99
Budapest	47.43	0.99	0.99
London	51.51	0.99	0.99
Moscow	55.75	0.96	1.00
Edinburgh	55.95	0.99	0.99
St. Petersburg	59.96	0.98	1.00

Table 4.4.3 Regression between mean-daily irradiation ($\overline{G}$) and maximum temperature (T_{max}): all locations.

Location	Latitude	T_{max}- $\overline{G}$	
		January-June	July-December
		r^2	r^2
Barcelona	41.28	0.99	0.96
Rome	41.95	0.98	0.96
Sofia	42.65	0.98	0.97
Sapporo	43.06	1.00	0.98
Varna	43.20	1.00	0.98
San Sebastian	43.35	0.98	0.93
Cannes	43.53	0.98	0.99
Toulouse	43.63	0.98	0.98
Florence	43.80	0.97	0.98
Bologna	44.53	0.99	0.98
Milan	45.43	0.99	0.99
Timisoara	45.76	0.96	0.98
Odessa	46.43	0.98	0.98
Quebec	46.80	0.99	0.92
Graz	47.00	0.99	0.98
Budapest	47.43	0.96	0.99
London	51.51	0.98	0.97
Moscow	55.75	1.00	0.97
Edinburgh	55.95	0.97	0.96
St. Petersburg	59.96	1.00	0.98

Table 4.4.4 Regression between mean-daily irradiation ($\overline{G}$) and minimum temperature (T_{min}): all locations.

Location	Latitude	T_{min}- $\overline{G}$	
		January-June	July-December
		r^2	r^2
Barcelona	41.28	0.99	0.98
Rome	41.95	0.99	0.98
Sofia	42.65	0.99	1.00
Sapporo	43.06	0.96	0.98
Varna	43.2	0.99	0.97
San Sebastian	43.35	0.99	0.98
Cannes	43.53	0.98	0.97
Toulouse	43.63	1.00	0.94
Florence	43.8	0.95	0.98
Bologna	44.53	0.98	0.94
Milan	45.43	0.98	0.97
Timisoara	45.76	0.99	0.98
Odessa	46.43	0.97	0.96
Quebec	46.8	0.99	0.94
Graz	47	1.00	0.98
Budapest	47.43	0.98	0.98
London	51.51	0.98	0.94
Moscow	55.75	0.97	0.92
Edinburgh	55.95	0.98	0.97
St. Petersburg	59.96	1.00	0.93

The much weaker correlations for the near-equatorial band have been reported by Swartman and Ogunlade (Swartman and Ogunlade 1967) and Bandyopadhyay et al (Bandyopadhyay, Bhadra, Raghuwanshi et al. 2008). The former study has respectively attempted regressions between $\overline{G}$ and precipitable water and between $\overline{G}$ and daily temperature range. However, the important point to note is that the T_{mean} itself or indeed the daily temperature range is dictated by the much more uniform movement of the sun within the tropics. This point is demonstrated via Figure 4.4.3 that for the 40 to 60 degree latitudes there is a close concordance between T_{mean} and $\overline{G}$ with noon altitude.

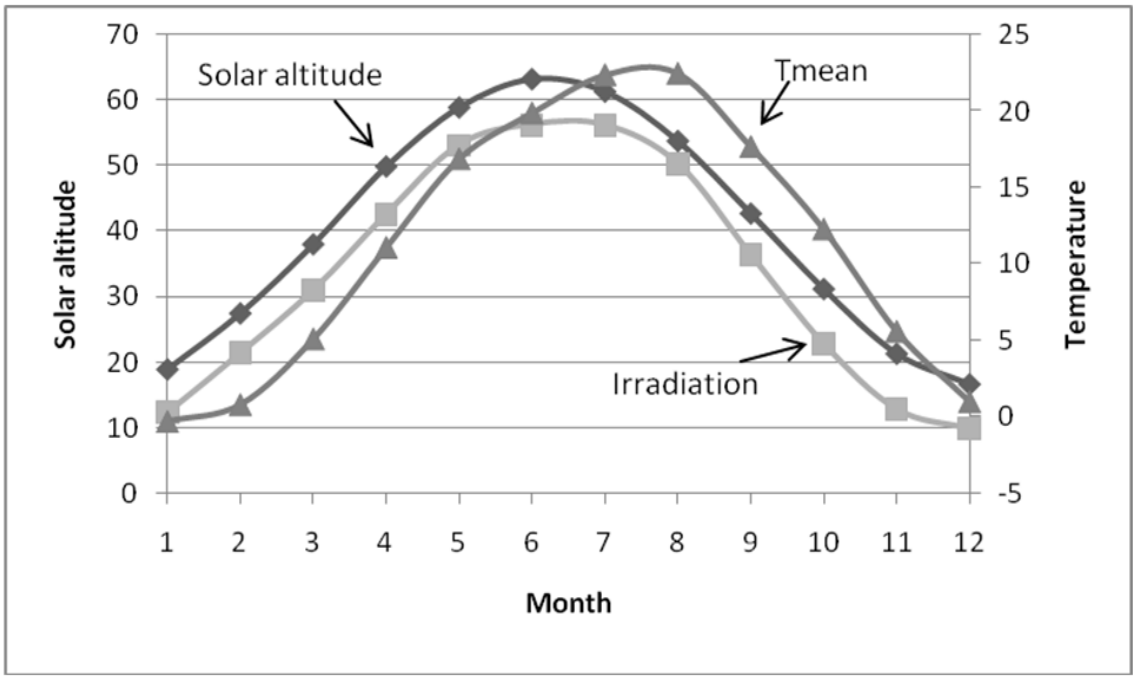

Figure 4.4.3 Solar altitudes at noon, irradiation (×10) and T_{mean} at 50° latitude.

Table 4.4.5 provides the proposed models that relate $\overline{G}$ to T_{mean}, T_{max} to $\overline{G}$, and T_{min} to $\overline{G}$. Note that there is a weaker correlation between T_{min} and $\overline{G}$. This may be explained as follows. Whereas during the daytime the sun's irradiation is the strongest contributor to the rise of temperature, after sunset, during nocturnal hours a number of factors determine the rate of heat loss from the landmass, i.e. direction and speed of wind, and duration and amount of precipitation (rain or snow). Thus a weaker correlation exists between T_{min} and $\overline{G}$.

This point is demonstrated in a greater detail via Figures 4.4.4 and 4.4.5. The time of occurrence for T_{max} is much more well-defined than T_{min}. The time of occurrence for T_{max} and T_{min} is important information as it enables one to obtain hourly temperatures for the 24-hour period. American Society of Heating, Refrigerating and Air-Conditioning Engineers (ASHRAE) (ASHRAE 2009) has provided the latter procedure and that will be the subject of discussion in Section 4.4.2.

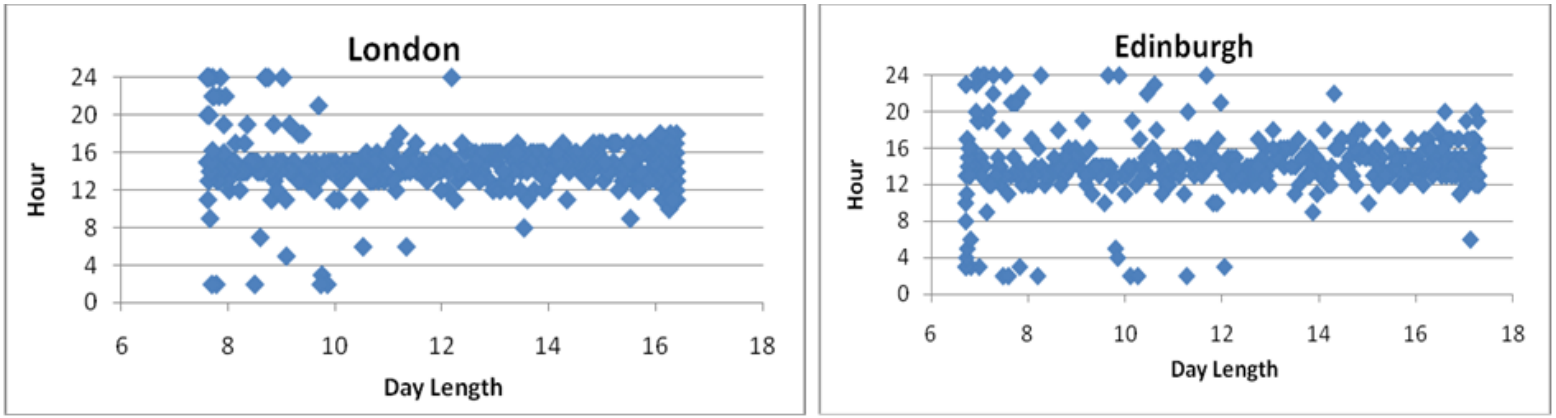

Figure 4.4. 4 Time of occurrence of maximum temperature.

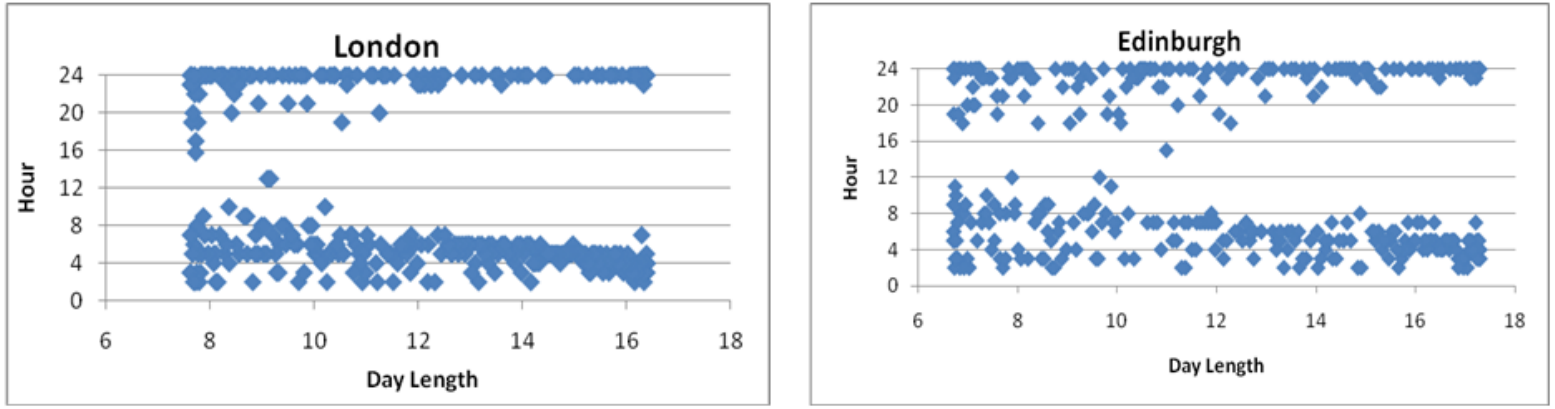

Figure 4.4.5 Time of occurrence of minimum temperature.

Table 4.4.5 Models for mean-daily irradiation ($\overline{G}$) based on mean temperature (T_{mean}), mean- maximum temperature (T_{max}) based on daily irradiation ($\overline{G}$) and mean-minimum temperature (T_{min}) based on daily irradiation ($\overline{G}$): all locations

Models	January-June	r^2	July-December	r^2
$\overline{G}$ to T_{mean}	$\overline{G} = 2.211 + 0.123 * T_{mean} + 0.005 * T_{mean}^2$	0.78	$\overline{G} = 0.955 + 0.078 * T_{mean} + 0.005 * T_{mean}^2$	0.86
T_{max} to $\overline{G}$	$T_{\max} = -2.47 + 4.66 * \overline{G} - 0.04 * \overline{G^2}$	0.72	$T_{\max} = -3.06 + 10.30 * \overline{G} - 0.80 * \overline{G^2}$	0.89
T_{min} to $\overline{G}$	$T_{\min} = -5.89 + 1.66 * \overline{G} + 0.25 * \overline{G^2}$	0.72	$T_{\min} = -5.45 + 6.19 * \overline{G} + 0.40 * \overline{G^2}$	0.76

To provide a better procedure to obtain T_{min} an attempt was made to relate the latter parameter to T_{mean} and T_{max}. Figure 4.4.6 shows an example plot for one location. The point to note here is that T_{mean} seems to be a close average of T_{min} and T_{max}. On the latter basis, T_{min} may thus be obtained as follows:

$$T_{\min} = 2T_{mean} - T_{\max} \qquad (4.4.1.1)$$

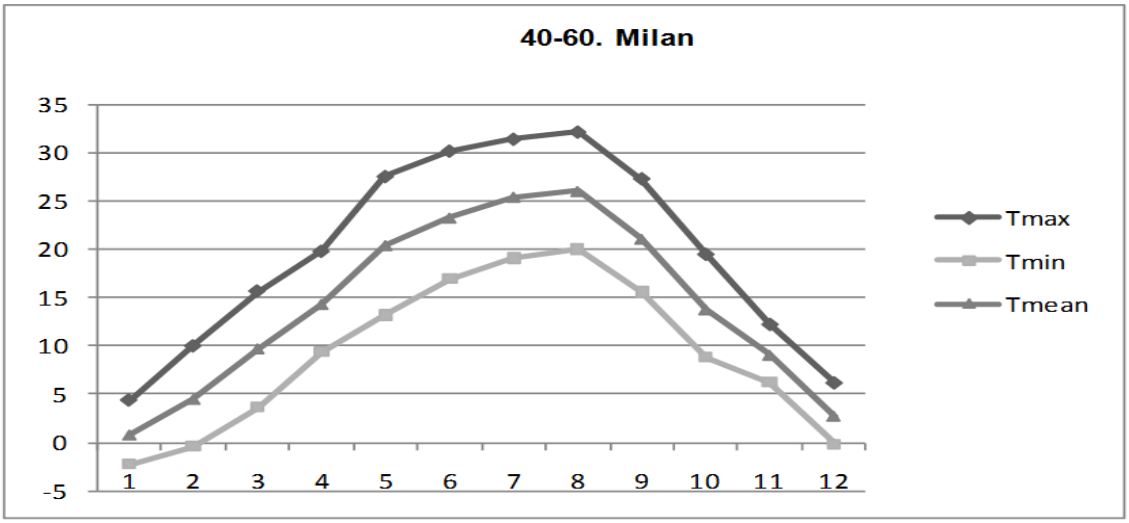

Figure 4.4.6 Inter-relationship between daily maximum, minimum and mean temperature for Milan.

Table 4.4.6 shows the correspondence between the T_{mean} values from the two sources – NASA and TuTiempo. The correspondence at latitudes north of 40-degree seems to be quite strong though and hence the T_{mean} data may be used inter-changeably.

Table 4.4.6 Regression between monthly-mean temperature (T_{mean}) data from the two sources - NASA and TUTIEMPO.

Location	Latitude	$T_{mean\text{-}TuTiempo}$-$T_{mean\text{-}NASA}$	
		Slope	r^2
Barcelona	41.28	1.17	0.99
Rome	41.95	1.20	0.95
Sofia	42.65	1.05	0.99
Sapporo	43.06	0.98	0.99
Varna	43.20	1.13	0.99
San Sebastian	43.35	1.21	0.98
Cannes	43.53	1.08	0.98
Toulouse	43.63	1.07	0.99
Florence	43.80	0.92	0.98
Bologna	44.53	0.85	0.98
Milan	45.43	1.12	0.99
Timisoara	45.76	1.01	0.98
Odessa	46.43	1.06	0.99
Quebec	46.80	1.06	0.97
Graz	47.00	1.03	0.98
Budapest	47.43	0.98	0.98
London	51.51	0.91	0.95
Moscow	55.75	1.14	0.98
Edinburgh	55.95	0.97	0.95
St. Petersburg	59.96	1.09	0.98

4.4.2 Models for hourly temperature

Accurate hourly data are required in very many applications. To meet this need, a simple model to estimate hourly temperature from daily records has been provided by the ASHRAE (ASHRAE 1997). A computer program to decompose daily- to hourly temperature has been provided by Muneer et al (Muneer, Abodahab N., Weir et al. 2000). That code is also available in Muneer's book (Muneer 2004). The daily maximum temperature that is achieved at a given location is dependent on the prevailing solar radiation, cloud-cover and wind profile. The earliest available models suggest a sinusoidal profile between the daily maximum and minimum temperatures. However more recent work of Hedrick (Hedrick 2009) and Thevenard (Thevenard 2009), ASHRAE (ASHRAE 2009) has further updated the latter model. Table 4.4.2.1 gives the hourly temperature profile, expressed in terms of a presently defined Z-parameter as define below:

$$Z = \frac{T_h - T_{\min}}{T_{\max} - T_{\min}} \qquad (4.4.2.1)$$

Where T_h temperature at selected hour, $T_{\min}$ is the minimum temperature of the day and $T_{\max}$ is the maximum temperature of the day.

ASHRAE (ASHRAE 2009) has suggested that this profile is representative of both dry-bulb and wet-bulb temperature variation on typical design days. The tabulated information provided by ASHRAE (ASHRAE 2009) has been cross-checked using averaged hourly data from 58 Turkish locations (Coskun, Oktay and Dincer 2010) and hourly data from three international locations, i.e. Edinburgh, London and Abu Dhabi. Table 4.4.2.2 includes that information.

Table 4.4.2.1 ASHRAE model for diurnal temperature swing.

Hour	Z	Hour	Z
1	0.12	13	0.95
2	0.08	14	1.00
3	0.05	15	1.00
4	0.02	16	0.94
5	0.00	17	0.86
6	0.02	18	0.76
7	0.09	19	0.61
8	0.26	20	0.50
9	0.45	21	0.41
10	0.62	22	0.32
11	0.77	23	0.25
12	0.87	24	0.18

Table 4.4.2.2 Performance of ASHRAE model for three international locations.

Location	Year	Slope	r^2	MBE (°C)	RMSE (°C)
Abu Dhabi	1997	0.99	0.77	-0.1	3.7
London	1990	0.97	0.93	-0.4	1.6
Edinburgh	1990	0.97	0.86	-0.3	1.7

Data from the above three international locations were then used to evaluate the ASHRAE model. Figure 4.4.2.1 and Table 4.4.2.2 present the evaluation which used four statistical indicators. These indicators are the slope of the best-fit regression line between the computed and measured values, coefficient of determination value (r^2) for the above best-fit line, mean bias error (MBE) and root mean square error (RMSE).

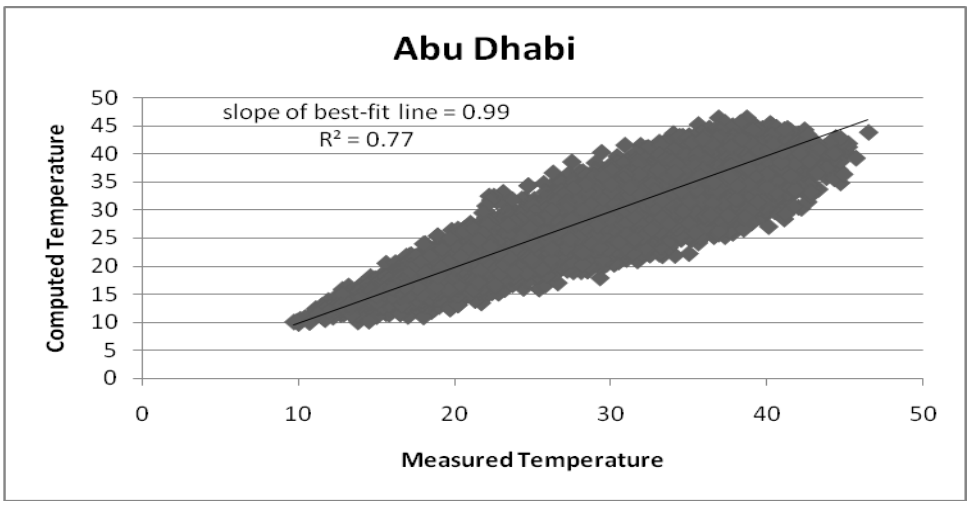

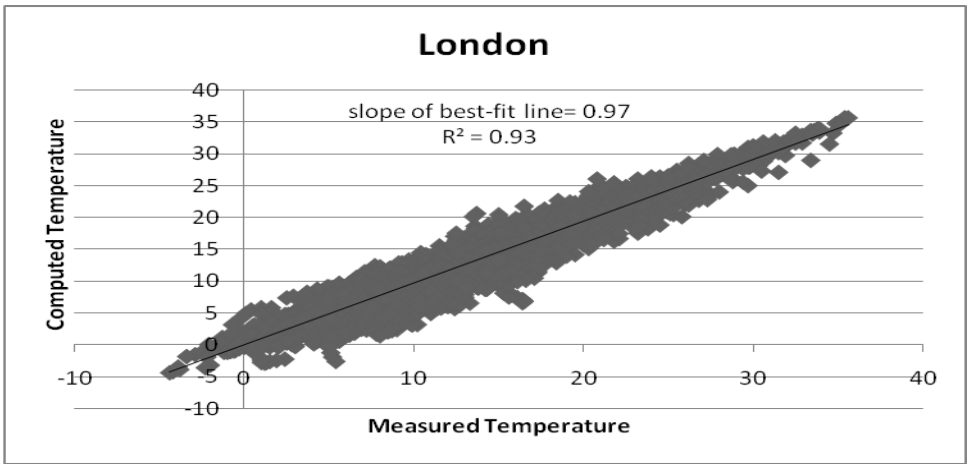

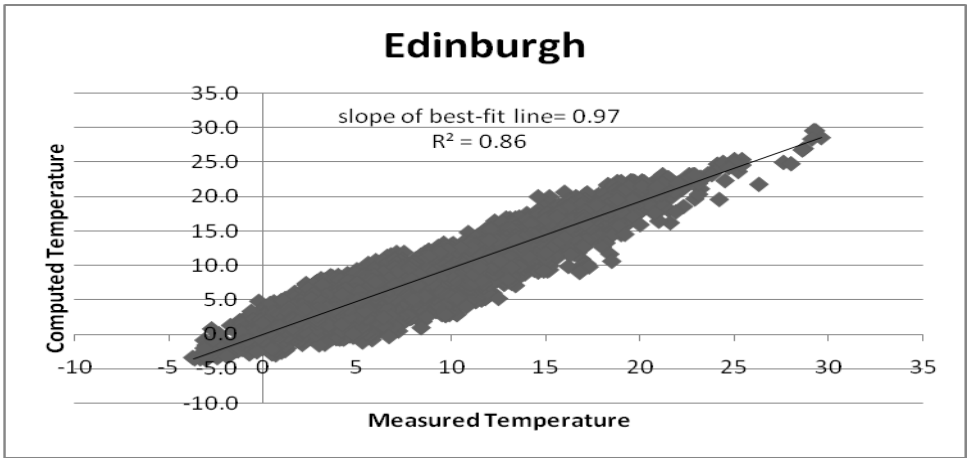

Figure 4.4.2.1 Performance of the ASHRAE model for three international locations.

The slope of the best-fit line shows that the model performs well for all locations in this study. The r^2 indicator for Abu Dhabi showed that the model slightly

under-performs in terms of data scatter. For the remaining stations, the r^2 values lie in the range 0.86 to 0.93 showing that the model performs well. The highest value of MBE is -0.4 °C for Edinburgh and the lowest is -0.1°C at Abu Dhabi. This shows a good agreement with the slope of the best-fit line where Abu Dhabi has the best value near to the desired value of 1. The RMSE value for Abu Dhabi is the highest with the value of 3.7°C and the lowest value of 1.6 °C was found for London.

Furthermore, a comparison between the ASHRAE temperature model and the mean-hourly temperature record for locations within the UK and Turkey was carried out. It is evident that the UK temperature trend very closely follows the ASHRAE model. A slight upward shift of temperatures was observed for Turkey for the ante meridian hours. Figure 4.4.2.2 shows that comparison.

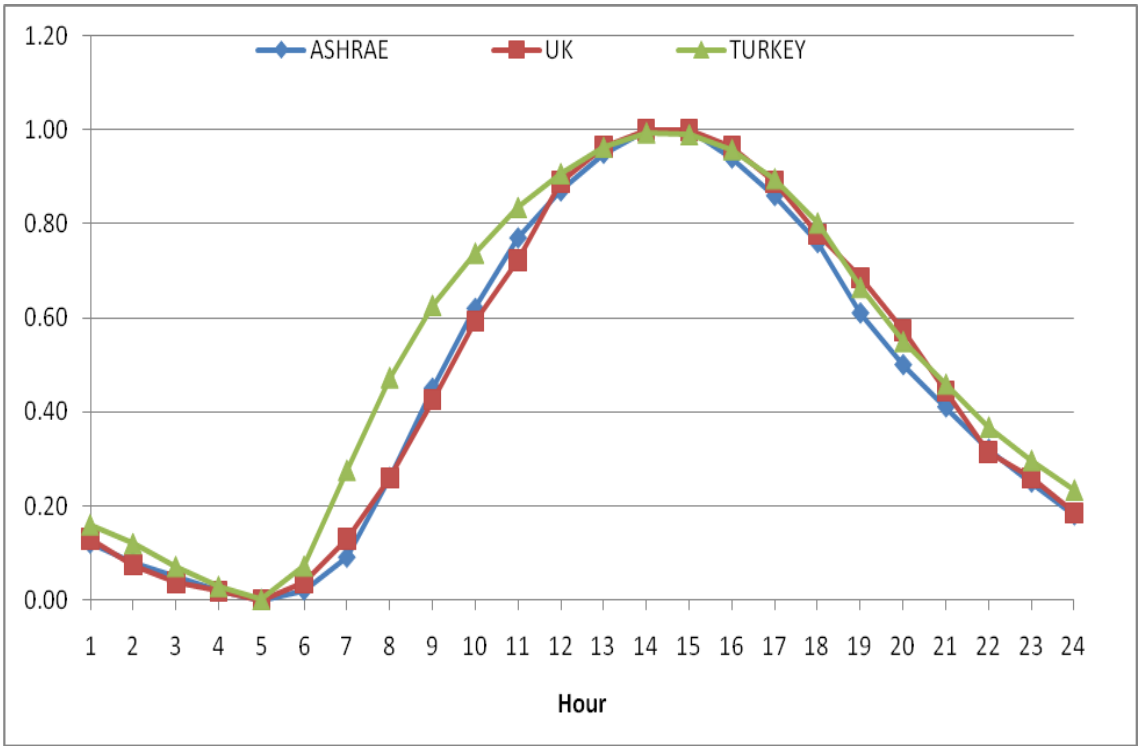

Figure 4.4.2.2 Comparison of mean-hourly temperature trend.

4.5 Conclusions

World-wide there are many more temperature measuring meteorological stations than those that measure solar radiation. Presently, a case has been made for the development of temperature-based mathematical models to obtain mean-daily irradiation. In contrast to the classical models that use daily temperature range, use was made of mean-daily temperature as the basic regressor. Furthermore, a procedure to decompose daily to hourly temperatures was also evaluated. It was found that the procedure, although originally developed using data from North American locations, produces reliable estimates of hourly temperature with a low MBE range that varied from -0.1°C to -0.4°C and the RMSE range that varied between 1.6°C and 3.7°C for three international locations.

Finally, there is large body of existing data on the above parameters measured across the world in recent years. These data may be used for further validation of the proposed model for different geographic areas, climatic zones and seasons.

5.0 Sol-air temperature and Illuminanace

Data sets from the UKCP09 were used in this study along with historical measured data for three locations to critically analyse the likely changes that may occur in the sol-air temperature and daylight illuminance profiles. These two parameters are important with respect to building design, i.e. the sol-air temperature is used to determine the building cooling load and the daylight illuminance affects window design. Building dwellers require natural lighting and also a view of the outside world (Roche, Dewey and Littlefair 2000; Galasiu and Veitch 2006; Cheung and Chung 2008). In a fully air-conditioned office building, 20-30% of total electricity is used for electric lighting (Chirarattananon, Chaiwiwatworakul and Pattanasethanon 2002; Krarti, Erickson and Hillman 2005) and it accounts for 10% of the energy consumption for residential buildings (Lam 1996). Proper lighting control linked to daylight can reduce building's electricity consumption (Loutzenhiser, Maxwell and Manz 2007; Doulos, Tsangrassoulis and Topalis 2008; Kurian, Aithal, Bhat et al. 2008).

This study provides altered profiles of sol-air temperature and daylight illuminance for the UKCP09 data for future years and for different emission scenarios.

5.1 Data sets

Long term hourly data from three locations in the UK was used for this study namely Bracknell, Manchester and Edinburgh. Muneer and Fairooz (Muneer and Fairooz 2002) quality control procedures were used to prepare 'cleaned' data sets.

Future data generated from the WG for the locations mentioned above were used. Three carbon dioxide (CO_2) emission scenarios i.e. Low Emission (LE), Medium Emission (ME) and High Emission (HE) at different time series were selected for this study, namely 2030, 2050 and 2080 scenarios. These data sets were selected because it covered different CO_2 emission scenarios and a wide range of time series from 2020 till the end of this century. Table 5.1.1 shows the details of all data that were presently used.

Table 5.1.1 Details of the data used in the present study.

Location	Latitude	Measured data	WG data
Bracknell	51.38	1981-1992	Control, 2030LE, 2030ME, 2030HE, 2050LE, 2050ME, 2050HE, 2080LE, 2080ME, 2080HE
Manchester	53.33	1982-1994	Control, 2030LE, 2030ME, 2030HE, 2050LE, 2050ME, 2050HE, 2080LE, 2080ME, 2080HE
Edinburgh	55.85	1976-1992	Control, 2030LE, 2030ME, 2030HE, 2050LE, 2050ME, 2050HE, 2080LE, 2080ME, 2080HE

5.2 Sol-air temperature

The sol-air temperature may be defined as the outside air temperature which, in the absence of solar radiation, would give the same temperature distribution and rate of heat transfer through wall (or roof) as exists due to the combined effects of the actual outdoor temperature distribution plus the incident solar radiation (O'Callaghan and Probert 1977).

Sol-air temperature (t_{eo}) for an exposed surface of slope *b* and orientation *a* may be obtained by considering the surface energy balance, by equating radiation gains with surface convective and conductive exchanges (evaporative losses due to evaporation of moisture at the surface are not considered in this technique).

$$a_{rad}G(b,a)+L^{*}(b)=h_{c}(T_{eo}-T_{ao})+E \qquad (5.2.1)$$

where a_{rad} is the surface short-wave absorptivity, $G(b,a)$ is the short-wave global irradiance (W/m^2) on surface of tilt *b* and orientation *a*, $L^*(b)$ is the net long-wave radiation exchange rate (W/m^2) on surface of tilt *b*, *h*c is the external surface convection coefficient due to wind (W/m^{2}K), T_{eo} is the (absolute) external surface temperature (K), T_{ao} is the (absolute) outside dry bulb air temperature of the convective flow over the surface (K) and *E* is the rate of energy flow rate into the construction (W/m^2). $L^*(b)$ may be estimated from :

$$L^*(b) = e_l\left(L_{sky}(b) + L_g(b) - \sigma T_{eo}^4\right) \quad (5.2.2)$$

where L^* (b) is the long-wave radiation energy exchange (W/m^2), L_{sky} (b) is the atmospheric long-wave radiation received directly from the sky (W/m^2), L_g (b) is the long-wave radiation received from the ground (W/m^2), e_l is the long-wave surface emissivity, σ is the Stefan-Boltzmann constant (5.6697 × 10^{-8}) (W/m^{2}K^4) and b is the inclination of the surface (°).

Note that the outgoing long-wave flux does not depend on the orientation of the emitting surface. The consequent long-wave radiation energy exchange on a sloping plane may then be expressed as a net balance.

The short-wave albedo of the ground is set at 0.2 and an estimate of the ground long-wave emissivity, normally set between 0.90 and 0.95, are needed to calculate the two radiative contributions from the ground. The convective heat transfer coefficient (h_c) may be estimated from the surface wind speed using the standard empirical relationship (CIBSE 2006):

$$h_c = 4 + 4v \quad (5.2.3)$$

where h_c is the convective heat transfer coefficient (W/m^{2}K), v is the wind velocity over the surface (m/s).

Rearranging Equation 5.2.1 and setting E=0, the following expression for the (absolute) sol-air temperature is obtained:

$$T_{eo} = \left\{\left[a_{rad}G(b,a) + L^*(b)\right]/h_c\right\} + T_{ao} \quad (5.2.4)$$

Substituting for L^*(b) from Equation 5.2.2 gives:

$$T_{eo} = \left\{\left[a_{rad}G(b,a) + e_l\left(L_{sky}(b) + L_g(b) - \sigma T_{eo}^4\right)\right]/h_c\right\} + T_{ao} \quad (5.2.5)$$

Rearranging Equation 5.2.5 produces the following fourth order non-linear equation:

$$\sigma T_{eo}^4 / h_c + T_{eo} - \left\{a_{rad} G(b,a) + e_l \left[L_{sky}(b) + L_g(b)\right]\right\} / h_c - T_{ao} = 0 \quad (5.2.6)$$

Equation 5.2.6 may be solved for T_{eo} using any suitable iterative process. The solution yields the value of T_{eo} (K). Then, finally:

$$t_{eo} = T_{eo} - 273.15 \quad (5.2.7)$$

where t_{eo} is the sol-air temperature (°C).

For more in-depth discussion reference is made to CIBSE Guide J (CIBSE 2002). *Note*: This section is a summary and extracted from Section 5.5 in CIBSE Guide J 2002.

5.2.1 Results and discussion

Data from three locations were used to obtain sol-air temperature according to the steps shown in Figure 5.2.2.1 and data sets details that are shown in Table 5.1.1. Comparison of future and present sol-air temperatures was carried out. The present data set that was used was the Chartered Institution of Building Services Engineers (CIBSE) Guide A 2006.

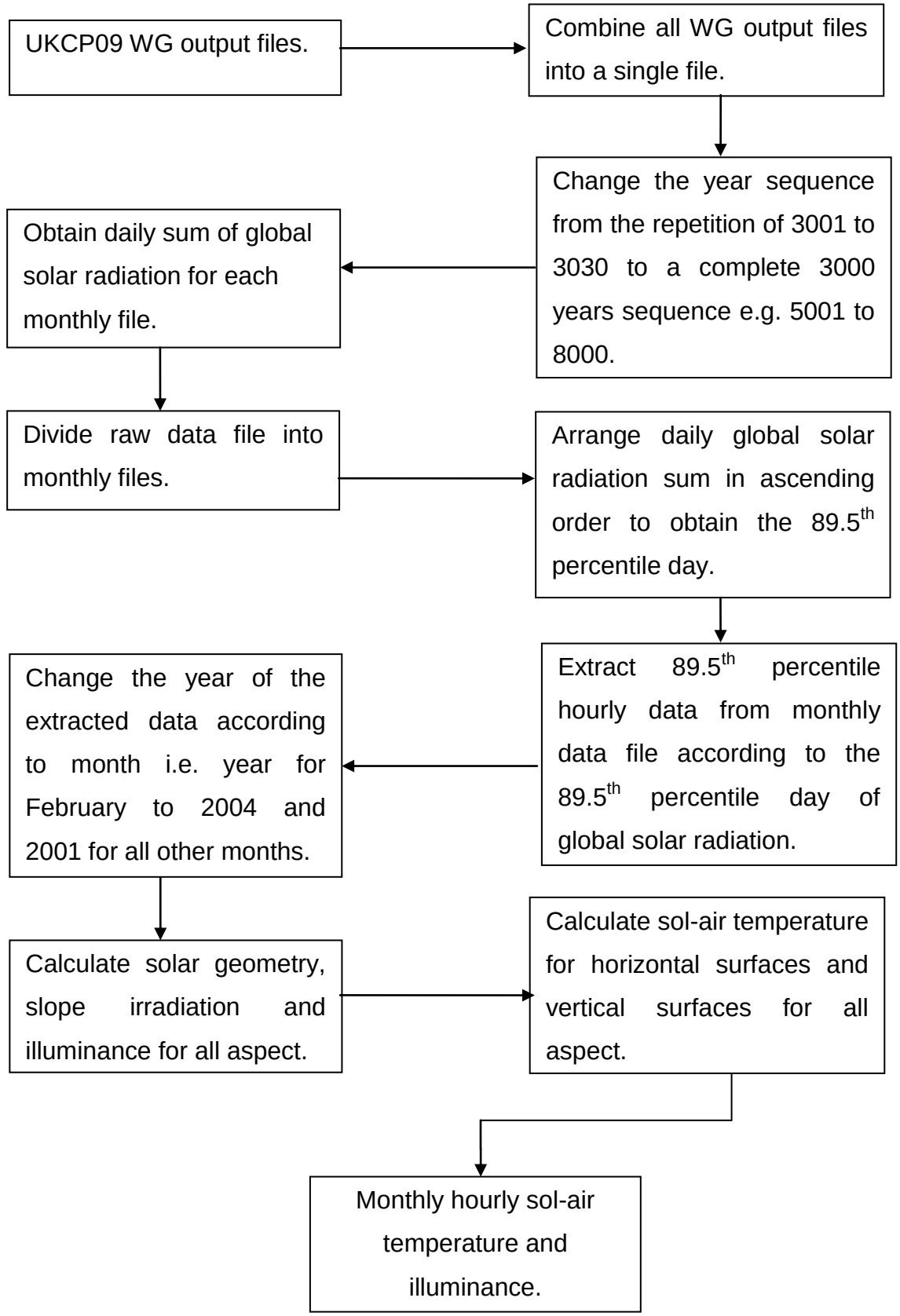

Figure 5.2.2.1 Process flow chart to obtain 89.5th percentile of sol-air temperature.

A complete set of monthly hourly sol-air temperature for the above three stations were obtained. Presently, however only sol-air temperature at 1300 hours corresponding to the 89.5th percentile of daily total radiation are presented. This hour was selected in view of the high solar radiation occurrence. Figures 5.2.2.2 to 5.2.2.4 show the sol-air temperature for Bracknell, Manchester and Edinburgh respectively for all WG data sets. For full table of sol-air temperature at 1300 hours please refer to Appendix A.

Furthermore, comparison was carried out for horizontal and south facing vertical surfaces between CIBSE Guide A 2006 and 2080HE. Table 5.2.2.1 show the comparison of monthly sol-air temperature for Bracknell, Manchester and Edinburgh respectively.

A dark-coloured horizontal surface has the highest sol-air temperature difference for all locations. A difference of 18.1°C for sol-air temperature for Bracknell, 19.0ºC for Manchester and 20.1°C for Edinburgh was found when the value of the year 2080HE was compared with the reference value (CIBSE Guide A, 2006).

For light-coloured horizontal surface, when comparing the value of 2080HE scenario data set with the reference value, a difference of 12.2°C, 12.7ºC and 13.8°C was found, respectively for Bracknell, Manchester and Edinburgh.

For vertical surfaces facing south (dark- as well as light-coloured), the highest sol-air temperature difference of 22.3°C and 16.2°C was found for Edinburgh, 12.2°C and 10.1°C for Bracknell and 12.6ºC and 10.6ºC or Manchester for the 2080HE data set when compared with the reference data.

From the comparison Table 5.2.2.1, most of the time the highest sol-air temperature difference of sol-air temperature occurred during the month of June. Besides that, two out of three locations, June has the highest sol-air temperature difference. Hence, the month of June was selected for further evaluation of the basic variables that were used to calculate sol-air temperature i.e. dry bulb temperature, sunshine duration and global solar radiation. Furthermore, from the monthly sol-air temperature Figures 5.2.2.2 to 5.2.2.4,

overlapping of sol-air temperature were evident among the WG projected data sets. To avoid this, only the Control, 2030LE, 2050ME and 2080HE projected data sets were selected for further evaluations.

Due to the same trend of monthly sol-air temperature for all locations, only Bracknell and Edinburgh were selected for further evaluations.

Note that, full tables of sol-air temperature for all scenarios, orientations and locations can be found at the attached compact disk (CD) together with this report.

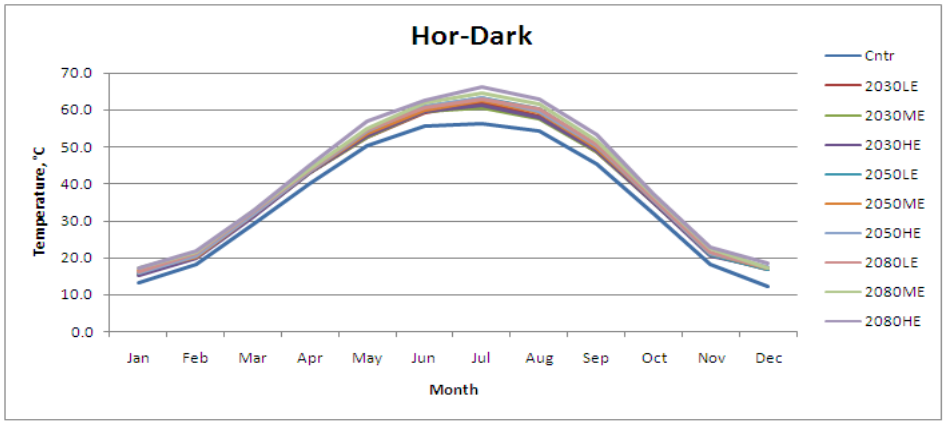

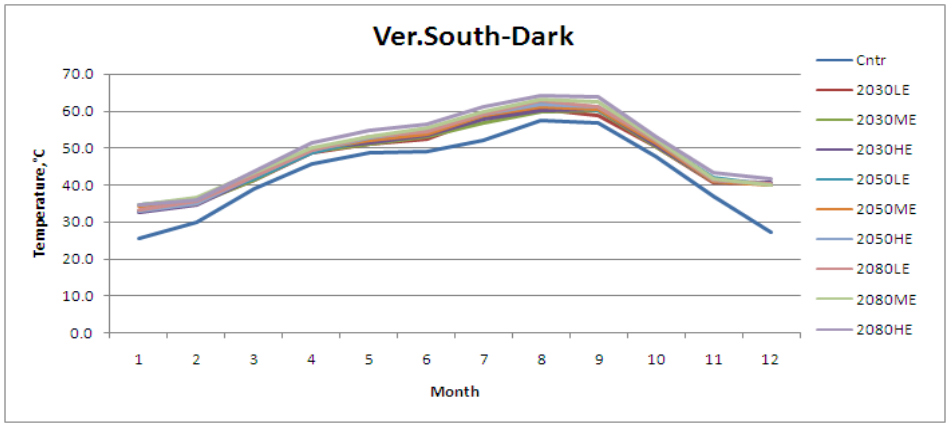

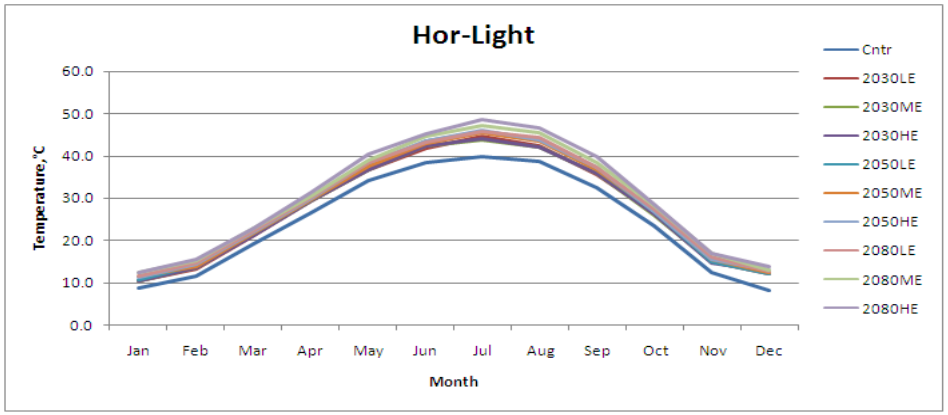

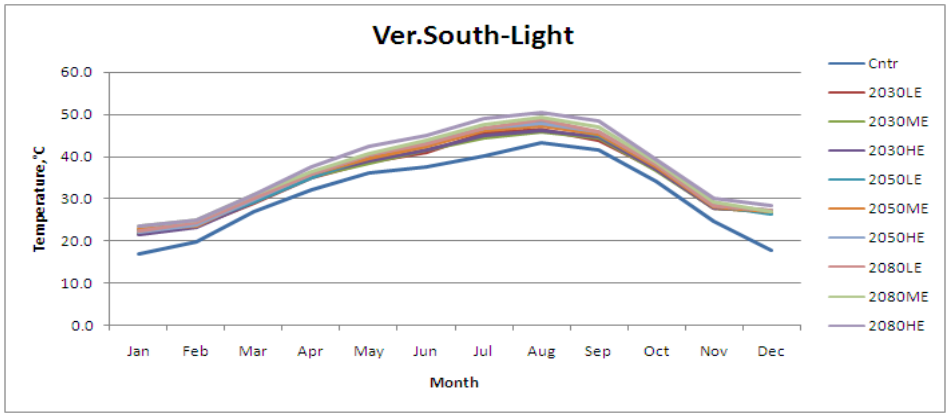

Figure 5.2.2.2 Monthly sol-air temperature for Bracknell at 1300 hours. Note: Hor-Light= Horizontal light coloured surface, Hor-Dark= Horiontal dark coloured surface, Ver.South-Dark= Vertical South facing dark coloured surfaces, Ver-South Light= Vertical South facing light coloured surface.

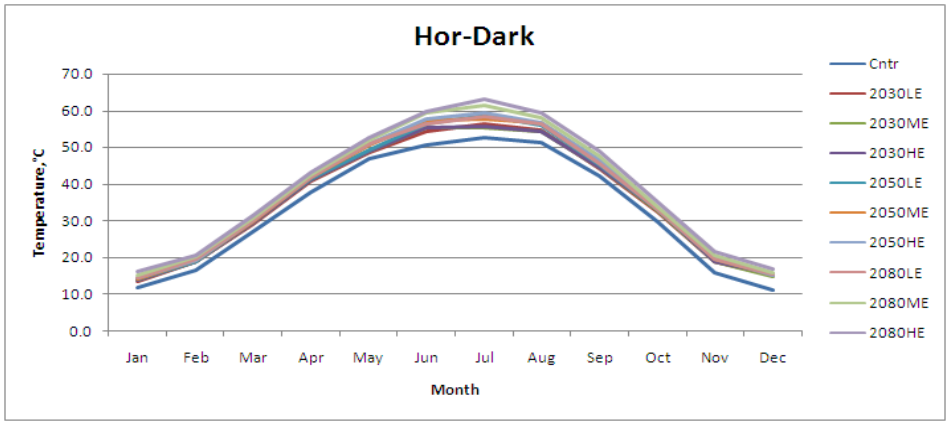

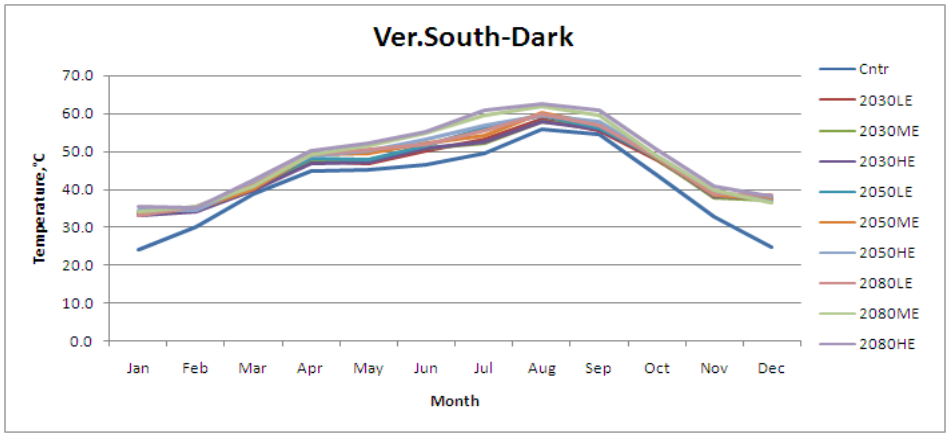

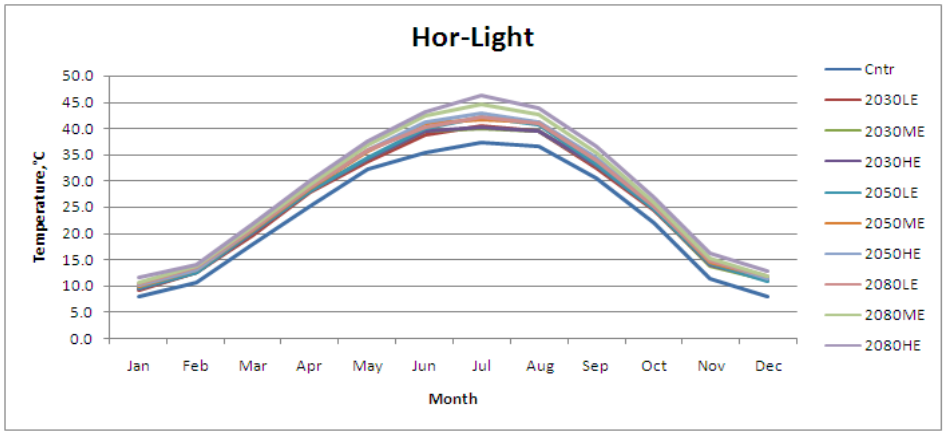

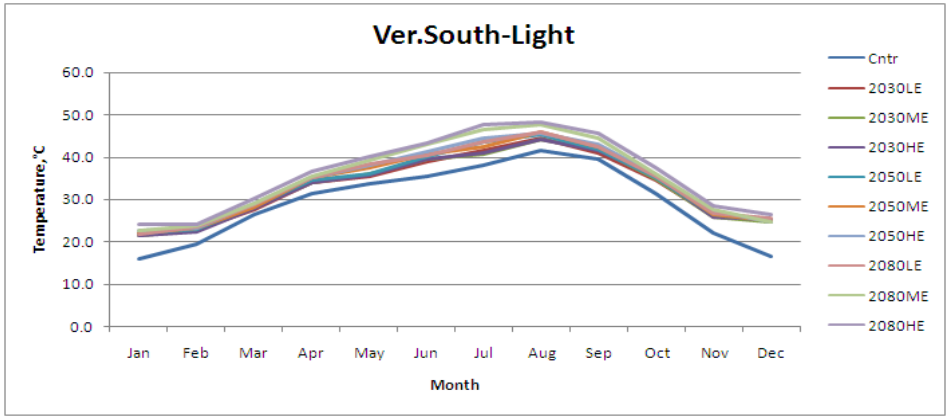

Figure 5.2.2.3 Monthly sol-air temperature for Manchester at 1300 hours. Note: Hor-Light= Horizontal light coloured surface, Hor-Dark= Horiontal dark coloured surface, Ver.South-Dark= Vertical South facing dark coloured surfaces, Ver-South Light= Vertical South facing light coloured surface.

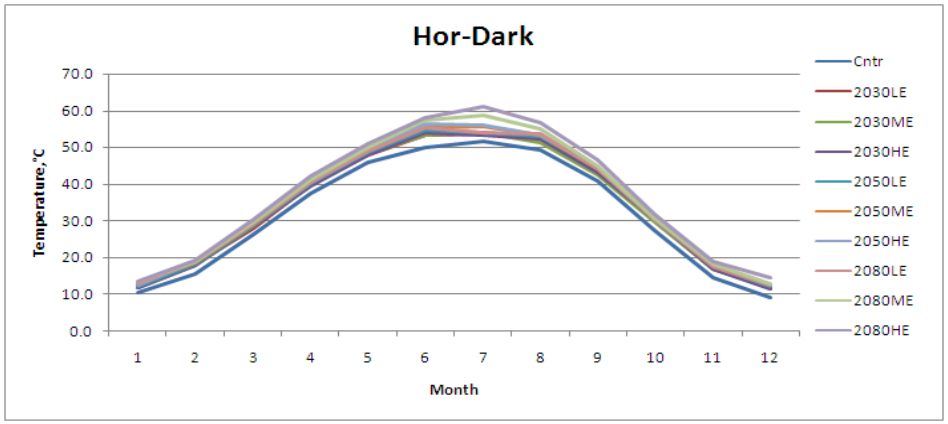

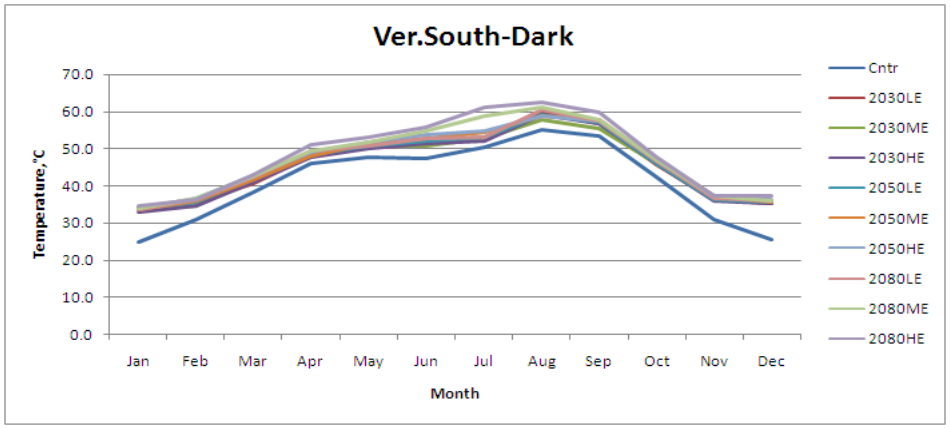

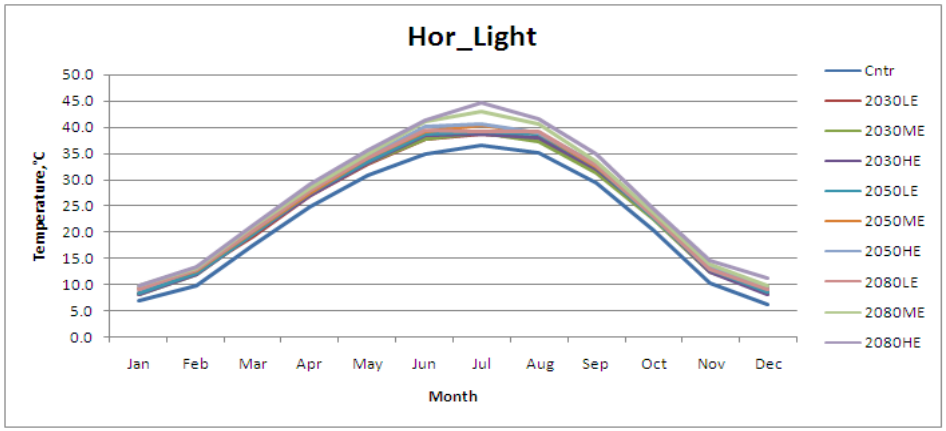

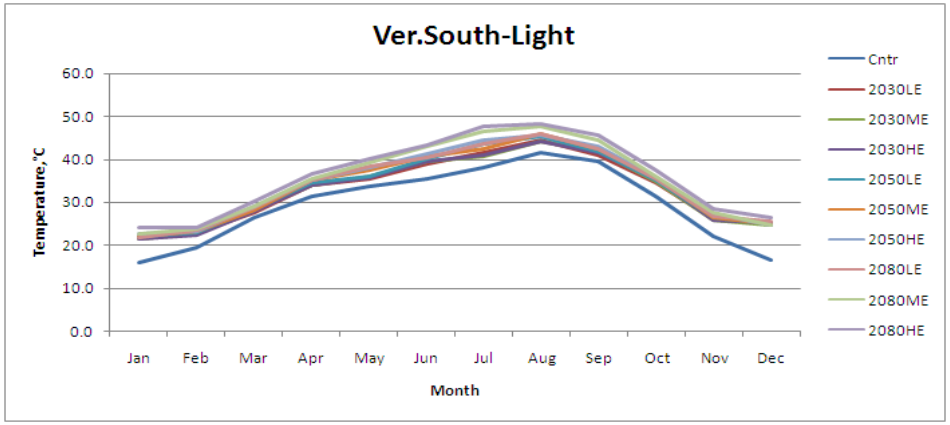

Figure 5.2.2.4 Monthly sol-air temperature for Edinburgh at 1300 hours. Note: Hor-Light= Horizontal light coloured surface, Hor-Dark= Horiontal dark coloured surface, Ver.South-Dark= Vertical South facing dark coloured surfaces, Ver-South Light= Vertical South facing light coloured surface.

Table 5.2.2.1 Differences of monthly sol-air temperature between CIBSE and 2080HE data set at 1300 hours. Note: Hor-Light= Horizontal light coloured surface, Hor-Dark= Horiontal dark coloured surface, Ver.S-Dark= Vertical South facing dark coloured surfaces, Ver.S Light= Vertical South facing light coloured surface.

Month	Bracknell				Manchester				Edinburgh			
	Hor-Dark	Hor-Light	Ver.S-Dark	Ver.S-Light	Hor-Dark	Hor-Light	Ver.S-Dark	Ver.S-Light	Hor-Dark	Hor-Light	Ver.S-Dark	Ver.S-Light
Jan	5.1	4.5	-0.5	1.7	6.1	5.4	3.5	4.5	5.5	5.1	2.7	4.2
Feb	4.4	3.8	-0.3	1.6	7.0	5.5	4.6	4.9	5.4	4.2	4.0	4.2
Mar	2.8	2.1	-0.9	0.6	7.9	5.7	5.9	5.5	11.7	8.5	12.5	10.0
Apr	8.9	5.3	8.0	5.8	7.2	4.7	4.9	4.3	12.3	8.4	11.7	9.2
May	16.3	10.4	11.9	9.3	12.6	8.8	8.3	7.3	16.1	10.6	13.2	10.4
Jun	13.3	8.5	6.4	5.8	19.0	12.7	12.1	10.2	20.1	13.8	13.4	11.5
Jul	18.1	12.2	12.2	10.1	16.1	11.5	11.0	9.8	17.8	12.4	13.4	11.0
Aug	15.8	10.6	12.1	9.7	15.9	11.3	12.6	10.6	18.8	13.1	17.6	13.7
Sep	13.6	9.9	12.0	10.1	12.7	9.3	11.8	9.7	18.3	12.5	22.3	16.2
Oct	8.2	6.2	6.0	5.8	10.6	8.9	9.0	8.7	10.0	7.4	12.9	9.9
Nov	4.5	3.8	1.0	2.3	5.7	4.8	3.0	3.9	4.4	3.3	4.0	3.8
Dec	7.8	7.3	1.4	4.1	8.3	7.5	4.8	5.9	8.7	9.0	-3.6	2.3

Note that the UKCP09 WG does not generate wind speed. The wind speed value was set to 3 m/s for all WG output data sets to obtain sol-air temperature following an analysis of wind speed frequency distribution. This wind speed distribution analysis was carried out by using measured data sets for each of the two locations. Figure 5.2.2.5 shows the wind speed frequency distributions for Bracknell and Edinburgh. Note that for both locations the most frequent value of wind speed lies in the 2 m/s to 4 m/s range. Hence 3 m/s value was presently selected as the most likely value.

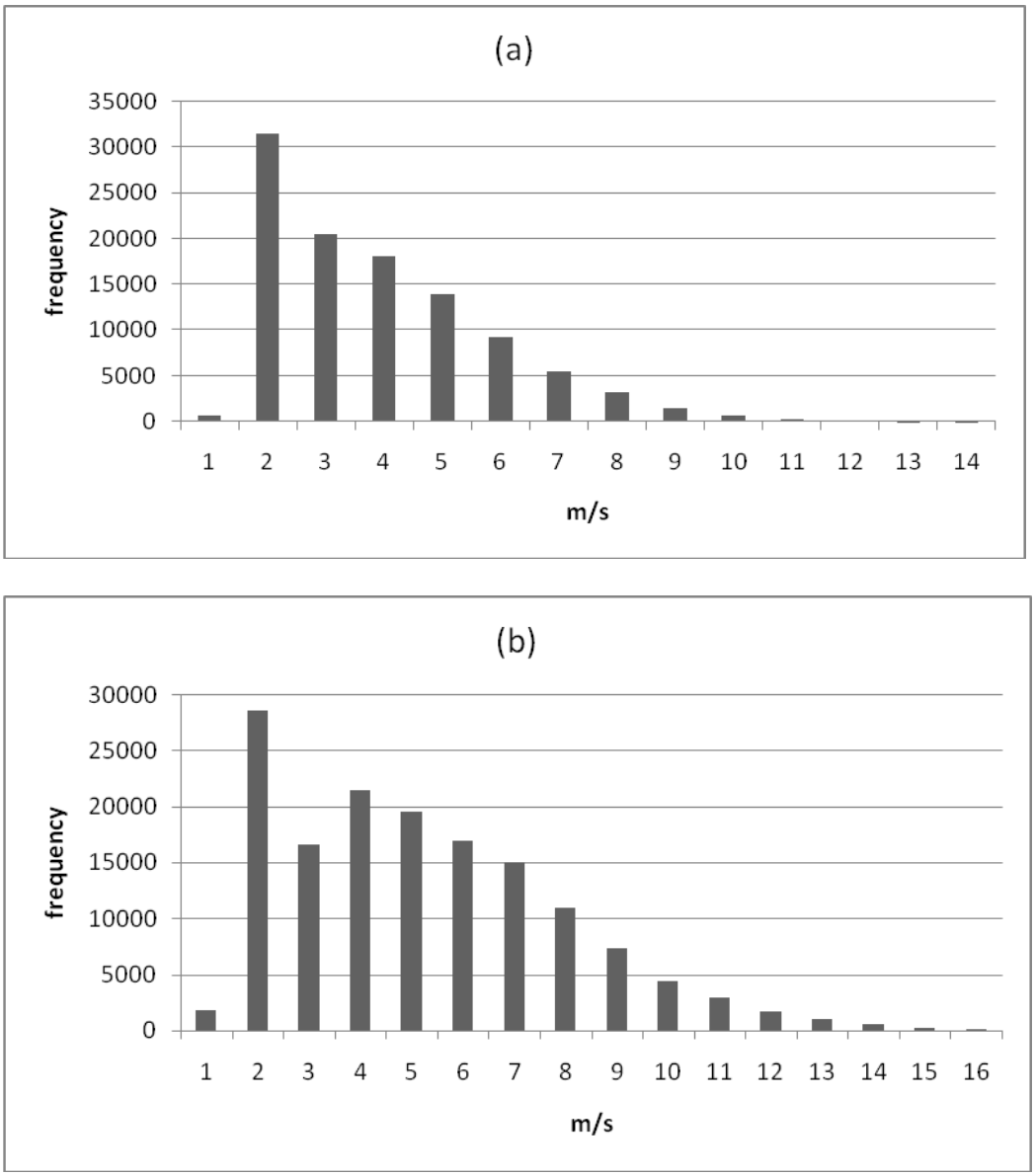

Figure 5.2.2.5 Measured wind speed distribution: (a) Bracknell year 1981-1992 (b) Edinburgh year 1976-1992.

5.3 Illuminance

For daylighting design, quantitative illuminance data are needed for window sizing and window shading system design. Global- and diffuse horizontal illuminance of the sky vault are needed for this task. Cumulative frequency curves of horizontal illuminance are usually used. Curves for the frequencies at which different horizontal global- (IL_g) and diffuse illuminance levels (IL_d) are exceeded are needed separately. Horizontal beam illuminance data (IL_b) are not normally used.

5.3.1 Analysing cumulative frequency illuminance data

First, the length of the working day must be defined. The cumulative illuminance data can be derived on a month-by-month or on an annual basis. Hunt (Hunt 1979) defined the standard UK working day for illumination design purposes as 09:00–17:30 Local Apparent Time (LAT) in winter and 08:00–16:30 LAT for the period between April and October to allow for British Summer Time. For practical reasons, the difference between LAT and Greenwich Meridian Time (GMT) was considered to be small enough to be neglected for the sites considered.

The cumulative frequency curves in common engineering use are usually based either on hour-by-hour observations of illumination or indirectly derived from hour-by-hour observations of irradiation. These irradiation data are converted into illuminance values by applying the appropriate luminous efficacy models. In both cases, the assumption, implicit in the conversion to cumulative illuminance, is that the mid-hour illuminance in klux is equal to the hourly illumination in klux hours divided by one hour.

The hour-by-hour conversion process from illumination to illuminance also presents difficulties in the sunrise and sunset hours (CIBSE 2002). During these hours, the sun will only be above the horizon for part of the hour, making the accurate estimation of the illuminance from the hourly illumination very difficult. This complication is frequently overlooked. Another important factor is that, in the winter months, the sun will be below the horizon for part of the working day.

This influences the maximum possible cumulative frequency of daylight provision in the winter months.

Muneer and Kinghorn (Muneer and Kinghorn 1997) have developed luminous efficacy models based on the UK observed data. The global and diffuse luminous efficacy algorithms given below enable the estimation of a long-term time series of diffuse and global horizontal illuminance from the respective hour-by-hour horizontal irradiation time series data. Kinghorn and Muneer (Kinghorn and Muneer 1998) found the following regression relationships for solar altitudes above 5 degrees:

$$K_G = 136.6 - 74.54Kt_h + Kt_h^2 \quad (5.3.1.1)$$

$$K_D = 130.2 - 39.82Kt_h + 49.97Kt_h^2 \quad (5.3.1.2)$$

where Kt_h is the hourly clearness index.

K_G and K_D are defined as follows:

$$K_G = IL_g / G \quad (5.2.3.3)$$

$$K_D = IL_d / D \quad (5.3.1.4)$$

where IL_g is the global illuminance on the horizontal plane (klux), G is the global irradiance on the horizontal plane (W/m^2), IL_d is the diffuse illuminance on the horizontal plane (klux) and D is the diffuse irradiance on the horizontal plane (W/m^2).

Note: This section is a summary and extracted from Section 5.6 in CIBSE Guide J 2002. For more in-depth discussion reference is made to CIBSE Guide J (CIBSE 2002).

5.3.2 Results and discussion

Comparisons of global and diffuse illuminance between results from the WG data sets and CIBSE Guide J 2002 were carried out. Figures 5.3.2.1 and 5.3.2.2 show the comparison of global illuminance and diffuse illuminance for Bracknell and Edinburgh respectively.

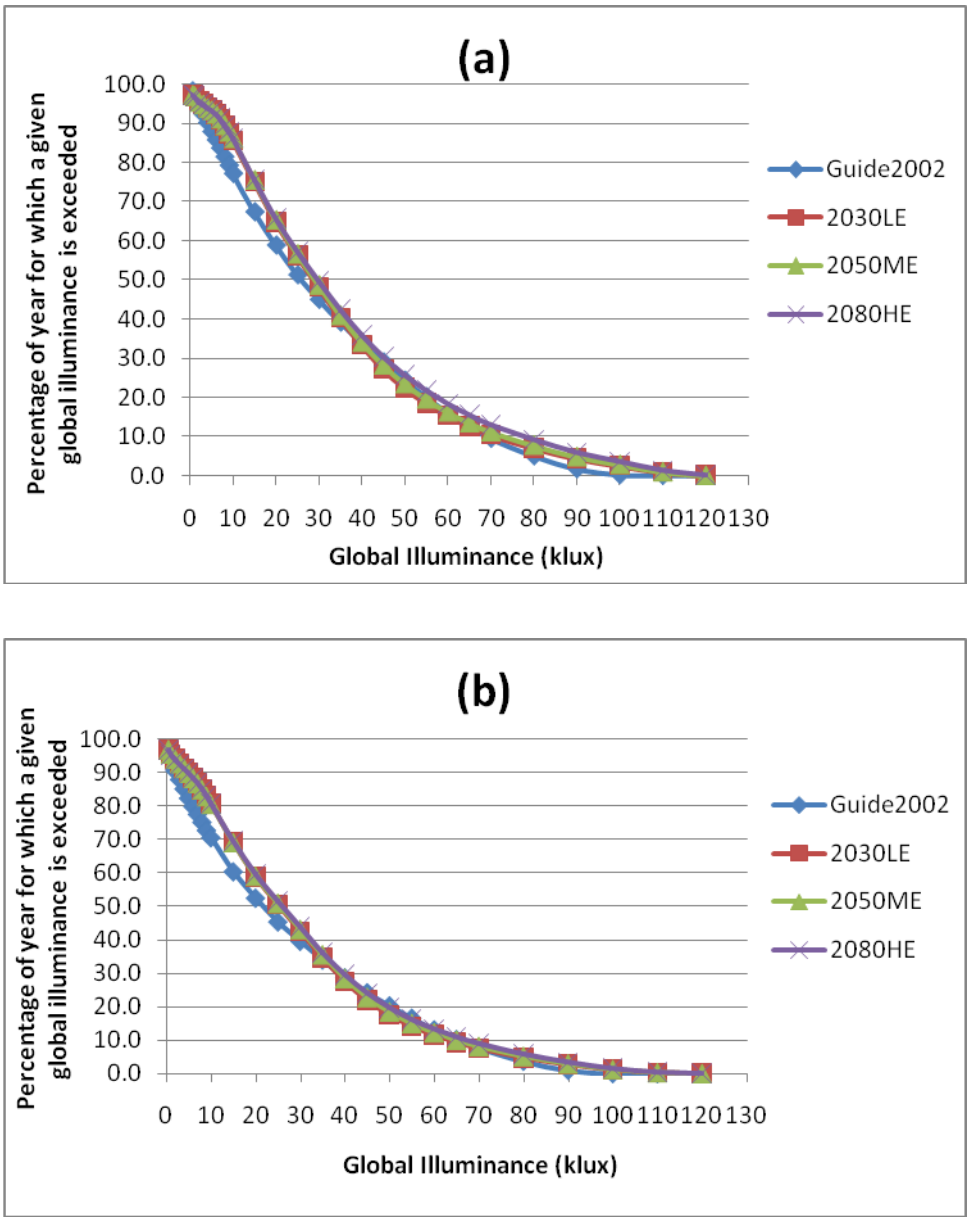

Figure 5.3.2.1 Frequency of occurrence of global illuminance for Bracknell (a) and Edinburgh (b). Note: Guide 2002= CIBSE Guide J 2002, LE= Low Emission, ME= Medium Emission, HE= High Emission

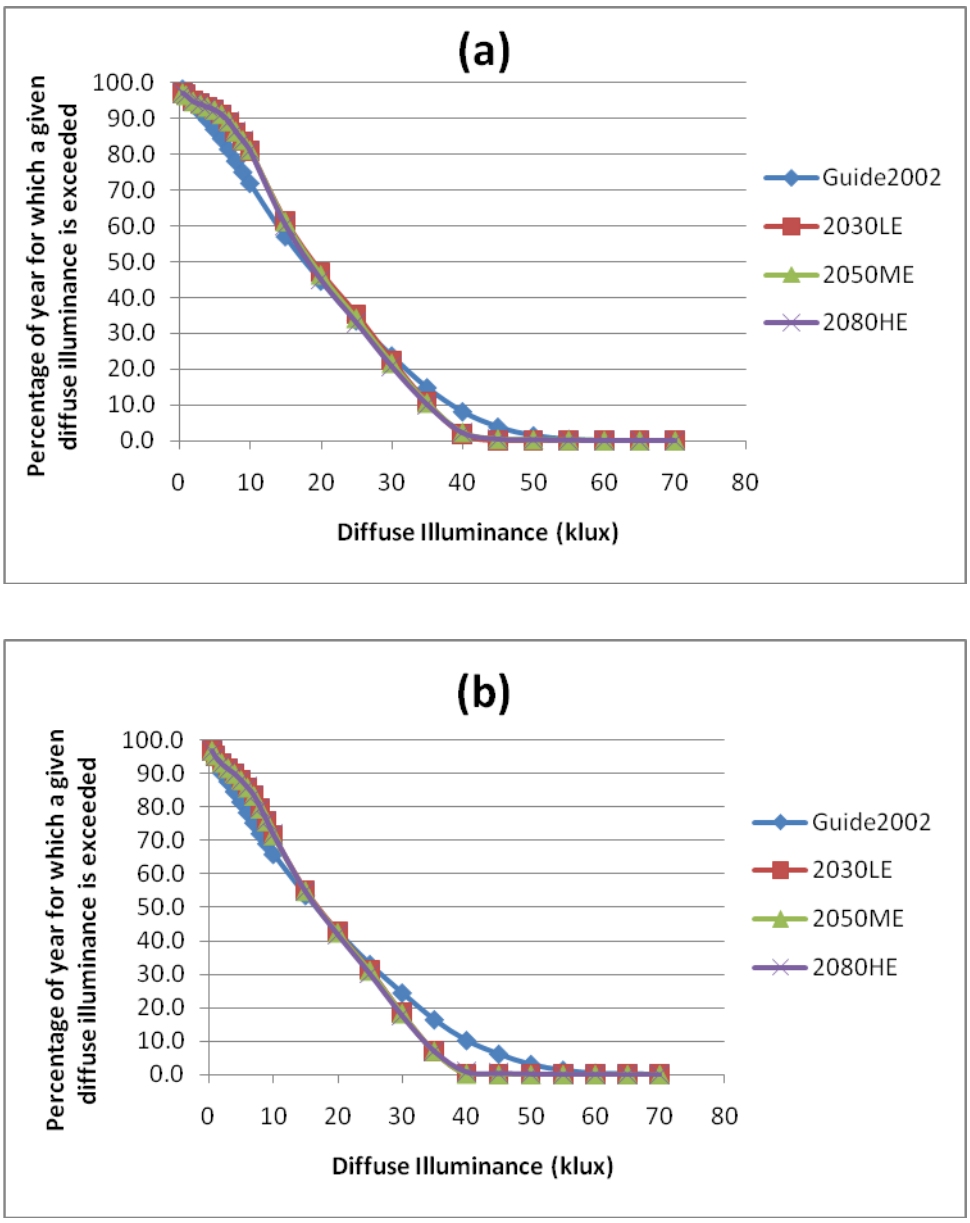

Figure 5.3.2.2 Frequency of occurrence of diffuse illuminance for Bracknell (a) and Edinburgh (b). Note: Guide 2002= CIBSE Guide J 2002, LE= Low Emission, ME= Medium Emission, HE= High Emission

For global illuminance, both locations show the same increasing trend of frequencies of occurrence for global illuminance for the 0 - 30 klux range for all WG scenarios when compared with CIBSE data. A similar trend of increased frequency of global illuminance for the 70 - 110 klux for Bracknell and 80 - 110 klux for Edinburgh is also apparent.

For diffuse illuminance, the frequencies of occurrence show an increase from 0 - 15 klux for Bracknell and 0 - 25 klux for Edinburgh for all WG scenarios. Both locations show gradual decrease of frequencies of occurrence as the diffuse illuminance level increases. For Bracknell, the CIBSE data shows that the frequencies of occurrence of diffuse illuminance are constantly higher than the WG scenarios for 30 - 50 klux range. For Edinburgh, the diffuse illuminance frequencies start to decrease for the 25 - 40 klux range for all WG scenarios. The frequencies of occurrence for CIBSE data are higher for the 25 - 50 klux.

The influence of latitude is greater for cumulative global illuminance frequency than for the diffuse component.

Note that, tables of frequencies of occurrence for all the above scenarios can be found at the attached compact disk (CD) together with this report.

5.4 Evaluation of projected data

Due to the changes in sol-air temperature and illuminance as discussed in the previous sub-sections, measured data and selected data sets from the UKCP09 WG as discussed previously i.e. control, 2030LE, 2050ME and 2080HE were used for this evaluation.

The UKCP09 WG data sets were generated through the UI provided by UKCP website. A single run of the WG produces 100, 30-year hourly future data files of the selected scenario and 100, 30-year hourly control data files. These files are then combined into one single file for each data type, i.e. control and future data files. In this study only the future data files were used. All files were combined by using Microsoft Windows® cmd program.

After combining all the files, the year variable has to be changed to an ascending sequential order from 1 to 3000. For this study the year numbers have been re-assigned the values of 5001 to 8000. This is because each of the output files from the WG contained the same year that started from 3001 to 3030. Furthermore, by changing the year sequence, the exact days for the selection of the 89.5^{th} percentile days can be identified and used for further

analysis in this study. The 89.5th percentile is used because data generated from the WG which exceed of 90th percentile has high uncertainties due to relatively short observed records of hourly data and rainfall model used in WG as discussed in the Annex of the WG report (Jones, Kilsby, Harpham et al. 2009).

In the next step the daily global solar radiation (gsr) is summed up from the constituent hourly values. The monthly daily solar radiation files were rearranged in ascending order according to daily solar radiation value. This process is used to identify the 89.5th percentile days. Hourly values corresponding to the 89.5th percentile days were then extracted.

All the above mentioned tasks were carried out using Microsoft Excel® and in-built Visual Basic for Application (VBA) tool. Figure 5.4.1 presents all of the above-mentioned steps.

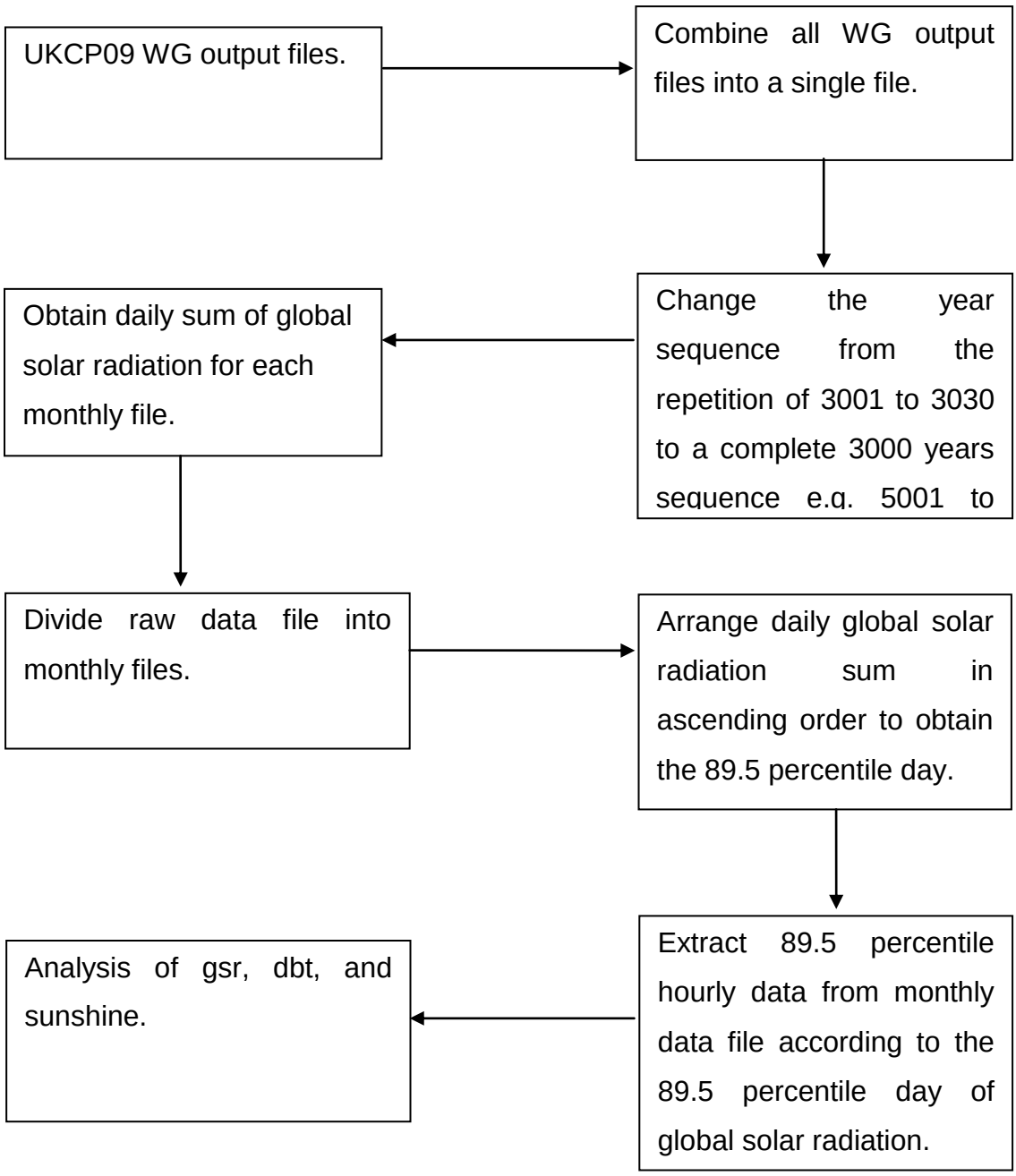

Figure 5.4.1 Process flow chart to obtain 89.5 percentile of gsr, dbt and, sunshine for analysis.

5.4.1 Results and discussion

Three basic variables from the WG output were analysed in detail namely sunshine duration (ss), global solar radiation (gsr) and dry-bulb temperature (dbt). All of these three variables are the basic inputs to most of the building simulation tools.

Sunshine duration is the main variable that is used to generate solar radiation in the WG as shown in Figure 2.10.1 in Chapter 2. Two selected locations i.e. Bracknell and Edinburgh as discussed in section 6.2.2 were analysed.

For Bracknell, future data set for 2050ME up to 2080HE show a full hour's sunshine from the 6th to the 20th hour of the day corresponding to the 89.5th percentile of daily total radiation. In contrast, the measured data set indicated only four full hours of sunshine, i.e. from the 11th to the 14th hour. Furthermore when comparing the control data with the measured data, the control data showed a longer sunshine duration in the earlier hours of the day i.e. from the 5th to the 10th hour. Figure 5.4.1.1 and 5.4.1.2 shows the sunshine duration for all data sets for Bracknell and Edinburgh respectively.

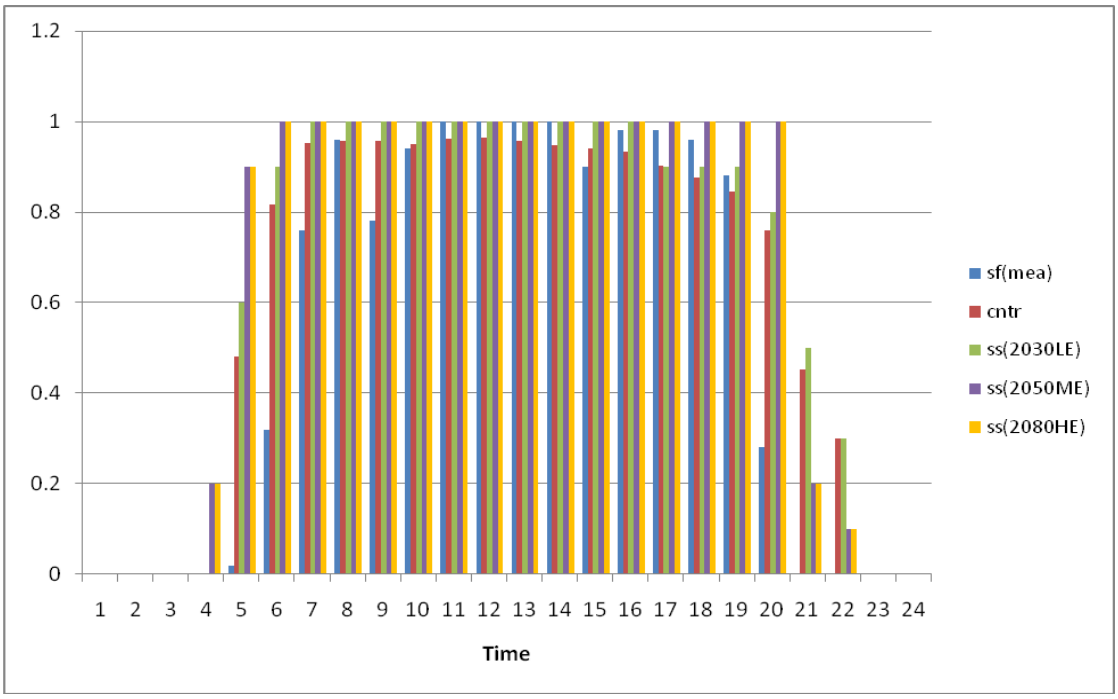

Figure 5.4.1.1 Comparison of future and measured sunshine corresponding to the 89.5th percentile of daily total radiation for June. Location: Bracknell. Note: sf= sunshine fraction, mea= measured data (1981-1992), cntr=control data from the WG, LE= Low Emission, ME= Medium Emission, HE= High Emission

As for Edinburgh, a significant difference is found throughout the day between the control and WG data sets. The values of sunshine duration for measured

data were found to be in the range of 0.4 and 0.8 hour for the 5th to the 20th hour of the day. However, for 2080HE data the corresponding hourly sunshine fraction were found to be in 0.8 to 1 range. Besides that, the control data also showed longer spells of sunshine for the entire day. The above difference of sunshine duration between the two data sets under discussion leads to the difference of gsr. This item will be discussed later.

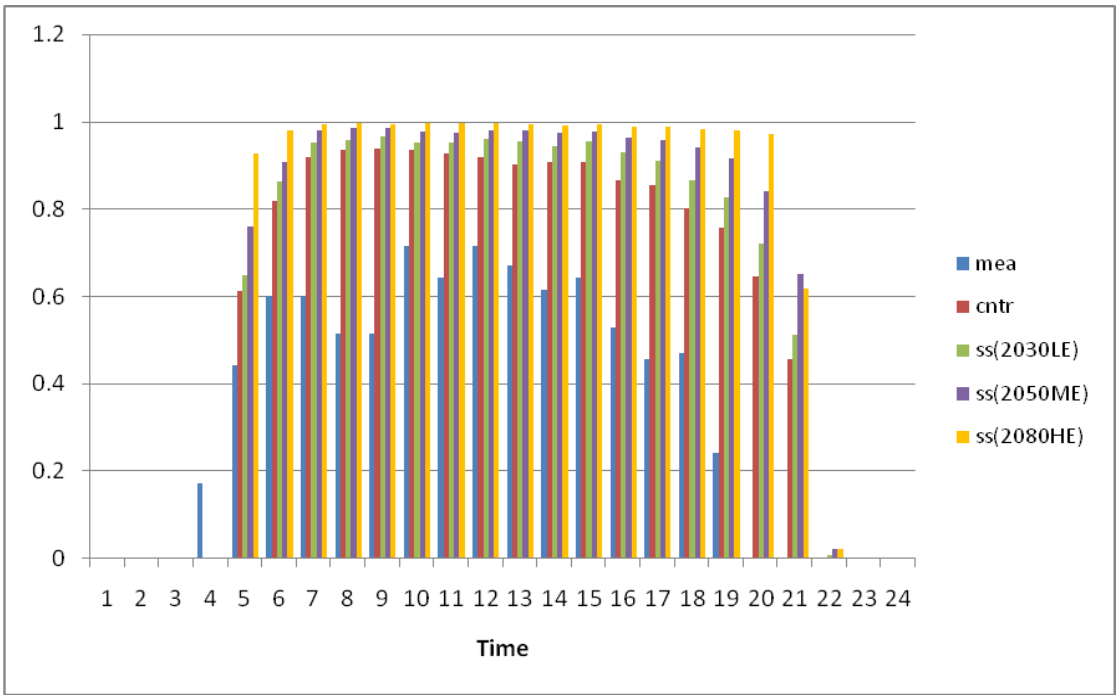

Figure 5.4.1.2 Comparison of future and measured sunshine corresponding to the 89.5th percentile of daily total radiation for June. Location: Edinburgh. Note: sf= sunshine fraction, mea= measured data (1976-1992), cntr=control data from the WG, LE= Low Emission, ME= Medium Emission, HE= High Emission

Of particular note was the anomalous occurrence in UKCP09 of late evening sunshine duration. For Bracknell and Edinburgh, the sunshine duration at hour ending 20 and beyond showed a substantial amount of predicted sunshine. As a result of this work, the following corrective action has been proposed for UKCP09 data set, i.e. to use the World Meteorological Office (WMO) rule that bright sunshine duration corresponds to irradiation exceeding 120W/m^2. (Wood, Muneer and Kubie 2003)

The second variable is the global solar radiation (gsr). The UKCP09 WG generates direct and diffuse radiation components. To obtain the gsr for these data sets, direct and diffuse radiation are added up. Figures 5.4.1.3 and 5.4.1.4 show hourly gsr for Bracknell and Edinburgh. At 13th hour of the day, significant differences of gsr were found for both locations. For Bracknell, the measured value of gsr is 818 Wh/m^2 and the 2080HE future value is 1002 Wh/m^2. This shows a significant increase of 184 Wh/m^2 or 22.5 percent. The same trend is to be seen for Edinburgh, with the measured data value being 789 Wh/m^2 and the 2080HE predicted value of 948 Wh/m^2. This is an increase of 159.2 Wh/m^2 or 20.2 percent.

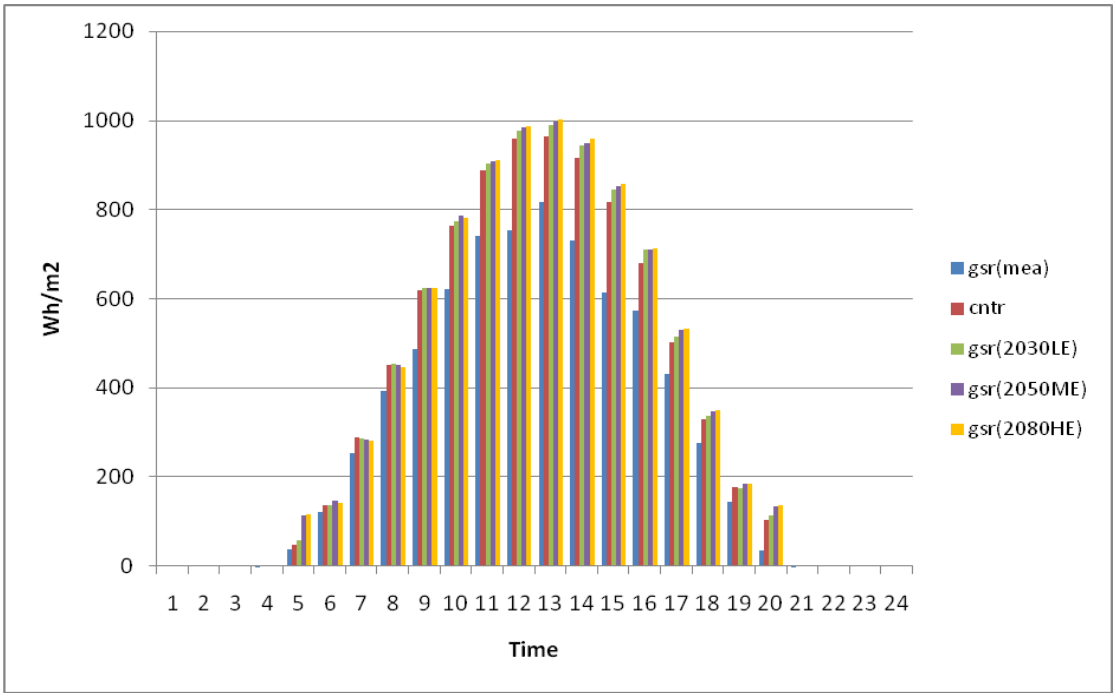

Figure 5.4.1.3 Comparison of future and measured hourly global solar radiation corresponding to the 89.5th percentile of daily total radiation for June. Location: Bracknell. Note: gsr= global solar radiation, mea= measured data (1981-1992), cntr=control data from the WG, LE= Low Emission, ME= Medium Emission, HE= High Emission.

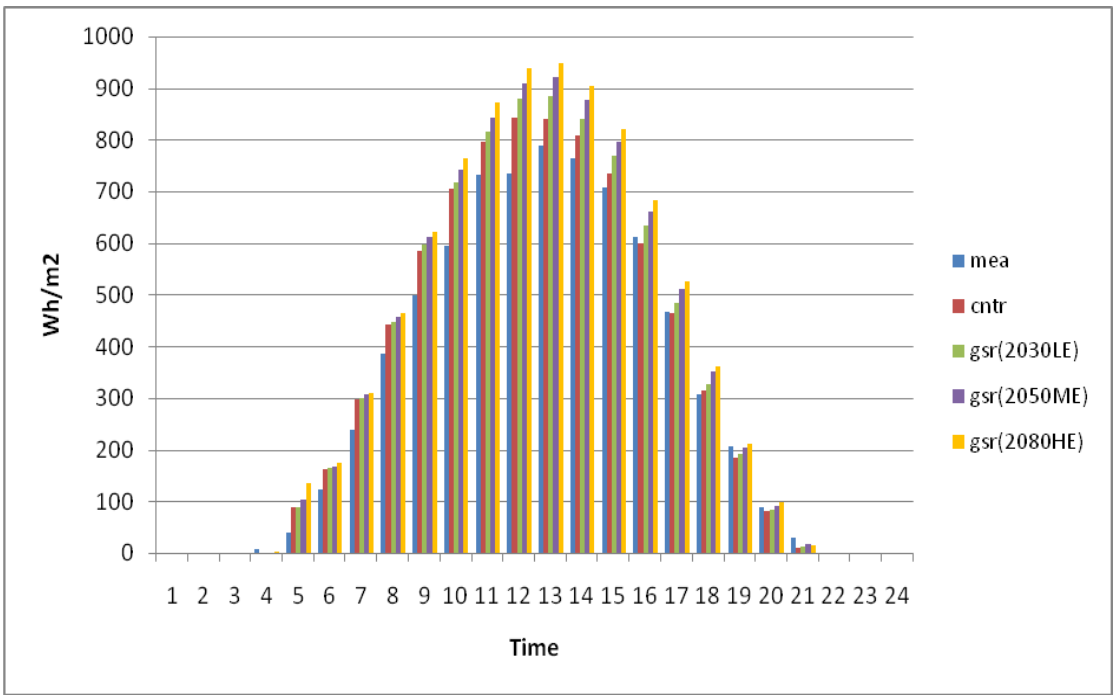

Figure 5.4.1.4 Comparison of future and measured hourly global solar radiation corresponding to the 89.5th percentile of daily total radiation for June. Location: Edinburgh. Note: gsr= global solar radiation, mea= measured data (1976-1992), cntr=control data from the WG, LE= Low Emission, ME= Medium Emission, HE= High Emission.

Furthermore, an evaluation of the change in diffuse to global radiation ratio (DRG) was carried out. The DRG values for Bracknell show a drastic decrease from 0.37 for measured data set to 0.13 for 2080HE future data set. For Edinburgh, the DRG decreases from 0.33 to 0.14. Figures 5.4.1.5 and 5.4.1.6 respectively show in greater detail the decreasing trend of DRG for Bracknell and Edinburgh. DRG value is used as an indicator of the sky's clarity. A drastic decrease in DRG of this magnitude signifies a radical shift in the character of solar climate for the future. The current solar climate of Bracknell is known for its above average turbidity, the latter stemming from the following factors: inland location, high density housing, proximity to Heathrow airport and M25 London orbital motorway. Whether such an extreme shift in the sky clarity will occur within a matter of 60 to 70 years is open to discussion.

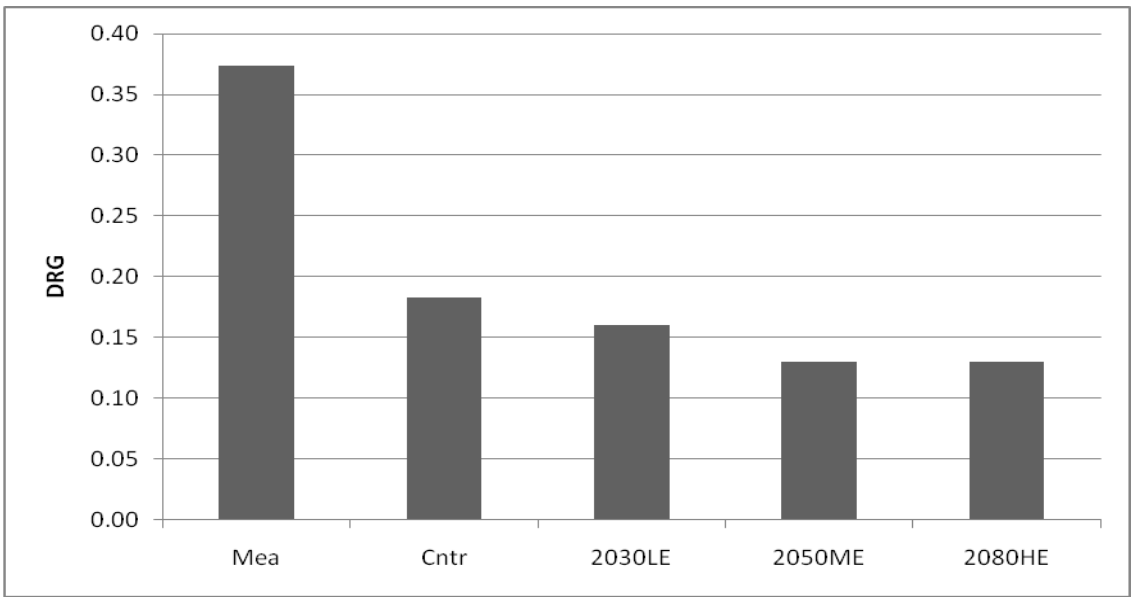

Figure 5.4.1.5 Comparison of future and measured diffuse to global radiation ratio (DRG) at 1300 hours corresponding to the 89.5th percentile of daily total radiation for June. Location: Bracknell Note: mea= measured data (1981-1992), cntr=control data from the WG, LE= Low Emission, ME= Medium Emission, HE= High Emission

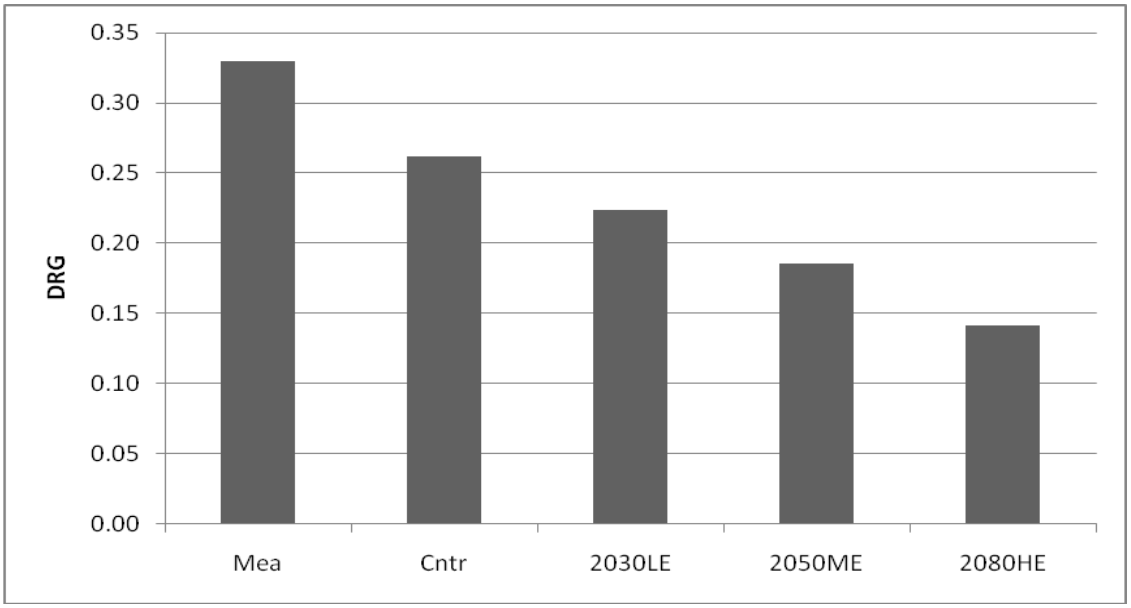

Figure 5.4.1.6 Comparison of future and measured diffuse to global radiation ratio (DRG) at 1300 hours corresponding to the 89.5th percentile of daily total radiation for June. Location: Edinburgh. Note: mea= measured data (1976-1992), cntr=control data from the WG, LE= Low Emission, ME= Medium Emission, HE= High Emission

The third variable under study is the dry bulb temperature (dbt). During the middle of the day i.e. 13th hour, the dbt for Bracknell shows an increment of as much as 3.7°C while comparing the measured value with the 2080HE data. An even higher increment occurs for Edinburgh with the difference being 5.5°C. This increase in future temperature is in line with the analysis of Betts et al (Betts, Sanderson, Hemming et al. 2009) who have shown that future temperature may increase by as much as 4°C. Hence summers warmer than the year 2003 may occur regularly if the predictions come true as discussed before in Chapter 1. This presents a great challenge to the building services industry. Figures 5.4.1.7 and 5.4.1.8 show the hourly dbt for Bracknell and Edinburgh.

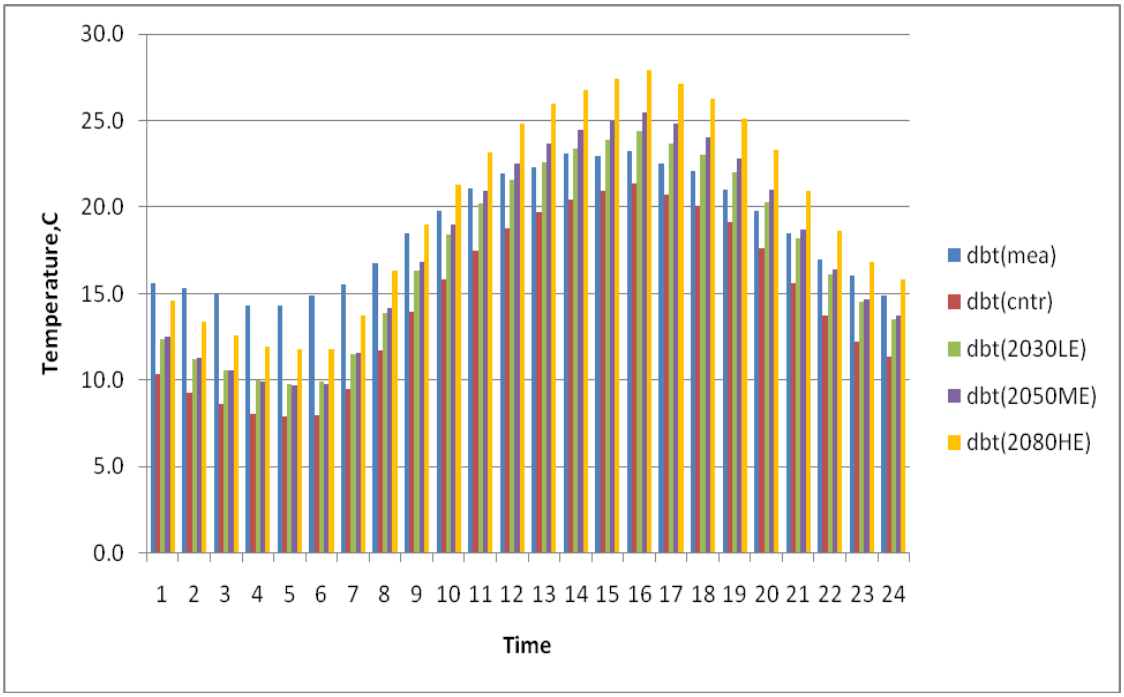

Figure 5.4.1.7 Comparison of future and measured hourly dry bulb temperature corresponding to the 89.5th percentile of daily total radiation for June. Location: Bracknell. Note: gsr= global solar radiation, mea= measured data (1981-1992), cntr=control data from the WG, LE= Low Emission, ME= Medium Emission, HE= High Emission

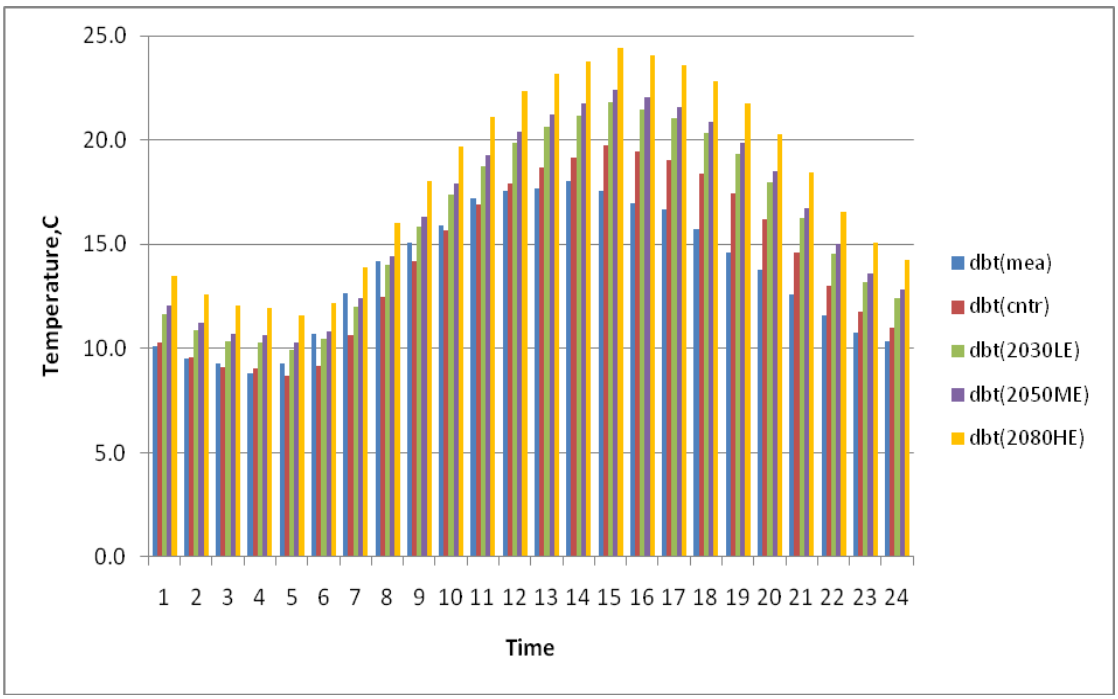

Figure 5.4.1.8 Comparison of future and measured hourly dry bulb temperature corresponding to the 89.5th percentile of daily total radiation for June. Location: Edinburgh. Note: gsr= global solar radiation, mea= measured data (1976-1992), cntr=control data from the WG, LE= Low Emission, ME= Medium Emission, HE= High Emission

5.5 Sensitivity test for sol-air temperature

An in-depth sensitivity test was carried out to analyze the impact of the constituent variables on sol-air temperature. These main basic variables are global solar radiation, dry bulb temperature and wind speed. The sensitivity test was performed in two stages described below.

For horizontal surfaces, where wind speed was set at 3 m/s with the changes being made to global solar radiation and dry bulb temperature incrementally. A 10 percent change in global solar radiation alone result in an increase of 6.2% in sol-air temperature for dark-coloured surface and 5.3% increase for light-coloured surface. An increase in the dry bulb temperature by 20 percent though increases sol-air temperature by 6 and 9% respectively for dark and light-coloured surfaces.

The second stage was to set the wind speed at 4 m/s. Without any changes in global solar radiation and dry bulb temperature, the sol-air temperature decrease by 8.9 and 6.5% respectively for dark and light-coloured surfaces. In the next step changes in global solar radiation and dry bulb temperature were applied. With a 20 percent change in dry bulb temperature and 10 percent change in global solar radiation, the sol-air temperature was found to increase by 3% for dark- and 7.3% for light-coloured surface.

For vertical surfaces, the same two-stage test was carried out. For the first stage, the wind speed was set at 3 m/s with an increment of 10 percent in global solar radiation, the sol-air temperature increased by 5.5% for dark-coloured surface and 4.6% for light surface. A 20 percent increment of dry bulb temperature produced a 13.8% increase in sol-air temperature for dark-coloured surface. The corresponding increase for light-coloured surface was 15.6%.

For the second stage where the wind speed set at 4 m/s and with no changes to dry bulb temperature and global solar radiation, a decrease in sol-air temperature of 8.1% for dark-coloured surface and 6.4% for light surface was found. Then an increase of 20 percent in dry bulb temperature and 10 percent of global solar radiation saw an increase of 5.3% and 8.4% for dark- and light-coloured surface respectively.

Note that the limit of global solar radiation and dry bulb temperature in the sensitivity test was set at 10% and 20% respectively. These limits were based on the difference between measured and the 2080HE WG data sets. Figures 5.5.1 and 5.5.2 show the sensitivity test's results for horizontal surfaces and vertical surfaces facing south. All values are expressed in percent.

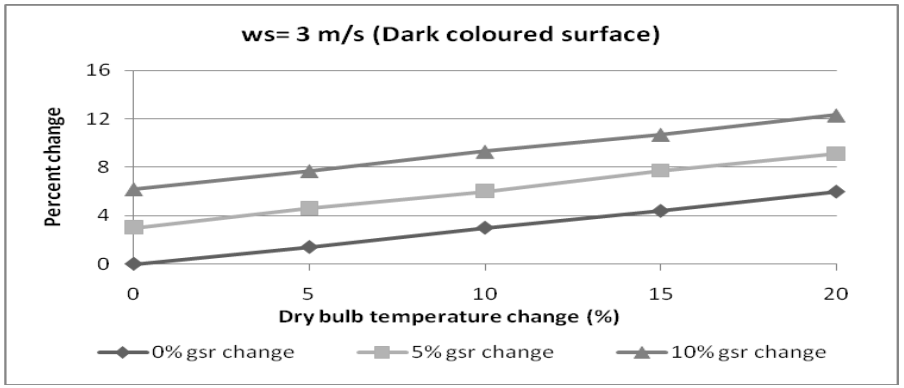

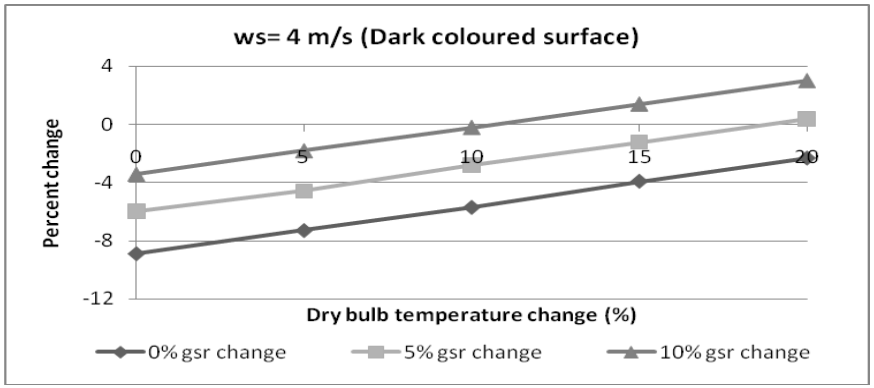

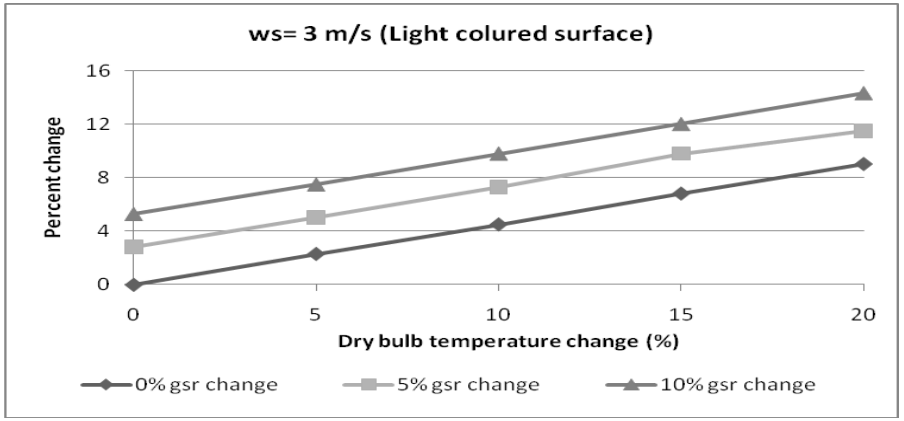

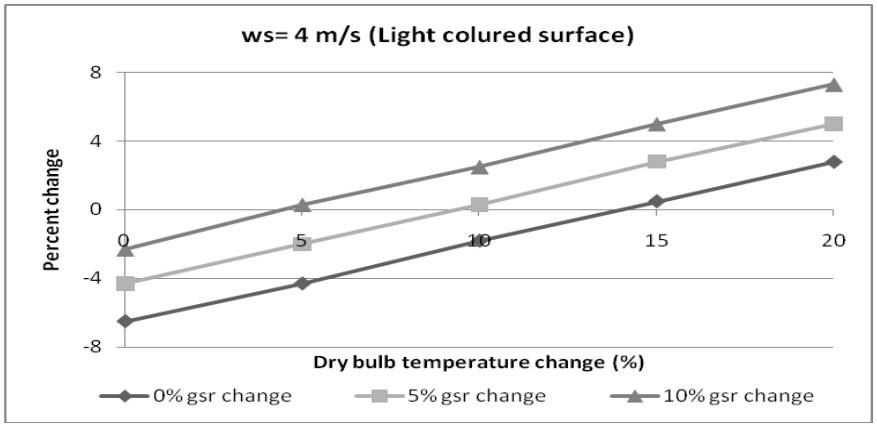

Figure 5.5.1 Percentage change of sol-air temperature in sensitivity test for horizontal surfaces. Note: ws=wind speed(m/s), gsr= global solar radiation.

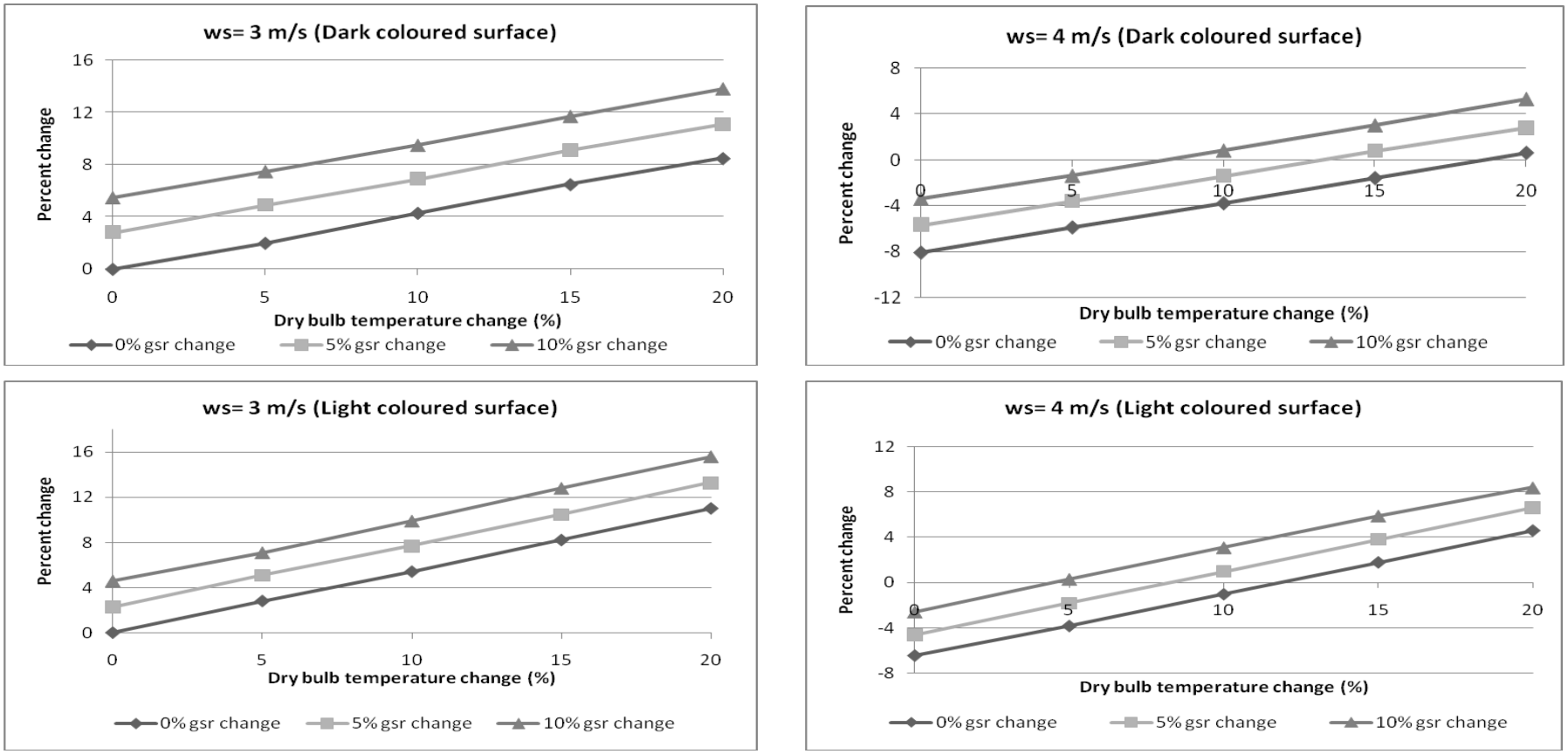

Figure 5.5.2 Percentage change of sol-air temperature in sensitivity test for vertical surfaces. Note: ws=wind speed(m/s), gsr= global solar radiation.

5.6 Conclusions

Data sets from the UKCP09 were used in this study along with the historical measured data for three locations i.e. Bracknell (London), Manchester and Edinburgh to critically analyse sol-air temperature and the likely change that may occur in the key climate variables, i.e. temperature, sunshine duration and solar irradiation.

Three carbon dioxide (CO_2) emission scenarios at different time series were selected, namely 2030 Low Emission, 2050 Medium Emission and 2080 High Emission scenarios. These data sets were selected because it covered different CO_2 emission scenarios and a wide range of time series from 2020 till the end of this century. Note that only results from Bracknell and Edinburgh are discussed in detail because the results for Manchester show the similar trend.

It was found that the UKCP09 data sets showed a substantial increase in temperature, sunshine and solar irradiation when compared with historical measured data. For Bracknell and Edinburgh the clear-day noon temperatures were respectively found to increase by nearly 4- and 6 Celsius within a span of 75 years. Likewise, the increase in the corresponding irradiation was around 20%, which when combined with the drastic temperature rise would pose a serious challenge for the cooling of buildings.

A study to investigate the impending changes in sol-air temperature and daylight illuminance was carried out. For the year 2080 High Emission scenario the sol-air temperature for dark-coloured horizontal surface has the highest difference i.e. for Bracknell and Edinburgh an increase of 13.3°C and 20.1°C respectively. For vertical surfaces facing south, sol-air temperature increases of 13.4°C and 11.5°C were found for dark- and light-coloured surfaces for Edinburgh, and 6.4°C and 5.8°C, respectively, for the latter surfaces, for Bracknell.

Besides that, a shifting trend of daylight illuminance is evident. For global illuminance, both locations show the same increasing trend of frequencies of

occurrence for global illuminance for the 0 - 30 klux range for all scenarios when compared with CIBSE data. A similar trend of increased frequency of global illuminance for the 70 - 110 klux for Bracknell and 80 - 110 klux for Edinburgh is also apparent. For diffuse illuminance, the frequencies of occurrence show an increase from 0 - 15 klux for Bracknell and 0 - 25 klux for Edinburgh for all scenarios. Both locations show gradual decrease of frequencies of occurrence as the diffuse illuminance level increases. For Bracknell, the CIBSE data shows that the frequencies of occurrence of diffuse illuminance are constantly higher than the future scenarios for 30 - 50 klux range. For Edinburgh, the diffuse illuminance frequencies start to decrease for the 25 - 40 klux range for all scenarios. The frequencies of occurrence for CIBSE data are higher for the 25 - 50 klux.

Furthermore, a study was conducted to investigate the cause of the shifting trend in daylight illuminance. It found that the predictions indicate a radical change in the characteristics of solar climate, i.e. from the present diffuse fraction (of total irradiation) of 0.37 which indicates mild turbidity, the value would drop to around 0.13 indicating clear skies with exceptionally low turbidity. This behaviour was somewhat anomalous. If the prediction comes true the severe reduction in the diffuse fraction would mean that beam irradiance would be of a high order and this would necessitate appropriate shading design for windows and atria. The drastic change in sol-air temperature and the shifting trend of daylight illuminance pose a great challenge to engineers.

From the above mentioned increase in solar irradiation and the frequent occurrence of clear skies, solar applications seems to have a promising future in the UK especially photovoltaic for electricity generation.

6.0 New Weather Generator (WG_v2)

In this chapter, communications with the UKCP WG modeller will be discussed. Furthermore, modifications made to the new WG_v2 will be reviewed. Analyses of the output data sets from the WG_v2 were carried out to compare with the Meteorological Office data sets (MetD) and the now old WG data sets. This is to check and verify whether the changes or modifications applied to the WG_v2 produce reasonable estimation.

6.1 Communication with UKCP

From the previous chapter's detailed analysis of the UKCP09 WG data, it was found that the UKCP09 WG data sets showed a substantial increase in temperature, sunshine and solar irradiation when compared with historical measured data. Hence, the results were presented to the UKCP project officer i.e. Dr. Colin Harpham who is the UKCP09 WG modeller.

Through the discussion, suggestions were given to UKCP to remodel the WG. The following suggestions were given to the UKCP modeller:

- To curtail all solar/daylight calculations that are related to solar altitude less than 10 degrees.
- To use the World Meteorological Office (WMO) rule that bright sunshine duration corresponds to irradiation exceeding 120W/m^2. (Wood, Muneer and Kubie 2003)

The above suggestions were taken into discussion at the UKCP WG meeting. After the meeting, the modeller decided to address the sunshine duration issue and remodel the WG. The test data set generated from the remodelled WG was supplied for further analysis.

Comparisons of sunshine duration were carried out for two months namely January and July. Data were extracted from the test and old data set provided corresponding to the 89.5th percentile of daily total radiation to get the average hourly sunshine duration.

The comparisons showed that for both months decreasing of sunshine duration occurred at most of the hours of the day as shown in Figure 6.1.1. Note should be taken particularly at those late evening hours where sunshine was found. In particular the month of July clearly showed that almost a full hour of sunshine was found at hour ending 20 and partial sunshine was found at hour ending 21. Care should be taken to deal with this late evening sunshine.

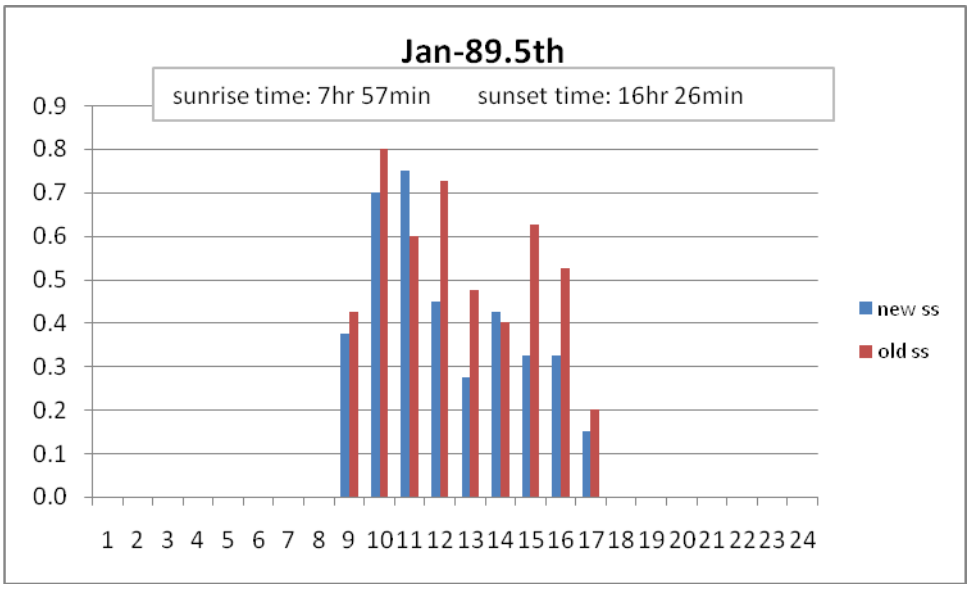

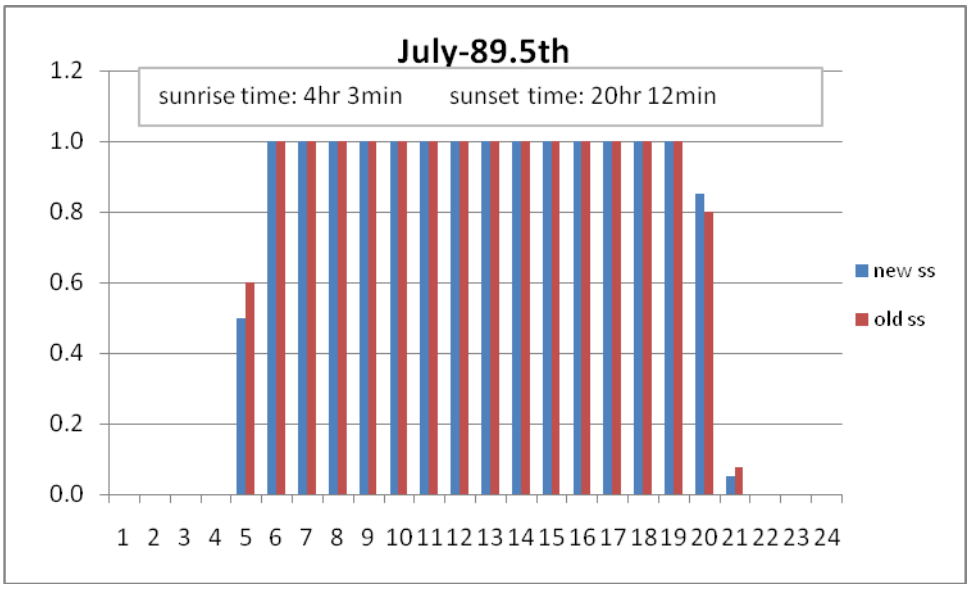

Figure 6.1.1 Comparisons of sunshine duration hours corresponding to the 89.5th percentile of daily total radiation for Heathrow. Note: old ss= UKCP09 data set, new ss= new data set provided by Dr. Colin Harpham with changes.

Following from the changes applied to the WG, a new version of WG were released on the 26th January 2011 and available through the UKCP User Interface (UI) online. An acknowledgement note was given from the modeller. The note is as follow:

"*This note provides recognition of the quality control work undertaken by Edinburgh Napier University staff under the COPSE project, namely Professor Tariq Muneer and Mr Yiengwei Tham, with respect to the UKCP09 Weather Generator (WG) sunshine hours output. The latter team advise me regarding problems related to sunshine data that were reported for very late evening hours and the time system. I had discussions with the above team to resolve the relevant issues and the WG has been updated accordingly. The new version will be released together with other improvements in the near future.*" – Dr. Colin Harpham (30 September 2010)

Note that all communications with WG modeller were attached in Appendix B.

6.2 Updates made to Weather Generator version 2.0

The UKCP report stated that "*In September 2010, a UKCP09 user brought to our attention that the outputs from the Weather Generator showed unrealistic changes in future sunshine hours when compared to changes in future cloud cover.*" (Stephens and Jones 2011) This corresponds to the email communications that were discussed in the previous section that the author is the user stated in the report.

As a result, a new version of WG was released; this is the Weather Generator version 2.0 in January 2011. There are four main updates included in the WG_v2. Following are the updates which are extracted from the UKCP web page (UKCIP 2011):

i) Rain fall extreme

A new statistical distribution has been implemented to better replicate historical extreme periods across the range of return periods at which it is applicable.

ii) Temperature extreme

Improvements have been made to heat duration by adding an extra dry spell transition.

iii) Improvement in sunshine hours

Modifications have been made to shorten the simulated day length to be consistent with measurements of effective sunshine.

iv) Changes in sunshine and vapour pressure

A new baseline has been produced for sunshine and vapour pressure to produce more realistic changes in future projections.

For more in-depth information about the WG version 2.0 please refer to the UKCP report and guidance web page:

http://ukclimateprojections.defra.gov.uk/content/view/1206/500/

Note that only changes in sunshine hours will be discussed in detail in the next section.

6.2.1 Improvement and changes to sunshine hours

The original WG produced or estimated daily sunshine from the moment the sun rose above the horizon. On the other hand, observational equipment does not begin recording until the sun is higher which lead to the WG over-estimated effective sunshine. Improvement or modifications were made to include a more realistic day length which was slightly shorter. This update now accurately reflects how sunshine is measured.

Due to the unrealistic changes in future sunshine hours, changes were made to the climatology's baseline in sunshine. The unrealistic changes were due to the choice of observed climatology used in generating the change factors and do not stem from errors in either the UKCP09 probabilistic data or the UKCP09 WG. Hence, a new observed baseline has been set up to produce more realistic changes.

Most of the variables required in the change factors are available in the projections whereas sunshine and vapour pressure are not available. Therefore, these variables are derived from available variables i.e. sunshine from cloud cover and vapour pressure from relative humidity and temperature.

6.3 Procedure to produce sunshine in Weather Generator

From the WG technical report, to calculate the future change in sunshine the following steps were to perform as shown in Figure 6.3.1 below.

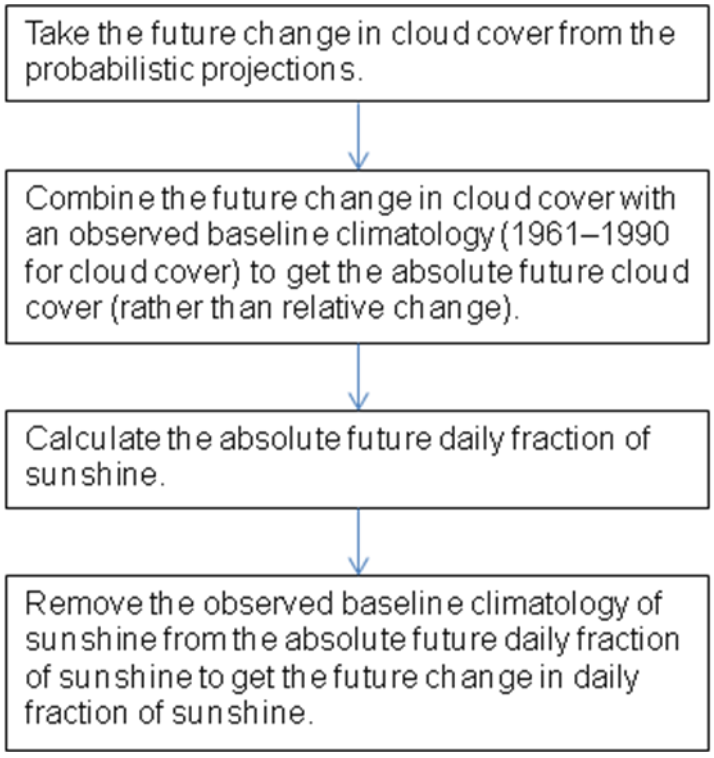

Figure 6.3.1 Steps to calculate future change in sunshine (Stephens and Jones 2011).

Sunshine is calculated from the total cloud cover assuming the following relationship:

$$SUNSHINE\_FRACTION = (1 - CLOUD\_FRACTION) \quad (6.3.1.1)$$

The use of observed baseline climatologies caused the problem with sunshine change factors for which the relationship in the above equation does not hold true. From the producers of the baseline climatologies, the observational baselines, cloud and sunshine, are derived from different measurements and do not always follow the above equation. Hence, this is not a problem with the climatologies, the projections or the weather generator. The problem lies in the assumptions that the project team took when deciding how to create the change factors.

To address the problem, new baseline climatology from the cloud baseline was created so that the above relationship remains constant for both the baseline and future climate. An example of the proposed change was demonstrated in the WG report. The following steps were taken to make the correction:

1. Generate a new baseline climatology for sunshine (derived from cloud cover) and vapour pressure (derived from RH and temperature).

2. Create validation plots of the new climatology to show the difference from the current sunshine and vapour pressure climatologies.

3. Implement the change under the UI so that the new climatologies are used when calculating change factor.

6.4 Data analysis

In this section, detail analysis was carried out in this section to determine the effects of the changes applied to the WG_v2 on sunshine and global solar irradiation.

6.4.1 Previous and improved Met. Office and WG Datasets

Data sets for two locations i.e. Bracknell and Edinburgh were downloaded from the WG version 2.0 UI. Two time series were selected i.e. 2030 and 2080. This two time series were selected because of the wide range of time which cover from 2020 till the end of the century. The selected CO_2 emissions scenarios were low emissions for 2030 and high emissions for 2080. These emissions scenario were selected because it covers the lower and the highest part of all the data sets that proposed in this study. Furthermore, data sets from the UK Meteorological Office (MetD) and the control data sets from the WG will be used along with the generated WG data sets. Table 6.4.1.1 shows the information of all data sets used.

Table 6.4.1.1 Details of the data used in the present study.

Location	Latitude	Data set
Bracknell	51.38ºN	Control, 2030LE,2080HE,MetD
Edinburgh	55.85ºN	Control, 2030LE,2080HE,MetD

6.4.2 Results and Discussions

WG_v2 data sets were analysed and compared with the now old WG data sets results from analyses carried out in the previous chapter. This is to evaluate the effects of the changes made to the projected future data from WG_v2. The procedures used to produce the 89.5th percentile for the WG_v2 is the same as the old WG as discussed in the previous chapter.

The first analysis was to look at the ratio of diffuse to global irradiation (DRG) for both the selected locations i.e. Bracknell and Edinburgh. Figure 6.4.2.1 shows side by side comparisons between the WG_v2 data sets, the old WG data sets and the Meteorological Office data sets (MetD). A drastic change was observed for all WG_v2 data sets when compare with the old WG data sets. The DRG ratio for control data sets increased from 0.18 to 0.26 for Bracknell and 0.26 to 0.33 for Edinburgh. For 2030LE scenario, the DRG ratio increased from 0.16 to 0.28 and 0.22 to 0.34 for Bracknell and Edinburgh respectively. The highest increased was observed for Edinburgh in the 2080HE scenario with an increase of 0.16 from 0.14 to 0.30. For Bracknell for the 2080HE data sets, an increase of 0.11 was observed from 0.13 to 0.24. From this analysis, the extreme clear sky conditions which was found in the old WG data sets from the previous analysis seems to be disappeared or not valid. Furthermore, the future projected data sets from the WG_v2 seem to produce more realistic future projections for the UK sky conditions when comparing the MetD data sets.

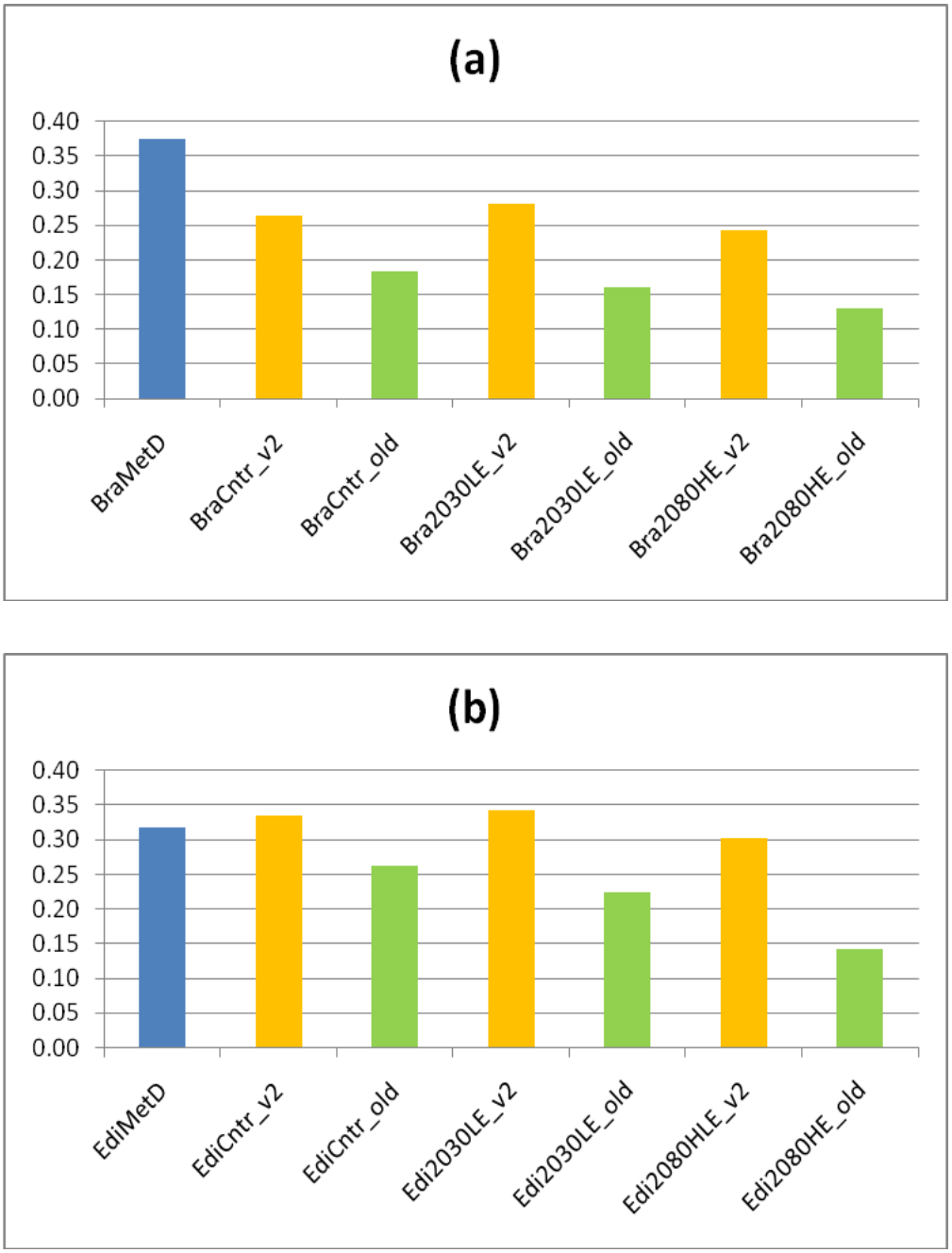

Figure 6.4.2.1 DRG for June at 1300 hrs at 89.5th percentile; (a) Bracknell and (b) Edinburgh. Note: MetD= Meteorological Office data set, old= old WG control data sets, v2= WG version 2.0 data sets, LE= Low Emissions, HE= High Emissions

Further analyses were carried out to evaluate the two main variables i.e. total global solar irradiation (GSR) and sunshine duration (SS). The first variable is the GSR. Figures 6.4.2.2 and 6.4.2.3 show the comparisons of GSR for Bracknell and Edinburgh respectively.

It is evident that a drastic decrease of GSR was found for the WG_v2 data sets when compared with the old WG data sets. The old WG data sets showed constant higher GSR values from the ninth till the 17^{th} hour of the day for Bracknell. For Edinburgh, the higher values of GSR were found from the ninth till 18^{th} hour of the day. Contrary, lower GSR values for the old WG were found at the early and late hour of the day. The highest GSR difference was found at 13^{th} hour of the day when comparing the 2080HE data sets which was 120 Wh/m^2 and 141 Wh/m^2 for Bracknell and Edinburgh respectively.

When comparing the MetD data sets with the WG_v2 data sets, increased of GSR was found thorough out the day especially for early and late evening hours. High GSR was found at these hours. Note should be taken where a difference of as much as 129 Wh/m^2 at the fifth hour and 193 Wh/m^2 at the 20^{th} hour of the day was found for Edinburgh and Bracknell respectively. Hence, it is advised that when using the projected data sets from the WG_v2 extra care should be taken. The user may exclude the first two hours and last two hours of the day when using the projected data for any solar application so that reasonable or good results could be obtained.

Note that data table used to produce Figure 6.4.2.2 and 6.4.2.5 are shown in Appendix C.

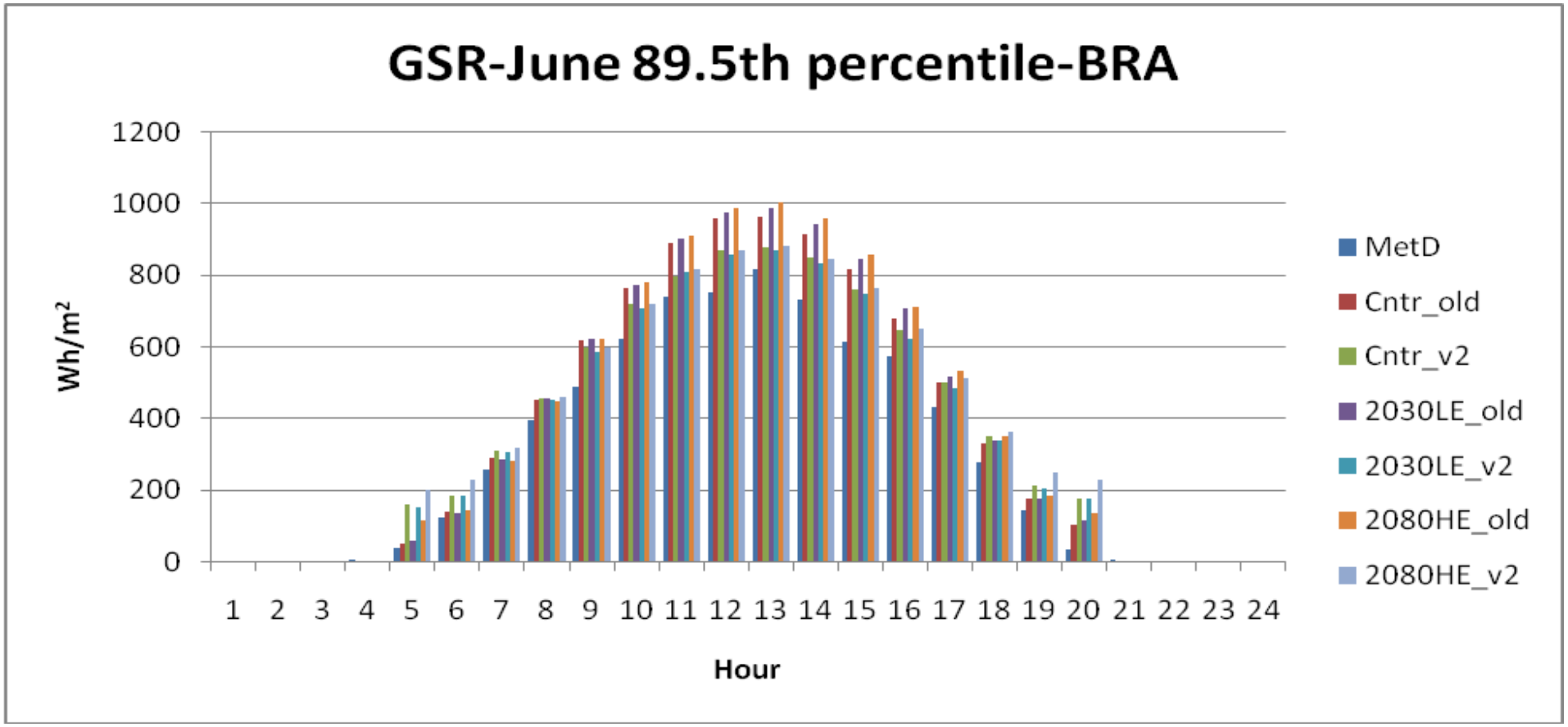

Figure 6.4.2.2 GSR comparison for Bracknell. Note: MetD= Meteorological Office data set, old= old WG control data sets, v2= WG version 2.0 data sets, LE= Low Emissions, HE= High Emissions.

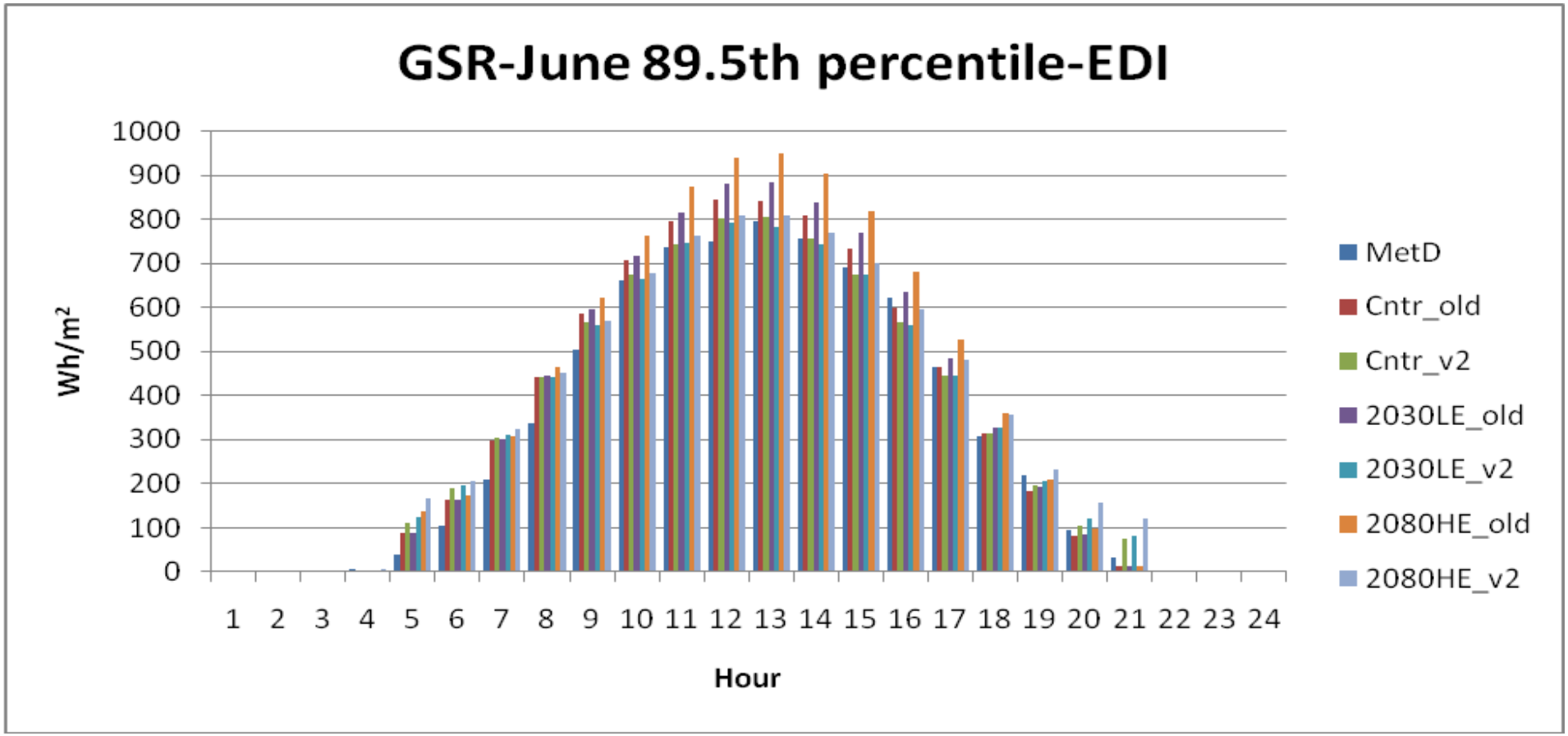

Figure 6.4.2.3 GSR comparison for Edinburgh. Note: MetD= Meteorological Office data set, old= old WG control data sets, v2= WG version 2.0 data sets, LE= Low Emissions, HE= High Emissions.

The second variable to be evaluated is the SS. When comparing the old WG and the WG_v2 data sets, drastic changes of SS were evident. For 2080HE data sets, decrease of SS was found at the early and late hours of the day i.e from fourth to sixth and 17th to 20th hour of the day for Bracknell. For Edinburgh, the differences were observed thorough the day. More distinct differences were found from the fourth to seventh and 18th to 21th hour . These decreases in the WG_v2 seem to be reasonable when comparing with the MetD data sets. Furthermore, SS which was found at very late hour of the day i.e 22nd hour of the day in the old WG data sets was not found in the GW_v2 data sets. This shows that the changes that applied to the WG_v2 seem to produce good or reasonable results.

A further comparison was carried out between the MetD data sets and the WG_v2 data sets. For the 2080HE WG_v2 data set, SS for Bracknell location shows that SS was higher during the early hour of the day and late hour of the day i.e. from fourth to seventh hour and 20th to 21st hour of the day. Contrary, higher SS was found starting from the 11th to 18th hour of the day for the MetD data set.

As for Edinburgh, higher SS was found throught out the day for the 2080HE WG_v2. Apparent differences were observed during the very late hour of the day i.e. the 19th to 21st hour of the day. SS was not found at all at the 21st hour of the day for the MetD data set where some SS was found for all the WG_v2 data sets.

Attention should be drawn to the disappearance of the SS value after sunset i.e the 22nd hour of the day from the WG_v2 data sets for both locations. Thus it is evident that the changes applied to the WG_v2 is working fine.

Note that difference of SS at the early and late hours of the day for both locations may be the main reason that big differences which were found in the GSR analysis. Figures 6.4.2.4 and 6.4.2.5 show the SS for Bracknell and Edinburgh.

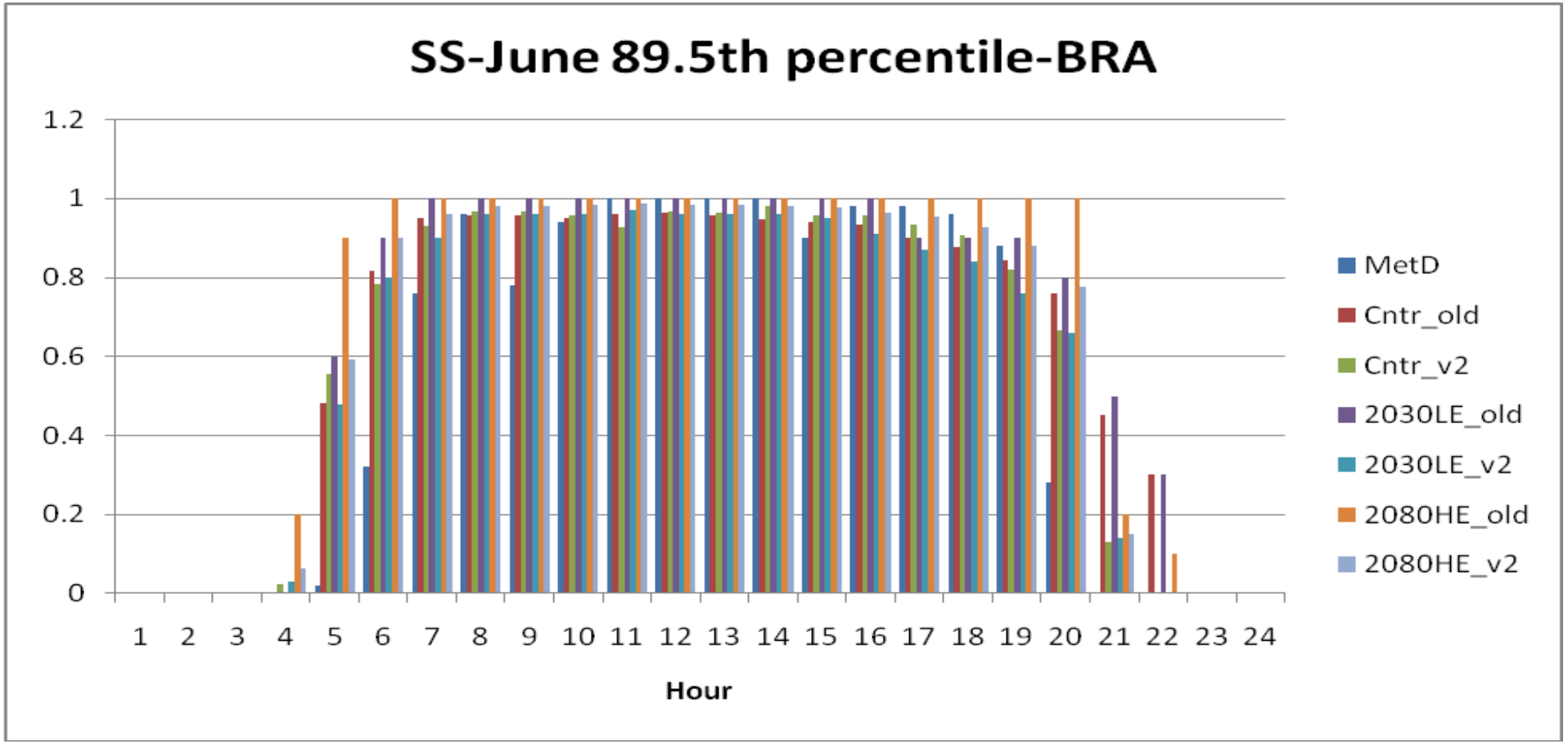

Figure 6.4.2.4 SS comparisons for Bracknell. Note: MetD= Meteorological Office data set, old= old WG control data sets, v2= WG version 2.0 data sets, LE= Low Emissions, HE= High Emissions.

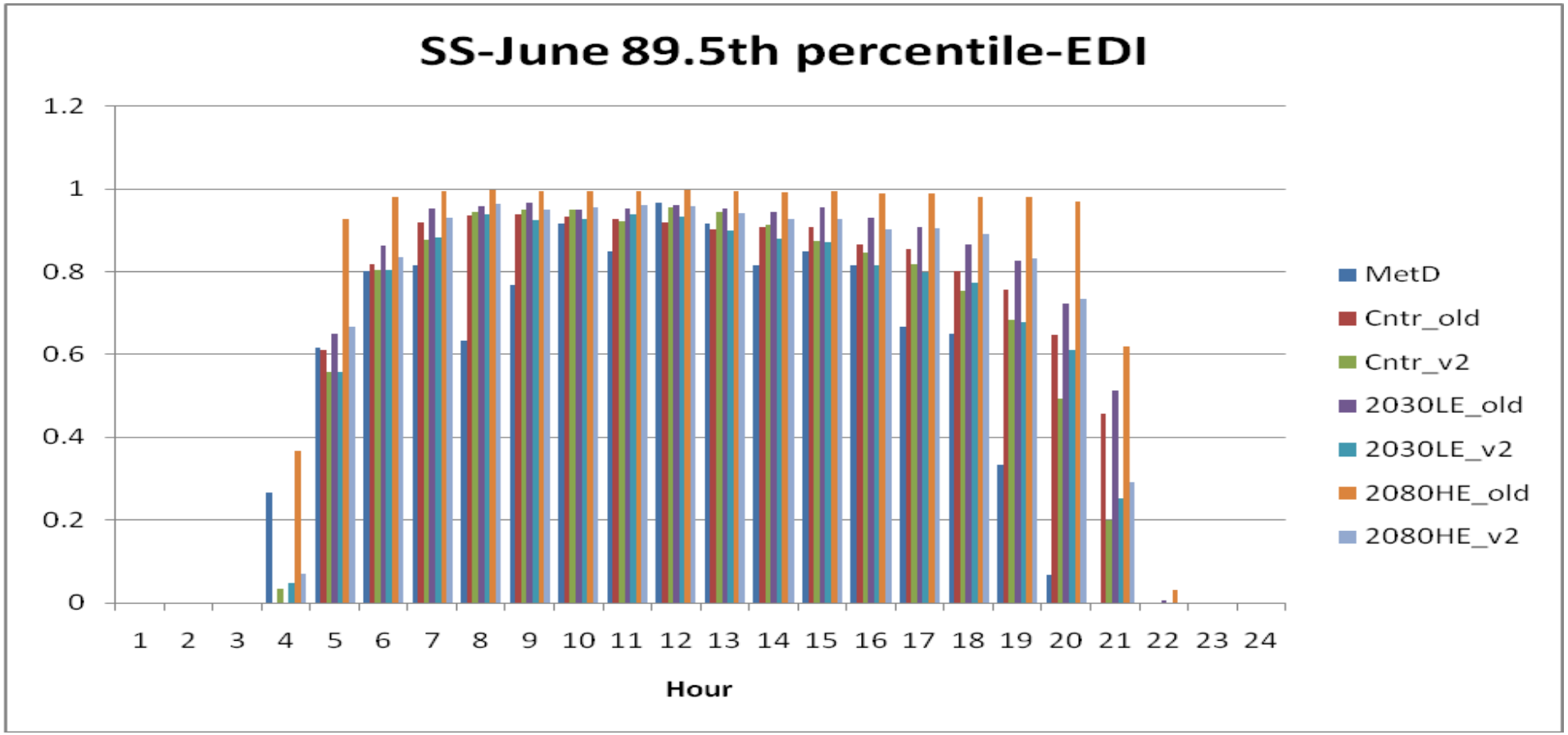

Figure 6.4.2.5 SS comparison for Edinburgh. Note: MetD= Meteorological Office data set, old= old WG control data sets, v2= WG version 2.0 data sets, LE= Low Emissions, HE= High Emissions.

6.5 Conclusions

From the analyses carried out on the WG_v2 data sets, it is evident that the projected data sets provide reasonable results. Note should be taken that high GSR values were found at the early and late hours of the day. This may be due to the effects of the SS values which were found at those hours as SS was used to derive the GSR values. For users who wish to use the WG_v2 data sets for solar applications, it is suggested that first two hours of the beginning and last two ending hours of the day to be excluded in the application to obtain reasonable simulation results.

Due to the increase of GSR in the projected WG_v2 data sets, PV application for electricity generation in the UK seems promising. Further analysis of possible implementation of PV is recommended.

7.0 Conclusions and future work

In this chapter the overall conclusions to this thesis will be presented. Potential future works will also be addressed.

7.1 Conclusions

The earth's climate system is changing and this is affecting all living creatures on it. As discussed in previous chapters solar radiation affects the earth climate system. Furthermore, the concentration of CO_2 in the atmosphere also plays an important role in trapping the excess heat or long wave radiation from escaping from the surface and atmosphere of the earth. The retention of this excess heat will increase the earth's temperature as a whole and thus change the climate system.

The UKCIP was established to co-ordinate research works that deal with climate change. Besides that, the UKCIP also produce projected future climate data according to CO_2 emissions scenarios so that mitigation and adaptation steps can be taken to keep the UK well prepared for climate change.

As part of the COPSE research group, this research work focuses on the projected solar radiation profile for the UK and detailed analysis were carried out in this respect. Following are the conclusions drawn from all the research analysis:

Evaluation of models

Due to the high cost of solar radiation measurement equipment and the need for highly trained personnel, measured solar radiation data is scarce. Hence, mathematical models are usually employed. Evaluations of models for the UK were carried out and the following conclusions were drawn:

1. The Liu-Jordan model performs well for estimating the average hourly global and diffuse radiation for the UK with errors normally distributed around zero, with 65%- and 100% points lying in the ±30 W/m^2 range respectively. At the individual hourly level however, a number of problems were observed. At low

sunset angles, the values predicted by the model were less reliable. Given the low absolute solar energy available at such angles though, this was not seen as a major defect.

A general weakness, however, was the model's inability to take account of the asymmetric distribution of radiation across solar noon. Because of this it underestimates global and diffuse radiation before noon and overestimates after noon for most of the UK locations.

2. For the clear-sky radiation models, the Page model performs better than the Yang model in semi-arid interior climatic locations as shown in the Aswan, Egypt and Jodphur, India results with an averaged accuracy of 96- and 99 percent respectively. As for the Yang model, it performs better than Page model in high humidity locations such as Bahrain with an averaged accuracy of 96 percent. For mild climatic locations such as Gerona, both models show good results with 99- and 97 percent of accuracy respectively for Page and Yang model. Hence, it is concluded that for semi-arid interior climatic conditions Page model is suitable and for humid climates Yang model is recommended.

3. From the evaluation work presently carried out for the two all-sky solar radiation models, i.e. MRM and Yang model, a consistently better overall performance was observed for the MRM than for the Yang model. In the 200-400 W/m^2 range, the higher accuracy of the MRM was particularly evident, which makes it the more suitable for use in the UK where conditions are frequently overcast and radiation levels typically fall below 400 W/m^2. Furthermore, this may be due to the reason that the Yang model was first developed for clear-sky conditions.

Solar radiation and temperature relations

Temperature is closely related to solar radiation. World-wide there are many more temperature measuring meteorological stations than those that measure solar radiation. Development of temperature-based mathematical models to obtain mean-daily irradiation have been carried out and found to be of good accuracy with an averaged r^2 of 0.74 for January to Jun and 0.84 for July to

December. In contrast to the classical models that use daily temperature range, use was made of mean-daily temperature as the basic regressor. Furthermore, a procedure to decompose daily to hourly temperatures was also evaluated. It was found that the procedure, although originally developed using data from North American locations, produces reliable estimates of hourly temperature.

UKCP09 data analysis

Data sets from the UKCP09 were used in this study along with the historical measured data for three locations i.e. Bracknell (London), Manchester and Edinburgh to critically analyse sol-air temperature and the likely change that may occur in the key climate variables, i.e. temperature, sunshine duration and solar irradiation.

Three carbon dioxide (CO_2) emission scenarios at different time series were selected, namely 2030 Low Emission, 2050 Medium Emission and 2080 High Emission scenarios. Note that only results from Bracknell and Edinburgh are discussed in detail because result for Manchester shows the similar trend.

It was found that the UKCP09 data sets showed a substantial increase in temperature, sunshine and solar irradiation when compared with historical measured data would pose a serious challenge for the cooling of buildings.

A study to investigate the impending changes in sol-air temperature and daylight illuminance was carried out. For the year 2080, high-emission scenario the sol-air temperature for dark-coloured horizontal surface has the highest difference of 20.1ºC. For vertical surfaces facing south, the highest sol-air temperature increases of 22.3ºC was found.

Besides that, a shifting trend of daylight illuminance is evident. For global illuminance, both locations show the same increasing trend of frequencies of occurrence for global illuminance for lower range (0-30 klux) for all scenarios when compared with CIBSE data. A similar trend of increased frequency of global illuminance for the higher range (70-120 klux) was also apparent. For

diffuse illuminance, the frequencies of occurrence show an increase lower range of illuminance for all scenarios.

Furthermore, a study was conducted to investigate the cause of the shifting trend in daylight illuminance. It found that the predictions indicate a radical change in the characteristics of solar climate, i.e. from the present diffuse fraction (of total irradiation) of 0.37 which indicates mild turbidity, the value would drop to around 0.13 indicating clear skies with exceptionally low turbidity. To the present researcher this behaviour was somewhat anomalous. If the prediction come true the severe reduction in the diffuse fraction would mean that beam irradiance would be of a high order and this would necessitate appropriate shading design for windows and atria. If such a drastic change in sol-air temperature and the shifting trend of daylight illuminance would occur that would pose a great challenge to building services engineers.

Weather Generator version 2.0 (WG_v2)

As a result from the old WG data analysis that was previously carried out, communications with the UKCP WG modeller was established. From the communications (see Appendix B), new version of WG was released i.e. WG_v2. Data analyses of WG_v2 data sets were carried out to determine the effects of the changes that have been applied to the WG_v2.

From the above data analyses, drastically decreased GSR was found in the WG_v2 data sets when compared with the old WG data sets. A substantial increase of GSR was found in the early and late hours when comparing between Met. Data and the WG_v2 data sets.

For SS, the same decreasing trend was found while comparing the WG_v2 with the old WG data sets. Increase of SS was also found in the WG_v2 data sets when comparing with the Met. Data sets during early and late hours of the day. This increase is the main cause of the increase in GSR that was previously mentioned as GSR was derived from SS.

Overall the WG_v2 produces reasonable projected GSR and SS. Note that care should be taken during early and late evening hour when using the WG_v2 for solar applications.

7.2 Future work

Throughout the research works carried out, the following possible future works are proposed:

- *Clear-sky radiation model*

  Further research may be undertaken using a combination of the Linke turbidity, precipitable water vapour and ozone layer data, so that a truly universal clear-sky radiation model could be developed. Furthermore, seasonal effects could be usefully taken into consideration as well.

- *Temperature and solar radiation relations*

  There is a large body of existing data from recent years on the temperature and radiation parameters measured across the world in recent years. This data could be used for further validation of the proposed model for different geographic areas, climatic zones and seasons.

- *UKCP09 projected data*

  Following from the communications with the UKCP modeller regarding the long sunshine hour at the late evening hour, further evaluations should be carried out to validate the application of the proposed solutions on the newly launched WG. Furthermore, the consistencies of the new projected data should also be validated.

  Validated mathematical solar radiation models e.g. MRM may be used to generate solar radiation data and incorporated in to the WG. This can be done by using the projected input variables to run the model.

Further work should be carried out to look at the turbidity of the UK sky conditions. From the evaluation works carried out in this research, the UK sky seems to have clearer condition in the future.

- *PV for electricity generation*

  Due to increase of GSR in the projected data sets, further research should be carried out to test the PV at different orientations for electricity generation. This is to provide an in-depth and thorough understanding of PV performance. Furthermore, different types of PV should also be tested for their performance in the projected scenarios.

  A thorough monetary or life cycle analysis for PV should be carried out to see the difference between current and projected future scenarios.

References

(1969). Observers Handbook. London, HSMO.

(2006). STERN REVIEW:The Economics of Climate Change.

Allen, R. (1995). Evaluation of procedures for estimating mean monthly solar radiation from air temperature, Food and Agriculture Organization of the United Nations (FAO).

Allen, R. G. (1997). "Self-Calibrating Method for Estimating Solar Radiation from Air Temperature." Journal of Hydrologic Engineering **2**(2): 56-67.

Angstrom, A. (1924). "Solar and terrestrial radiation." Quart J R Met Soc(50): 121–124.

Ångström, A. K. (1924). "On the computation of global radiation from records of sunshine." Arkiv. Geof **2**(22): 471.

Angus, R. C. (1995). Illuminance models for the United Kingdom. Edinbirgh, Edinburgh Napier University. **PhD**.

Annandale, J. G., N. Z. Jovanovic, N. Benadé and R. G. Allen (2002). "Software for missing data error analysis of Penman-Monteith reference evapotranspiration." Irrigation Science **21**(2): 57-67.

Anon. "ACTIVE SOLAR TRACKING SYSTEM." Retrieved 25 November, 2010, from http://www.middletonsolar.com/products/product12.htm.

Anon. "Measurement Equipment." Retrieved 4 April, 2011, from http://users.du.se/~ffi/SERC/Hybrid/technical_data.htm.

ASHRAE (1997). Handbook of Fundamentals. Atalanta, American Society of Heating, Refrigerating and Air-Conditioning Engineers.

ASHRAE (2009). Handbook of Fundamentals. Atalanta, American Society of Heating, Refrigerating and Air-Conditioning Engineers.

Bandyopadhyay, A., A. Bhadra, N. S. Raghuwanshi and R. Singh (2008). "Estimation of monthly solar radiation from measured air temperature extremes." Agricultural and Forest Meteorology **148**(11): 1707-1718.

Betts, R., M. Sanderson, D. Hemming, M. New, J. Lowe and C. Jones (2009). Regional climate changes at 4+°C. International Climate Conference: 4 Degrees and beyond, Oxford University.

Bird, R. E. and R. L. Hulstrom (1979). Application of Monte Carlo Technique to Insolation Characterisation and Prediction, US SERI Tech.**:** 38.

Black, E., M. Blackburn and G. Harrison (2004). "Factors contributing to the summer 2003 European heat wave." Weather(59): 217-223.

Bristow, K. L. and G. S. Campbell (1984). "On the relationship between incoming solar radiation and daily maximum and minimum temperature." Agricultural and Forest Meteorology **31**(2): 159-166.

Burton, A., H. J. Fowler, S. Blenkinsop and C. G. Kilsby (2010). "Downscaling transient climate change using a Neyman-Scott Rectangular Pulses stochastic rainfall model." Journal of Hydrology **381**(1-2): 18-32.

Calosi, P., D. T. Bilton and J. I. Spicer (2008). "Thermal tolerance, acclimatory capacity and vulnerability to global climate change." Biology Letters **4**(1): 99-102.

Campbell, G. (1977). An Introduction to Environmental Biophysics., Springer.

Celik, A. N., T. Muneer and P. Clarke (2009). "A review of installed solar photovoltaic and thermal collector capacities in relation to solar potential for the EU-15." Renewable Energy **34**(3): 849-856.

Chandrasekhar, S. and D. D. Elbert (1954). "The illumination and polarization of the sunlit sky on Rayleigh scattering." Trans. Amer. Phil. Soc. **44**: 643.

Cheung, H. D. and T. M. Chung (2008). "A study on subjective preference to daylit residential indoor environment using conjoint analysis." Building and Environment **43**(12): 2101-2111.

Chirarattananon, S., P. Chaiwiwatworakul and S. Pattanasethanon (2002). "Daylight availability and models for global and diffuse horizontal illuminance and irradiance for Bangkok." Renewable Energy **26**(1): 69-89.

CIBSE (2002). CIBSE Guide J Weather Solar and Illuminance Data, The Charted Institution of Building Services.

CIBSE (2002). Guide J:Weather, solar and illuminance data. K. Butcher, The Chartered Institution of Building Services Engineers.

CIBSE, Ed. (2006). Environmental Design. CIBSE Guide A. London, The Chartered Institution of Building Services Engineers.

Clima, T. "Shadow Ring CM 121 Typ B." Retrieved 4 April, 2011, from http://www.thiesclima.com/global_radiation.html.

Collares-Pereira, M. and A. Rabl (1979). "The average distribution of solar radiation- correlations between diffuse and hemispherical and between daily and hourly insolation values." Solar Energy(22): 155.

Colliver, D. G., Ed. (1991). Solar Energy in Agriculture:Energy in World Agriculture. Amsterdam, Elsevier.

Coskun, C., Z. Oktay and I. Dincer (2010). A novel approach to cooling degree-hour calculation: an application for 58 cities in Turkey. 5th International Ege Energy Symposium. , Pamukkale University, Turkey.

Coulson, K. L. (1959). "Characteristics of radiation emerging from top of a Rayleigh atmosphere." Plane Space Sci.(1): 265.

Coulson, K. L. (1975). Solar and Terrestrial Radiation. New York, Academic Press.

Cowpertwait, P. S. P., C. G. Kilsby and P. E. O'Connell (2002). "A space-time Neyman-Scott model of rainfall: Empirical analysis of extremes." Water Resour. Res. **38**(8): 1131.

Dave, J. V. (1964). "Importance of higher order scattering in a molecular atmosphere." J. Opt. Soc. Amer. **54**: 307.

Dave, J. V. (1979). "Extentsive data sets of the diffuse radiation in realistic atmospheric models with aerosols and common absorbing gases." Solar Energy **21**: 361-369.

De Jong, R. and D. W. Stewart (1993). "Estimating global solar radiation from common meteorological observations in Western Canada." Can J Plant Sci (73): 509-518.

DECC (2010). Feed-in tariffs: Government's response to the summer 2009 consultation**:** p47.

DECC (2011). UK CLIMATE CHANGE SUSTAINABLE DEVELOPMENT INDICATOR:2009 GREENHOUSE GAS EMISSIONS, FINAL FIGURES.

DEFRA (2008). Climate Change Act 2008: CHAPTER 27. D. f. E. F. a. R. Affairs.

DEFRA. (2009). "EU landfill directive: landfill directive briefing paper." Retrieved 4 April, 2011, from http://archive.defra.gov.uk/environment/waste/strategy/legislation/landfill/documents/landfilldir.pdf.

Deutsch, C. A., J. J. Tewksbury, R. B. Huey, K. S. Sheldon, C. K. Ghalambor, D. C. Haak and P. R. Martin (2008). "Impacts of climate warming on terrestrial ectotherms across latitude." Proceedings of the National Academy of Sciences **105**(18): 6668-6672.

Doulos, L., A. Tsangrassoulis and F. Topalis (2008). "Quantifying energy savings in daylight responsive systems: The role of dimming electronic ballasts." Energy and Buildings **40**(1): 36-50.

Draper, N. and H. Smith (1998). Applied regression analysis. New York, Wiley.

Driesse, A. and D. Thevenard (2002). "A test of Suehrcke's sunshine-radiation relationship using a global data set." Solar Energy(72): 167.

Drummond, A. J. (1956). "On the measurement of sky radiation." Arch. Met. Geoph. Biokl. **B7**: 413-436.

Ekström, M., P. D. Jones, H. J. Fowler, G. Lenderink, A. Buishand and D. Conway (2007). "Regional climate model data used within the SWURVE project. 1: Projected changes in seasonal patterns and estimation of PET." Hydrology and Earth System Sciences **11**: 1069-1083.

Envco. (2009). "Albedometer - Global and Reflected Radiation." Retrieved 4 April, 2011, from http://www.envcoglobal.com/catalog/product/analog-solar-radiation-sensors/albedometer-global-and-reflected-radiation.html.

EPLAP. "NORMAL INCIDENCE PYRHELIOMETER." Retrieved 4 April, 2011, from http://www.eppleylab.com/.

ESRA (2000). European Solar Radiation Atlas Paris, Ecole des Mines.

ESRA (2000). European Solar Radiation Atlas 2000. Vol. 1: Fundamentals and maps. Ecole des mines de, Paris, Les Presse de l'Ecole.

EST-UK. (2011). "Feed-in Tariff scheme." Retrieved 4 April, 2011, from http://www.energysavingtrust.org.uk/Generate-your-own-energy/Sell-your-own-energy/Feed-in-Tariff-scheme#about.

Fröhlich, C. (2006). "Solar Irradiance Variability Since 1978." Space Science Reviews **125**(1): 53-65.

Galasiu, A. D. and J. A. Veitch (2006). "Occupant preferences and satisfaction with the luminous environment and control systems in daylit offices: a literature review." Energy and Buildings **38**(7): 728-742.

Geuymard, C. (2000). "Prediction and performance assessment of mean hourly global radiation." Solar Energy **68**: 285.

Geuymard, C. and H. D. Kambezidis (2004). Solar spectral radiation. Solar radiation and daylight models. T. Muneer. Oxford, Elsevier Ltd**:** 221-302.

Gipe, P. (2009). "Britain To Launch Innovative Feed-in Tariff Program in 2010 " Retrieved 4 April, 2011, from http://www.renewableenergyworld.com/rea/news/article/2009/07/britain-to-launch-innovative-feed-in-tariff-program-in-2010.

Grag, H. P. and S. N. Grag (1985). "Correlation of monthly-average daily global, diffuse and beam radiation with bright sunshine hours." En. Conv. Mgmt(25): 409.

Guan, L. (2009). "Preparation of future weather data to study the impact of climate change on buildings." Building and Environment **44**(4): 793-800.

Gueymard, C. A. (2003a). "Direct solar transmittance and irradiance predictions with broadband models. Part 1: detailed theoretical performance assessment " Solar Energy(74): 355-379.

Gueymard, C. A. (2003b). "Direct solar transmittance and irradiance predictions with broadband models. Part II: validation with high quality measurements " Solar Energy(74): 381-395.

Halthore, R. N. (1999). Measurement and modeling of shortwave irradiance componentsin cloud-free atmosphere. S. G. Pandalai. Research Signpost,Trivandrum, India.

Hansen, J., M. Sato, R. Ruedy, P. Kharecha, A. Lacis, R. Miller, L. Nazarenko, K. Lo, Schmidt, G. A., G. Russell, I. Aleinov, S. Bauer, E. Baum, B.

Cairns, V. Canuto, M. Chandler, Y. Cheng, A. Cohen, A. Del Genio, G. Faluvegi, E. Fleming, A. Friend, T. Hall, C. Jackman and J. Jonas, Kelley, M., Kiang, N. Y., Koch, D., Labow, G., Lerner, J., Menon, S., Novakov, T., Oinas, V., Perlwitz, Ja., Perlwitz, Ju., Rind, D., Romanou, A., Schmunk, R., Shindell, D., Stone, P., Sun, S., Streets, D., Tausnev, N., Thresher, D., Unger, N., Yao, M., and Zhang, S. (2007). "Dangerous human-made interference with climate: a GISS model study." Atmospheric, Chemistry and Physics **7**(9): 2287-2312.

Hargreaves, G. (1994). "Simplified coefficients for estimating monthly solar radiation in North America and Europe." Dept. Paper, Department of Biology and Irrigation Engineering, Utah State University.

Hargreaves, G. and Z. Samani (1982). "Estimating potential evapotraspiration." J Irrig Drain Eng,ASCE(180): 225-30.

Hargreaves, G. L., G. H. Hargreaves and J. P. Riley (1985). "Irrigation Water Requirements for Senegal River Basin." Journal of Irrigation and Drainage Engineering **111**(3): 265-275.

Hawas, M. and T. Muneer (1983). "Correlation between global radiation and sunshine data for India." Solar Energy(30): 289.

Hawas, M. and T. Muneer (1984). "Study of diffuse and global radiation characteristics in India." En. Conv. Mgmt(24): 143.

Hedrick, R. (2009). Generation of hourly design-day weather data (RP-1363), ASHRAE Research Project. **Final Report**.

Hunt, D. R. G. (1979). "The use of artificial lighting in relation to daylight levels and occupancy." Building and Environment **14**(1): 21-33.

Hunt, L. A., L. Kuchar and C. J. Swanton (1998). "Estimation of solar radiation for use in crop modelling." Agricultural and Forest Meteorology **91**(3-4): 293-300.

Ineichen, P. (2006). "Comparison of eight clear sky broadband models against 16 independent data banks." Solar Energy(80): 468-478.

Instruments, E. (2004). "Sky Scanner MS-321LR." Retrieved 4 April, 2011, from http://www.eko-usa.com/products/am/MS-321LR/MS-321LR.html.

Instruments, E. (2005). "Pyrgeometer: MS-202/MS-202F." Retrieved 4 April, 2011, from http://www.eko-usa.com/products/am/MS-202_MF-11/MS-202/MS-202.html.

IPCC (2007). Climate Change 2007: The Physical Science Basis. Cambridge, UK, Intergovernmental Panel on Climate Change.

Iqbal, M. (1979). "Prediction of hourly diffuse solar radiation from measured hourly global radiation on a horizontal surface." Solar Energy **24**: 491.

Jain, S. and P. C. Jain (1988). "A comparison of Ångström-type correlations and the estimation of monthly average daily global irradiation." Solar Energy(40): 93.

Janda, K. B. (2011). "Buildings don't use energy: people do " Architectural Science Review **54**: 15-22.

Jones, P. (2011). "Global Temperature Record." Retrieved 4 April, 2011, from http://www.cru.uea.ac.uk/cru/info/warming/.

Jones, P. D., C. G. Kilsby, C. Harpham, V. Glenis and A. Burton (2009). UK Climate Projections science report: Projections of future daily climate for the UK from the Weather Generator., University of Newcastle,UK.

Kambezidis, H. and N. Papanikolaou (1989). Total solar irradiance on inclined surfaces with arbitrary orientations in Greece. Proc. of the General Assembly of the European Geophysical Society Barcelona, Spain.

Kambezidis, H., B. Psiloglou and B. Synodinou (1997). "Comparison between measured and models for daily solar radiation on tilted surfaces in Athens, Greece." J. Renew. Energy **10**: 505.

Keeling, R. F., S. C. Piper, A. F. Bollenbacher and J. S. Walker (2009). Atmospheric Carbon Dioxide Record from Mauna Loa.

Kendrick, D. e. a. (1994). Guide to recommended practice of daylight measurement. Wein, Austria, International Commission on Illumination (CIE).

Kiehl, J. T. and K. E.Trenberth (1997). "Earth's Annual Global Mean Energy Budget. ." American Meteorological Society(78): 197-208.

Kilsby, C. G., P. D. Jones, A. Burton, A. C. Ford, H. J. Fowler, P. James, A. Smith and R. L. Wilby (2007). "A daily weather generator for use in climate change studies." Environmental Modelling and Software(22): 1705-1719.

Kinghorn, D. and T. Muneer (1998). "Daylight illuminance frequency distribution: Review of computational techniques and new data for UK locations." Lighting Research and Technology **30**(4): 139-150.

Kopp, G., G. Lawrence and G. Rottman (2005). "The Total Irradiance Monitor (TIM): Science Results." Solar Physics **230**(1): 129-139.

Koussa, M., A. Malek and M. Haddadi (2009). "Statistical comparison of monthly mean hourly and daily diffuse and global solar irradiation models and a Simulink program development for various Algerian climates." Energy Conversion and Management **50**(5): 1227-1235.

Krarti, M., P. M. Erickson and T. C. Hillman (2005). "A simplified method to estimate energy savings of artificial lighting use from daylighting." Building and Environment **40**(6): 747-754.

Kurian, C. P., R. S. Aithal, J. Bhat and V. I. George (2008). "Robust control and optimisation of energy consumption in daylight-artificial light integrated schemes." Lighting Research and Technology **40**(1): 7-24.

Lam, J. C. (1996). "An analysis of residential sector energy use in Hong Kong." Energy **21**(1): 1-8.

Latif, M. (2010). "Uncertainty in climate change projections." Journal of Geochemical Exploration **In Press, Corrected Proof**.

Leckner, B. (1978). "The spectral distribution of solar radiation at the earth's surface-elements of a model." Solar Energy(20): 143-150.

Liu, B. Y. H. and R. C. Jordan (1960). "The inter-relationship and characteristic distribution of direct, diffuse and total solar radiation." Solar Energy(4): 1.

Liu, D. L. and B. J. Scott (2001). "Estimation of solar radiation in Australia from rainfall and temperature observations." Agricultural and Forest Meteorology **106**(1): 41-59.

Lobell, D. B. and C. B. Field (2007). "Global scale climate-crop yield relationship and the impacts of recent warming." Environ Res Lett.

Loeb, N. G., B. A. Wielicki, D. R. Doelling, G. L. Smith, D. F. Keyes, S. Kato, N. Manalo-Smith and T. Wong (2009). "Toward Optimal Closure of the Earth's Top-of-Atmosphere Radiation Budget." Journal of Climate **22**(3): 748-766.

Lof, G. O. G., Duffie, J.A. and Smith, C.O (1966). World distribution of solar radiation. Engineering Experiment Station Report Madison, USA, University of Wisconsin. **21**.

Loutzenhiser, P. G., G. M. Maxwell and H. Manz (2007). "An empirical validation of the daylighting algorithms and associated interactions in building energy simulation programs using various shading devices and windows." Energy **32**(10): 1855-1870.

Lutherbacher, J., D. Dietrich, E. Xoplanki, M. Grosjean and H. Wanner (2004). "European seasonal and annual temperature variability, trends and extreme since 1500." Science **303**: 1499-1503.

MacLeay, I., K. Harris and A. e. a. Annut (2010). Digest of United Kingdom energy statistics (DUKES) 2010 :Chapter 7: Renewable sources of energy.

Madkour, M. A., M. El-Metwally and A. B. Hamed (2006). "Comparative study on different models for estimation of direct normal irradiance (DNI) over Egypt atmosphere." Renew. Energy(31): 361-382.

Madkour, M. A., El-Metwally, M. and Hamed, A. B. (2006). "Comparative study on different models for estimation of direct normal irradiance (DNI) over Egypt atmosphere " Renew. Energy **31**: 361-382.

McCaskill, M. R. (1990a). "Prediction of solar radiation from rainday information using regionally stable coefficients." Agricultural and Forest Meteorology **51**(3-4): 247-255.

McCaskill, M. R. (1990b). "An efficient method for generation of full climatological records from daily rainfall." Australian Journal of Agricultural Research **41**: 595-602.

Meteorological Office, I. (1980). Aerological Data at India Part III: Radiation Data 1971 Pune, India, India Meteorological Office.

Meza, F. and E. Varas (2000). "Estimation of mean monthly solar global radiation as a function of temperature." Agricultural and Forest Meteorology **100**(2-3): 231-241.

Monteith, J. L. (1959). "The reflection of short-wave radiation by vegetation." Q. J. Roy. Met. Soc. **85**: 392.

Montgomery, D. and E. Peck (1992). Introduction to linear regression analysis. New York, Wiley.

Muneer, T. (2004). Solar radiation and daylight models. Oxford, Elsevier Ltd.

Muneer, T., Abodahab N., G. Weir and J. Kubie (2000). Windows in Buildings. Oxford, Elsevier.

Muneer, T. and F. Fairooz (2002). "Quality control of solar radiation and sunshine measurements – lessons learnt from processing worldwide databases." Building Serv. Eng. Res. **23**(3): 151-166.

Muneer, T. and M. S. Gul (1998). "Detailed evaluation of a meteorological radiation model using long-term data from UK locations." En. Conv. Mgmt **38**: 303.

Muneer, T. and M. S. Gul (2000). "Evaluation of sunshine and cloud cover based models for generating solar radiation data." Eng. Conv. Mgmt **41**: 461-482.

Muneer, T., M. S. Gul and H. Kambezedis (1998). "Evaluation of an all-sky meteorological radiation model against long-term measured hourly data." Eng. Conv. Mgmt **39**(3): 303-317.

Muneer, T., M. S. Gul, H. Kambezedis and S. Allwinkle (1996). A simple meteorological radiation model. Join Charted Institution of Building Services Engineer/American Society of Heating Refregerating and Air-conditioning Engineers Conf., Harrogate.

Muneer, T. and D. Kinghorn (1997). "Luminous efficacy of solar irradiance: Improved models." Lighting Research and Technology **29**(4): 185-191.

Muneer, T. and G. S. Saluja (1985). "A brief review of models for computing solar radiation on inclined surfaces." Energy Conversion and Management **25**(4): 443-458.

Myers, D. R. (2005). "Solar radiation modelling and measurements for renewableenergy applications: Data and model quality." Energy **30**(9): 1517-1531.

N.B. Foster, a. L. W. F. (1953). "A photoelectric sunshine recorder." Bull. Am. Met. Soc.(34): 212.

Nagrial, M. and T. Muneer (1984). Relationship between global radiation and sunshine hours for Pakistan. Proc. Int. Conf. on Science- Past, Present and Future, Islamabad, Pakistan.

NASA. (2011, 18 January 2011). "Glory Mission." Retrieved 4 April, 2011, from http://www.nasa.gov/mission_pages/Glory/overview/index.html.

NovaLynx. (2011). "240-1070-L Campbell-Stokes Pattern Sunshine Recorder." Retrieved 4 April, 2011, from http://www.novalynx.com/240-1070.html.

NREL. (1993). "Quality Assessment with SERI_QC." Retrieved 4 April, 2011, from http://rredc.nrel.gov/solar/pubs/seri_qc/.

NREL. (2009). "Solar Photovoltaic Technology." Retrieved 4 April, 2011, from http://www.nrel.gov/learning/re_photovoltaics.html.

O'Callaghan, P. W. and S. D. Probert (1977). "Sol-air temperature." Applied Energy **3**(4): 307-311.

OECD (2008). OECD Environmental Outlook to 2030.

Page, J. K. (1961). Proc U.N. Conf. on New Sources of Energy. paper no. 35/5/98.

Page, J. K. (1977). The estimation of monthly mean value of daily short wave irradiation on vertical and inclined surfaces from sunshine records for latitude 60ºN to 40ºS. . BS32, Department of Building Science, University of Sheffield, UK

Page, J. K. (1997). Proposed quality control procedures for the Meteorological Office data tapes relating to global solar radiation, diffuse solar radiation, sunshine and cloud in UK. London, UK, the Charted Institution of Building Services Engineers

Page, J. K. and R. Lubens (1986). Climate in the United Kingdom. London, HMO.

Painter, H. E. (1981). The performance of a Campbell–Stokes sunshine recorder compared with a simultaneous record of the normal incidence irradiance. Meterological.

Perez, R., P. Ineichen and R. Seals (1990). "Modelling daylight availability and irradiance components from direct and global irradiance." Solar Energy **44**: 271.

Pisimanis, D., V. Notaridou and D. P. Lalas (1987). "Estimating direct, diffuse and global radiation on an arbitrarily inclined plane in Greece." Solar Energy **39**(3): 159.

Raval, A. and V. Ramanathan (1989). "Observational determination of the greenhouse effect." Nature **342**(6251): 758-761.

Rawlins, F. (1984). "The accuracy of estimates of daily global irradiation from sunshine records for the United Kingdom." Met. Mag.(113): 187.

Richardson, C. W. (1985). "Weather simulation for crop management models." Transactions of the ASABE **28**(5): 1602-1606.

Rivington M., Matthews K.B. and B. K. (2002). A Comparison of Methods for Providing Solar Radiation Data to Crop Models and Decision Support Systems. Integrated Assessment and Decision Support: Proceedings of the 1st biennial meeting of the International Environmental Modelling and Software Society, University of Lugano, Switzerland.

Roche, L., E. Dewey and P. Littlefair (2000). "Occupant reactions to daylight in offices." Lighting Research and Technology **32**(3): 119-126.

Sabine CL, T. T. (2010). "Estimation of anthropogenic CO2 inventories in the ocean." Annual Review of Marine Science **2**: 175-198.

Sakera, Z. (1956). "Recent developments in the study of the polarization of skylight." Adv. Geophys(3): 43.

Salazar, G. A. (2011). "Estimation of monthly values of atmospheric turbidity using measured values of global irradiation and estimated values from CSR and Yang Hybrid models. Study case: Argentina." Atmospheric Environment **45**(15): 2465-2472.

Saluja, G. S. and P. Robertson (1983). Design of passive solar heating in the northern latitude locations. Proc. Solar World Congress, Perth, Australia.

Samani, Z. (2000). "Estimating Solar Radiation and Evapotranspiration Using Minimum Climatological Data." Journal of Irrigation and Drainage Engineering **126**(4): 265-267.

Schar, C., P. L. Vidale, D. Luthi, C. Frei, C. Haberli, M. A. Liniger and C. Appenzeller (2004). "The role of increasing temperature variability in European summer heatwaves." Nature **427**(6972): 332-336.

Schulze, R. E. (1976). "Physically based method of estimating solar radiation from sun-cards." Argricul. Met.(16): 85.

Scott, P. A., D. A. Stone and M. R. Allen (2004). "Human contribution to the European Heatwave of 2003." Nature **432**: 610-614.

Sims, R. E. H. (2004). "Renewable energy: a response to climate change." Solar Energy **76**(1-3): 9-17.

Stephens, A. and P. Jones (2011). Modifications to fix the discrepancies between observed baseline climatology and future change in sunshine and vapour pressure, UK Climate Projections.

Suehrcke, H. (2000). "On the relationship between duration of sunshine and solar radiation on the earth surface: Ångström's equation revisited." Solar Energy(68): 417.

Swartman, R. and O. Ogunlade (1967). Solar radiation estimates from common parameters. Proceedings of Solar Energy Conference.

Tang, W., K. Yang, J. He and J. Qin (2010). "Quality control and estimation of global solar radiation in China." Solar Energy **84**(3): 466-475.

Thevenard, D. (2009). Updating the ASHRAE climatic data for design and standards (RP-1453). ASHRAE Research Project. **Final Report**.

Thornton, P. E. and S. W. Running (1999). "An improved algorithm for estimating incident daily solar radiation from measurements of temperature, humidity, and precipitation." Agricultural and Forest Meteorology **93**(4): 211-228.

Turton, S. M. (1987). "Relationship between total radiation and sunshine duration in the humid tropics." Solar Energy(38): 353.

UKCIP. (2010, 15/10/2010). "About UKCIP." Retrieved 4 April, 2011, from http://www.ukcip.org.uk/about-ukcip/.

UKCIP. (2011, 15 March 2011). "About the Weather Generator version 2.0." Retrieved 4 April, 2011, from http://ukclimateprojections.defra.gov.uk/content/view/1206/500/.

UNFCCC (1994). United Nations Framework Convention on Climate Change.

Whillier, A. (1956). "The determination of hourly values of total radiation from daily summations." Arch. Met. Geoph. Biokl. **Series B**(7): 197.

WHO. (2009). "10 facts on climate change and health." Retrieved 4 April, 2011, from http://www.who.int/features/factfiles/climate_change/en/index.html.

Williams, J. W., S. T. Jackson and J. E. Kutzbach (2007). "Projected distributions of novel and disappearing climates by 2100 AD." Proceedings of the National Academy of Sciences **104**(14): 5738-5742.

WMO (2003). Manual on the Global Observing System. Geneva, World Meteorological Organization.

WMO (2006). Guide to meteorological instruments and methods of observation. Geneva, Switzerland, World Meteorological Office.

Wood, J., T. Muneer and J. Kubie (2003). "Evaluation of a New Photodiode Sensor for Measuring Global and Diffuse Irradiance, and Sunshine Duration." Journal of Solar Energy Engineering **125**(1): 43-48.

Yang, K., G. W. Huang and N. Tamai (2001). "A Hybrid model for estimating global solar radiation." Solar Energy **70**(13).

Yang, K., Huang, G.W. and Tamai, N. (2001). "A hybrid model for estimating global solar radiation " Solar Energy **70**: 13.

Yang, K., T. Koike and B. Ye (2006). " Improving estimation of hourly, daily and monthly solar radiation by importing global data sets." Agri. and Forest Meteorology (137): 43-55.

Yang, K., Koike, T. and Ye, B. (2006). "Improving estimation of hourly, daily and monthly solar radiation by importing global data sets." Agri. and Forest Meteorology **137**: 43-55.

Younes, S., R. Claywell and T. Muneer (2005). "Quality control of solar radiation data: Present status and proposed new approaches." Energy **30**: 1533-1549.

Zhou, J., Y. Wu and G. Yan (2005). "General formula for estimation of monthly average daily global solar radiation in China." Energy Conversion and Management **46**(2): 257-268.

Appendices

Appendix A: Table of monthly sol-air temperature at 1300 hours for Bracknell (London), Manchester and Edinburgh.

Bracknell: Horizontal dark coloured surface sol-air temperature (ºC)

Month	Cntr	2030LE	2030ME	2030HE	2050LE	2050ME	2050HE	2080LE	2080ME	2080HE
Jan	13.1	15.5	15.4	15.2	15.7	16.5	16.0	16.3	17.2	17.3
Feb	18.1	20.0	20.2	20.0	20.8	20.3	20.7	21.1	21.7	21.9
Mar	28.9	31.3	31.5	31.0	31.9	31.7	32.0	32.4	32.8	32.8
Apr	40.0	43.0	43.1	42.9	43.4	43.3	43.5	43.7	44.0	44.9
May	50.1	52.7	52.7	52.9	54.1	53.7	54.3	54.6	55.0	56.9
Jun	55.4	59.2	59.8	59.6	60.8	60.1	60.9	60.5	61.9	62.6
Jul	56.2	61.9	60.7	61.2	63.1	62.7	63.3	62.8	64.5	66.1
Aug	54.3	58.1	57.8	57.8	60.2	59.5	59.7	60.3	61.4	62.8
Sep	45.4	48.6	48.8	48.8	50.0	49.8	50.4	50.6	51.8	53.3
Oct	31.9	35.5	34.9	35.2	35.8	35.9	35.7	36.1	37.0	37.6
Nov	18.0	20.8	20.7	20.4	20.8	21.3	21.2	21.7	22.7	22.9
Dec	12.1	16.9	17.1	17.3	16.7	17.0	17.5	17.2	17.4	18.6

Note: Cntr= control, LE= Low Emissions, ME= Medium Emissions, HE= High Emissions

Bracknell: Horizontal light coloured surface sol-air temperature (ºC)

Month	Cntr	2030LE	2030ME	2030HE	2050LE	2050ME	2050HE	2080LE	2080ME	2080HE
Jan	8.9	10.6	10.5	10.4	10.7	11.6	11.2	11.4	12.4	12.5
Feb	11.7	13.4	13.6	13.4	14.1	13.7	14.2	14.5	15.1	15.5
Mar	19.3	21.4	21.5	21.1	21.8	21.7	22.0	22.3	22.9	22.8
Apr	26.6	29.4	29.4	29.3	29.6	29.7	29.9	30.1	30.3	31.3
May	34.2	36.7	36.6	36.8	37.8	37.5	38.2	38.4	38.7	40.5
Jun	38.4	41.9	42.4	42.3	43.4	42.8	43.5	43.2	44.5	45.3
Jul	39.7	44.7	43.7	44.1	45.7	45.4	45.9	45.6	47.0	48.6
Aug	38.8	42.3	42.0	42.0	44.1	43.4	43.6	44.3	45.2	46.6
Sep	32.5	35.6	35.8	35.7	36.8	36.6	37.1	37.3	38.3	39.8
Oct	23.4	26.5	26.1	26.2	26.8	26.9	26.7	27.1	28.1	28.6
Nov	12.5	15.0	14.9	14.7	14.9	15.5	15.5	15.9	16.9	17.1
Dec	8.2	12.3	12.5	12.7	12.0	12.5	12.9	12.6	12.8	14.0

Note: Cntr= control, LE= Low Emissions, ME= Medium Emissions, HE= High Emissions

Bracknell: Vertical dark coloured surface facing south sol-air temperature (ºC)

Month	Cntr	2030LE	2030ME	2030HE	2050LE	2050ME	2050HE	2080LE	2080ME	2080HE
Jan	25.4	33.0	33.0	32.7	34.6	34.2	33.0	33.2	34.5	34.5
Feb	29.9	35.2	35.1	34.8	36.3	35.0	35.1	35.6	36.4	35.8
Mar	38.9	41.3	41.5	42.0	41.7	42.9	42.3	42.2	43.2	43.6
Apr	45.5	48.6	49.0	49.6	48.6	49.8	49.4	49.3	50.0	51.2
May	48.4	51.1	51.0	51.5	52.3	52.2	52.7	52.9	53.1	54.8
Jun	48.9	52.4	53.3	53.3	54.2	53.9	54.6	54.4	55.4	56.3
Jul	51.9	57.9	56.8	57.7	58.7	58.7	59.2	58.9	60.0	61.2
Aug	57.3	60.3	59.7	60.1	62.2	61.2	61.8	62.6	63.3	64.1
Sep	56.7	58.6	60.2	60.4	60.1	60.4	61.2	61.1	62.5	63.8
Oct	47.6	50.5	50.5	50.7	51.9	51.4	52.2	51.8	52.5	52.9
Nov	36.9	40.8	41.0	41.0	42.1	41.1	41.5	41.2	41.8	43.1
Dec	27.0	40.3	40.5	40.9	40.1	40.1	40.2	40.3	40.0	41.6

Note: Cntr= control, LE= Low Emissions, ME= Medium Emissions, HE= High Emissions

Bracknell: Vertical light coloured surface facing south sol-air temperature (ºC)

Month	Cntr	2030LE	2030ME	2030HE	2050LE	2050ME	2050HE	2080LE	2080ME	2080HE
Jan	16.9	21.7	21.7	21.5	22.7	22.9	22.0	22.3	23.4	23.4
Feb	19.8	23.5	23.5	23.3	24.4	23.6	23.8	24.2	25.0	24.7
Mar	26.9	29.0	29.2	29.3	29.3	30.1	29.8	29.9	30.8	31.0
Apr	32.2	35.1	35.3	35.7	35.1	35.9	35.8	35.8	36.3	37.4
May	36.1	38.6	38.5	38.9	39.7	39.6	40.2	40.3	40.6	42.3
Jun	37.7	41.1	41.7	41.8	42.7	42.4	43.1	42.8	44.0	44.8
Jul	40.2	45.4	44.5	45.2	46.3	46.2	46.7	46.5	47.6	48.9
Aug	43.3	46.4	45.9	46.3	48.1	47.3	47.7	48.6	49.3	50.3
Sep	41.5	43.7	44.6	44.9	44.9	45.2	45.7	45.8	47.0	48.4
Oct	34.1	36.9	36.7	37.0	37.7	37.6	38.0	38.0	38.7	39.2
Nov	24.6	27.7	27.8	27.8	28.4	28.2	28.4	28.4	29.1	30.0
Dec	17.7	26.8	27.0	27.3	26.5	26.8	27.1	27.0	26.9	28.4

Note: Cntr= control, LE= Low Emissions, ME= Medium Emissions, HE= High Emissions

Manchester: Horizontal dark coloured surface sol-air temperature (ºC)

Month	Cntr	2030LE	2030ME	2030HE	2050LE	2050ME	2050HE	2080LE	2080ME	2080HE
Jan	11.7	13.5	13.8	13.7	14.1	14.1	14.5	14.6	15.1	16.1
Feb	16.4	18.9	18.8	18.7	18.8	19.3	19.4	19.7	20.0	20.3
Mar	27.0	29.1	29.5	29.3	29.9	29.7	30.2	30.2	30.6	31.3
Apr	37.9	41.0	41.1	41.0	41.4	41.8	42.1	42.0	42.5	43.3
May	46.8	48.5	49.1	48.8	49.3	50.6	51.0	51.1	52.2	52.8
Jun	50.8	54.5	55.4	55.4	56.2	57.2	57.9	56.4	59.4	59.9
Jul	52.7	56.4	55.4	55.7	58.6	57.5	59.4	58.4	61.6	63.2
Aug	51.3	54.6	54.3	54.4	55.7	56.5	56.6	56.3	58.2	59.5
Sep	42.2	44.2	44.7	44.6	45.2	46.1	46.6	45.7	47.6	48.9
Oct	29.7	32.4	32.6	32.8	32.9	33.5	33.2	33.3	33.9	34.9
Nov	15.9	19.1	18.9	18.9	19.4	19.6	20.0	19.7	20.6	21.4
Dec	11.2	15.1	14.9	15.3	15.0	15.3	15.3	15.6	15.7	16.8

Note: Cntr= control, LE= Low Emissions, ME= Medium Emissions, HE= High Emissions

Manchester: Horizontal light coloured surface sol-air temperature (ºC)

Month	Cntr	2030LE	2030ME	2030HE	2050LE	2050ME	2050HE	2080LE	2080ME	2080HE
Jan	8.0	9.2	9.4	9.4	9.8	9.8	10.2	10.3	10.7	11.7
Feb	10.6	12.7	12.5	12.5	12.6	13.0	13.2	13.4	13.9	14.2
Mar	18.0	19.7	20.0	20.0	20.5	20.4	20.8	20.7	21.4	21.9
Apr	25.1	27.9	28.0	28.0	28.2	28.5	28.9	28.7	29.4	30.1
May	32.1	33.8	34.2	34.1	34.4	35.4	35.9	35.9	36.9	37.6
Jun	35.4	38.8	39.4	39.4	40.0	40.8	41.3	40.2	42.5	43.0
Jul	37.3	40.5	39.9	40.1	42.1	41.6	43.0	42.2	44.7	46.2
Aug	36.5	39.6	39.4	39.4	40.5	41.2	41.3	41.0	42.8	43.8
Sep	30.4	32.5	32.8	32.8	33.2	34.0	34.5	33.8	35.4	36.6
Oct	21.9	24.4	24.6	24.7	24.8	25.4	25.2	25.2	25.9	26.9
Nov	11.3	13.9	13.9	13.8	14.3	14.5	14.9	14.6	15.5	16.3
Dec	7.9	11.1	11.1	11.4	11.1	11.4	11.4	11.6	11.9	13.0

Note: Cntr= control, LE= Low Emissions, ME= Medium Emissions, HE= High Emissions

Manchester: Vertical dark coloured surface facing south sol-air temperature (ºC)

Month	Cntr	2030LE	2030ME	2030HE	2050LE	2050ME	2050HE	2080LE	2080ME	2080HE
Jan	24.0	33.7	33.3	33.2	33.7	33.8	34.3	33.0	34.2	35.6
Feb	29.9	34.3	34.5	34.1	34.6	34.8	34.4	35.3	35.5	35.1
Mar	38.5	39.7	40.5	39.9	40.7	40.3	41.4	40.9	41.0	42.6
Apr	44.7	47.3	47.2	47.0	48.2	49.3	48.8	49.1	49.1	50.2
May	45.1	46.8	47.6	47.1	47.9	49.4	50.2	50.4	51.6	52.2
Jun	46.5	50.0	50.9	50.8	51.5	52.4	53.1	51.8	54.9	55.3
Jul	49.4	53.2	52.1	52.4	56.1	54.4	57.0	55.5	59.5	60.8
Aug	55.7	58.5	57.8	57.9	59.5	60.3	59.6	59.8	61.8	62.6
Sep	54.5	55.5	56.3	55.9	56.3	57.4	58.0	56.8	59.5	60.8
Oct	43.8	47.6	48.0	48.5	48.4	48.7	48.8	48.5	48.9	50.5
Nov	32.6	38.4	37.8	38.2	38.5	38.6	39.3	38.8	39.9	40.7
Dec	24.6	37.7	37.0	37.8	37.7	37.5	36.6	38.2	36.6	38.2

Note: Cntr= control, LE= Low Emissions, ME= Medium Emissions, HE= High Emissions

Manchester: Vertical light coloured surface facing south sol-air temperature (ºC)

Month	Cntr	2030LE	2030ME	2030HE	2050LE	2050ME	2050HE	2080LE	2080ME	2080HE
Jan	16.0	21.8	21.6	21.6	22.0	22.1	22.6	21.9	22.8	24.0
Feb	19.5	22.8	22.9	22.6	22.9	23.2	23.1	23.7	24.1	24.0
Mar	26.4	27.6	28.1	27.9	28.5	28.3	29.0	28.7	29.1	30.3
Apr	31.3	33.9	33.9	33.9	34.5	35.3	35.2	35.2	35.6	36.5
May	33.7	35.4	36.0	35.7	36.2	37.5	38.1	38.2	39.4	40.0
Jun	35.6	39.0	39.6	39.6	40.2	40.9	41.4	40.5	42.9	43.4
Jul	38.1	41.4	40.7	40.9	43.5	42.5	44.4	43.4	46.5	47.9
Aug	41.7	44.4	44.0	44.1	45.4	46.0	45.7	45.8	47.7	48.4
Sep	39.6	41.1	41.6	41.4	41.8	42.7	43.2	42.3	44.5	45.6
Oct	31.5	34.6	35.0	35.3	35.3	35.7	35.7	35.6	36.1	37.4
Nov	21.9	26.1	25.8	26.0	26.4	26.6	27.1	26.7	27.7	28.5
Dec	16.5	25.1	24.7	25.3	25.1	25.1	24.6	25.7	24.9	26.2

Note: Cntr= control, LE= Low Emissions, ME= Medium Emissions, HE= High Emissions

Edinburgh: Horizontal dark coloured surface sol-air temperature (ºC)

Month	Cntr	2030LE	2030ME	2030HE	2050LE	2050ME	2050HE	2080LE	2080ME	2080HE
Jan	10.2	12.0	11.9	11.9	12.2	13.0	12.7	12.8	13.5	13.4
Feb	15.5	18.2	18.0	17.8	18.1	18.6	18.9	19.0	19.1	19.1
Mar	26.3	28.2	28.7	28.7	28.7	29.0	29.4	29.4	30.0	30.3
Apr	37.4	39.7	40.2	39.7	40.3	40.3	40.7	40.6	41.3	42.1
May	45.9	48.0	48.4	48.2	48.6	49.3	49.4	49.0	49.9	50.8
Jun	49.9	53.4	53.5	54.1	54.8	55.3	56.3	55.4	57.4	58.1
Jul	51.5	53.7	54.1	53.5	54.2	55.6	56.0	54.1	58.9	61.0
Aug	49.2	52.3	51.5	52.3	53.0	53.1	53.3	53.5	55.0	56.5
Sep	40.7	43.0	42.7	43.4	44.2	44.1	44.4	44.3	45.0	46.5
Oct	27.4	29.9	29.9	30.3	30.2	30.6	30.5	30.4	31.0	31.7
Nov	14.3	17.0	16.8	16.8	17.4	17.5	17.9	17.4	18.3	18.9
Dec	9.0	11.8	11.9	11.5	12.0	12.5	12.6	12.4	13.0	14.3

Note: Cntr= control, LE= Low Emissions, ME= Medium Emissions, HE= High Emissions

Edinburgh: Horizontal light coloured surface sol-air temperature (ºC)

Month	Cntr	2030LE	2030ME	2030HE	2050LE	2050ME	2050HE	2080LE	2080ME	2080HE
Jan	6.9	8.3	8.2	8.2	8.4	9.3	9.0	9.1	9.8	9.7
Feb	9.9	12.2	12.1	12.0	12.2	12.6	12.9	13.0	13.2	13.3
Mar	17.6	19.1	19.6	19.7	19.6	20.0	20.3	20.2	20.9	21.3
Apr	24.7	27.0	27.2	26.9	27.4	27.5	28.0	27.9	28.4	29.3
May	30.9	32.9	33.2	33.2	33.5	34.1	34.3	34.0	34.8	35.6
Jun	34.9	37.8	37.9	38.3	38.7	39.1	40.0	39.4	40.9	41.5
Jul	36.5	38.7	39.0	38.6	39.2	40.3	40.6	39.2	42.9	44.8
Aug	35.1	37.9	37.4	37.9	38.6	38.7	39.0	39.1	40.4	41.7
Sep	29.5	31.6	31.4	31.8	32.5	32.5	32.8	32.7	33.4	34.8
Oct	20.3	22.5	22.5	22.9	22.8	23.2	23.1	23.0	23.6	24.4
Nov	10.3	12.5	12.4	12.4	12.9	13.1	13.5	13.0	13.9	14.5
Dec	6.3	8.6	8.6	8.2	8.7	9.3	9.4	9.1	9.8	11.2

Note: Cntr= control, LE= Low Emissions, ME= Medium Emissions, HE= High Emissions

Edinburgh: Vertical dark coloured surface facing south sol-air temperature (ºC)

Month	Cntr	2030LE	2030ME	2030HE	2050LE	2050ME	2050HE	2080LE	2080ME	2080HE
Jan	24.9	33.9	34.2	33.0	33.9	33.5	33.8	33.6	33.9	34.6
Feb	30.9	35.5	34.6	34.7	35.5	35.7	36.5	36.1	36.5	36.3
Mar	38.4	40.8	41.3	41.2	41.9	41.7	42.6	42.5	42.6	42.9
Apr	46.0	47.9	49.2	47.8	48.3	48.1	49.0	49.5	49.5	51.1
May	47.8	50.2	50.6	50.3	50.6	51.4	51.6	50.9	51.6	53.2
Jun	47.4	50.9	50.9	51.5	52.1	52.6	53.6	52.8	54.9	55.7
Jul	50.4	52.5	52.9	52.3	53.0	54.4	54.7	53.1	58.9	61.2
Aug	55.1	59.7	57.9	59.2	59.1	58.7	58.8	60.5	61.2	62.5
Sep	53.5	56.6	55.5	57.0	57.1	57.6	57.5	57.6	57.9	59.8
Oct	42.3	45.7	46.0	46.0	46.0	46.5	46.6	46.9	47.0	47.6
Nov	31.0	36.1	36.2	36.1	36.1	37.1	37.3	36.7	37.4	37.3
Dec	25.6	35.3	35.5	35.5	35.6	35.5	36.2	35.8	36.0	37.1

Note: Cntr= control, LE= Low Emissions, ME= Medium Emissions, HE= High Emissions

Edinburgh: Vertical light coloured surface facing south sol-air temperature (ºC)

Month	Cntr	2030LE	2030ME	2030HE	2050LE	2050ME	2050HE	2080LE	2080ME	2080HE
Jan	16.2	21.8	21.9	21.3	21.8	22.0	22.0	22.0	22.5	22.9
Feb	19.9	23.5	22.9	22.9	23.4	23.8	24.3	24.2	24.5	24.5
Mar	26.3	28.1	28.7	28.6	29.0	29.0	29.7	29.6	30.0	30.3
Apr	32.0	34.0	34.8	33.9	34.3	34.2	35.1	35.4	35.5	36.8
May	34.7	36.8	37.2	37.1	37.3	38.1	38.2	37.8	38.6	39.8
Jun	36.1	39.1	39.1	39.6	40.0	40.4	41.3	40.7	42.4	43.1
Jul	38.5	40.6	40.9	40.5	41.1	42.2	42.5	41.2	45.7	47.7
Aug	40.9	44.7	43.6	44.4	44.7	44.5	44.6	45.7	46.6	47.8
Sep	38.8	41.5	40.8	41.7	42.1	42.4	42.5	42.5	43.0	44.6
Oct	30.3	33.1	33.2	33.4	33.3	33.8	33.8	33.9	34.3	34.9
Nov	20.8	24.6	24.6	24.5	24.7	25.4	25.7	25.1	25.9	26.2
Dec	16.6	23.0	23.1	23.0	23.2	23.4	23.8	23.5	23.9	25.2

Note: Cntr= control, LE= Low Emissions, ME= Medium Emissions, HE= High Emissions

Appendix B: E-mail communications

From: Muneer, Tariq [mailto:T.Muneer@napier.ac.uk]

Sent: 21 May 2010 11:21

To: Colin Harpham

Cc: Tham, Yieng Wei

Subject: Discussion we had yesterday re: solar data in UKCP09 database

Colin,

I am grateful for the exchange of emails yesterday. I reiterate what I said yesterday, i.e.

1. It would have been better if we were consulted before the data was released. That way we could have quickly checked and spotted that a full hour or a significant amount of sunshine was not reported for very late evening hours. As you know the WMO rule is that bright sunshine duration is that which corresponds to irradiation exceeding 120W/m2 (see attached jpg file). I append a relevant article of ours (Article #1: Woodsunshine1.pdf) . I understand that your colleagues were under pressure to meet the deadline for release of data hence consultation was not possible.

2. Furthermore, it would have been better if you had calculated daily radiation from daily bright sunshine duration as those models are very reliable. They operate with a high accuracy. You could then have decomposed daily- to hourly irradiation using established and validated techniques such as those highlighted in Article #2 (BSE350547.pdf) that is also appended. Hourly sunshine may then be obtained from the latterly computed hourly irradiation. Once again those models are validated for UK and are provided in my book (T Muneer, Solar radiation and daylight models, Elsevier, Oxford, 2004).

I'd be grateful if you kindly let me know what course of action would you be taking with respect to above concerns. It would also be helpful to find out 'who does what', i.e. the role of Mr Murphy at Met Office and the role of CRU.

Thanking you.

Professor Tariq Muneer, BEng(Hons), MSc(Hons), PhD, DSc, CEng, MIMechE, FCIBSE, Millennium Fellow

Professor of Energy Engineering

School of Engineering and Built Environment

EDINBURGH NAPIER UNIVERSITY

10 Colinton Road, Edinburgh EH10 5DT, Scotland, UK

Tel: (0131) 455 2541 Fax: (0131) 455 2264

email: T.Muneer@Napier.ac.uk

From: Colin Harpham [mailto:c.harpham@uea.ac.uk]

Sent: 24 May 2010 09:59

To: Muneer, Tariq

Cc: Tham, Yieng Wei

Subject: RE: Discussion we had yesterday re: solar data in UKCP09 database

Dear Tariq,

Thank you for the articles.

Daily radiation is calculated from daily sunshine hours, and from tests against observed (which were constrained by the poor availability of observed radiation data) the output compared favourably. The hourly WG component is initially calibrated on observed data (including sunshine hours) and the inter variable relationships need to be maintained, so while deriving sunshine from radiation may be moreaccurate we have the additional constraint that it needs to preserve its relationship with rainfall and temperature. However the sum of the hourly sunshine and radiation do match the daily (it is during this adjustment process that I have allowed unrealistic amounts to occur at the endpoints). We are having an ARCADIA WG meeting tomorrow when this will be discussed - I'll let you know the outcome.

If the endpoints problem is resolved would this affect a building model since the total amount will stay the same?

Phil Jones – CRU project leader

Colin Harpham – CRU WG model for variables other than rainfall.

Chris Kilsby – Newcastle project leader. Rainfall model, integration of the CRU component and embedding into the BADC web interface.

James Murphy – climate change – RCMs

Regards

Colin

From: Muneer, Tariq

Sent: 24 May 2010 10:20

To: Colin Harpham

Cc: Tham, Yieng Wei

Subject:RE: Discussion we had yesterday re: solar data in UKCP09 database

The building industry relies heavily on hourly datasets and hence if one was not careful then the end sunshine hours may be 'trusted' faithfully and used in all manner of calculations, e.g. daylight availability and so on. We may be able to guard against such action by curtailing all solar/daylight calcs that are related to solar altitude less than say 10 degrees. Daylight is an important resource though and there are formulae provided for energy available even for solar altitude less than 0 degrees (twilight).

We'll need to think long and hard on this issue. Is it possible for you to visit us for a brainstorming session? You said you had a little bit of money left over in your kitty and that ought to cover your travel costs. We won't charge you anything.

From: Colin Harpham [mailto:c.harpham@uea.ac.uk]

Sent: 27 May 2010 09:25

To: Muneer, Tariq

Cc: Tham, Yieng Wei

Subject: RE: Discussion we had yesterday re: solar data in UKCP09 database

Dear Tariq,

After discussions at the WG meeting I am going to resolve the endpoints problem in the hourly data. In your formula for sunrise and sunset I notice there is provision for less than 0 degrees (6,12 and 18) – can these formulas be easily modified to cater for +10 deg?

So far as increased future sunshine is concerned these change factors are calculated elsewhere and supplied to the WG at runtime. I have requested the script for this calculation in an effort to check the process from start to finish.

As this originates from an UKCP09 help desk query any meetings should probably involve them, they like to be kept informed so in the near future I had better send them an update.

Regards

Colin

From: Muneer, Tariq [mailto:T.Muneer@napier.ac.uk]

Sent: 27 May 2010 14:21

To: Colin Harpham

Cc: Tham, Yieng Wei

Subject: RE: Discussion we had yesterday re: solar data in UKCP09 database

We'll try to send you a code that'll calculate daily sunshine duration for solar altitude > +10 deg. In what form do you want the code? FORTRAN or EXCEL workbook with VBA code?

From: Colin Harpham [c.harpham@uea.ac.uk]

Sent: 27 May 2010 14:27

To: Muneer, Tariq

Cc: Tham, Yieng Wei

Subject:RE: RE: Discussion we had yesterday re: solar data in UKCP09 database

FORTRAN please.

Thanks

Colin

From: Harpham Colin Dr (ENV) [mailto:C.Harpham@uea.ac.uk]

Sent: 21 July 2010 10:01

To: Muneer, Tariq

Cc: Jones Philip Prof (ENV)

Subject: radiation

Dear Tariq,

I have recently been looking at the WG hourly sunshine distribution and I noticed that I still get a mismatch between sunshine hours and radiation at the day's end (i.e. a sunshine value but no radiation). However, I have compared modelled hourly radiation output with Finningley and find for midsummer that there are observations from 0400-2100 hrs whereas the MRM only has output from 0400 -1900 hrs. To provide better consistency with observed would you recommend I alter the 7deg solar angle hard coded in the routine? Unfortunately I have very limited observed radiation data to do any testing with.

Regards

Colin

Dr Colin Harpham

From: Muneer, Tariq [mailto:T.Muneer@napier.ac.uk]

Sent: 21 July 2010 11:57

To: Harpham Colin Dr (ENV)

Subject: RE: radiation

Pls call me on 0131-455-2541

thanks

From: Harpham Colin Dr (ENV) [mailto:C.Harpham@uea.ac.uk]

Sent: 21 July 2010 13:53

To: Muneer, Tariq

Subject: RE: radiation

Tariq,

Attached is a sample for the Finningley grid cell. NB this version of the WG outputs wind speed (in data column 5) so there is an extra column compared to UKCP09 output.

Regards,

Colin

From: Muneer, Tariq

Sent: 21 July 2010 13:58

To: Tham, Yieng Wei

Subject: FW: radiation

Let us check this

From: Tham, Yieng Wei [mailto:Y.Tham@napier.ac.uk]

Sent: 26 July 2010 14:51

To: Harpham Colin Dr (ENV); Muneer, Tariq

Subject: RE: radiation

hi Colin,

Would you please send us the old version of the Finningley file from the UKCP09 WG so that we can check on the data.

Regards,

Tham

From: Tham, Yieng Wei [mailto:Y.Tham@napier.ac.uk]

Sent: 28 July 2010 13:37

To: Harpham Colin Dr (ENV); Muneer, Tariq

Subject: RE: radiation

Hi Colin,

Attached is the short report of our findings on the sunshine duration for the new and old data sets.

Regards,

Tham

From: Harpham Colin Dr (ENV) [mailto:C.Harpham@uea.ac.uk]

Sent: 28 July 2010 15:50

To: Tham, Yieng Wei; Muneer, Tariq

Subject: RE: radiation

Hi Tham,

I'm a bit confused by your comments as I can find no non-zero ss hrs at 2200 and the largest value at 2100 is 0.6 in June.

Cheers

Colin

From: Tham, Yieng Wei [mailto:Y.Tham@napier.ac.uk]

Sent: 28 July 2010 16:07

To: Harpham Colin Dr (ENV); Muneer, Tariq

Subject: RE: radiation

Hi Colin,

The time system that I am using is hour ending and not hour starting which is used in the WG. For example, hour ending at 22 will be 2100 for the WG file. Hope this will clarify your doubt.

Regards,

Tham

From: Harpham Colin Dr (ENV) [mailto:C.Harpham@uea.ac.uk]

Sent: 28 July 2010 16:49

To: Tham, Yieng Wei; Muneer, Tariq

Subject: RE: radiation

Hi Tham,

The WG times will refer to the previous hours amount i.e. 2100 records the measurement for 2000-2100 - same as observed.

Cheers

Colin

From: Tham, Yieng Wei

Sent: 29 July 2010 09:39

To: Muneer, Tariq

Subject: RE: radiation

Hi Prof,

I am not sure what he tries to clarify. Please meet to discuss.

Regards,

Tham

From: Muneer, Tariq [T.Muneer@napier.ac.uk]

Sent: 29 July 2010 10:35

To: Tham, Yieng Wei

Cc: Harpham Colin Dr (ENV)

Subject: RE: radiation

I am also somewhat confused. The best thing would be to have a phone chat with Colin.

Colin,

What time can you call us?

From: Harpham Colin Dr (ENV) [mailto:C.Harpham@uea.ac.uk]

Sent: 29 July 2010 19:59

To: Muneer, Tariq; Tham, Yieng Wei

Subject: RE: radiation

sorry, forgot to set my out of office reply, I'll be in Monday Tham if you want to give me a call. What I'm saying is that 2200 in the WG file relates to the previous hour. ie. for the WG 2200 is the hour ending.

Not quite sure what you mean by hour starting.

cheers

Colin

From: Muneer, Tariq [T.Muneer@napier.ac.uk]

Sent: 30 July 2010 14:17

To: Harpham Colin Dr (ENV); Tham, Yieng Wei

Subject: RE: radiation

We know what you are saying. In view of this we say that you still have a problem. Will phone you on Monday. Pls say when?

From: Harpham Colin Dr (ENV) [mailto:C.Harpham@uea.ac.uk]

Sent: 03 August 2010 11:30

To: Muneer, Tariq; Tham, Yieng Wei

Subject: RE: radiation

New attached. I have also tried to improve the relationship between sunshine hours and direct radiation (re the >120 constraint) - this has provided a useful improvement for around summer, not so successful for around winter.

Cheers

Colin

From: Muneer, Tariq [mailto:T.Muneer@napier.ac.uk]

Sent: 03 August 2010 11:42

To: Harpham Colin Dr (ENV); Tham, Yieng Wei

Subject: RE: radiation

I suggest that you use a < 10 degree solar altitude cut-off for winter, i.e. when the solar altitude < 10 degree, then zero sunshine duration

---

From: Harpham Colin Dr (ENV) [mailto:C.Harpham@uea.ac.uk]

Sent: 03 August 2010 14:37

To: Muneer, Tariq; Tham, Yieng Wei

Subject: RE: radiation

I cannot fiddle with the daylength because hourly sunshine totals must be consistent with the daily. The >120Wm2 is only applicable to post 2000 MO stations using the new equipment (there are many non-MO stations that do not use it yet) and the WG is calibrated on 1960-1995 data and consequently is expected to model that period for the control run. I have just been comparing Finningly direct radiation with sunshine hours and for winter there are many instances of sub 120Wm2 entries (I spotted one entry as low as 25Wm2) with a full hours sunshine. I imagine the new equipment produces quite different records which are not going to be directly compatible/comparable with the old.

When I subtracted diffuse from global there are a few negative numbers floating about which makes me wonder about the quality of the observed data.

Any idea why this should occur?

Colin

From: Muneer, Tariq

Sent: 03 August 2010 15:05

To: Harpham Colin Dr (ENV); Tham, Yieng Wei

Subject: RE: radiation

Attachments: Fairooz1.pdf

I attach an article on QC that we wrote a while ago. Note that QC of solar data is quite a horrendous task and now is not the time for you to start these procedures. The problem that you are mentioning is quite familiar one and is picked up in the controls that we undertook for CIBSE database.

T Muneer

From: Tham, Yieng Wei

Sent: 04 August 2010 09:31

To: Muneer, Tariq

Subject: new test location from Colin

Hi Prof,

Attached is the result of ss for the new location that Colin sent.

Regards,

Yieng Wei Tham

From: Muneer, Tariq [mailto:T.Muneer@napier.ac.uk]

Sent: 04 August 2010 11:25

To: Harpham Colin Dr (ENV); Tham, Yieng Wei

Subject: FW: new test location from Colin

Tham and I have examined your data (see attached file for clear days) and we think u r now on the right track. If you wish you may correct all files using your newer method.

Please confirm what's your next step.

Thanks.

From: Harpham Colin Dr (ENV) [C.Harpham@uea.ac.uk]

Sent: 04 August 2010 12:44

To: Muneer, Tariq; Tham, Yieng Wei

Subject: RE: new test location from Colin

Actually clear days will be little different, the error was in a routine for dealing with partial sunshine days and I am certain that has now been corrected. I'll do further tests just to make sure.I believe the plan is to release the MK2 version after September; this modification will get rolled out with improvements to rainfall/temperature.

I'll update UKCIP so they are aware of the outcome.

Thanks for the paper on QC of radiation/sunshine measurement, very interesting but not confidence inspiring.

Regards,

Colin

From: Roger Courtney [mailto:roger.courtney@ntlworld.com]

Sent: 28 September 2010 17:22

To: Geoff Levermore

Cc: Chris Underwood; Muneer, Tariq

Subject: Sunshine data - BSERT paper

Geoff,

As agreed at the COPSE meeting, I spoke to Roger Street about the way that Tariq's paper had influenced the revision of the CP09 data. I said it would be published in BSERT and that it would be good to have a formal acknowledgement of the point in the journal. He suggested that this might come from Colin Harpham who had actually made the changes. So I spoke to Colin who was agreeable to the suggestion.

I think it is now a matter of direct liaison with Colin over the words and how they will appear in BSERT.

Roger

From: Muneer, Tariq

Sent: 29 September 2010 09:51

To: Roger Courtney; Geoff Levermore; Tham, Yieng Wei

Cc: Chris Underwood

Subject: RE: Sunshine data - BSERT paper

I am very grateful to Roger for taking this up with Roger Street and Colin Harpham. I'll work with Tham to produce a short draft which will then be circulated to all of you and also sent to Colin Harpham.

From: Tham, Yieng Wei

Sent: 30 September 2010 14:10

To: Harpham Colin Dr (ENV)

Cc: Muneer, Tariq

Subject: RE: Sunshine data - BSERT paper

Hi Colin,

Here is the proposed words that will appear in BSERT:

[This note provides recognition of the quality control work undertaken by Edinburgh Napier University staff under the COPSE project, namely Professor Tariq Muneer and Mr Yiengwei Tham, with respect to the earlier draft of the UKCP09 data set. The latter team advise me regarding problems related to sunshine data that were reported for very late evening hours and the time system. I had discussions with the above team to resolve the relevant issues. Corrective actions was then taken by self and a new, improved UKCP09 data set (MK2) has thus been produced. The new version of the Weather Generator has also been updated accordingly.]

Please let us know if this ok.

Regards,

Yieng Wei Tham

From: Muneer, Tariq [mailto:T.Muneer@napier.ac.uk]

Sent: 30 September 2010 14:23

To: Tham, Yieng Wei; Harpham Colin Dr (ENV)

Subject: RE: Sunshine data - BSERT paper

Colin,

I'd like to correct what Tham has written. The following text got to be agreed between us. Only then BSERT may be approached for a proper insertion.

From: Harpham Colin Dr (ENV) [C.Harpham@uea.ac.uk]

Sent: 01 October 2010 08:46

To: Muneer, Tariq; Tham, Yieng Wei

Subject: RE: Sunshine data - BSERT paper

Tariq,

Just to clarify - the WG produces the output data in response to user requests, so there is no actual data stored. Perhaps something along the lines:

[This note provides recognition of the quality control work undertaken by Edinburgh Napier University staff under the COPSE project, namely Professor Tariq Muneer and Mr Yiengwei Tham, with respect to the UKCP09 Weather Generator (WG) sunshine hours output. The latter team advise me regarding problems related to sunshine data that were reported for very late evening hours and the time system. I had discussions with the above team to resolve the relevant issues and the WG has been updated accordingly. The new version will be released together with other improvements in the near future.]

Cheers

Colin

From: Muneer, Tariq [mailto:T.Muneer@napier.ac.uk]

Sent: 01 October 2010 13:33

To: Harpham Colin Dr (ENV); Tham, Yieng Wei

Subject: RE: Sunshine data - BSERT paper

This looks fine. There is one small error, i.e. instead of 'advise' please change it to 'advised' and re-send the email.

From: Harpham Colin Dr (ENV) [C.Harpham@uea.ac.uk]

Sent: 01 October 2010 13:43

To: Muneer, Tariq; Tham, Yieng Wei

Subject: RE: Sunshine data - BSERT paper

[This note provides recognition of the quality control work undertaken by Edinburgh Napier University staff under the COPSE project, namely Professor Tariq Muneer and Mr Yiengwei Tham, with respect to the UKCP09 Weather Generator (WG) sunshine hours output. The latter team advised me regarding problems related to sunshine data that were reported for very late evening hours and the time system. I had discussions with the above team to resolve the relevant issues and the WG has been updated accordingly. The new version will be released together with other improvements in the near future.]

Amended as requested,

Colin

Appendix C: Tables of comparison for WG_v2.

Tables of comparison of SS for Bracknell.

Mth	Hr	MetD	Cntr_old	Cntr_v2	2030LE_old	2030LE_v2	2080HE_old	2080HE_v2
6	1	0	0.0	0	0.0	0	0	0.0
6	2	0	0.0	0	0.0	0	0	0.0
6	3	0	0.0	0	0.0	0	0	0.0
6	4	0.0	0.0	0.0	0.0	0.0	0.2	0.1
6	5	0.0	0.5	0.6	0.6	0.5	0.9	0.6
6	6	0.3	0.8	0.8	0.9	0.8	1	0.9
6	7	0.8	1.0	0.9	1.0	0.9	1	1.0
6	8	1.0	1.0	1.0	1.0	1.0	1	1.0
6	9	0.8	1.0	1.0	1.0	1.0	1	1.0
6	10	0.9	1.0	1.0	1.0	1.0	1	1.0
6	11	1.0	1.0	0.9	1.0	1.0	1	1.0
6	12	1.0	1.0	1.0	1.0	1.0	1	1.0
6	13	1.0	1.0	1.0	1.0	1.0	1	1.0
6	14	1.0	0.9	1.0	1.0	1.0	1	1.0
6	15	0.9	0.9	1.0	1.0	1.0	1	1.0
6	16	1.0	0.9	1.0	1.0	0.9	1	1.0
6	17	1.0	0.9	0.9	0.9	0.9	1	1.0
6	18	1.0	0.9	0.9	0.9	0.8	1	0.9
6	19	0.9	0.8	0.8	0.9	0.8	1	0.9
6	20	0.28	0.8	0.7	0.8	0.7	1	0.8
6	21	0	0.5	0.1	0.5	0.1	0.2	0.2
6	22	0	0.3	0	0.3	0	0.1	0.0
6	23	0	0.0	0	0.0	0	0	0.0
6	24	0	0.0	0	0.0	0	0	0.0

Tables of comparison of SS for Edinburgh.

Month	Hour	MetD	Cntr_old	Cntr_v2	2030LE_old	2030LE_v2	2080HE_old	2080HE_v2
6	1	0	0.0	0	0.0	0	0.0	0
6	2	0	0.0	0	0.0	0	0.0	0
6	3	0	0.0	0	0.0	0	0.0	0
6	4	0.3	0.0	0.0	0.0	0.0	0.4	0.1
6	5	0.6	0.6	0.6	0.6	0.6	0.9	0.7
6	6	0.8	0.8	0.8	0.9	0.8	1.0	0.8
6	7	0.8	0.9	0.9	1.0	0.9	1.0	0.9
6	8	0.6	0.9	0.9	1.0	0.9	1.0	1.0
6	9	0.8	0.9	0.9	1.0	0.9	1.0	0.9
6	10	0.9	0.9	0.9	1.0	0.9	1.0	1.0
6	11	0.9	0.9	0.9	1.0	0.9	1.0	1.0
6	12	1.0	0.9	1.0	1.0	0.9	1.0	1.0
6	13	0.9	0.9	0.9	1.0	0.9	1.0	0.9
6	14	0.8	0.9	0.9	0.9	0.9	1.0	0.9
6	15	0.9	0.9	0.9	1.0	0.9	1.0	0.9
6	16	0.8	0.9	0.8	0.9	0.8	1.0	0.9
6	17	0.7	0.9	0.8	0.9	0.8	1.0	0.9
6	18	0.7	0.8	0.8	0.9	0.8	1.0	0.9
6	19	0.3	0.8	0.7	0.8	0.7	1.0	0.8
6	20	0.1	0.6	0.5	0.7	0.6	1.0	0.7
6	21	0	0.5	0.2	0.5	0.3	0.6	0.3
6	22	0	0.0	0	0.0	0	0.0	0
6	23	0	0.0	0	0.0	0	0.0	0
6	24	0	0.0	0	0.0	0	0.0	0

Tables of comparison of GSR for Bracknell (Wh/m^2).

Month	Hour	MetD	Cntr_old	Cntr_v2	2030LE_old	2030LE_v2	2080HE_old	2080HE_v2
6	1	0	0.0	0	0.0	0	0	0
6	2	0	0.0	0	0.0	0	0	0
6	3	0	0.0	0	0.0	0	0	0
6	4	1.6	0.0	0.0	0.0	0.0	0	0.0
6	5	37.8	48.9	158.4	57.8	152.5	115.8	200.5
6	6	122.2	138.0	185.6	137.2	184.6	143.3	227.1
6	7	255.4	289.8	309.9	287.5	305.6	280.8	319.5
6	8	393.8	452.5	455.8	454.1	450.5	447.7	459.1
6	9	487.0	618.0	597.7	624.1	586.7	624	596.8
6	10	621.4	763.7	718.0	773.5	709.4	781.8	720.9
6	11	742.0	888.3	797.6	903.7	808.5	910.6	817.3
6	12	753.8	958.9	869.9	977.0	859.5	985.9	871.3
6	13	818.0	964.9	876.3	988.5	870.7	1001.9	881.8
6	14	731.2	915.2	848.9	943.1	832.6	958.6	846.4
6	15	614.8	815.9	758.8	843.7	747.1	857.3	764.9
6	16	574.8	680.3	645.8	709.2	622.0	712	649.1
6	17	430.8	502.0	499.9	515.0	482.4	532.9	511.3
6	18	277.2	329.4	350.6	336.4	339.0	349.5	364.4
6	19	144.6	176.4	211.4	175.6	205.5	184.3	247.6
6	20	35.6	103.6	177.2	113.1	176.3	137.1	228.2
6	21	1.0	0.0	0.0	0.0	0.0	0	0
6	22	0	0.0	0	0.0	0	0	0
6	23	0	0.0	0	0.0	0	0	0
6	24	0	0.0	0	0.0	0	0	0

Tables of comparison of GSR for Edinburgh (Wh/m^2).

Month	Hour	MetD	Cntr_old	Cntr_v2	2030LE_old	2030LE_v2	2080HE_old	2080HE_v2
6	1	0	0.0	0	0.0	0	0.0	0
6	2	0	0.0	0	0.0	0	0.0	0
6	3	0	0.0	0	0.0	0	0.0	0
6	4	7.7	0.5	2.1	0.5	3.3	3.0	7.4
6	5	37.8	88.7	112.6	88.3	123.9	136.0	166.9
6	6	103.7	163.7	188.4	165.0	195.2	174.3	206.7
6	7	207.8	298.9	305.6	301.3	311.4	308.7	324.5
6	8	336.8	442.7	440.6	446.8	443.3	463.9	453.0
6	9	503.7	585.5	565.9	596.6	559.3	621.6	570.5
6	10	660.7	706.5	673.4	716.9	665.0	764.5	678.1
6	11	736.3	795.7	742.6	815.5	748.3	873.4	761.5
6	12	751.5	843.7	802.8	880.5	792.6	939.6	807.3
6	13	794.7	841.3	805.7	885.4	784.0	948.2	807.3
6	14	756.8	807.7	757.6	839.7	742.2	904.5	769.1
6	15	692.3	733.9	673.6	768.9	673.1	820.1	701.6
6	16	622.7	598.9	566.5	634.6	560.7	682.6	595.5
6	17	464.8	463.4	444.7	485.3	446.0	525.8	481.0
6	18	307.5	314.4	314.1	328.4	326.1	360.2	355.4
6	19	218.8	184.1	197.4	191.5	205.8	210.5	232.2
6	20	96.0	81.8	104.1	85.0	120.7	98.5	158.0
6	21	31.3	11.4	76.5	12.7	83.0	13.7	120.4
6	22	0	0.0	0	0.0	0	0.0	0
6	23	0	0.0	0	0.0	0	0.0	0
6	24	0	0.0	0	0.0	0	0.0	0

Appendix D: List of publications

Journals:

1. **N Caliskan, E Jadraque, Y Tham, T Muneer** (***In Press, Corrected Proof***, *Available online 5 February 2011*) *"Evaluation of the accuracy of mathematical models through use of multiple metrics"* International Journal of Sustainable Cities and Society. doi:10.1016/j.scs.2011.02.001
2. **E J Gago, S Etxebarria, Y Tham, Y Aldali, T Muneer** (2011) *"Inter-relationship between mean-daily irradiation and temperature, and decomposition models for hourly irradiation and temperature."* Int. J. Low-Carbon Tech **6**(1): 22-37
3. **Y.Tham, T. Muneer** (2011) *Sol-air temperature and daylight illuminance profiles for the UKCP09 data sets.* Building and Environment **46**(6):1243-1250
4. **Y. Tham, T. Muneer, G. J. Levermore, D. Chow** (first published on December 2, 2010) *"An examination of UKCIP CP02 and CP09 data sets for the UK climate related to their use in building design."* Building Service Engineering. doi:10.1177/0143624410389396
5. **Y. Tham, T. Muneer, B. Davison**. (2010). *"Estimation of hourly averaged solar irradiation: evaluation of models."* Building Service Engineering **31**(1): 9-25
6. **Y. Tham, T. Muneer, B. Davison** (2009). *"A generalized procedure to generate clear-sky radiation data for any location."* Int. J. Low-Carbon Tech. **4**(4): 205-212
7. **Y. Tham, T. Muneer, B. Davison** (2009). *"Evaluation of simple all-sky models to estimate solar radiation for the UK."* Int. J. Low-Carbon Tech. **4**(4): 258-264

Conferences:

1. **Y. Tham, T. Muneer, B. Davison** (2010) *"Evaluation Of Hourly-Averaged Solar Radiation Model"* 2nd United Kingdom-Malaysia Engineering Conference, London
2. **T. Muneer, Y. Tham, B. Davison** (2010) *"Generation of solar radiation data for world-wide sites – Review and validation of models"*,5th International Ege Energy Symposium and Exhibition, Denizli, Turkey.